



HAL
open science

Advanced microscopies for the study of motility behavior in predating *Myxococcus xanthus*

Sara Rombouts

► **To cite this version:**

Sara Rombouts. Advanced microscopies for the study of motility behavior in predating *Myxococcus xanthus*. Bacteriology. Université Montpellier, 2021. English. NNT : 2021MONTT084. tel-03637407

HAL Id: tel-03637407

<https://theses.hal.science/tel-03637407>

Submitted on 11 Apr 2022

HAL is a multi-disciplinary open access archive for the deposit and dissemination of scientific research documents, whether they are published or not. The documents may come from teaching and research institutions in France or abroad, or from public or private research centers.

L'archive ouverte pluridisciplinaire **HAL**, est destinée au dépôt et à la diffusion de documents scientifiques de niveau recherche, publiés ou non, émanant des établissements d'enseignement et de recherche français ou étrangers, des laboratoires publics ou privés.

THÈSE POUR OBTENIR LE GRADE DE DOCTEUR DE L'UNIVERSITÉ DE MONTPELLIER

En Biophysique

École doctorale : Sciences chimiques et biologiques pour la santé, ED 168

Unité de recherche : Centre de Biochimie Structurale, UMR5048 U1054

Advanced microscopies for the study of motility behavior in predating *Myxococcus xanthus*

Présentée par Sara Rombouts
Le 26 Novembre 2021

Sous la direction de Marcelo Nollmann

Devant le jury composé de

Pascal Hersen, Directeur de Recherche, Institut Curie, Paris

Vincent Calvez, Directeur de Recherche, Institut Camille Jordan (ICJ), Lyon

Sophie Helaine, Professeur des Universités, Harvard Medical School, Boston

Tam Mignot, Directeur de Recherche, Laboratoire de Chimie Bactérienne (LCB), Marseille

Pierre-Emmanuel Milhiet, Directeur de Recherche, CBS, Montpellier

Andrea Parmeggiani, Professeur des Universités, Laboratoire Charles Coulomb, Montpellier

Antoine Le Gall, Chargé de Recherche, CBS, Montpellier

Marcelo Nollmann, Directeur de Recherche, CBS, Montpellier

Rapporteur

Rapporteur

Examineur

Examineur

Membre du Jury

Président du Jury

Co-encadrant

Directeur de Thèse



UNIVERSITÉ
DE MONTPELLIER

Acknowledgements

First, I would like to thank the jury, Dr. Sophie Helaine, Dr. Tam Mignot, Dr. Pierre-Emmanuel Milhiet and Prof. Andrea Parmeggiani, and the rapporteurs Dr. Vincent Calvez and Dr. Pascal Hersen. Thank you for investing your time to read and report on my work. I would like to specially thank Dr. Tam Mignot for the ongoing collaboration and the exciting scientific interactions we had. With this, I would also like to thank your team for their expertise and for teaching me the ins and outs of this wonderful bug, *Myxococcus xanthus*.

My most sincere thank you is directed towards my PI and thesis director, Dr. Marcelo Nollmann. Because of his drive, knowledge and expertise, I have seen some of the most challenging and state-of-the-art projects come to life. He is always trying to get the best out of everyone, allowing people to grow. I personally enjoyed the one-to-one meetings, in which he was always available to deeply discuss scientific problems with no question ever too much. As a biologist, I had the opportunity to learn an immense amount of microscopy and data-analysis skills, for which I was always given the time. In his team, I had the privilege to work with Dr. Jean-Bernard Fiche and Dr. Antoine Le Gall. Aside from the scientific expertise they have and their willingness to always help everyone, they fulfill indispensable roles by solving many day-to-day problems. I had the chance to collaborate with both in various projects, and can honestly say it has been a pleasant experience.

Further, I would like to thank all the people working on bacteria in our team over the years, Antoine, Baptiste, Hernan, Antonio and recently Anna. I have enjoyed the many interactions we had, discussing dedicated topics in journal clubs and debating over scientific results. Alongside them, my heart goes out to all current and former team members, Christophe, Marie, Franziska, Diego, Sergio, Andres and Markus. And last but not least, I cannot express enough how grateful I am for having had Julian, Marion and Olivier as fellow PhD students in the team. They are, without a doubt, the best colleagues I could have hoped for, always supportive, uplifting and helpful.

Aside from my team, I would like to thank Dr. Pierre-Emmanuel Milhiet for inviting me into his team to carry out the work I did using AFM. A special thank you is in place for Dr. Luca Costa, for teaching me how to run all AFM experiments, but also to be a great office mate (with Arianna).

To all of my friends, Oscar, Thales and Arianna from CBS, Constance, Amélie, Amandine and Jacqueline from the Van De Perre Team, Marisa, Mieke, Nina, Hannah and Nena from the KUL, I say thank you. It would have never been the same without you. Cheers to all the weekly apéro's, to the virtuel apéro's during the pandemic, to the wedding, to all the trips between Belgium and Montpellier,... Cheers to all of you!

I would like to thank my family. My brother and sister, Rob and An, for giving me a pat on the back when I needed it and for being both extremely funny and loving people. A wholehearted thank you to my mother. Mama, what an inspiration you continuously have been. Thank you for being the strong woman you are and for teaching me to always believe in myself. From the little things to the big life changing decisions, you have always supported my dreams.

And finally, the biggest thank you to the main man, my homie, my bestie, my Mathieu. Thank you for your continuous support and your love. I could not have done this without you.

Table of Contents

I	Introduction	1
1	Collective behavior in the natural world	2
2	Collective behavior in multicellular bacteria	2
2.1	Underlying sources of community heterogeneity	2
2.2	Cooperative microbial behaviors	3
2.3	Filamentous multicellular bacteria	4
2.4	Biofilms	6
2.4.1	Biofilm formation.....	6
2.4.2	Phenotypic heterogeneity as a result of division of labor	8
2.4.3	Intercellular cooperation through Quorum Sensing	9
3	<i>Myxococcus xanthus</i> as a prokaryotic model system for social behavior.....	10
3.1	The <i>M. xanthus</i> lifecycle	10
3.1.1	The developmental cycle	11
3.1.2	The vegetative cycle	13
	The predation strategy.....	13
	Prey searching and sensing	14
	Prey killing and consumption	14
3.2	Motility.....	16
3.2.1	Adventurous motility	16
3.2.2	Social motility	17
3.2.3	The Frz system	18
3.2.4	Rippling	19
3.3	Cooperation giving rise to the <i>M. xanthus</i> life cycle	19
3.3.1	Cheating and policing	21
4	Objectives	22
II	Results	24
1	BactoTracker: dynamic imaging combined with AI-based semantic segmentation and single-cell tracking enables the study of <i>M. xanthus</i> predation	25
2	Multi-scale dynamic imaging reveals synergistic interplay between specialized cells in multicellular bacterial communities	26
3	Transcriptome heterogeneity in <i>M. xanthus</i> colonies	28
3.1	Introduction	28
3.2	RNA FISH labeling optimization in cells harvested from liquid cultures	29
3.3	RNA FISH labeling optimization in biofilms.....	33
3.4	Nutrient-dependent differential gene expression in <i>M. xanthus</i>	35
3.5	Differential gene expression in predating biofilms	37
3.6	Discussion	37
4	Obstacle sensing by <i>M. xanthus</i>.....	40

4.1	Abstract.....	40
4.2	Introduction	41
4.2.1	Mechanosensitivity in the bacterial membrane	41
4.3	Correlative AFM and Fluorescence Microscopy.....	43
4.4	The experimental system: <i>Myxococcus xanthus</i>	44
4.4.1	The sample preparation.....	44
4.4.2	AFM tip size and shape	47
4.4.3	The experimental set-up.....	48
4.5	Results.....	50
4.6	Conclusion.....	51
III	<i>Conclusion and perspectives.....</i>	52
IV	<i>Annex</i>	55
1	Material and Methods.....	56
2	Review: RNA Imaging in Bacteria	66
V	<i>References</i>	68

List of Abbreviations

AFM	Atomic Force Microscopy
Agl-Glt	Adventurous gliding and gliding transducer
AHL	N-acylated homoserine lactone
A-motility	Adventurous motility
BAP	Biofilm-associated proteins
c-di-GMP	cyclic diguanylate
ECM	Extracellular matrix
(e)DNA	(extracellular) deoxyribonucleic acid
EF-TU	Elongation Factor Thermo Unstable
EHB	Enhancer binding proteins
EPS	Exopolysaccharide
FA	Focal adhesion
FISH	Fluorescence In Situ Hybridization
FOV	Field of view
GAP	GTPase activating protein
GAPDH	Glyceraldehyde-3-Phosphate Dehydrogenase
(sf)GFP	(superfolder) Green Fluorescent Protein
GTP	Guanosine triphosphate
IF	Immunofluorescence
IM	Inner-membrane
kDa	kilo-Dalton
MMPs	Multicellular magnetotactic prokaryotes
(m)RNA	(messenger) Ribonucleid Acid
OM	Outer-membrane
OME	Outer-membrane exchange
OMV	Outer-membrane vesicle
PP	Primary probe
(p)ppGpp	Guanosine penta- and tetraphosphate
ROI	Region of interest
SDS-PAGE	Sodium dodecyl sulphate-polyacrylamide gel electrophoresis
SEM	Scanning electron microscopy
S-motility	Social motility
SP	Secondary probe
WT	Wildtype
YFP	Yellow Fluorescent Protein
γ -PGA	poly- γ -DL glutamic acid

List Of Figures

Figure 1. Social interactions among individuals in a population.....	3
Figure 2. Multicellular lifeforms among bacteria.....	4
Figure 3. Stages of biofilm development	8
Figure 4. The lifecycle of <i>M. xanthus</i>	11
Figure 5. <i>M. xanthus</i> fruiting bodies	13
Figure 6. Predation of <i>M. xanthus</i> over <i>E. coli</i>	14
Figure 7. <i>E. coli</i> prey plasmolysis due to contact-dependent killing	15
Figure 8. The adventurous (A-) motility system.....	17
Figure 9. The social (S-) motility system.....	18
Figure 10. Probe design and labeling of sfGFP transcript in <i>Myxococcus xanthus</i> from liquid culture	31
Figure 11. Influence of formamide concentration on melting temperatures and RNA labeling	32
Figure 12. IF and RNA FISH labeling in printed <i>M. xanthus</i> cells.....	35
Figure 13. Differential expression of sfGFP under EF-TU promoter in <i>M. xanthus</i>	36
Figure 14. Motility systems of <i>M. xanthus</i>	43
Figure 15. The AFM-SMLM set-up	44
Figure 16. A-motility of <i>M. xanthus</i> on poly-L-lysine coated surfaces.....	47
Figure 17. Bead attachment to the Nanosensors ATEC-CONT.....	48
Figure 18. Fluorescence of Nanotools Biosphere B1000-CONT.....	49
Figure 19. Different configurations for probing <i>M. xanthus</i> cells	50
Figure 20. Tip-cell collision induced cell reversal.....	51

List of Tables

Table 1. Tested surface coating and respective results.	46
Table 2. List of bacterial strains.	56
Table 3. Sequences of probe set for sfGFP target transcript and read-out oligos.	61

I Introduction

1 Collective behavior in the natural world

Collective behavior is a phenomenon which can be observed in all layers of life (Bak-Coleman et al. 2021). It describes the coordinated and cooperative behavior of individuals within a group and is therefore inherently driven by communication and interactions between the individuals of this group. It is generally a facultative trait exploited for the adaptation to environmental pressures with the aim to gain a common fitness advantage. The most apparent form of collective behavior can be observed between higher-order organisms giving rise to fish schools, bird flocks, ant trails and honeybee swarms (David J. T. Sumpter 2010; D. J. T. Sumpter 2006). In these multi-organism systems, social behavior provides protection from possible predators, enhances foraging abilities and facilitates locomotion (Biro, Sasaki, and Portugal 2016). Collective cell migration can also be observed between single cells in multicellular organisms driving processes such as morphogenesis and wound healing in physiological conditions and cancer invasion and metastasis in pathophysiological conditions (Nguyen et al. 2016; Hinohara and Polyak 2019; Kurosaka and Kashina 2008; Bertolaso and Dieli 2017). Interestingly, bacterial cells have also been observed to cooperate, challenging the historical paradigm installed by Robert Koch describing micro-organisms as solitary unicellular organisms thriving in pure cultures and causing disease (J. A. Shapiro 1998; James A. Shapiro 1988). Early observations in bacteria of complex and coordinated collective cell behaviors, such as developmental transitions in *Streptomyces* and *Myxobacteria* and swarming of *Proteus* species, were thought to be exceptions (J. A. Shapiro 1998). However, over the last few decades, a plethora of bacteria have been described to exploit intercellular cooperation to a greater or lesser extent for adaptability purposes, often resulting in phenotypic heterogeneity and ultimately in cell specialization and differentiation (Avery 2006).

2 Collective behavior in multicellular bacteria

Historically, bacteria have been studied as unicellular organisms in homogeneous cell cultures. All experimental observations regarding cellular processes were based on bulk measurements of cells in planktonic state and were extrapolated as being representative for all cells within the culture. More recent studies, however, have shown that bacteria from seemingly isogenic populations can show phenotypic variety (Avery 2006). Such diversification is thought to occur after exploration of the environment and help bacteria optimize fitness and community survival.

2.1 Underlying sources of community heterogeneity

One of the sources of phenotypic heterogeneity is the accumulation of mutations in a subset of cells in genetically identical populations, creating diverging cell lineages. For example, clonal plating of a mucoid strain of the gram-negative *Pseudomonas fluorescens* results in hybrid colonies consisting of the original strain and a newly developed genetic variant. This evolutionary process allows the colony to gain a new collective spreading phenotype which is thought to help gain territory (W. Kim, Levy, and Foster 2016). *P. fluorescens* has also been described to genetically diversify in liquid cultures. The various phenotypes enable the bacteria to exploit different environmental niches, such as the air-culture interface, liquid phase and the less aerobic bottom of the culture flask (Rainey and Travisano 1998). A second source of phenotypic heterogeneity is noisy or stochastic gene expression (Raj and van Oudenaarden 2008), underpinned by the stochastic nature of transcription and translation allowing the development of different phenotypes in clonal populations. This can be beneficial for

bacterial communities because varying phenotypes can promote adaptability and survival under environmental pressure, a concept referred to as bet hedging (Veening, Smits, and Kuipers 2008; Dhar and McKinney 2007; Smits, Kuipers, and Veening 2006; de Jong, Haccou, and Kuipers 2011). An example of this phenotypic heterogeneity is the stochastic generation of non-growing or dormant cells called persisters. In *E. coli* batch monocultures, a proportion of cells will naturally enter a transient persister state (Keren et al. 2004; Lewis 2007; Shah et al. 2006). Additionally, clinically relevant species, such as *Mycobacterium tuberculosis* and *Salmonella enterica* species, develop persisters to overcome antibiotic treatment and relapse infection (Veening, Smits, and Kuipers 2008; Fisher, Gollan, and Helaine 2017).

Finally, phenotypic heterogeneity can result from cooperation between bacterial cells. Already in 1964, Hamilton used mathematical models to study social interactions between relatives in a population and its outcomes for fitness (Hamilton 1964). Based on his work, four different interactions between individuals could be defined, each describing the costs and benefits for the individual performing the behavior (the actor), and for the individual not performing the behavior (the recipient) (S. A. West, Griffin, and Gardner 2007) (**Figure 1**). Social interactions are: 'Selfish' when they are costly for the recipient and beneficial for the actor; 'Spite' when they are costly for both actor and recipient; (Hamilton 1964, 1970); 'altruistic' when the interaction is beneficial for the recipient but costly for the actor; and 'mutualistic' when the interaction is beneficial for both (Sachs et al. 2004; Hamilton 1964). These behaviors represent social interactions but are not always cooperative. In fact, a requirement to define intercellular interactions as cooperative is that the behavior carried out by an actor benefits the recipient, and thus cooperation is either altruistic or mutual (S. A. West, Griffin, and Gardner 2007). Furthermore, cooperation is a hallmark of division of labor, an important strategy adopted by many prokaryotic species in which cooperating individuals carry out specific tasks (Stuart A. West and Cooper 2016; Van Gestel, Vlamakis, and Kolter 2015). Division of labor implies the specialization of individual cells into specific tasks or behaviors for the benefit of other cells in the population to increase the inclusive fitness for all individuals. This specialization ultimately leads to phenotypic heterogeneity in isogenic bacterial populations.

Actor / Recipient	-	+
-	Spite	Selfish
+	Altruism	Mutualism

Figure 1. Social interactions among individuals in a population. Interactions can be advantageous (+) or disadvantageous (-) for the actor or recipient.

2.2 Cooperative microbial behaviors

In the past decades, a multitude of microbial behaviors were described to be cooperative (Gregory J. Velicer 2003; Stuart A. West et al. 2007; Crespi 2001; Brown and Buckling 2008). This includes, among others, the production of public goods, such as iron-chelating siderophores (Kramer, Özkaya, and Kümmerli 2020), exoenzymes for nutrient digestion and antibiotics breakdown (Dugatkin

et al. 2005; Folse and Allison 2012; E. Rosenberg, Keller, and Dworkin 1977), anti-competitor toxins (L. Chao and Levin 1981; Doekes, de Boer, and Hermsen 2019; Kerr et al. 2002) and quorum sensing molecules (Parsek and Greenberg 2005). An example of public goods is the production of proteases by a subset of *B. subtilis* cells in a stationary phase liquid culture. These proteases are released in the medium and allow the degradation of proteins into small peptides which freely diffuse through the medium and serve as a nutrient source for all cells (Veening, Igoshin, et al. 2008). Additionally, many cooperative microbial behaviors require cell self-organization, for example for collective cell motility (Köhler et al. 2000; Gregory J. Velicer and Yu 2003; Li et al. 2003), or for the formation of multicellular structures such as biofilms (Nadell, Xavier, and Foster 2009; Nadell et al. 2008; Xavier, Martinez-Garcia, and Foster 2009), hyphae (Claessen et al. 2006) and fruiting bodies (Curtis, Taylor, et al. 2007; S. S. Branda et al. 2001). Bacterial multicellularity is generally a facultative trait, although several magnetotactic prokaryotes (MMPs) have been described to be obligate multicellular organisms and shares hallmark features of classical multicellularity observed in eukaryotic species, including morphological differentiation, programmed cell death and patterning (Claessen et al. 2014; Lyons and Kolter 2015; Keim et al. 2004). However, the formation of eukaryotic and bacterial multicellularity differs in many aspects. Eukaryotic multicellular organisms arise from the proliferation of one ancestral somatic cell or zygote (Brunet and King 2017). Conversely, bacterial multicellularity can arise from three different processes: i) the formation of syncytial filaments, ii) clustered or filamentous growth and, iii) cell aggregation (Lyons and Kolter 2015; Claessen et al. 2014; Aguilar, Eichwald, and Eberl 2015) (**Figure 2**).

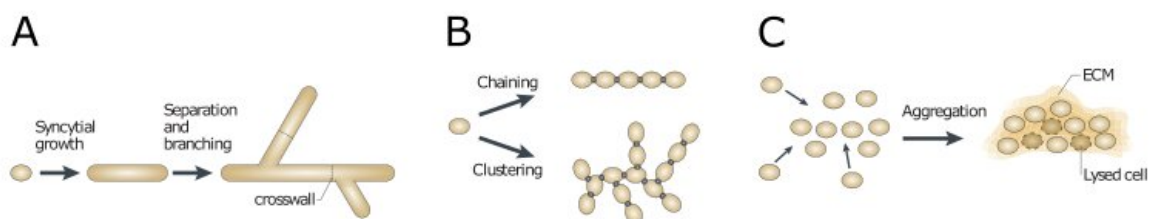


Figure 2. Multicellular lifeforms among bacteria. In syncytial filaments, cross walls are formed in elongated hyphae (A). Chained or clustered growth of cells results in filamentous structures (B). Multiple cells can aggregate into dense colonies or biofilms embedded in an ECM (C). Adapted from (Claessen et al. 2014).

2.3 Filamentous multicellular bacteria

Both syncytial filaments and clustered growth result in chain-like multicellular structures but differ significantly in how they are formed. Syncytial filaments, which can be found in *Streptomyces coelicolor* and other actinobacteria, emerge by the formation of cross walls in elongated hyphae making up a vegetative mycelium (Flärdh 2003; Flärdh and Buttner 2009). The cross walls are made up of cell division structures placed at irregular intervals and separate adjacent and connected compartments. Bacterial conjugation experiments evidenced that different compartments interact to exchange genetic information (Kataoka, Seki, and Yoshida 1991). In these bacteria, division of labor is important under starvation conditions. Starvation induces the formation of aerial hyphae from the vegetative mycelium by the formation of branches that break the surface-tension of the liquid-air interface and grow in the air (McCormick and Flärdh 2012; Flärdh and Buttner 2009). In aerial hyphae,

a tightly-regulated developmental cascade enables the formation of apical sporogenic cells, which contain a subapical stem cell and a prespore compartment in which ultimately a spore develops (McCormick and Flårdh 2012). Two different mechanisms of cooperation between the vegetative and developmental cell types can be distinguished. On the one hand, a portion of vegetative cells in the mycelium undergo programmed cell death so that nutrients are released in the environment, which is beneficial for the initial formation of aerial hyphae (Chater et al. 2010; Wildermuth 1970; Miguélez, Hardisson, and Manzanal 1999; A. Manteca et al. 2007; Á. Manteca, Fernández, and Sánchez 2005). On the other hand, vegetative cells within the mycelium secrete proteases in the environment for the breakdown of substrate mycelium which serves a nutrient source for sporulation (Kang and Lee 1997; Chater et al. 2010). In both cases, division of labor increases the fitness of the overall cell population by ensuring survival under starvation conditions.

Alternatively, filamentation of cells due to chained or clustered growth arises from incomplete cell fission after division (Grosberg and Strathmann 2007; Claessen et al. 2014; Aguilar, Eichwald, and Eberl 2015). One of the best documented examples of this permanent chaining of clonal cells are the cyanobacteria. Several species of the cyanobacteria are known to grow as multicellular filamentous colonies (Rippka, Deruelles, and Waterbury 1979; Schirrmeyer, Antonelli, and Bagheri 2011). The development of different phenotypes is especially important. Cyanobacteria are organisms that can perform both carbon fixation through photosynthesis and nitrogen fixation (Flores and Herrero 2010; Haselkorn 1978). In the process of nitrogen fixation, the enzyme nitrogenase reduces the available nitrogen (N_2) to ammonia (NH_3). However, the by-product oxygen (O_2) produced during photosynthesis irreversibly inactivates nitrogenase. Therefore, these two processes are incompatible in the same cell. Some cyanobacteria solve this incompatibility issue by regulating the two processes in time with a circadian clock (Bergman 1997; Cohen and Golden 2015). However, most filamentous cyanobacteria resort to a more efficient division of labor strategy to segregate these processes in space (Rossetti et al. 2010). In short, a subset of vegetative cells differentiate into nitrogen-fixing heterocysts while the majority of vegetative cells carry out the task of photosynthesis (Kumar, Mella-Herrera, and Golden 2010). Heterocysts and photosynthetic vegetative cells cooperate through an intercellular proteinaceous network that ensures nutrient redistribution through the molecular exchange of photosynthetically-fixed sugars and nitrogen (Merino-Puerto et al. 2011; Golden and Yoon 2003). In response to adverse environmental conditions, photosynthetic vegetative cells differentiate into spore-like cells, an additional phenotype called akinetes (Meeks and Elhai 2002; Flores and Herrero 2010). Finally, several cyanobacteria produce a motile phenotype, called hormogonia, when nutrient availability or light exposure changes (Meeks and Elhai 2002; Tamulonis, Postma, and Kaandorp 2011). Hormogonia are short filaments that play an essential role in bacterial dispersal over short distances and are only capable of photosynthesis as these filaments lack heterocyst cells. Both hormogonia and akinetes are transient phenotypes. Akinetes will germinate in favorable environmental conditions and hormogonia return to a sessile lifestyle after which cell division is induced so that vegetative cells accumulate and heterocysts differentiate.

Aside from the example of cyanobacteria, there are a multitude of species that also adopt a filamentous lifestyle. Generally, this is a transient phase because clustered growth and filamentation leads to important drawbacks, such as decreased motility and buoyancy, and increased competition for resources due to the increased local cell density (Bonner 1998; Grosberg and Strathmann 2007). Therefore, bacterial species only induce this growth strategy to overcome stress and unfavorable environmental conditions, but disassemble the filaments once conditions become less hostile.

Predatory stress is one possible cause of stress-induced filamentation. Often, predators consume their prey by ingestion through phagocytosis. Certain bacteria reversibly form chain-like structures to increase their size and thus, protect themselves against size-selective phagocytosis (Jousset 2012; Hahn, Moore, and Höfle 1999; Corno Gianluca and Jürgens Klaus 2006). An example of this are the *Flectobascillus* species that induce or enrich filamentous phenotypes when they are co-cultured with the bacterivorous flagellate *Ochromonas* (Corno 2006). Clinically relevant species also exploit their morphological plasticity in an adaptive response to their environment. One example is *Mycobacterium tuberculosis* which forms filaments during proliferation in macrophages (Chauhan et al. 2006). In addition, some species, such as *B. subtilis* and *Lactococcus lactis*, go through a transient filamentous stage during biofilm development (Nelson and Young 2000; Potluri, de Pedro, and Young 2012; Pérez-Núñez et al. 2011; Kobayashi Kazuo 2007).

2.4 Biofilms

The last and probably most diverse group of multicellular bacterial life-forms are biofilms. Biofilms are generally defined as sessile aggregations of cells embedded in an extracellular matrix (ECM). They can be viewed as a transient or reversible community state, because switching between aggregate and planktonic state highly depends on growth conditions and environmental stressors (Monds and O'Toole 2009). The induction of biofilm formation in numerous species was shown to cause substantial changes in gene expression, leading to extensive phenotypic variation. The benefits of this heterogeneity include increased resistance to chemical compounds, such as antibiotics, to predation and to host-defense mechanisms (Kiedrowski and Horswill 2011; Donlan Rodney M. and Costerton J. William 2002; Abebe 2020; Monds and O'Toole 2009). Because of this, biofilms pose major problems for human health, as they are able to colonize most medical devices and implants. This colonization of indwelling devices represents almost half of all nosocomial infection cases reported in United States hospitals every year (Khatoon et al. 2018; Rodrigues 2011; Darouiche 2004). Therefore, biofilms are among the best-studied forms of bacterial multicellularity.

2.4.1 Biofilm formation

Biofilm development is a multi-step process that involves three loosely-defined stages: i) reversible and irreversible initial attachment, ii) biofilm maturation, and iii) dispersion or cell detachment (Khatoon et al. 2018; Armbruster and Parsek 2018). The mechanisms of biofilm formation are in general similar between bacterial species, however there are slight differences. The initial attachment of planktonic cells to a substrate is promoted by increased intracellular concentrations of cyclic diguanylate (c-di-GMP) (Jenal, Reinders, and Lori 2017) and is mediated by hydrophobic, electrostatic and steric interactions, protein adhesion, Van der Waals forces and bacterial appendages, including pili and flagella (Floyd, Eberly, and Hadjifrangiskou 2017; Bjarnsholt 2013; Gupta et al. 2016; Joo and Otto 2012; Veerachamy et al. 2014; Stoica et al. 2017) (**Figure 3a**). This attachment is reversible when the interaction between the bacterial cell and the substrate is too weak. For example, the extent of attachment of bacteria to medical implants is highly dependent on the surface properties of the bacteria, on the material of the medical device, and on environmental parameters such as temperature and pressure (Gupta et al. 2016; Khatoon et al. 2018). In contrast, bacterial cells can become irreversibly immobilized on the surface and initiate the formation of a monolayer (Gupta et al. 2016) (**Figure 3b**). In clinically-relevant species of *Staphylococcus*, over 20 surface-associated

adhesins have been characterized that mediate initial cell attachment and intercellular adhesion during maturation (Speziale et al. 2014; N. D. Hammer and Skaar 2011; Paharik and Horswill 2016).

Successively, biofilm maturation describes the phase in which attached cells grow to create complex multilayered structures by interacting among themselves (Gu et al. 2013; Gupta et al. 2016; G. Wei et al. 2015) (**Figure 3c-d**). Intercellular interactions during stage I of the maturation are mediated by autoinducer or quorum sensing molecules, such as N-acylated homoserine lactone (AHL) and result in the expression of biofilm-specific genes. In stage II, the biofilm increases in size and thickness. An essential process in biofilm maturation is the production of ECM by secretion of exopolysaccharides (EPS), extracellular DNA (eDNA) and proteins (Aguilar, Eichwald, and Eberl 2015). The most prevalent ECM component is EPS, a polymeric macromolecule with an essential role in facilitating and maintaining cohesion between cells and in forming a physical barrier that protects cells within the biofilm from environmental stresses, such as antibiotics and pH variations (Veerachamy et al. 2014; Gupta et al. 2016; Aguilar et al. 2009). EPS chemical composition and contribution to the biofilm also depends on the bacterial strain and the conditions in which the biofilm matures. For example, two different polymers are important for *B. subtilis* biofilm development, namely poly- γ -DL glutamic acid (γ -PGA) and EPS. In the undomesticated strain NCIB3610 of *B. subtilis* EPS is primarily secreted (S. S. Branda et al. 2001; Steven S. Branda et al. 2005). Conversely, γ -PGA, and not EPS, stimulates biofilm formation in other undomesticated strains (Morikawa et al. 2006; Stanley and Lazazzera 2005). *P. aeruginosa* excretes at least three different EPS products, Pel, Psl and alginate (Gupta et al. 2016). The former two seem to be most important for biofilm development in laboratory conditions. The latter plays an unimportant role in biofilm formation on abiotic surfaces and is essential for biofilm development in pathological conditions (Aguilar et al. 2009).

A second important component of the ECM is eDNA. eDNA plays an essential role in intercellular communication and biofilm stabilization as an interconnecting compound (Vilain et al. 2009; Steinberger and Holden 2005; Izano et al. 2008; Jurgisek and Bakaletz 2007). Additionally, eDNA plays a role in biofilm formation, as evidenced in *P. aeruginosa* where biofilm formation is inhibited after treatment with DNase I (Whitchurch 2002).

Last but not least, ECM contains a non-negligible protein fraction. Proteins are mostly involved in maintaining robustness and integrity of the biofilm (Aguilar, Eichwald, and Eberl 2015). One example of such proteins are the lectins which have been studied in many bacteria including *P. aeruginosa*, *Azospirillum brasilense* and *Burkholderia cenocepacia* (Inhülsen et al. 2012; Funken et al. 2012; Danhorn and Fuqua 2007). Lectins are assumed to be involved in creating an EPS-protein network because they contain a sugar-binding site specific for EPS and additional binding sites for proteins (Neu and Lawrence 2010). In *B. subtilis*, two other proteins, BslA and TasA, are known to play an essential role in the biofilm development (Romero et al. 2010, 2011; Ostrowski et al. 2011). Lastly, large surface proteins or Biofilm-Associated Proteins (BAP) promote intercellular interactions and contribute to ECM integrity in several *Staphylococcus* strains (Lasa and Penadés 2006).

During biofilm maturation, the available resources are being depleted and toxic metabolic by-products can accumulate (Khatoun et al. 2018; Gupta et al. 2016). To get rid of waste and regain access to nutrients, the biofilm regulates itself by dispersion or detachment of single cells or clumps (**Figure 3e-f**). This process is highly regulated and induced by nutrient starvation or oxygen depletion in aerobic biofilms. In short, a cascade of autophosphorylation and activation of c-di-GMP phosphodiesterase enables the degradation of c-di-GMP (Oppenheimer-Shaanan, Steinberg, and

Kolodkin-Gal 2013; Jenal, Reinders, and Lori 2017). This results in the dissolving of EPS and the release of cells which return to a planktonic state. Alternatively, bacteria in the biofilm can produce saccharolytic enzymes which locally impair the EPS integrity after which cells are released (Gupta et al. 2016). In pathological species, the dispersal of biofilms provides a mechanism by which infection can easily spread and cause chronic infection. This is referred to as metastatic seeding and is a major problem in disease treatment (Masters et al. 2019; Eiff et al. 2005; Y. Chao et al. 2015). Therefore, the study of dissolving of EPS is of clinical interest as it might provide alternative methods to treat biofilms and prevent the spreading of infections (Grande et al. 2014; Oppenheimer-Shaanan, Steinberg, and Kolodkin-Gal 2013).

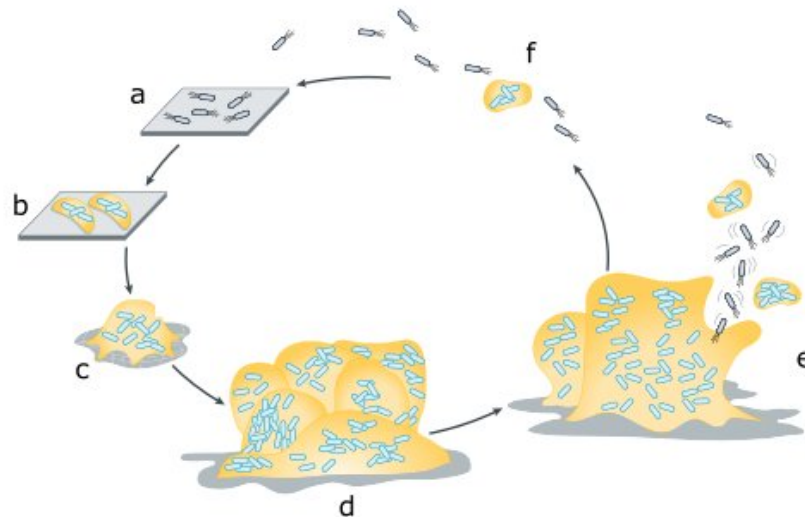


Figure 3. Stages of biofilm development. Biofilm formation is initiated by planktonic cells irreversibly attaching to a surface (a) after which a monolayer of cells is formed, and the ECM (yellow) is produced (b). The biofilm then increases in size (c) and ultimately forms a large multilayered structure tightly embedded in ECM (d). Finally, cells or aggregates of cells can be dispersed from the biofilm into a planktonic state again (e). Adapted from (Rumbaugh and Sauer 2020).

2.4.2 Phenotypic heterogeneity as a result of division of labor

Despite the fairly general formation mechanism, biofilms can be morphologically very diverse, ranging from air-water interface pellicles to solid surface associated communities including micro- and macro-colonies and fully diversified biofilms. This organizational plasticity allows the adaptation of biofilm architecture in response to global and local environmental changes (Bridier et al. 2017). As a result of these continuous adaptations, cells in a mature biofilm will differentiate and specialize to carry out specific tasks and cooperate among each other. This process is generally referred to as division of labor and ultimately leads to extensive phenotypic heterogeneity (Stewart and Franklin 2008; An and Parsek 2007). In *B. subtilis* microcolonies (i.e. not yet fully matured biofilms) it was shown that phenotypic heterogeneity can drive cell differentiation into sporulating cells (Veening, Stewart, et al. 2008). Conversely, cells in more mature *B. subtilis* colonies sporulate at preferential sites (S. S. Branda et al. 2001). In these *B. subtilis* biofilms, the sporulation process is preceded by death of a subpopulation of cells, in a process called cannibalism whereby cells expressing toxins lyse a fraction of their sensitive neighbors (López et al. 2009). In addition to sporulating cells and cannibals, mature biofilms contain other differentiated phenotypes including motile cells, matrix producers, surfactin producers, degradative enzyme producers and competent cells (López and Kolter 2010).

Many of those cell behaviors are localized in distinct subpopulations and their occurrence is dynamically regulated throughout biofilm development (Vlamakis et al. 2008). For example, motile cells are dominant in early biofilm formation and matrix producers became dominant during matrix maturation. Moreover, each specialized cell in the biofilm seems to play a key role in the proper initiation and maturation of the biofilm as *B. subtilis* biofilms containing mutants for matrix components TasA and EPS were shown to have a considerably smaller fraction of sporulating cells (Aguilar et al. 2010; Dragoš et al. 2018). Spatially segregated phenotypes can also be found in the Staphylococcus species *S. aureus* and *S. epidermidis*. More precisely, protein and DNA synthesis were shown to be carried out in specific zones by a subset of cells, which may indicate that most cells in the biofilm are metabolically inactive (Rani et al. 2007). Additionally, in *P. aeruginosa* biofilms the expression of the housekeeping gene, *acpP*, and quorum sensing regulated genes, *phzA1* and *aprA*, is not homogeneous and cells in fairly close proximity showed significantly different gene expression patterns (Lenz et al. 2008). Altogether, these findings support that biofilms are phenotypically heterogeneous and a high degree of spatial organization of these phenotypes exists.

2.4.3 Intercellular cooperation through Quorum Sensing

Intercellular cooperation between cells is essential in biofilms. Living within a biofilm entails clear advantages, but it is also metabolically costly to produce and maintain ECM components. To minimize the energetic investment for the cells, gene expression is tightly regulated by a high degree of cell-cell communication through quorum sensing molecules (Rutherford and Bassler 2012; Ng and Bassler 2009). These small molecules are produced by single cells, secreted and diffused through the environment and detected by other cells. The perceived concentration of these molecules is a measure for cell density, allowing bacterial cells to recognize others around them (Mukherjee and Bassler 2019). Because the molecules for quorum sensing are species-specific, bacteria can recognize close relatives or kin and other non-kin species (Schluter et al. 2016). When a critical concentration is reached, indicating a critical cell density, these molecules act as a trigger for gene expression. Quorum sensing has been studied extensively in a multitude of species, including *P. aeruginosa*, *V. cholerae*, *Pantoea stewartii* and the plant-pathogen *Xanthomonas campestris*, and was identified as an important mechanism for the production and degradation of EPS during biofilm development (von Bodman, Majerczak, and Coplin 1998; Koutsoudis et al. 2006; Sakuragi and Kolter 2007; Dow et al. 2003; Torres et al. 2007; B. K. Hammer and Bassler 2004). In *P. aeruginosa*, it was also shown to be an important mechanism for eDNA excretion (Barken et al. 2008).

Myxobacteria represent a special case of multicellular aggregates, with *Myxococcus xanthus* being the most-studied species to date. *M. xanthus* cells do not form a sessile and stationary biofilm. Instead, *myxococcus* cells associate in a highly dynamic manner. Their social and coordinated motility allows them to enter the developmental cycle, resulting in spore-filled fruiting bodies. Additionally, their collective motion enables them to prey on other cells, which gives them a keen advantage in multispecies environments. Behavioral and phenotypic heterogeneity in mature predating biofilms of *M. xanthus* are the focus of this thesis.

3 *Myxococcus xanthus* as a prokaryotic model system for social behavior

Myxococcus xanthus is a gram-negative bacterium that belongs to the order of the Myxococcales, otherwise referred to as the Myxobacteria. Myxobacteria belong to the class of the Deltaproteobacteria (L. Shimkets and Woese 1992). Up until this day, several tens of Myxobacteria species have been described and can be subdivided in three sub-orders: i) the Sorangiineae, ii) the Nannocystineae, and iii) the Cystobacterineae, the sub-order to which *M. xanthus* belongs (Garcia et al. 2010; L. J. Shimkets, Dworkin, and Reichenbach 2006; Mohr 2018). This phylogenetic subdivision is the result of the isolation and study of mostly terrestrial samples (Dawid 2000; Reichenbach 1999; Garcia et al. 2010; Spröer, Reichenbach, and Stackebrandt 1999). More recently, however, myxobacterial species were isolated from marine samples (Brinkhoff et al. 2012; T. Iizuka et al. 1998). From an evolutionary point of view, these halotolerant species diverge from the terrestrial species and phylogenetically cluster in a sub-order distinct from the other three characterized sub-orders (Jiang et al. 2010; Brinkhoff et al. 2012). The constant or ongoing discovery and characterization of novel myxobacteria from environmentally diverse samples showcases the great diversity that can be found within this order. Indeed, Myxobacteria can be found virtually everywhere on this planet, ranging from glaciers to tropical nutrient-rich soils (Mohr et al. 2016, 2017; Dawid 2000; Takashi Iizuka et al. 2006; Powell et al. 2015; REICHENBACH and H 1993; Reichenbach 1999; Y.-Q. Zhang et al. 2005). In addition to being widespread, they are also abundant. Zhou *et al.* studied several terrestrial soil samples and found that myxobacteria represent a fraction of the total bacterial community, ranging from 0,4% to 4,5% (Zhou et al. 2014). The fact that myxobacteria represent such large fractions in bacterial communities suggests that they play vital roles in local bacterial ecology. However, one should be careful with interpreting and extrapolating observed phenotypes or behaviors from one environmental niche to another as certain cell specializations might be only advantageous in defined ecological conditions.

3.1 The *M. xanthus* lifecycle

M. xanthus is a rod-shaped bacterium that represents a model organism used to understand self-organization and how cell motility gives rise to social behavior (Y. Zhang, Ducret, et al. 2012). *M. xanthus* is found predominantly in forest soil, a very diverse ecosystem containing a multitude of species. To ensure survival in this complex environment, *M. xanthus* adopts a multicellular social lifestyle (**Figure 4**) that enables it to colonize their ecosystem and respond rapidly to environmental stimuli such as nutrient availability (Dworkin 1963). In short, when the external environment becomes unfavorable and nutrients are sparse, *M. xanthus* cells enter the developmental cycle and aggregate together to form spore-filled fruiting bodies. When conditions become favorable again, vegetative cells proliferate and become motile to actively search for nutrients, either in the form of macromolecules available in the environment or in the form of prey in a process called bacterial predation (Muñoz-Dorado et al. 2016).

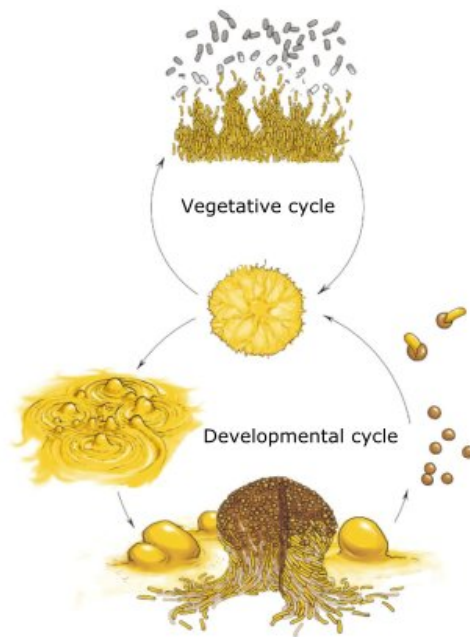


Figure 4. The lifecycle of *M. xanthus*. During the vegetative cycle, *M. xanthus* cells (yellow) swarm out in search for nutrients or prey (grey). During the developmental cycle, *M. xanthus* cells aggregate together to form fruiting bodies (bottom) that release spores back into the environment (right). Adapted from (Muñoz-Dorado et al. 2016).

3.1.1 The developmental cycle

The developmental cycle is initiated under nutrient depleted conditions, more specifically when amino acids become sparse, and under sufficient cell density (Kaplan and Plamann 1996). In the first phase of the developmental cycle, growth is arrested and early-functioning eukaryotic-like enhancer binding proteins (EBBs) will enable σ^{54} RNA polymerase to transcribe early developmental genes (Kroos 2007; Kroos and Inouye 2014; Caberoy et al. 2003; Giglio et al. 2011). In this phase, *M. xanthus* cells induce, very similarly to *E. coli*, the stringent response which allows the inhibition of protein synthesis and the accumulation of the second messenger guanosine penta- and tetraphosphate ((p)ppGpp) (Harris, Kaiser, and Singer 1998; Manoil and Kaiser 1980a, 1980b). Additionally, the A-signal, which is a set of peptides and amino acids released by extracellular protease activity, is produced under the regulatory control of the *asg* genes (Plamann, Kuspa, and Kaiser 1992; Kuspa, Plamann, and Kaiser 1992a). In short, *AsgA* detects nutrient depletion and will consecutively promote phosphorylation of *AsgB*. This leads to the expression of genes that are responsible for the production of the A-signal (Konovalova, Wegener-Feldbrügge, and Søggaard-Andersen 2012). Together, the A-signal and EBPs control the accumulation of the transcription regulator *MrpC* and its N-terminally truncated form *MrpC2* (H. Sun and Shi 2001a, 2001b; Ueki and Inouye 2003). Altogether, these components stimulate the production of the C-signal, which is a 17 kDa cell surface bound protein (Crawford and Shimkets 2000; Konovalova, Löbach, and Søggaard-Andersen 2012; Gronewold and Kaiser 2007; Konovalova, Wegener-Feldbrügge, and Søggaard-Andersen 2012). In the last stage of the developmental cycle, *MrpC* and *MrpC2* bind to the *fruA* promoter region and directly activate expression of the transcription factor *FruA* (Nariya and Inouye 2006; Ueki and Inouye 2003). Finally, *FruA* and *MrpC2*, together with the C-signal, regulate expression of the *dev* operon, which is directly involved in spore formation (J.-S. Lee et al. 2011; Mittal and Kroos 2009a, 2009b; Son, Liu, and Kroos

2011). In addition to the dev operon, MrcP and MrpC2 also bind to promoter regions of many other developmentally-regulated genes to regulate their expression (Robinson et al. 2014).

Intercellular communication by means of the A- and C-signals are especially important for cell density sensing and aggregation of cells through the regulation of cell motility. A- and C-signal production and abundance coincides with specific stages of development. For example, the A-signal is produced and accumulated one to two hours after starvation induction (Kuspa, Kroos, and Kaiser 1986). This leads to the onset of cell aggregation and to coordinated group movement toward aggregation centers. Further changes in cell motility and the beginning of aggregation centers can be observed four to six hours after starvation (Lars Jelsbak and Sørensen 2002). The C-signal, on the other hand, is essential for aggregation in later phases of the developmental cycle. Its concentration continuously increases after starvation, and reaches medium levels at 8-18h post-starvation (Dale Kaiser 2003). This, in turn, coincides with the completion of the aggregation process after 24h (Claessen et al. 2014). Finally, formation of fruiting bodies leads to a sharp, local increase in the C-signal triggering sporulation (Dale Kaiser 2003). Sporulation is completed approximately 72h after nutrient depletion, with nascent fruiting bodies containing around 10^5 - 10^6 spores (Diodati et al. 2014). From the moment starvation is induced and (p)ppGpp is being accumulated, more than 2000 genes are differentially expressed (Giglio et al. 2011). This involves the temporal regulation of gene activity so that groups of genes are up- or downregulated during specific phases of development.

During development, two kinds of differentiated cells are produced: i) spores, which represent 10% of developing cells, and ii) peripheral rods, which account for around 30% (O'Connor and Zusman 1991) (**Figure 5**). Peripheral rods are cells located around and between fruiting bodies, and just like vegetative cells, are rod-shaped and metabolically active. However, they do not proliferate and, as a recent study showed, they display a different transcriptional program than nutrient-stressed stationary-phase cells (Whitfield et al. 2020). In the past, it was suggested that peripheral rods act as persister cells that consume low levels of nutrients available in nutrient-limited environments, inadequate for vegetative growth or spore germination (O'Connor and Zusman 1991; Higgs et al. 2013). Both peripheral rods and spores return to the vegetative state when nutrients become abundant again, however, peripheral rods are able to respond faster because they do not need to germinate (David R. Zusman et al. 2007). Therefore, both strategies are often seen as complementary to ensure survival in a wide range of environmental conditions (L. J. Shimkets 1999; D. Kaiser, Robinson, and Kroos 2010; Mauriello, Mignot, et al. 2010; Y. Zhang, Ducret, et al. 2012). Alongside spores and peripheral rods, the remaining fraction of around 60% of developing cells lyse by the end of the developmental cycle. Programmed cell death is thought to occur from the onset of aggregation early on in the developmental cycle up until the final stages of fruiting body maturation (Nariya and Inouye 2008; Wireman and Dworkin 1977; B. Lee et al. 2012). Just as for filamentous *Streptomyces coelicolor* cells and biofilms-forming *B. subtilis* cells, cell lysis is thought to provide nutrients for neighboring starving cells (Muñoz-Dorado et al. 2016; Berleman et al. 2006).

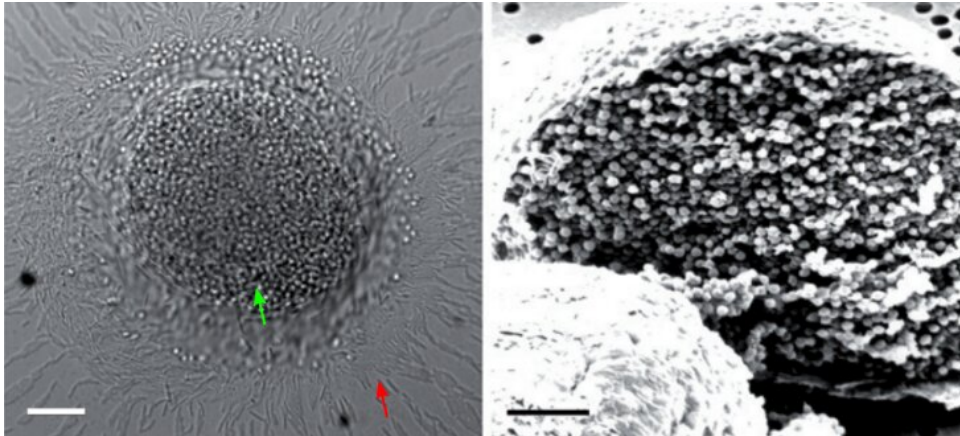


Figure 5. *M. xanthus* fruiting bodies. Fruiting bodies are surrounded by peripheral rods (red arrow) and consist of spherically shaped spores (green arrow) (left) that organize themselves into 3D mounts (right). Scalebars = 15 μ m. Adapted from (David R. Zusman et al. 2007) (left) and (D. R. Zusman and O'Connor 1991) (right).

3.1.2 The vegetative cycle

When nutrients become available again, spores germinate into proliferating rod-shaped cells. These vegetative cells move over solid surfaces in search for nutrients as a coordinated assembly, or otherwise called a swarm. Nutrients can be either in the form of freely diffusing macromolecules or in the form of prey. Bacterial predation is the process in which predator cells kill and consume other bacterial cells (the prey). Over the past hundred years, a multitude of myxobacteria were described as predators, including *M. xanthus* (Eugene Rosenberg and Varon 1984). *M. xanthus* was identified as an epibiotic predator, meaning that it remains on the outside in the extracellular space when killing, lysing and consuming their prey (Thiery and Kaimer 2020). *M. xanthus* is able to target a wide variety of microorganisms as prey, ranging from other gram-positive and gram-negative bacteria to fungi and parasites, and grow exclusively on the remains of these prey organisms (Livingstone, Morphew, and Whitworth 2017; Morgan et al. 2010; Eugene Rosenberg and Varon 1984; Mendes-Soares and Velicer 2013; Shilo 1970; Pham et al. 2005; Bull, Shetty, and Subbarao 2002; Berleman et al. 2006).

The predation strategy

Predation is seemingly initiated by several pioneering *M. xanthus* cells that explore the area around the colony to identify possible nutrient sources in a process referred to as scouting (Keane and Berleman 2016) (**Figure 6**). Surface colonizing scouts and branching cell groups are thought to drive the advancement of a *M. xanthus* colony through the prey colony (Keane and Berleman 2016). Often, the *M. xanthus* predation strategy is referred to as ‘wolf-pack predation’, meaning that cells, like a pack of wolves, attack their prey by encircling them in a coordinated manner. Such a strategy implies that the predator should be numerous as compared to the prey. However, several studies examining predation between *M. xanthus* and various prey species showed that *M. xanthus* can successfully attack and predate on very dense colonies of prey cells (Berleman et al. 2008; Pérez et al. 2011, 2014). In this case, *M. xanthus* cells gradually percolate through the dense prey colony while killing and consuming the prey (**Figure 6b-d**). Therefore, the predation strategy of *M. xanthus* on dense prey colonies is also often referred to as a ‘frontal attack’ (Pérez et al. 2016).

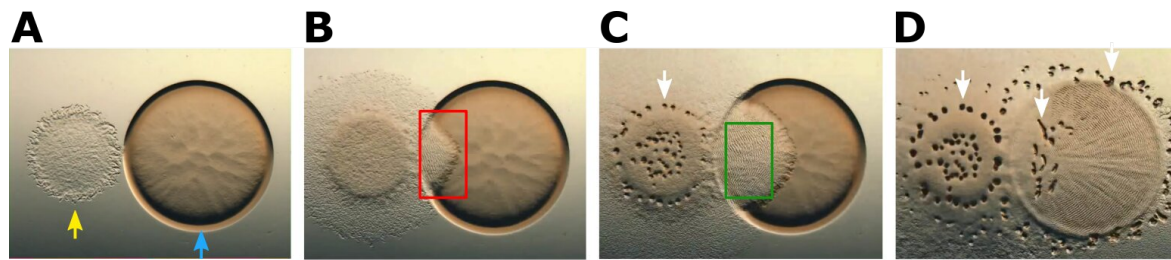


Figure 6. Predation of *M. xanthus* over *E. coli*. A) A dense colony of *M. xanthus* (yellow arrow) is inoculated at millimeter distance from a dense colony of *E. coli* (blue arrow) on a hard (1.5%) agar surface. Over time the *M. xanthus* colony will move out of the original inoculation perimeter. B) Upon encounter with the *E. coli* colony, *M. xanthus* cells will invade the prey colony while killing prey cells, creating a predation zone (red box). C) At the original inoculation location of *M. xanthus*, fruiting bodies develop (white arrow). In the predation zone, a collective behavior, called rippling, emerges (green box). D) After the whole *E. coli* colony is killed, fruiting bodies develop around and within the perimeter where the *E. coli* colony was originally inoculated. Images sampled from timelapse, courtesy of Berleman and Kirby (Berleman and Kirby 2009).

Prey searching and sensing

Interestingly, *M. xanthus* attack strategy depends on the predator density but also on other factors, such as the density of prey cells or the mechanical properties of the surface (Hillesland, Lenski, and Velicer 2007). On the one hand, evolution experiments showed that *M. xanthus* cells develop increased foraging capabilities under sparse prey conditions (Hillesland, Velicer, and Lenski 2009). As a trade-off, *M. xanthus* cells seemed to have a reduced capability to form fruiting bodies. On the other hand, the solidity of the substrate influenced the predation efficiency, with harder agar surfaces increasing the search proficiency (Hillesland, Lenski, and Velicer 2007).

The question remains, however, as to what drives the movement of *M. xanthus* cells towards prey. When placing *M. xanthus* cells on a hard agar surface adjacent to a prey colony, *M. xanthus* cells radially migrate out of the original inoculation point in search for nutrients (Berleman et al. 2006). In an attempt to unravel which genes may be responsible for the detection of prey, Livingstone and colleagues performed transcriptome profiling of both predator (*M. xanthus*) and prey (*E. coli*) in mixed liquid cultures (Livingstone et al. 2018). Strikingly, only 12 out of 7300 *M. xanthus* genes were differentially expressed when mixed with live prey cells, but 1319 genes were differentially expressed when mixed with heat-killed prey, suggesting that the *M. xanthus* transcriptional response is more efficiently triggered by the availability of nutrients than by the presence of live prey. Also surprisingly, prey cells themselves showed differential expression of more than 1500 genes when in contact with live predator cells and around 500 genes when in contact with the supernatant of predator culture. This suggests that prey cells can react to secreted metabolites from the predator cells. Furthermore, upregulated genes in prey cells belong, among others, to pathways involved in antibiotics and secondary metabolite production. This suggests that prey cells might induce defense mechanisms when confronted with predators (Livingstone et al. 2018). Altogether, the above-mentioned results do not confirm nor reject the hypothesis of prey sensing or predataxis by *M. xanthus* during prey searching.

Prey killing and consumption

Once *M. xanthus* cells encounter prey cells, they enter the second phase of predation in which they kill the prey and consume the nutrients released by prey lysis. To date, it remains unclear which

mechanisms are in place to achieve prey killing. On the one hand, myxobacteria have been reported to be capable of killing prey cells from a distance, presumably by the secretion of secondary metabolites, antibiotics and Outer-Membrane Vesicles (OMVs) containing lethal cargo (Berleman and Kirby 2009; Evans et al. 2012; Findlay 2016; Xiao Yao et al. 2011). Myxobacteria are known to encode in their large genome a myriad of bioactive compounds. These compounds can be secreted as such but can be brought into the extracellular space by OMVs. OMVs contain large numbers of metabolites and enzymes including peptidases, phosphatases and lipases of which some are exclusively found in OMVs (Berleman et al. 2014; Kahnt et al. 2010; Whitworth 2015). This suggests that OMVs complement the function of other secreted metabolites. It was indeed shown that both prey *E. coli* and *P. aeruginosa* could be killed by *M. xanthus* produced OMV-free supernatant alone, and by OMVs alone (Evans et al. 2012). When exposed to an OMV-containing supernatant, the predatory activity increased. Additionally, when the enzyme GAPDH was added OMV-mediated prey killing was enhanced. GAPDH is secreted by *M. xanthus* cells, and thus can possibly be seen as a public good (Curtis, Atwood, et al. 2007; Evans et al. 2012; Whitworth and Morgan 2015; Whitworth, Slade, and Mironas 2015). As a moonlighting protein, it has several known functions including facilitation membrane fusion (Wang et al. 2014). When the membrane of OMVs was lysed by french-pressing, however, predatory activity was impaired (Evans et al. 2012). Not surprisingly, it has been suggested that OMV-mediated killing requires the fusion of the OMV membrane to the membrane of the prey cells and that GAPDH and OMVs work synergistically to achieve this.

On the other hand, microscopic evidence shows the killing of single prey cells by *M. xanthus* cells in a contact-dependent manner (Berleman and Kirby 2009; Shilo 1970; McBride and Zusman 1996; W. Zhang et al. 2020; Seef et al. 2021) (**Figure 7**). Regardless of whether the killing mechanism is contact-dependent or contact-independent, killing of prey cells occurs only in relatively close proximity to the *M. xanthus* cells (McBride and Zusman 1996; Berleman and Kirby 2009).

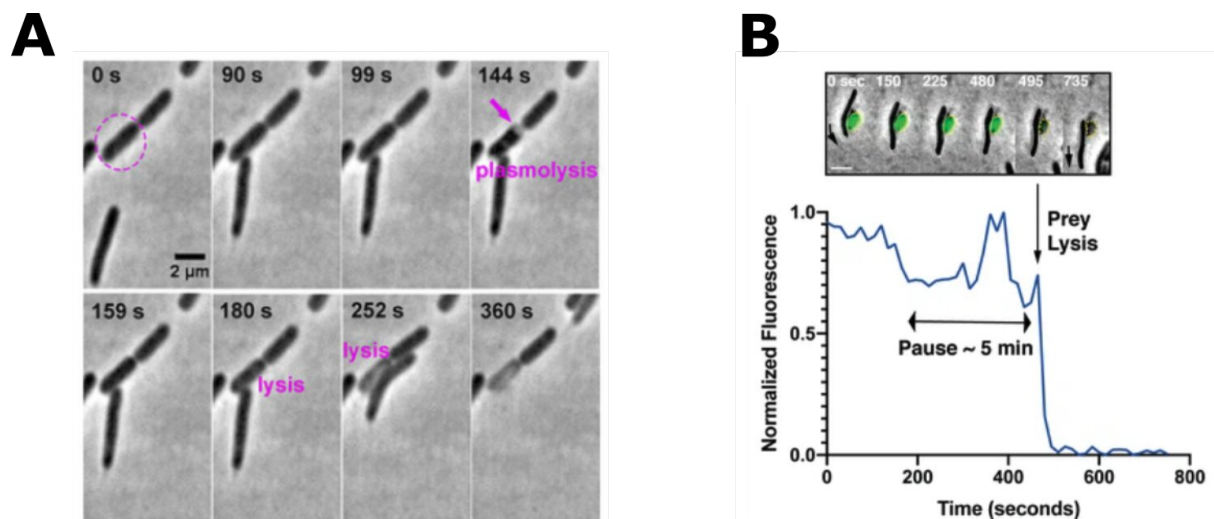


Figure 7. *E. coli* prey plasmolysis due to contact-dependent killing. A) *E. coli* cell (encircled in pink) undergoes plasmolysis upon contact-dependent killing by *M. xanthus*. Scalebar = 2 μm . Adapted from (W. Zhang et al. 2020). B) GFP-labeled *E. coli* cell undergoes plasmolysis. The GFP fluorescence drops instantaneously after a pause of 5 min after contact with the *M. xanthus* cell, indicating *E. coli* cell lysis. Scalebar = 2 μm . Adapted from (Seef et al. 2021).

3.2 Motility

M. xanthus cells rely on their ability to move over solid surfaces through all stages of their life cycle. To do so, these rod-shaped cells use motility approaches allowing them to glide along their long axis creating a leading and lagging cell pole. Every so often, cells change the direction of motion by reversing. During reversal the lagging and leading poles are exchanged. For a long time, it was unclear which mechanisms underlie cell movement and reversal. In 1979, however, not one but two genetically separate motility systems were identified in a screening study. These were called adventurous (A-) motility and social (S-) motility (Jonathan Hodgkin and Kaiser 1979). Cells only became completely immobile in mutants containing perturbations in both sets of genes, thus *M. xanthus* cells use either A- or S- motilities to glide.

Since this discovery, researchers have wondered why *M. xanthus* may have two distinct and independent motility systems instead of one, given that maintaining both of them carries a cost to the cell and the species. To answer this question, several studies evaluated the effects of environmental conditions. First, it was observed that both motility systems perform quite differently on various surfaces. More specifically, the hardness of the surfaces, evaluated by modulating the agar concentration of the substrate, had tremendous effects (Shi and Zusman 1993). The A-motility system was more effective on more rigid surfaces, while the S-motility system was more performant on soft surfaces. In fact, the A-motility system did not even permit gliding at all on soft surfaces. Not surprisingly, wild-type cells were able to swarm proficiently over a wider range of surfaces as compared to the respective motility mutants. Additionally, the effect of nutrient availability, both as diffusible nutrients and prey, was evaluated (Hillesland and Velicer 2005). Cells using the S-motility system were most efficient in swarming and colony expansion when in high-nutrient conditions on soft surfaces. In nutrient-limited conditions, however, the S-motility system was not effective at all on both hard and soft surfaces and was even outperformed by the A-motility system on hard surfaces.

3.2.1 Adventurous motility

In the pioneering screening study of Hodgkin and Kaiser it was shown that mutations in the set of genes coding for the A-motility system seemed to affect mostly the movement of single cells, hence the name adventurous motility (Jonathan Hodgkin and Kaiser 1979). The cell movement driven by the A-motility system was later determined to be a 'gliding motility' approach, meaning that cells propel themselves forward over a surface without extracellular appendages, such as flagella (Burchard 1981; Islam and Mignot 2015). A-motile cells use a molecular machinery, called the Agl-Glt machinery, instead (Luciano et al. 2011). The Agl-Glt machinery is a multiprotein apparatus consisting of two subcomplexes: i) the molecular motor AglRQS, and ii) the GltA-K complex (Luciano et al. 2011; M. Sun et al. 2011; Jakobczak et al. 2015; Nan et al. 2011; Balagam et al. 2014) (**Figure 8a**). The AglRQS motor is an inner-membrane associated complex made up of TolQR like proteins. This complex functions as a proton pump and is thus responsible for the necessary force generation through the proton motive force to propel movement (Cascales et al. 2000). The GltA-K complex, on the other hand, spans the entire cell envelope and is thus associated with the inner-membrane, periplasm and outer-membrane. This multiprotein sub complex is attached to the AglRQS motor in the inner-membrane and ensures the attachment of the complete Agl-Glt apparatus to the substrate. Several cytoplasmic proteins have been identified as well, including AglZ, MglA and MreB (Treuner-Lange et al. 2015; Mauriello, Mouhamar, et al. 2010; Galicia et al. 2019; Hartzell and Kaiser 1991). These proteins mostly play essential roles in A-motility by recruiting and assembling the Agl-Glt machinery

at the leading pole in motile cells. In short, the Ras-like G-protein MglA is bound to GTP (MglA-GTP) and localizes at the leading pole. There, MglA-GTP interacts with the MreB actin cytoskeleton. Consequently, the AlgRQS motor and the inner membrane complex are recruited and assembled at the leading pole where they anchor via AglZ to MreB. This sub-complex then moves intracellularly along a helical path in a counter-clockwise manner without producing movement of the cell (Faure et al. 2016) (**Figure 8b**). Upon encountering the basal membrane, the motor-inner membrane Agl-Glt sub-complex docks into the outer membrane sub-complex. Conformational changes induced by this docking are thought to lead to the attachment of the external sub-complex to the surface, and to the formation of a Focal Adhesion (FA) site (Faure et al. 2016). Force exerted by the Agl-Glt complex at the FA then powers the movement of the cell body along its long axis following a clockwise rotation (Faure et al. 2016). FAs retain a fixed position relative to the surface when the cell is motile (Mignot et al. 2007). Finally, FAs are disassembled at the lagging pole by the GTPase activating protein (GAP) MglB which localizes at the lagging pole (Treuner-Lange et al. 2015).

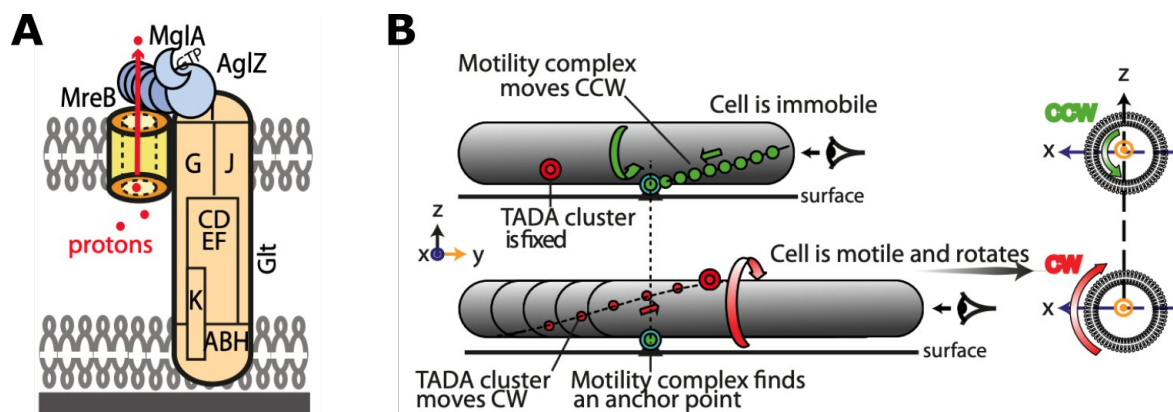


Figure 8. The adventurous (A-) motility system. A) Schematic of the A-motility machinery that is assembled at a FA consisting of inner-membrane associated AgIRSQ motor generating the proton motive force, the Glt complex, AglZ, MglA-GTP and MreB. B) The helical intracellular movement of motor proteins while cells are immobile (top) and mobile (bottom). Adapted from (Faure et al. 2016).

3.2.2 Social motility

Aside from the A-motility machinery, Kaiser and Hodgkin identified another set of genes for which mutants were heavily impaired in their capacity to move over surfaces as groups (Jonathan Hodgkin and Kaiser 1979). This kind of motility was termed social (S-) motility and is mediated by type IV pili. Type IV pili assemble extracellularly at the leading pole and power motion by extending forward, attaching to a substrate or a neighboring cell and retraction, like a retractile motor (Skerker and Berg 2001) (**Figure 9a-b**). S-motile cells can, just like A-motile cells, reverse. This process is mediated by MglA, however, the precise mechanism remains unclear (Mercier and Mignot 2016; Hartzell and Kaiser 1991; Jonathan Hodgkin and Kaiser 1979; Thomasson et al. 2002). Recently it was shown that pili could be assembled at both poles of the cell body but that MglA-GTP indirectly plays a role in the polar activation of the type IV pilus machinery (Mercier et al. 2020).

The complete pilus machinery is a multiprotein assembly which spans the cell envelope consisting of an outer membrane pore, four interconnected ring structures in the periplasm and cytoplasm, a cytoplasmic disc and dome, a periplasmic stem and the PilA protein which makes up the pilus itself (Chang et al. 2016). Assembly of the pilus machinery occurs in an outside-in manner, where

first the PilQ protein forms a multimeric pore in the outer-membrane (Friedrich, Bulyha, and Søgaard-Andersen 2014). It is then hypothesized from cryo-electron tomography studies that the assembly occurs sequentially (Chang et al. 2016) as follows (**Figure 9c**): TsaP polymerizes into a ring-like structure around the PilQ pore; both TsaP and PilQ are anchored to the peptidoglycan but it remains unclear whether this happens before or after their multimerization; once the outer membrane complexes are formed, a periplasmic structure is assembled by polymerization of PilP and PilO:PiLN proteins; then PilO and pil N interact with the presumably cytoplasmic proteins PilC and PiLM. The formation of the PiLM and PilC ring likely allows the subsequent assembly of minor pilins consisting of PilA; finally, the fully assembled PiLM ring recruits the ATPase PilB, the protein involved in mediation of pilus extension. In contrast to the PilB protein localizing predominantly at the leading cell pole, the protein PiIT, which mediates pilus retraction, was found to localize mostly at the lagging cell pole (Bulyha et al. 2009). Only occasionally, PiIT was found to localize on the leading cell pole. These observations led to the hypothesis that the spatial segregation of PilB and PiIT allow temporal separation of extension and retraction events. Aside from the PilB and PiIT involvement in pilus extension and retraction, the exopolysaccharide (EPS) fraction of the extracellular matrix (ECM) material was found to act as an anchor for the pilus and to trigger pilus retraction (Li et al. 2003). EPS is secreted by *M. xanthus* cells and deposited on the underlying substrate as a cell moves over that substrate, leaving behind what is called a slime trail of EPS and other ECM components (Wolgemuth et al. 2002). These slime trails are actively followed by reversing cells retracing their own path, but also by other cells which reorient their motion direction upon encounter of a slime-trail (Burchard 1982; Berleman et al. 2016). Therefore, EPS plays a significant role in the social behavior of *M. xanthus* (Keane and Berleman 2016; Patra et al. 2016).

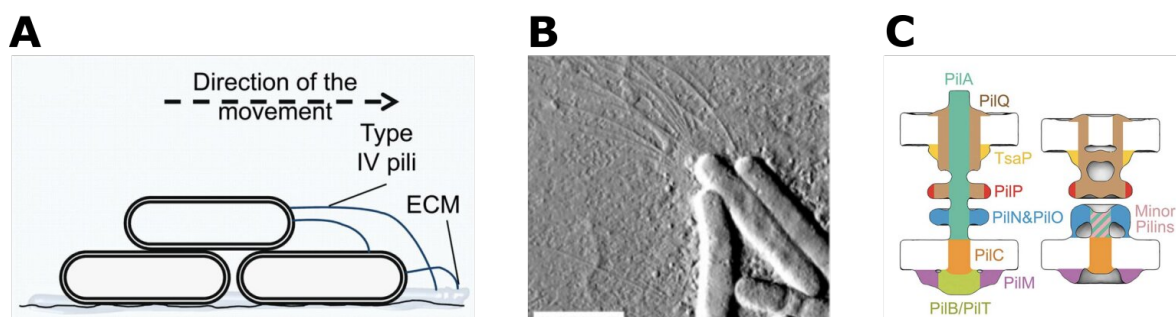


Figure 9. The social (S-) motility system. A) Type IV pili are assembled at the leading pole of the cell and drag the cell forward by extending the pilus forward, attaching to deposited EPS in the ECM and retracting the pilus. Adapted from (Muñoz-Dorado et al. 2016). B) An AFM deflection-mode image of single *M. xanthus* cells with pili assembled at the leading pole. Scalebar = 2 μ m. Adapted from (Pelling et al. 2005). C) Schematic of the pilated (left) and empty (right) basal body of the Type IV pilus containing the inner-membrane associated components PilC/M/B/T, the periplasmic associated components TsaP and PilP/N/O/Q and the outer-membrane associated components PilA/Q. Adapted from (Chang et al. 2016).

3.2.3 The Frz system

As was established in the sections above, the polar assembly of both the A- and S-motility systems is controlled by the localization of MglA-GTP. MglA, in turn, is under the control of the chemotactic Frz pathway, homologous to the well-defined Che pathway in *E. coli* (Ward and Zusman 1997). Mutants in the Frz system do not aggregate as wild-type cells, and thus are heavily impaired in

collective cell motion, surface colonization and fruiting body formation (Ward and Zusman 1997; McBride, Weinberg, and Zusman 1989; Bustamante et al. 2004). Aside from the implications for multicellular behavior, mutations in Frz proteins deeply affect single cell reversal frequency (Blackhart and Zusman 1985).

The Frz system is a multiprotein signal-transduction cascade activated by unknown triggers. The most upstream protein identified in this cascade is the methyl-accepting chemotaxis protein FrzCD, a cytosolic receptor that together with FrzA, activates the autophosphorylation of the histidine-kinase FrzE (Bustamante et al. 2004; Guiseppi et al. 2019; Mercier and Mignot 2016). FrzE can then transfer its phosphoryl group to the cytosolic response regulators FrzX, FrzZ or RomR, which have direct or indirect effects on MglA (Guzzo et al. 2018). RomR has a dual function as it interacts with both MglA-GTP at the leading cell pole in motile cells, as well as with MglB at the lagging cell pole (Keilberg et al. 2012; Y. Zhang, Guzzo, et al. 2012). As mentioned before, the GAP activity of MglB inhibits the localization of MglA-GTP at the lagging pole, and thus has consequences to the establishment of cell polarity. FrzX was recently shown to localize at the lagging pole upon activation by FrzE and to work together with RomR to trigger reversal (Guzzo et al. 2018).

3.2.4 Rippling

Both during the developmental cycle and during predation, the large-scale coordinated cell movement phenomenon, called rippling, is triggered (Konovalova, Petters, and SØgaard-Andersen 2010; Berleman et al. 2006). During this process, *M. xanthus* cells laterally align and collectively oscillate in a synchronous manner to form multiple parallel wavefronts, or ripples. These wavefronts contain high densities of cells interspaced by regions with very few cells. The distance between two travelling wavefronts is defined as the wavelength and was shown to decrease during predatory rippling with the local concentration of prey and to increase as time progresses (Berleman et al. 2008). Additionally, rippling was shown to affect predation efficiency in genetic strains or physiological conditions in which rippling was inhibited (Berleman et al. 2006). In the absence of prey however, rippling can be initiated in areas where nutrient substrates such as peptidoglycan monomers and chromosomal DNA are present (Berleman et al. 2006; L. J. Shimkets and Kaiser 1982). Up until this day, however, it remains unclear what cues trigger the onset of rippling and what is the precise function of rippling during predation. Previous studies hypothesized that rippling may play a role in the consumption of nutrients, as rippling occurs only in areas where prey or prey lysis products were originally located (Berleman et al. 2006).

3.3 Cooperation giving rise to the *M. xanthus* life cycle

From the previous paragraphs, it is clear that several mechanisms confer *M. xanthus* the ability to behave in a collective manner. In the next paragraph, I will review some of the most important cooperation mechanisms used by *M. xanthus*.

A key mechanism giving rise to the multicellular life cycle of *M. xanthus* is social movement of cells. S-motility, for example, is a cell contact dependent behavior that assembles a large number of cells in close proximity with the consequence of increasing the swarm expansion rate (Dale Kaiser and Crosby 1983). Additionally, S-motility is driven by the secretion and deposition of EPS (Lu et al. 2005), which allows adhesion of cells to the substrate and cohesion between cells within swarms (Arnold and Shimkets 1988; Hu et al. 2016). Additionally, EPS facilitates cooperative movement by acting as a

lubricant for cells to slide on (Gibiansky et al. 2013). For S-motility mutants it has been shown that an alternative collective swarming phenotype can evolve relying on A-motility and increased production of extracellular fibril material, which interconnects the cells (Gregory J. Velicer and Yu 2003; Dana and Shimkets 1993). Despite the cost of the enhanced production of the fibril matrix, colony expansion was significantly increased. In summary, EPS can be considered as a public good because it is a component of the ECM secreted in the extracellular space and shared between cells in high density swarms. Secretion of EPS has a cost to the cell producing it but has positive effects on the overall movement of *M. xanthus* swarms. Therefore, EPS production is a typical example of cooperativity.

Cooperation is also thought to be essential for predation. Predation efficiency is highly dependent on the predator cell density, suggesting that a large number of cells cooperate as a predatory unit (wolf-pack) (Berleman and Kirby 2009; McBride and Zusman 1996). High cell densities have been proposed to be advantageous when killing occurs by means of secreted lysing metabolites and outer-membrane vesicles (OMVs) as this results in higher concentrations of killing agents in the environment. Therefore, collective motion of many cells can increase the efficiency of killing. In addition, the secreted products can be seen as public goods because their antimicrobial activity results in the release of lysis products which provide a nutrient source for all surrounding cells, another sign of cooperation.

Additionally, formation of multicellular fruiting bodies during the developmental cycle relies on the cooperation between thousands of cells. The assembly of collective groups of cells requires two quorum sensing signals. The A-signal functions as a monitor for local cell density and is produced in response to starvation (Harris, Kaiser, and Singer 1998; Pathak, Wei, and Wall 2012) in the premature stages of development (Harris, Kaiser, and Singer 1998; Pathak, Wei, and Wall 2012). Only when sufficient levels of A-signal are detected in the environment, indicating that a minimally required number of cells are in starvation, the expression of early-developmental genes is triggered (Kuspa, Plamann, and Kaiser 1992b; Pathak, Wei, and Wall 2012). In more advanced stages of development, cells cooperatively aggregate to form fruiting bodies, a process mediated by the C-signal, a morphogen transmitted in the population by pole-to-pole cell-cell contacts (S. K. Kim and Kaiser 1990a; L. Jelsbak and Sogaard-Andersen 2000; L. J. Shimkets 1999; Kruse et al. 2001; S. K. Kim and Kaiser 1990b).

Lastly, Outer Membrane Exchange (OME) is a cooperation mechanism complementary to the ones directly influencing motility, predation, germination or fruiting body formation. OME describes the process by which outer membrane (OM) components, such as OM lipoproteins, proteins, lipids and putative signals, are exchanged between individual *M. xanthus* cells in a contact-dependent manner through transient fusion of OMs between cells (Pathak et al. 2012; Vassallo et al. 2015; Dey and Wall 2014; X. Wei, Pathak, and Wall 2011). OME can transiently restore motility in nonmotile mutants by transferring functional motility proteins from motile cells to the mutants (J. Hodgkin and Kaiser 1977; Nudleman, Wall, and Kaiser 2005; Wall, Wu, and Kaiser 1998), and heal cells showing lipopolysaccharide defects (Vassallo et al. 2015). Even though the rescuing of damaged or mutant cells by healthy cells seems to imply an unidirectional and altruistic process, OME is actually a mutual cooperative behavior, as OME is a bidirectional process and moreover, healed cells can contribute to group behavior (Pathak et al. 2012; X. Wei, Pathak, and Wall 2011; Nudleman, Wall, and Kaiser 2005).

3.3.1 Cheating and policing

Heterogeneity in a population is oftentimes advantageous, but can also leave space for non-producers or so-called social cheaters (G. J. Velicer, Kroos, and Lenski 2000; Fiegna and Velicer 2005). Cheaters gain a fitness advantage over producers as they do not have the metabolic costs associated with producing yet they reap the benefits of cooperation through the availability of public goods (Gregory J. Velicer and Vos 2009). This leads to an increase of cheaters in the population over time and finally, they will outcompete cells producing public goods eventually leading to the collapse of the social structure (Fiegna and Velicer 2003). This is often referred to as the ‘tragedy of the commons’ principle (Rankin, Bargum, and Kokko 2007).

M. xanthus has a few mechanisms in place to presumably help prevent exploitation and maintain a healthy population. The population can control public goods sharing by kin recognition (Sah and Wall 2020; Cao et al. 2015), whereby cells only interact with genetically-closely related members of a population and exclude non-kin. For example, the genetic variation between spores of the same fruiting body is significantly lower as compared to the variation between spores of multiple fruiting bodies isolated from soil, indicating that genetically related cells cluster together in space (Kraemer and Velicer 2011; Vos and Velicer 2009). In fact, OME only occurs between kin and thus, cooperative sharing of OM associated material is limited to related cells (Pathak et al. 2012, 2013; Cao et al. 2015).

Another mechanism that *M. xanthus* uses to limit exploitation is based on cell-cell surveillance or policing. When repeatedly exposing a laboratory strain proficient in cooperative fruiting body formation to a developmental cheater strain, the cooperative strain rapidly evolves by increasing fitness in presence of the cheater and relative to the cooperative ancestor strain (Manhes and Velicer 2011). Additionally, the evolved strain enhances the ancestor productivity, and inhibits cheaters. However, the mechanism by which this cell-cell surveillance happens remains to be elucidated.

4 Objectives

Over the last few decades, *M. xanthus* has become a popular model system to study bacterial predation. The process of predation, and more specifically prey foraging and the gradual eradication of prey colonies, relies heavily on surface colonization, which *M. xanthus* achieves by moving out of their colony perimeter. Macroscopic qualitative studies of *M. xanthus* predation over *E. coli* have shown that collective motion drives multicellular phenomena, such as rippling, during predation. However, it remains unclear how single-cell motion behavior influences colony penetration and the gradual percolation through the prey colony, and more specifically, what are the respective roles of the adventurous (A-) and social (S-) motility systems in this process. Answering these questions was the main goal of my thesis. For this, I developed four specific aims:

Aim1: Development of microscopy and image analysis method to track the dynamics of M. xanthus and prey single-cells during predation.

To achieve this aim, I first established a classical predation assay in the lab in which a high-density colony of *M. xanthus* is spotted at a millimeter distance from a high-density colony of *E. coli*. Over time, *M. xanthus* cells move out of their original colony perimeter and invade the prey colony. By carefully modulating the density of prey, I was able to create a prey colony, delimited by the spotting perimeter, in which medium-sized (several tens of microns), 2D micro colonies (or islands) of *E. coli* formed. Together, this allowed me to follow bacterial predation in a 2D high-throughput microscopy assay.

Second, I developed a method for large-scale timelapse imaging with a high spatial resolution to resolve single bacterial cells. We combined this with a 2D Artificial intelligence-based method for automatic semantic segmentation, and with a method to reconstruct 2D trajectories of moving *M. xanthus* cells. The development of such a high-throughput imaging modality and the downstream segmentation and tracking analysis allows for the first time to focus on a very large region of interest, exceeding the traditional Field-Of-View (FOV) size used for high resolution acquisition, while following thousands of motile *M. xanthus* cells, even in denser swarms, as they travel through the prey colony. The single-cell trajectory reconstruction method which I built enabled me to follow *M. xanthus* cells, even in denser swarms. The complete imaging and analysis methodology is described in Chapter 1 of the results section.

Aim2: Study of the roles of A- and S-motility systems during predation.

I used the method developed in Aim1 to study the role of the two motility systems during predation. The fact that I was able to resolve single-cell masks and their respective trajectories in this complex sample allowed me to look at bacterial predation from a data-driven perspective and quantitatively describe cell behavior. I focused on the predation forefront where the *M. xanthus* colony protrudes towards unexplored prey colony regions. Overall, I found that different classes could be described, and that the presence and functionality of some of these classes depends on the motility system. I found that A-motile cells play key roles in driving predator advancement through the prey

colony. And finally, I found that both motility systems play synergistic roles when it comes to predation efficiency. These results are presented in chapter 2 of the results section.

Aim 3: Development of spatial transcriptomics to identify bacterial cell states during predation.

From microscopy timelapsing assays, a great variation of functionality and motion behavior among *M. xanthus* cells can be observed. Additionally, a wide range of behaviors have been described as well based on macroscopic-scale qualitative studies of the predation assay. To study whether this behavioral diversity arises from cell specialization, as can be observed in eukaryotic systems, I set out to explore the transcriptome of single *M. xanthus* cells in predating colonies. To do so, I developed a workflow which allows me to label RNA species of interest in fixed cells while conserving the spatial context of the cell in the colony. I validated this workflow by studying the transcriptomic levels of one target RNA species, expressed under the promoter of the EF-TU gene, involved in translation and associated with cell growth, metabolic activity and proliferation. The workflow optimization and the results of target RNA species profiling are elaborated in chapter 3 of the results section.

Aim 4: Develop methods to probe whether A-motility can be controlled by external, non-biological stimuli.

Finally, I explored whether A-motility driven *M. xanthus* cell motion can be influenced by non-biological stimuli. More specifically, I aimed at understanding whether cell reversal, an important event that *M. xanthus* cells use to alter their direction of movement, could be mechanically induced. For this, I resorted to a correlative AFM-optical microscopy method allowing me to use the AFM tip to mechanically probe A-motile *M. xanthus* cells and simultaneously image the cell response. This work is described in chapter 4 of the results section.

II Results

- 1 BactoTracker: dynamic imaging combined with AI-based semantic segmentation and single-cell tracking enables the study of *M. xanthus* predation

BactoTracker: dynamic imaging combined with AI-based semantic segmentation and single-cell tracking enables the study of *M. xanthus* predation

Sara Rombouts¹, Jean-Bernard Fiche¹, Tâm Mignot², Marcelo Nollmann¹

¹ *Centre de Biochimie Structurale, CNRS UMR 5048, INSERM U1054, Université de Montpellier, 60 rue de Navacelles, 34090, Montpellier, France*

² *Laboratoire de Chimie Bactérienne, Marseille, France.*

Abstract

The ability of cellular motility that exists in various bacterial species is one of the main characteristics that promotes survival by allowing rapid and efficient reaction to changes in the micro environment. The gram-negative soil bacterium *Myxococcus xanthus* has been studied for decades as a model organism for bacterial predation. By gliding over solid surfaces, a *M. xanthus* colony explores its environment in search for nutrients. Once a prey colony is identified, *M. xanthus* cells penetrate this colony while lysing prey cells. Over time, bacterial predation of *M. xanthus* over *E. coli* has been studied extensively in macroscopic assays. However, this colony-wide process is thought to rely on intercellular coordination between individual *M. xanthus* cells. Here we propose a large-scale high-throughput microscopy-based approach which allows us to follow the process of predation with high spatial and temporal resolution and over long periods of time. For this, we combine a deep learning-based approach for semantic cell segmentation with a single-cell tracking approach, which enables us to follow single cells for hours. This strategy will enable the quantitative characterization of the macroscopic predation phenomenon with single cell resolution.

Introduction

Myxococcus xanthus is a gram-negative bacterium that lives in soil. To survive in this complex ecosystem, it has developed a social lifestyle based on its capacity to move over a surface in a collective and coordinated manner (Dworkin 1963; Zhang et al. 2012). This motility allows them to seek prey in the environment (predation during vegetative growth), or to induce collective motion towards aggregation centers to form spore-filled fruiting bodies (developmental program) (Muñoz-Dorado et al. 2016). Both phenomena, predation and fruiting body formation, exceed the length scales of the single cell and arise from the strong coordinated dynamics of individual cells (Zhang et al. 2012). The process of predation occurs in several phases: i) exploration of the environment in search for nutrients, ii) identification of prey, iii) progression of swarms containing dozens of cells towards prey, iv) killing of the prey and v) take-up of nutrients (Keane and Berleman 2016). The occurrence of these cellular behaviors suggest that they all contribute to successful and efficient predation. However, it remains unclear how and to what extent intra- and intercellular behaviors affect this complex process.

Due to experimental and technical constraints, it has been challenging to study single cell behavior within the macroscopic context of bacterial predation. First, bacterial predation between *M. xanthus* and *E. coli* is a colony-phenomenon that exceeds the length scales accessible with high-resolution microscopy imaging. Therefore, it is challenging to capture an area that is large enough to provide indispensable context while being able to resolve single bacterial cells. Second, even if a large area could be microscopically captured, cells in a predation context have a tendency to be densely packed. Most *M. xanthus* cells associate themselves to form swarms, and *E. coli* cells form microcolonies or islands. To automatically detect cells in such dense areas is challenging with classical methods, such as intensity thresholding and watershed. Even though a number of softwares for cell segmentation, such as SuperSegger (Stylianidou et al. 2016), Oufi (Paintdakhi et al. 2016) and the MicrobeJ plugin for ImageJ (Ducret, Quardokus, and Brun 2016), became available over time and are very performant in a specific range of experimental conditions, these methods do not provide sufficient segmentation performance when the imaging mode varies (e.g. brightfield acquisition instead of phase-contrast), cells are too densely packed or species are intermixed. Recently, however, an artificial intelligence based solution for semantic cell segmentation of complex microbial communities was proposed (Panigrahi et al. 2021).

Finally, predation is a dynamic process, where *M. xanthus* cells are continuously gliding and *E. coli* cells disappear over time as a result of prey cell lysis due to *M. xanthus* killing. The study of single cell behavior in this context would ideally require a method that can follow single cells over time. This not only implies a single-cell resolving timelapsing imaging method, but also implies an adequate tracking method. SuperSegger, for example, is able to track bacterial growth in micro-sized stationary colonies over time (Stylianidou et al. 2016). *M. xanthus* cells, however, actively glide and thus, tracking of those cells requires alternative methods. Tracking of isolated or small groups of cells is often done with MicrobeJ (Ducret, Quardokus, and Brun 2016), but other methods were proposed to track *M. xanthus* cells as well (Chen, Alber, and Chen 2016; Liu et al. 2012). Most of these methods do not fit the experimental conditions we used to image the predation sample over time.

Here, we designed a workflow enabling us to provide an answer to these challenges. First, we developed a high-throughput microscopy-based method combining brightfield and fluorescence imaging that allows us to image a large area of the predation sample over time. To do so, a hardware-accelerated, automated microscope was implemented for the acquisition of the predation process with high spatial and temporal resolutions. Additionally, we developed a deep-learning approach for semantic cell segmentation of densely packed and multispecies regions. Lastly, we built a tracking method that allows us to efficiently follow motile *M. xanthus* cells, either as solitary cells or in densely packed regions, in the experimental timescales used for imaging.

Results

Workflow

Preparation of the predation assay

The predation assay was constructed as was described before by Berleman and colleagues (Berleman et al. 2006). In short, a colony of *M. xanthus* was spotted at a millimeter distance from a colony of *E. coli* on a hard agar surface of 1,5% (Fig. 1A). Over time, *M. xanthus* cells migrate out of the original colony perimeter in search for nutrients. When the *E. coli* colony is reached, *M. xanthus* penetrates the prey colony, creating a predation zone, and lyses prey cells in the *E. coli* islands. To be able to rely on 2D cell segmentation and tracking, we ensured that the density of *E. coli* was low enough so that 2D microcolonies (or islands) were formed and did not contain multiple layers. Generally, the sample was imaged after 48-72 hours of initial spotting of the colonies, which corresponds to the *M. xanthus* cells having advanced halfway through the prey colony. To limit any background signal during high resolution fluorescence imaging, the agar pad was made as thin as possible with an Ultrapure agar (Invitrogen).

Mosaic approach for large area imaging

To image a large region of interest (ROI) of the forefront of the predation assay, exceeding the size of the field of view (FOV) allowed by the microscope, a mosaic imaging approach was used (Fig. 1B). The ROI was constructed by acquiring 3-by-3 tiles of 2048x2048 pixels (pixel size calibrated to 106 nm), with each tile corresponding to the FOV size captured by the s-cmos camera. These tiles were imaged in a serpentine pattern to minimize stage displacement between successive images. For each tile, a 3D z-stack was simultaneously acquired in the brightfield channel and in the fluorescence channels, that minimally included the fluorescence signal emitted only by *E. coli* cells necessary for semantic cell segmentation. To account for possible tilt in the sample or for agar pad deformation, the z-stack spanned 1.5-2.5 μ m (7-9 planes, interspaced by 250-300nm) so that each bacterial cell could be captured in focus. An imaging cycle, corresponding to one time point in the timelapse, was completed when all z-stacks for each of the 9 FOVs were acquired in both brightfield and fluorescence modes. Live axial drift correction based on the reflection of an IR laser beam (785 nm) allowed us to maintain the focus during the course of the experiment (>6h). By repeating the 3x3 mosaic imaging cycle, a time lapse of a large area of the predation assay was constructed (~600x600 μ m). This fully-automatic acquisition was performed on a microscopy set-up optimized for speed, allowing to complete a full imaging cycle in ~35 s. This imaging speed is important to ensure that the semantic masks from the same cell acquired at consecutive time points could be linked together (see below). As the single-cell tracking approach used to follow motile *M. xanthus* cells for hours relies on connecting cell masks over time, therefore it is essential that some overlap between masks is maintained between consecutive acquisitions. As *M. xanthus* cells move on average 3.8-5.0 μ m/min (Spormann and Kaiser 1995), and their cell length is on average 4-5 μ m (Patra et al. 2016), this implies that a cell on average moves approximately 50% of its cell length in 35 s. Generally, 700 imaging cycles were acquired per experiment, corresponding to 6.5 hour long acquisition and at least 12600 z-stacks (700 Imaging cycles * 9 ROIs per Imaging cycle * 2 z-stacks (brightfield and *E. coli* fluorescence) per ROI).

Image pre-processing

Pre-processing involved the conversion of 3D stacks to 2D images, the input for semantic cell segmentations (Fig. 1C). To convert the z-stacks of the *E. coli* fluorescence to a 2D image, the z-stacks were deconvolved (Huygens, SVI) and a standard deviation image was calculated from all planes. The 3D to 2D conversion of the brightfield stacks was more complex, as the in-focus plane could vary in a FOV due to sample tilt and deformations in the agar pad. To account for this, each 2048x2048 pixels FOV was divided into 4-by-4 512x512 pixels sub-images. For each of those sub-images the in-focus

plane was found based on image contrast and sharpness and retained to reconstitute an in-focus 2D image. This process was repeated for all FOVs in the timelapse, creating 12600 2D images.

*Semantic segmentation of *M. xanthus* and *E. coli* cells*

To extract single cell masks and classify them as either *E. coli* cell or *M. xanthus* cells, we relied on a deep learning approach (see section below) which uses for each FOV the corresponding 2D brightfield image and the 2D *E. coli* fluorescence image as inputs, and outputs a semantically segmented image (Fig. 1D). The output image contains for each pixel a confidence value indicating to which class the pixel belongs to.

Reconstructing the large area image

The next step involved the assembly of 3x3 mosaics by tiling (Fig. 1E). Each image (i.e. 2048x2048 pixels image) was acquired with a theoretical overlap of 200 pixels with its neighbouring images. We used image cross-correlation to find the pixel-precision overlap between any two neighboring images (Python package scikit-image). When tiling the mosaic together, a smooth transition between images in the overlap region was ensured by using an alpha blending method with a decreasing transparency gradient. Once the large 3x3 tiled image was constructed, a drift correction was applied. This offset was calculated by cross correlating the *E. coli* segmented image of the middle FOV (time $t=n$) with respect to the reference middle FOV of the first image (time $t=1$).

*Post-processing of *M. xanthus* masks*

After image post-processing, the *M. xanthus* masks in this large image are post-processed to get a binary image containing only the masks corresponding to single *M. xanthus* cells (Fig. 1F). In the first step of mask post-processing, pixels with high confidence values are retained. Then for each mask, the neighboring pixels with gradually lower confidence values are evaluated. Pixels with lower confidence are retained only when the mask area does not increase more than 5%. If the mask area increases more than 5%, it is assumed that these pixels fuse neighboring cell masks and therefore, the pixels are rejected. The output of this pixel selection procedure is a binary image with 4-connected *M. xanthus* cell masks. These masks are then filtered for size, rejecting all masks with an area lower than 100 pixels. This ensures that wrongly assigned *E. coli* masks, which are smaller than *M. xanthus* cells, are rejected as much as possible from the segmented image. Additionally, a filtering was applied to reject fused cell masks which could not be detected in the pixel selection step. As *M. xanthus* are rod-shaped cells, their backbone should represent a line without any branchpoints. This was used to detect and reject mask fusions by calculating the backbone of all masks and detecting cells with branch points in their backbones. Furthermore, pole-to-pole mask fusions were detected by calculating the tortuosity of the mask. The tortuosity is defined as the ratio between the length of the backbone and the distance between its endpoints, and is thus a measure for the curvature of the mask. The mask was rejected when this ratio exceeds the threshold of two. The masks that were retained after mask post-processing were used to reconstruct single-cell trajectories.

Building single cell trajectories

We developed a single-cell tracking approach in which *M. xanthus* masks are connected over time (Fig. 1G). For solitary cells, this is a straightforward approach as we can rely on the overlap of masks between consecutive time points. However, for cells in dense groups, such as swarms, this is more complicated. To deal with cells in these dense regions, we rely on the parameters of the cell masks, including the overlap of masks in time, the cell length and the mask area, and a ranking approach to reconstruct the trajectories. This approach allowed us to follow several thousands *M. xanthus* cells migrating between *E. coli* islands during predation (see below).

AI-based semantic segmentation

The training database

The semantic segmentation approach that we used to segment the multispecies images was based on a convolutional neural network (CNN) with a U-net architecture implemented in MATLAB. Important for this CNN to properly classify pixels is the training of the network with ground truth data. The ground truth image database must contain representative data for different experimental conditions. For the predation assay, this means that we need to include images with high concentrations of *M. xanthus* (such as in *M. xanthus* swarms), of *E. coli* (such as in *E. coli* islands) and of both. Additionally, images where both species can be found in very close proximity to each other and even intermixed were also included in the training data set.

From experiments, 40 260x260 pixels images were selected satisfying the criteria described above (Fig. 2A). These images were manually annotated for five classes: i) background, ii) *M. xanthus* body, iii) *M. xanthus* contour, iv) *E. coli* body and v) *E. coli* contour. The cell contour of cells in densely packed regions was allowed to overlap and was included as a distinct class as this forced the network to physically separate single cell bodies. From these 260x260 images, training images of 128x128 pixels were sampled. The robustness of the semantic segmentation of input images with varying focal planes was increased by augmenting the training database with out-of-focus training images. In an additional data augmentation step, the 260x260 image was rotated 45° to create a 182x182 pixels image from which a number of additional training images were sampled. The corresponding out-of-focus images were again included in the training database. This process was repeated for all 40 260x260 pixels images and resulted in a large, diverse and representative training image database consisting of the sampled annotated images and its corresponding brightfield and *E. coli* fluorescence images. Finally, an automatic data-augmentation step was applied on all images in the training database, including image flip and noise addition.

Semantic segmentation with five independent U-nets

This training database was used to train the U-net. The performance of the trained network, defined by the ability of a network to accurately classify a pixel to a class, was evaluated in a validation step in which a subset of the training database is used and in which a Normalization Confusion Matrix is constructed (Fig. 2B). This matrix represents how well the network predicts the class of a given pixel with respect to the ground truth, and thus indicates the degree of correctly assigned classes. The network was able to accurately assign the classes Background, *M. xanthus* body and *E. coli* body. The assignment of the *M. xanthus* contour and *E. coli* contour classes were more challenging and were often intermixed with the respective cell body class or the background. This does not pose an immediate problem, as the classes for cell contour were only included to well separate masks in regions where bacteria were densely packed. However, it is imperative for the single-cell tracking to segment masks of single cells and avoid fusion of masks. Therefore, we adopted a strategy in which five networks were independently trained. Each network used a 2048x2048 pixels in-focus 2D brightfield image and the corresponding 2D standard deviation deconvolved fluorescence image of *E. coli* as input (Fig. 2C). Each of these five networks semantically segment the input data, resulting in an output image with a confidence value ranging between 0 and 5 for assignment of the pixels to each of the classes. This strategy allowed us to converge to an accurate result for which limited post-processing of the segmented masks was required for further analysis.

Single-cell tracking

After post-processing, each *M. xanthus* mask was assigned a unique cell identifier (ID). Single-cell trajectories were then reconstructed by connecting the unique cell IDs of masks over time.

The single-cell tracking approach that we developed consists of three distinct stages: i) pairwise tracking, ii) filtering pairwise tracking and iii) track reconstruction (Fig. 3).

In the first stage of the tracking, a pair-wise approach was used to connect the masks in consecutive images in time, creating pairs of linked masks (Fig. 3A). This was done by selecting for each mask at time t the possible candidate masks at time $t+1$. Candidates are selected based on the enlarged bounding box of the mask of interest (t), knowing that *M. xanthus* cells will only be able to move at most a few micrometers in the time separating two consecutive frames. Then, for the mask of interest (t) and the candidates ($t+1$), the cell length, the mask area and the overlap of the mask (t) and each candidate ($t+1$) was calculated. These parameters were used in Analytical Hierarchy Processing, an algorithm for analyzing complex decisions and ranking alternatives from most to least suitable (Saaty 1986). Here, this algorithm was used to rank the candidates ($t+1$) from most to least likely to represent the same cell and thus, to be connected to the mask of interest at time t . This process is repeated for all masks at time t and results in the pairwise connection of unique cell IDs at times t and $t+1$. When only one candidate at time $t+1$ can be selected, for example in regions where *M. xanthus* cells are not very dense, this cell was automatically connected to the mask of interest at time (t). When no candidate at time ($t+1$) can be selected, the track was stopped.

In regions where cells are densely packed, multiple assignments of the same candidate can frequently occur. This means that for two or more masks at time (t) the same candidate at time ($t+1$) was ranked most suitable for connecting to the mask. Such multiple assignments were filtered out and a reverse pairwise tracking was performed, meaning that the optimal mask at time (t) will be selected to connect to the multiple assigned candidates at time ($t+1$) (Fig. 3B). This finally resulted in unique pairwise connections for each pair of consecutive images over time.

Finally, all pairs of connected masks were linked to each other, so that the full tracks were reconstructed and could be visualized (Fig. 3C).

Discussion

In this article, we propose an imaging, cell segmentation and tracking framework for the study of predation of *M. xanthus* on *E. coli*. Our high-throughput, high resolution microscopy method allows the acquisition of large imaging areas in a timelapse manner by employing a mosaic imaging scheme. We propose a deep learning-based semantic segmentation approach for the reconstruction of single-cell *M. xanthus* and *E. coli* masks. And finally, we present a method that enables the tracking of motile *M. xanthus* cells. Additionally, we show that pre-processing of images for semantic segmentation and post-processing of masks for tracking is limited, which diminishes computational time and resources for the analysis of these large datasets.

The workflow proposed here allowed us to overcome several challenges that occur when dealing with complex samples such as the predation assay. First, mosaic imaging allows the visualization of extensive areas without sacrificing resolution and thus, thousands of predator and prey cells can be observed in their spatial context (position within the community). Mosaic approaches have been proposed before, mostly for the imaging of large biological specimens such as tissue slices (Chow et al. 2006; Price et al. 2006) and are often incorporated in commercial microscopes. Adding a time component, rendering the large-scale imaging modality dynamic, however, is more complicated. Depending on the movement patterns one wants to study, a certain imaging speed needs to be respected. In the case of motile *M. xanthus* cells, we defined a maximal interval of approximately 35 s between two consecutive frames to accurately track single cells. To respect this time constraint, we resorted to an in-house developed fully-automated hardware-accelerated microscope. Additionally, fast mosaic acquisition is desired for the time correlation of tiles in dynamic samples.

Second, we developed a deep learning based method for cell segmentation as traditional methods did not suffice to accurately generate binary masks in densely packed regions, e.g. *E. coli* cells in microcolonies or *M. xanthus* in swarms. Interestingly, the field of deep-learning based segmentation applied to biological problems is a fast developing field of research, with increasing numbers of publications and a multitude of accessible and even open-source packages coming out (Hallou et al. 2021; Greener et al. 2021). Here, we used a semantic segmentation approach based on a U-net trained to classify pixels to background, to *M. xanthus* body or contour, or to *E. coli* body or contour. Building the training image database containing ground truth images was a straightforward process, however, manual annotation of images can be quite laborious. Despite the fact that U-nets are reported to require less large training databases, a variety of representative example images of experimental conditions needs to be included (Falk et al. 2019). Data-augmentation methods provide a solution to minimize the amount of human input (Shorten and Khoshgoftaar 2019). An additional challenge when working with fully-automated microscopy systems is that the optimal focal plane cannot be selected manually but is determined by an autofocus system. To make the segmentation robust for images with varying focal planes, we included out-of-focus images to the training database.

Lastly, we exploit the timelapse data by reconstructing single-cell trajectories of motile *M. xanthus* cells. By using a ranking approach for complex decision making (Saaty 1986), we were able to track cells relatively efficiently in solitary states, small groups or dense swarms.

Taken together, this workflow opens the door for the quantitative study of bacterial predation of *M. xanthus* on *E. coli*. However, we predict that this workflow is easily transferable to different complex and multispecies systems which require the dynamic study of its bacterial components.

Acknowledgements

This project was funded by the European Union's Horizon 2020 Research and Innovation Program (Grant ID 724429) (M.N.). We acknowledge the Bettencourt-Schueller Foundation for their prize 'Coup d'élan pour la recherche Française', the France-BioImaging infrastructure supported by the French National Research Agency (grant ID ANR-10-INBS-04, "Investments for the Future"). Additional funding was provided by the European Union's Horizon 2020 Research and Innovation Program (Grant ID 885145) (T.M.).

Methods

Bacterial strains

The bacterial strains used in this work can be found in the table below.

Strain	Genotype	Strain origin
<i>E. coli</i> HU-mCherry	MG1655 HU-mCherry	Espeli laboratory collection
<i>M. xanthus</i>	DZ2 wildtype	Mignot laboratory collection
<i>M. xanthus</i> cytosolic-sfGFP	DZ2 pSWU19-pm3068-sfGFP	Mignot laboratory collection

Bacterial cultures

E. coli cells used in predation assays were grown overnight in 10 ml Luria-Bertani (LB) medium at 32°C under agitation (200 rpm). To ensure that *E. coli* cells were in exponential phase after overnight growth, a 1:10 dilution of the starter culture was made in fresh LB medium and incubated for approximately four hours.

M. xanthus cells were grown overnight in 10 ml Casitone Yeast Extract (CYE) rich medium as was described before (Bustamante et al. 2004) at 32°C under agitation (200 rpm), supplemented with antibiotics (Ampicillin 1 µg/ml) when necessary. Cells were harvested when the OD₆₀₀ reached 0.1-0.5.

Predation assays

Bacterial predation was established in laboratory conditions by setting up a predation assay. In short, *E. coli* and *M. xanthus* cells were harvested from the LB and CYE media, respectively. Cells were concentrated by centrifugation on a tabletop centrifuge at 2100 g for 5 min at room temperature and resuspended in CF medium (10 mM MOPS (pH 7.6), 1 mM KH₂PO₄, 8 mM MgSO₄, 0.02% (NH₄)₂SO₄, 0.2% sodium citrate, 0.015% bacto casitone peptone). *M. xanthus* cells were concentrated to an OD₆₀₀ of 5, *E. coli* cells were concentrated to an OD₆₀₀ of 0.005. Cell suspensions of 1 µl were spotted at close distance of approximately 1 mm on CF 1.5% agar pads supported on a coverslip.

The agar pads used for time lapse imaging were made with ultrapure agar (UltraPure Agarose 1000, Invitrogen) to limit autofluorescence by impurities in the agar solutions. Pads were made by pipetting 550 µl of melted agar onto a 25mm coverslip and by placing a second coverslip on the drop of agar, allowing the latter to solidify between two flat surfaces. Once the agar pad was made, the top coverslip was removed and the agar was cut to a diameter of 20 mm.

The prepared predation assays were then placed onto a layer of CF 1.5% agar in a petri dish and the petri dish was closed with parafilm to avoid agar pad evaporation and drying. Samples were incubated 24h to 48h on 32°C to allow *M. xanthus* cells to invade the *E. coli* colony.

Microscopy

Fast time lapse and hubble imaging were done on a homemade fully-automated hardware-accelerated wide-field epifluorescence microscope built on a RAMM modular microscope system (Applied Scientific Instrumentation). Samples were imaged using a 60x Plan-Achromat water-immersion objective (NA = 1.2, Nikon, Japan). The objective lens was mounted on a closed-loop piezoelectric stage (Nano-F100, Mad City Labs Inc. - USA). Illumination was provided by a

brightfield illumination source and 2 lasers (OBIS-488 nm and Sapphire-LP-561 nm, Coherent – USA). Images were acquired using a sCMOS camera (ORCA Flash 4.0V3, Hamamatsu – Japan), with a final pixel size calibrated to 106 nm. A custom-built autofocus system was used to correct for axial drift in real-time and maintain the sample in focus. Software-controlled microscope components, including camera, stages, brightfield illumination and lasers were run using a custom-made software package developed in LabView 2015 (National Instrument).

Fast time lapse imaging

For imaging of the predation assay, the sample was covered with an imaging coverslip. The imaging coverslip was washed consecutively with acetone, Milli-Q water, 70% ethanol (v/v) and Milli-Q water, and flamed to remove any fluorescence impurities and residues. The coverslip was cooled down to room temperature and placed hermetically on the sample while avoiding bubbles between the sample and the coverslip. The sample was mounted in an attofluor and onto the microscope for imaging. A region of interest spanning an area of approximately 0.36 mm² was selected. This large area was imaged by constructing a mosaic patchwork of 3 by 3 fields of view (FOVs) or mosaic tiles of 2048x2048 pixels, each theoretically overlapping with 200 pixels. An imaging cycle, in which the 3-by-3 mosaic was imaged by sample displacement following a snake-like pattern, was thus made up of 9 consecutive acquisitions. For each FOV, a 3D-stack was acquired to account for sample tilt in brightfield and in the fluorescence channel of 561 nm for *E. coli* carrying a HU-mCherry fusion. An additional fluorescent channel was added for *M. xanthus* when the used strain was carrying a fluorescent protein as well. A 3D-stack was generally made up of 7-12 planes interspaced with 250-500 nm. Exposure times were set at 50 ms. The laser powers used were kept at low intensity to limit phototoxic effects on the live cells during time lapse acquisition. Brightfield illumination was attenuated with a neutral density filter with optical density two. Imaging cycles were generally completed in 30-40 seconds and were repeated 700 times to construct an hours-long time lapse series of the mosaic area.

Treatment of fast time lapse data

To increase imaging speed, all images from one imaging cycle were pooled into one DCIMG file. First, the DCIMG files were converted to tiff files with software from Hamamatsu and sorted for each FOV, channel and time point. Tiff images of the fluorescent channel of *E. coli* were deconvolved with Huygens Professional version 20.04 (Scientific Volume Imaging, the Netherlands, <https://svi.nl/>). Deconvolved *E. coli* stacks were z-projected by calculating the standard deviation. 3D brightfield stacks were converted to 2D images by dividing each stack in 16 ROIs of 512x512 pixels, selecting automatically or manually the in-focus plane for each ROI and restitching the 16 ROIs. The code for calculating the in-focus brightfield image (im_straighter_FTL.m or im_straighter_FTL_manual.m) can be found in https://github.com/jbfiche/DCIMG_to_TIFF_conversion/tree/master/Fast_TL_windows. 2D brightfield and *E. coli* fluorescence images were used as input for an in-house developed MATLAB code using a convolutional neural network with U-Net architecture for semantic segmentation (Ronneberger, Fischer, and Brox 2015; Van Valen et al. 2016). Semantic segmentation was performed with five independently trained networks to converge towards a high confidence result, outputting an image with pixel values representing the pixel assignment confidence to a given class. The code for semantic segmentation (Reconstruct_image_FCN_FTL.m) can be found in https://github.com/jbfiche/Deep_Learning_segmentation/tree/Myxo_segmentation_predation_fluo_Unet/For_image_reconstruction.

Segmented images were then used to reconstruct the mosaic image by tiling the 9 images. Exact image overlap for tiling was calculated by image-based pixel-resolution cross correlation. Drift in time was corrected by aligning the mosaic images based on cross correlation calculated from segmented images of stationary *E. coli* microcolonies. *M. xanthus* segments from mosaic images were post-processed to reduce segmentation artefacts. In short, binary masks were generated from

the masks by exploiting the assignment of confidence values, masks were filtered for size and finally, tortuous masks and fused masks were rejected. *E. coli* masks were post-processed to avoid overlap between *E. coli* and *M. xanthus* masks and filtered for size to reject isolated pixels. The code for cross-correlation calculation (`MosaicImages_CC_BFNormalized_MyxoSegmented.py` and `Mosaic_DriftCorrection_GlidingRef_MiddelROI5.py`), and tiling, drift correction and mask post-processing (`function_DriftCorr_MosaicTiling_Ecoli.m`) can be found in https://github.com/SaraRombouts/ProjectFTL_Predation.

Single cell tracking

Single cell trajectories were reconstructed with an in-house developed MATLAB pipeline. For each timepoint in the time lapse image series, pairwise tracks were constructed between cells in frame k and cells in frame $k+1$. Briefly, the enlarged bounding box of the cell mask in frame k was utilized to select a number of possible candidates in frame $k+1$. Ultimately, the optimal candidate was found by ranking the candidates with Analytical Hierarchy Processing (AHP) (Saaty 1986) based on several parameters of the masks including cell area, cell length and mask overlap area between the cell and its candidates. To correct for multiple assignments of a candidate, an inverse AHP approach was used in which the optimal cell from frame k was selected for the candidate of frame $k+1$. Finally, pairwise tracks over all timepoints were combined to form complete single cell trajectories. The code for single-cell trajectory reconstruction (`function_Tracking_TiledMosaic.m`) can be found in https://github.com/SaraRombouts/ProjectFTL_Predation.

Figure Legends

Figure 1: Workflow of the proposed method for large area time lapse imaging, semantic segmentation and single-cell tracking.

A) Sample preparation of a predation assay. A colony of *M. xanthus* (yellow) is spotted at a millimeter distance from a colony of *E. coli* (blue) on a hard agar surface. This sample is then incubated for 48-72 hours before imaging the forefront of the predation zone (red boxed area).

B) Mosaic imaging of the predation forefront. The region of interest (ROI) is imaged by dividing it into a 3-by-3 mosaic made up of 2048x2048 pixels Field Of Views (FOVs). For each FOV at least two z-stacks are acquired, one for the brightfield channel and one for the *E. coli* fluorescence channel. The acquisition of each mosaic FOV with its corresponding z-stacks acquired in a snake-like pattern makes up an imaging cycle. By repeating the acquisition of imaging cycles, a timelapse is constructed of the large ROI.

C) Pre-processing of the z-stacks into 2D images. The *E. coli* fluorescence z-stack is deconvolved and a 2D standard deviation image is calculated from the deconvolved z-stack. The brightfield z-stack is divided into 4x4 small ROIs, and for each small ROI the in-focus plane is selected. A 2D in-focus brightfield image is reconstituted by retaining all selected planes. Scalebars = 20 μm .

D) Semantic segmentation of *E. coli* (blue) and *M. xanthus* (yellow) with a deep learning based method. A semantically segmented image is calculated from the 2D fluorescence and brightfield images for all FOVs in all imaging cycles of the timelapse. Scalebar large image = 50 μm , scalebar zoom = 20 μm .

E) Image post-processing to reconstruct the large ROI and to drift-corrected over time. By calculating the cross correlation of the overlap region between neighboring FOVs, their corresponding pixel-precise positioning in the mosaic can be determined. After the tiling of the mosaic, a drift correction is applied based on the cross-correlation between the middle FOV at time t with the middle reference FOV reference at time $t=1$.

F) Post-processing of the masks to reject all improper masks. Raw output *M. xanthus* masks of the semantic segmentation are first converted to a binary image based on their confidence values, masks are then filtered for size and finally fused masks are rejected based on backbone branch points and tortuosity. Scalebars = 20 μm .

G) Single-cell tracking of motile *M. xanthus* cells. Trajectories are reconstructed by connecting the *M. xanthus* cell masks over time (left) Scalebar = 5 μm . This tracking method allows us to reconstruct thousands of tracks in a tiled mosaic (right) Scalebars = 50 μm .

Figure 2: Semantic segmentation with MATLAB-based U-net algorithm.

A) Example annotated image for the set-up of the training image database. From a 260x260 pixel image annotated for the ground truth, a number of training images (128x128 pixels) were sampled. For each sampled training image, several out-of-focus brightfield and fluorescence images were included as well. The 260x260 pixels image was then 45° rotated from which additional training images were sampled. Out-of-focus brightfield and fluorescence images were included again. Scalebars = 5 μm .

B) Normalized Confusion Matrix for a trained U-net. From this matrix, the accuracy of pixel assignment to a given class predicted by the trained network is evaluated by comparing it to the ground truth.

C) Semantic segmentation of experimental input images. The input for the U-net are a 2048x2048 pixels brightfield and its corresponding fluorescence image. Segmentation is performed by five independently trained networks that output an image containing the confidence value for all pixel assignments for each class. Scalebars = 50 μm .

Figure 3: Schematic of single-cell tracking approach.

A) Pairwise tracking to connect all masks at time t to their corresponding masks at time $t+1$. For each mask at a given time point (time t), candidate masks for connection are selected in the consecutive time point (time $t+1$) based on the bounding box of the mask (t). For the mask (t) and candidates ($t+1$), three parameters are calculated: i) the cell length based on its backbone, ii) the cell area and the overlap between the mask (t) and iii) the mask of the candidate ($t+1$). These parameters are the input for the Analytical Hierarchy Processing (AHP) which rank the candidates from most suitable to least suitable for connection and finally. This process is repeated for all masks (t) and results in a list of pairwise connections.

B) Filtering and correction of multiple assignments in pairwise connection lists. To account for multiple assignments of a candidate, a reverse AHP step is included in which the most suitable mask (t) is selected for the candidate ($t+1$). The list of pairwise connections is then corrected, for masks (t) that were not selected in the reverse AHP the trajectory is stopped.

B) Full track reconstruction. From the lists containing pairwise mask connections for all timepoints, the full tracks can be reconstructed over the full length of the timelapse. Scalebar = 50 μm .

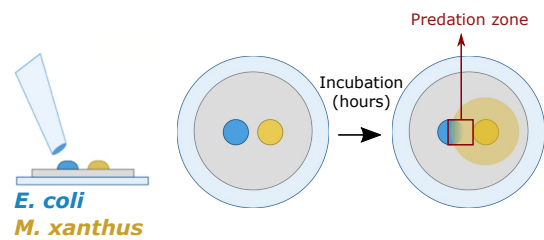
References

- Berleman, James E., Tatiana Chumley, Patricia Cheung, and John R. Kirby. 2006. "Rippling Is a Predatory Behavior in *Myxococcus Xanthus*." *Journal of Bacteriology* 188 (16): 5888–95.
- Bustamante, Víctor H., Irma Martínez-Flores, Hera C. Vlamakis, and David R. Zusman. 2004. "Analysis of the Frz Signal Transduction System of *Myxococcus Xanthus* Shows the Importance of the Conserved C-Terminal Region of the Cytoplasmic Chemoreceptor FrzCD in Sensing Signals." *Molecular Microbiology*. <https://doi.org/10.1111/j.1365-2958.2004.04221.x>.
- Chen, Jianxu, Mark S. Alber, and Danny Z. Chen. 2016. "A Hybrid Approach for Segmentation and Tracking of *Myxococcus Xanthus* Swarms." *IEEE Transactions on Medical Imaging* 35 (9): 2074–84.
- Chow, S. K., H. Hakoziaki, D. L. Price, N. A. B. MacLean, T. J. Deerinck, J. C. Bouwer, M. E. Martone, S. T. Peltier, and M. H. Ellisman. 2006. "Automated Microscopy System for Mosaic Acquisition and Processing." *Journal of Microscopy* 222 (Pt 2): 76–84.
- Ducret, Adrien, Ellen M. Quardokus, and Yves V. Brun. 2016. "MicrobeJ, a Tool for High Throughput Bacterial Cell Detection and Quantitative Analysis." *Nature Microbiology* 1 (7): 16077.
- Dworkin, Martin. 1963. "NUTRITIONAL REGULATION OF MORPHOGENESIS IN MYXOCOCCUS XANTHUS." *Journal of Bacteriology* 86 (1): 67–72.
- Falk, Thorsten, Dominic Mai, Robert Bensch, Özgün Çiçek, Ahmed Abdulkadir, Yassine Marrakchi, Anton Böhm, et al. 2019. "U-Net: Deep Learning for Cell Counting, Detection, and Morphometry." *Nature Methods* 16 (1): 67–70.
- Greener, Joe G., Shaun M. Kandathil, Lewis Moffat, and David T. Jones. 2021. "A Guide to Machine Learning for Biologists." *Nature Reviews. Molecular Cell Biology*, September. <https://doi.org/10.1038/s41580-021-00407-0>.
- Hallou, Adrien, Hannah G. Yevick, Bianca Dumitrascu, and Virginie Uhlmann. 2021. "Deep Learning for Bioimage Analysis in Developmental Biology." *Development* 148 (18). <https://doi.org/10.1242/dev.199616>.
- Keane, Ryan, and James Berleman. 2016. "The Predatory Life Cycle of *Myxococcus Xanthus*." *Microbiology* 162 (1): 1–11.
- Liu, Xiaomin, Cameron W. Harvey, Haitao Wang, Mark S. Alber, and Danny Z. Chen. 2012. "Detecting and Tracking Motion of *Myxococcus Xanthus* Bacteria in Swarms." *Medical Image Computing and Computer-Assisted Intervention: MICCAI ... International Conference on Medical Image Computing and Computer-Assisted Intervention* 15 (Pt 1): 373–80.
- Muñoz-Dorado, José, Francisco J. Marcos-Torres, Elena García-Bravo, Aurelio Moraleda-Muñoz, and Juana Pérez. 2016. "Myxobacteria: Moving, Killing, Feeding, and Surviving Together." *Frontiers in Microbiology* 7 (May): 781.
- Paintdakhi, Ahmad, Bradley Parry, Manuel Campos, Irnov Irnov, Johan Elf, Ivan Surovtsev, and Christine Jacobs-Wagner. 2016. "Oufiti: An Integrated Software Package for High-Accuracy, High-Throughput Quantitative Microscopy Analysis." *Molecular Microbiology* 99 (4): 767–77.
- Panigrahi, Swapnesh, Dorothée Murat, Antoine Le Gall, Eugénie Martineau, Kelly Goldlust, Jean-Bernard Fiche, Sara Rombouts, Marcelo Nöllmann, Leon Espinosa, and Tâm Mignot. 2021. "MiSiC, a General Deep Learning-Based Method for the High-Throughput Cell Segmentation of Complex Bacterial Communities." *eLife* 10 (September). <https://doi.org/10.7554/eLife.65151>.

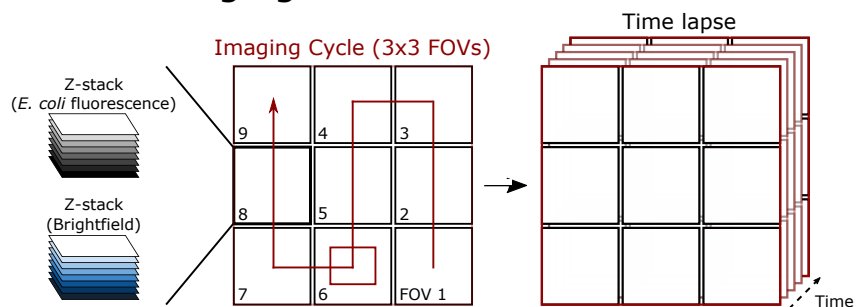
- Patra, Pintu, Kimberley Kissoon, Isabel Cornejo, Heidi B. Kaplan, and Oleg A. Igoshin. 2016. "Colony Expansion of Socially Motile Myxococcus Xanthus Cells Is Driven by Growth, Motility, and Exopolysaccharide Production." *PLoS Computational Biology* 12 (6): e1005010.
- Price, Diana L., Sunny K. Chow, Natalie A. B. Maclean, Hiroyuki Hakozaiki, Steve Peltier, Maryann E. Martone, and Mark H. Ellisman. 2006. "High-Resolution Large-Scale Mosaic Imaging Using Multiphoton Microscopy to Characterize Transgenic Mouse Models of Human Neurological Disorders." *Neuroinformatics* 4 (1): 65–80.
- Ronneberger, Olaf, Philipp Fischer, and Thomas Brox. 2015. "U-Net: Convolutional Networks for Biomedical Image Segmentation." In *Medical Image Computing and Computer-Assisted Intervention – MICCAI 2015*, 234–41. Springer International Publishing.
- Saaty, Thomas L. 1986. "Absolute and Relative Measurement with the AHP. The Most Livable Cities in the United States." *Socio-Economic Planning Sciences* 20 (6): 327–31.
- Shorten, Connor, and Taghi M. Khoshgoftaar. 2019. "A Survey on Image Data Augmentation for Deep Learning." *Journal of Big Data* 6 (1): 60.
- Spormann, A. M., and A. D. Kaiser. 1995. "Gliding Movements in Myxococcus Xanthus." *Journal of Bacteriology* 177 (20): 5846–52.
- Stylianidou, Stella, Connor Brennan, Silas B. Nissen, Nathan J. Kuwada, and Paul A. Wiggins. 2016. "SuperSegger: Robust Image Segmentation, Analysis and Lineage Tracking of Bacterial Cells." *Molecular Microbiology* 102 (4): 690–700.
- Van Valen, David A., Takamasa Kudo, Keara M. Lane, Derek N. Macklin, Nicolas T. Quach, Mialy M. DeFelice, Inbal Maayan, Yu Tanouchi, Euan A. Ashley, and Markus W. Covert. 2016. "Deep Learning Automates the Quantitative Analysis of Individual Cells in Live-Cell Imaging Experiments." *PLoS Computational Biology* 12 (11): e1005177.
- Zhang, Yong, Adrien Ducret, Joshua Shaevitz, and Tãm Mignot. 2012. "From Individual Cell Motility to Collective Behaviors: Insights from a Prokaryote, Myxococcus Xanthus." *FEMS Microbiology Reviews* 36 (1): 149–64.

Figure 1

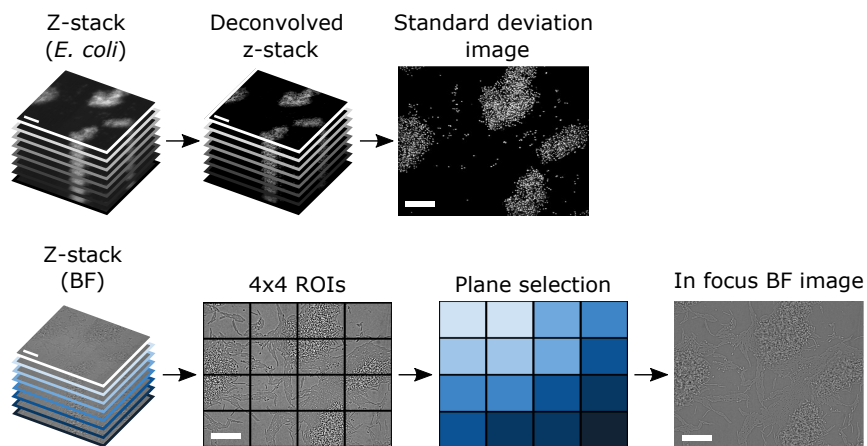
A Sample preparation



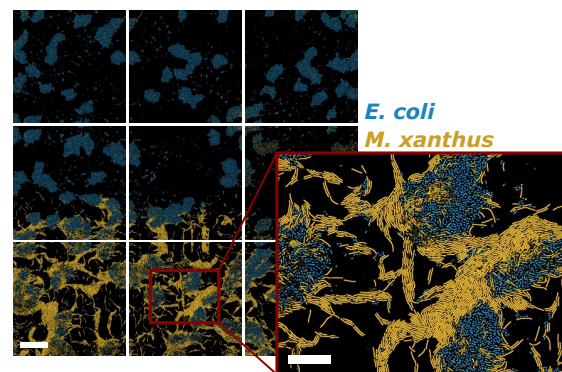
B Mosaic Imaging



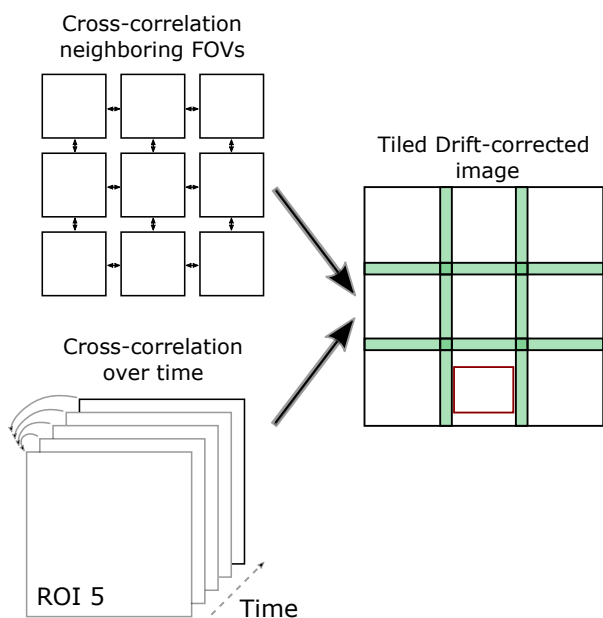
C Image pre-processing



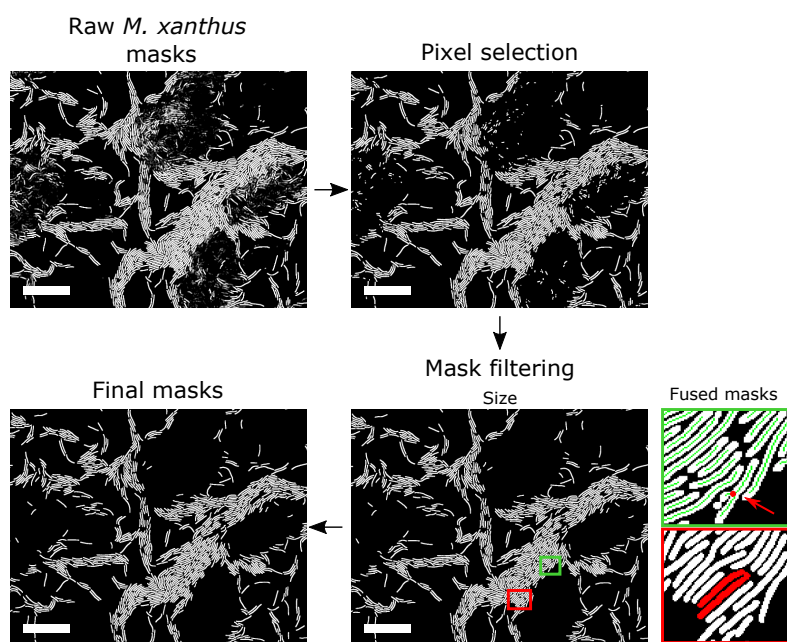
D Semantic segmentation



E Image post-processing



F Mask post-processing



G Single-cell tracking

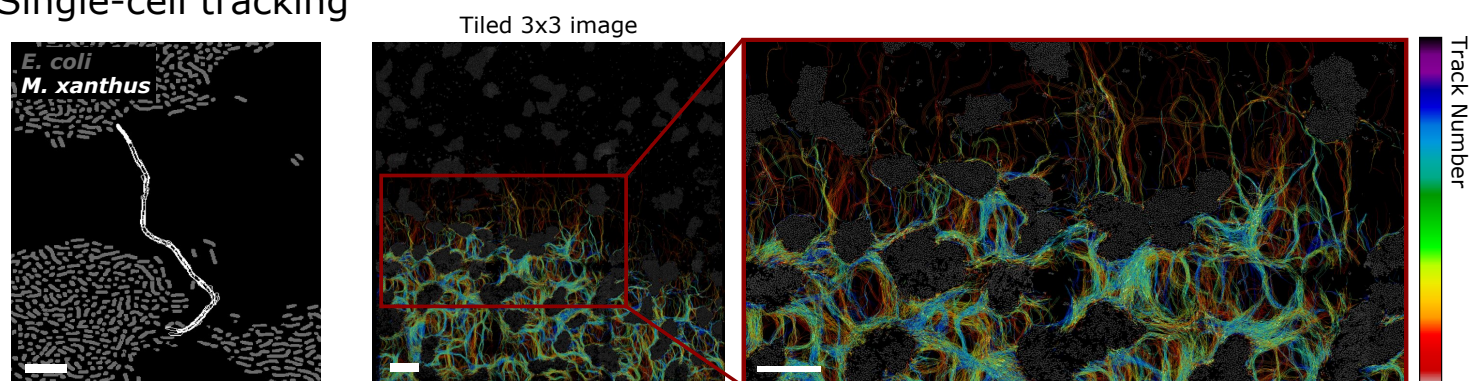
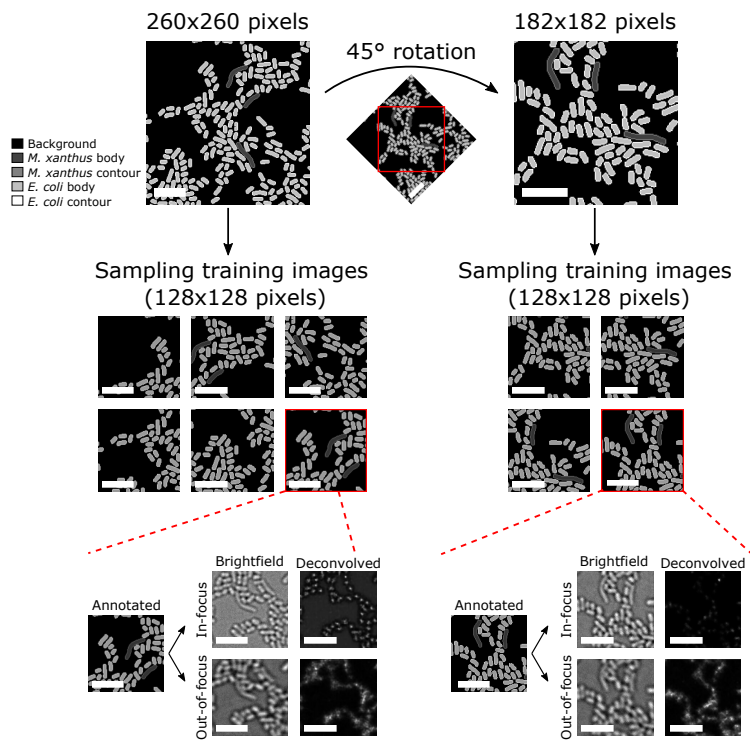


Figure 2

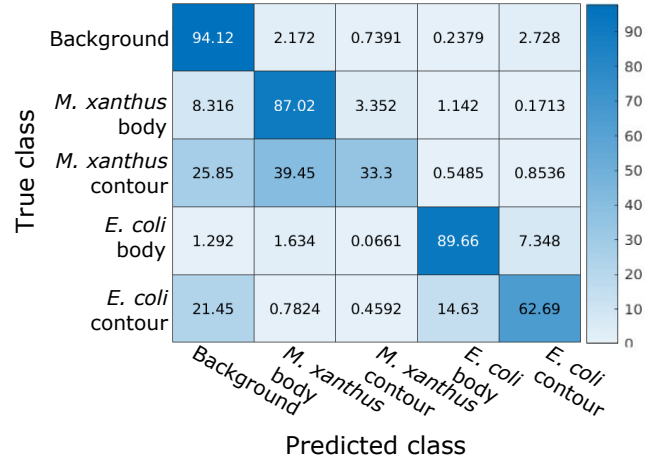
A

Training images



B

Normalized Confusion Matrix (%)



C

Semantic segmentation

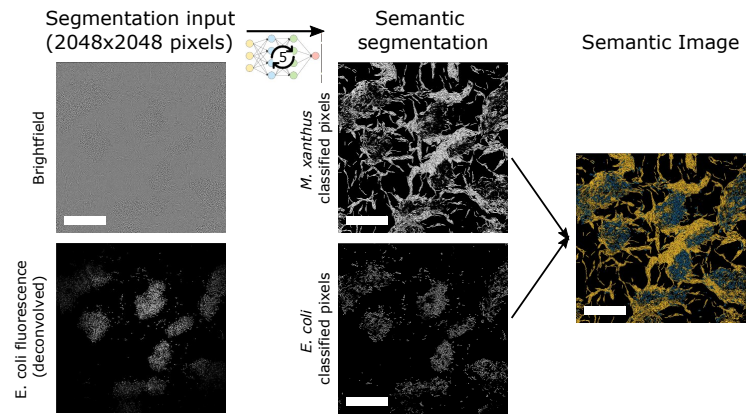
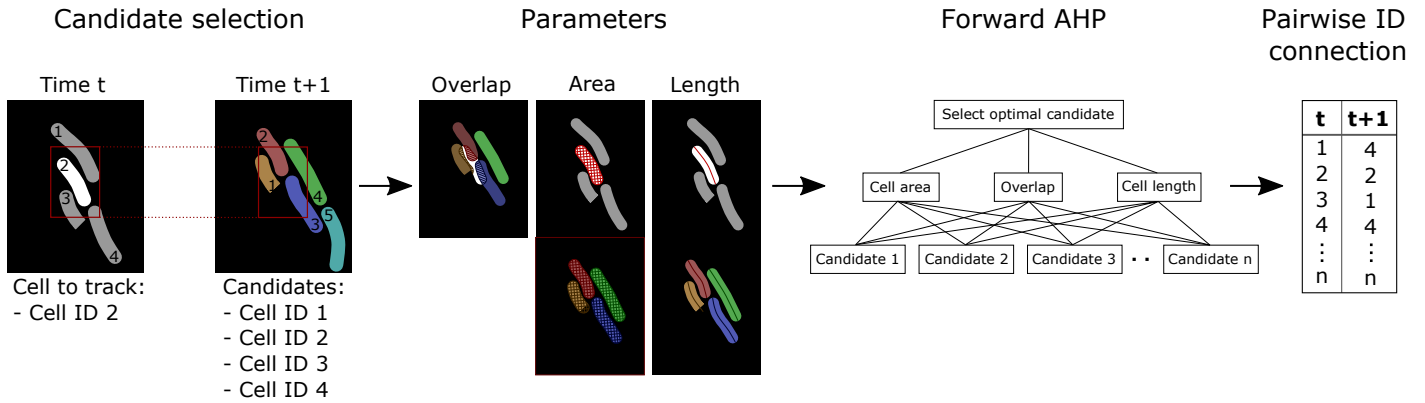
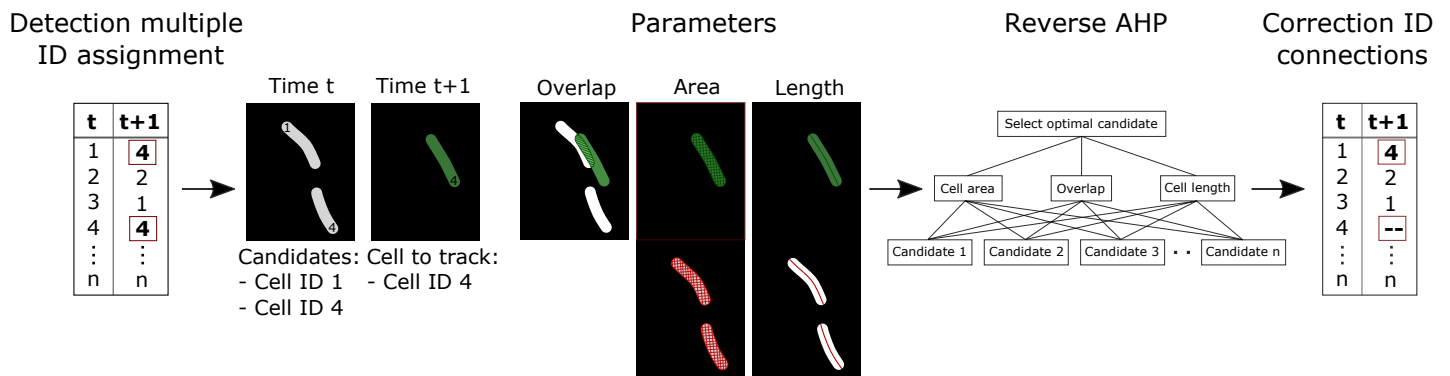


Figure 3

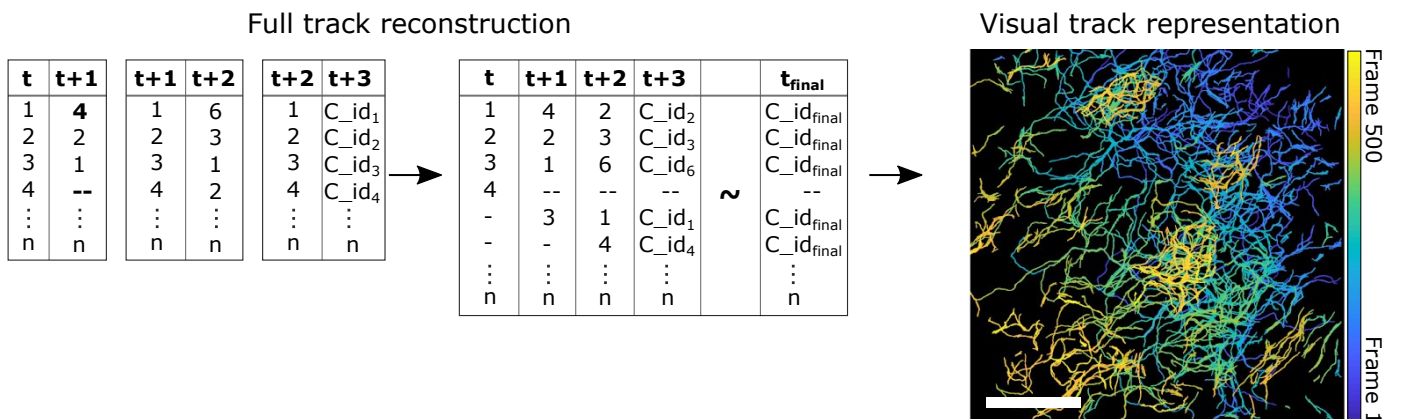
A Pairwise tracking



B Filtering PW tracks



C Track reconstruction



2 Multi-scale dynamic imaging reveals synergistic interplay between specialized cells in multicellular bacterial communities

Multi-scale dynamic imaging reveals synergistic interplay between specialized cells in multicellular bacterial communities

Sara Rombouts¹, Antoine Le Gall¹, Jean-Bernard Fiche¹, Anna Mas¹, Tâm Mignot², Marcelo Nollmann¹

¹ *Centre de Biochimie Structurale, CNRS UMR 5048, INSERM U1054, Université de Montpellier, 60 rue de Navacelles, 34090, Montpellier, France*

² *Laboratoire de Chimie Bactérienne, Marseille, France.*

Abstract

Collective organisms in nature are capable of a wide range of motility patterns to find food, reproduce or avoid predation. Importantly, the motility characteristics of individuals must be flexible and efficiently transmitted from the individual to the scale of the population to quickly adapt to environmental changes. Remarkably, multicellular systems can also display collective movement to achieve similar goals. *Myxococcus xanthus*, a soil predatory bacterium, assembles multicellular biofilms to collectively predate on other microorganisms. To achieve this, *M. xanthus* uses two genetically-independent motility molecular machines. Adventurous (A) motility drives the movement of individual cells to forage, while social (S) motility powers the collective motion of large groups of cells behind the invasion front. Here, we investigated the roles and interplay between these motility systems during *M. xanthus* predation by developing a novel multiscale cell-tracking method to follow single prey and predator cells in dense biofilms over extended time periods and areas. We found that foraging groups comprise both A- and S-motile cells, with A-motility being key to increase foraging area, ensure directional movement, and form trails. Surprisingly, A-motile cells were frequently present in large multicellular groups and their presence drastically affected their dynamic behavior. As a consequence, collective cell groups failed to follow trails efficiently, resulting in a diminished performance. Finally, we show that the synergistic action of A- and S-motile cells within collective groups led to increased prey killing. Together, our results show how individuals coordinate the collective behavior of specialized groups of cells and synergistically enhance colony adaptation and efficiency of predation.

Introduction

Collective movement is employed by many organisms, including fish, birds and ants, for the rapid exploration and predation of local resources (“Collective Motion” 2012). Remarkably, multicellular systems can also display collective movement to achieve similar goals. For instance, neutrophils swarming to kill invading microorganisms (Chtanova et al. 2008; Urban and Backman 2020; Kienle and Lämmermann 2016), and bacterial predation within the gut microbiota (Kern et al. 2021) or in natural ecosystems (Thiery and Kaimer 2020).

Myxococcus xanthus is a social bacterium that assembles multicellular biofilms (swarms) to collectively hunt and attack other microorganisms, including bacteria, fungi and yeast by a wolf-pack mechanism (Kaiser 2003; Muñoz-Dorado et al. 2016; Mercier and Mignot 2016; Thiery and Kaimer 2020). To achieve this aim, *M. xanthus* cells glide over solid surfaces by two independent motility mechanisms (Kaiser 2003; Nan and Zusman 2011). Social (S-) motility pulls cells forward by extending and retracting Type IV pili (Merz et al. 2000; Skerker and Berg 2001), whereas Adventurous (A-) gliding assembles a multicomponent focal adhesion engine powered by proton-motive force to propel the cell (Mignot et al. 2007; Faure et al. 2016). Notably, since their discovery (Hodgkin and Kaiser 1977), A- and S-motility were thought to specialize in entirely different tasks: A-motility in driving the movement of single cells at the colony edges (Kaiser 2003; Mercier and Mignot 2016), and S-motility in promoting the multi-cellular, coordinated movement of cells within swarms (Kaiser 1979; Muñoz-Dorado et al. 2016; Mercier and Mignot 2016). More recently, A-motility and contact-dependent killing were shown to be necessary for prey colony penetration (Seef et al. 2021). However, the specific roles, added values, and possible synergies of these motility systems during predation are unknown.

Here, we investigated the roles of each of these motility mechanisms during *Myxococcus* predation by developing a novel high-throughput method to track single prey and predator cells in dense biofilms over extended periods, with high temporal and spatial resolutions. This technology allowed us to detect four multicellular groups of cells with distinct properties. Notably, we found that A-motile cells are present in all multicellular groups, including swarms, and are required to ensure their directional movement. In addition, A-motility within multicellular groups was needed for their ability to create and to follow trails during predation. Finally, efficient prey killing required the synergistic action of both A- and S-motilities.

Results

Monitoring dynamics of predation at single-cell resolution

We were interested in studying the dynamics of bacterial predation with single-cell resolution. For this, we implemented a time-resolved version of bactoHubble, an imaging-based method that enables visualization of whole bacterial communities with single-cell resolution (Panigrahi et al. 2021). For our implementation, we built a robotized microscope able to acquire 3D, multiple-color images of large areas at diffraction-limited resolutions for long time periods (~hours) (Fig. 1A). Three-dimensional acquisitions enabled correction of axial drift and compensation of axial deformations in the substrate by adaptive reprojection, which produced in-focus 2D images (Methods). To cope with this high acquisition throughput —over ten thousand images per experiment— we implemented a deep learning automatic semantic segmentation approach coupled to an algorithm that links cell masks at different times to enable the retrieval of single-cell trajectories in 2D over long periods (~7 hours) (Fig. 1B) (Methods, and Rombouts *et al.*, *in preparation*).

Next, we used a two-pronged approach to retrieve spatial organization information from semantic, single-cell segmentation of prey and predator (Fig. 1C). First, we produced a Voronoi tessellation based on the middle points of the backbones of each *M. xanthus* mask (Fig. 1D, and Methods). Thus, the area of the polygon associated to each cell mask provided a proxy for local cell density: *M. xanthus* cells with large voronoi areas were relatively isolated from other *M. xanthus* cells, whereas cells associated with small voronoi areas were located in high cell density regions (Fig. 1D, arrows). Second, we partitioned groups of *M. xanthus* cells into clusters by linking together cells located in close spatial proximity (Fig. 1E, and Methods), and calculated the number of cells in each cluster and its size. These cluster statistics were associated with voronoi local density measurements to quantify the local environment of each single *M. xanthus* cell at each specific time during predation.

By representing each *M. xanthus* cell by its density and cluster size, we observe that single cells tend to scatter along an L-shaped, continuous distribution (Fig. 1F). From this distribution, we defined four cell classes (Fig. 1G): (1) scouts are small groups of cells (1-20) isolated from the main colony, typically localizing ahead of the forefront of the invading wave; (2) swarm cells lie within large cell clusters (>600 cells) and are always closely packed with other cells; (3) loners form small clusters of only 1-2 cells and lie close to the colony forefront; and (4) rafts form smaller clusters than swarms and occupy busy regions in proximity of the forefront. The full significance of this classification emerges when the behavior of A- or S- mutants during *E. coli* predation are explored.

Loss of S-motility (A+S⁻, Δ pilA) led to colonies displaying scouts, loners and rafts, but not swarms (Fig. 1H, blue arrow), consistent with the classical result of Hodkin (Dale Kaiser 2003). In contrast, loss of A-motility (A-S⁺ Δ GltJ-Nter222) produced communities with scouts, loners, rafts and swarms, similar to wild-type (Fig. 1I). This result seems in contrast to the classical view by which A-motility is required to produce isolated single cells (Muñoz-Dorado et al. 2016). To understand this apparent discrepancy, we compared scout trajectories in wild-type and A-S⁺ communities (Fig. 1I, red arrow). We observed that scouts in A-S⁺ colonies traveled considerably shorter distances than wild-type or than A+S⁻ cells (Fig. 1J, see wild-type in Fig. 1G). Next, we analyzed the distributions of instantaneous speeds and overall directionality of movement for scouts in these three conditions. Notably, A-S⁺ scouts displayed a marked reduction in speed (Fig. 1K, Supplementary Fig. 1A), and a clear reduction in directed motion counterbalanced by a gain in Brownian and confined movements (Fig. 1L). This result is in line with the finding that during colony expansion single *M. xanthus* cells move only if they carry a complete A-motility system (Dale Kaiser 2003). All in all, these findings suggest that scouts that can rely on A-motility move at faster speeds and more directionally through the prey than purely S-motile scouts.

A-motile cells are present in all cell classes and are required to direct collective cell movement

To further understand the role of A-motility in collective cell movement, we imaged AglZ, an integral component of the Agl-Glt machinery that assembles polar clusters in A-motile cells (Mignot et al. 2007; Faure et al. 2016). Assembly of polar AglZ clusters is a necessary, but not a sufficient, condition for A-motility. As expected, small groups of cells often displayed polar AglZ clusters (Fig. 2A), consistent with our result that scouts and loner movement requires A-motility (Fig. 1). Surprisingly, however, small groups of cells (scouts/rafts) as well as cells in large cell groups (rafts/swarms) also frequently displayed polar AglZ clusters (Fig. 2B). Thus, these results would suggest that both A- and S-motile cells may be present within larger cell groups.

To test this hypothesis, we mixed cultures of mCherry-labeled A+S- cells with GFP-labeled A-S+ cells, spotted them together, and imaged them during predation (Fig. 2C). Notably, A+S- and A-S+ cells thoroughly intermingled both in small (scouts/rafts) and large (swarms) cell populations, in support of our previous observation (Fig. 2B). In addition, both motility mutants moved together away from the spotting site to reach the prey, consistent with both gliding machineries being active within both small and large cell groups. Taken together, these results suggest that A-motility may not only be used by isolated cells away from the forefront, but may also play a functional role in collective cell movements.

We tested this prediction by a multi-pronged approach. First, we monitored whether A-motility and S-motility mutants induced changes in cell populations by subtracting the density/cluster-size histograms of pure cultures of A-S+ and A+S- communities by that of wild-type communities (Fig. 2D). Interestingly, removal of A-motility led to an overall reduction in the accessible Voronoi area for rafts and swarms (Fig. 2D, cyan box), thus these collective cell groups tend to remain closer to the community forefront in absence of A-motility.

Next, we investigated the functional role of A-motility in the movement of collective clusters by measuring the instantaneous speed for different collective cell groups. In wild-type communities, larger cell groups tended to move faster than smaller groups (Fig. 2E, see Methods). To detect whether the lack of A- or S-motilities changed this behavior, we normalized speed/cluster-size histograms of A-S+ and A+S- by that of the wild-type (Figs. 2F-G). Remarkably, removal of A-motility led to a large decrease in instantaneous speeds for all cell classes (scouts/loners/rafts/swarms). Interestingly, removal of S-motility led to a smaller reduction in the instantaneous speeds of scouts, loners and rafts (swarms were not detected in this strain, Fig. 1H).

All in all, these results show that A-motile cells intermingle and play a functional role in the collective movement of all cell populations. Thus, an important question is whether collective cell groups are pre-established or can dynamically change during predation. To answer this question, we followed the criteria established above (Fig. 1F) to monitor whether single cells changed their state as scout/loner/raft/swarm during their movement. We represented these single-cell state changes using a line plot where each cell class was assigned to a corner of a square, thus transitions appear as straight lines between states (Fig. 2H). Changes between different cell states were common in single trajectories (Fig. 2I) and occurred very frequently (Fig. 2J).

To get a more general picture of this behavior, we overlapped single-cell trajectories color-coded by trail density (Fig. 2K). The most common transitions were between swarms and rafts, thus rafts frequently break away from swarms but can also join them back. Interestingly, single cells disassembled from or joined rafts very often. The routes to become scouts typically involved either loner cells or rafts moving away from the forefront. Finally, single loner cells could also detach from swarms at a low frequency.

To quantify these population exchanges, we calculated the state transition probabilities (Fig. 2L). Remarkably, forward and reverse transitions between states were equally probable, ensuring

constant steady-state populations over our acquisition time. Importantly, state transitions were also frequent and symmetric in communities lacking A- or S-motility (Figs. 2M-N), thus state re-equilibration dynamics are independent of either motility system. Overall, these results show that transitions between collective cell groups are extremely frequent and bi-directional and do not require either motility system, ensuring that these groups remain properly populated during the advancement of the predation wave.

A-motile cells drive the ability of multicellular groups to form and follow trails

Next, we investigated the role of A-motility in the directional movement of collective cell groups by first analyzing whether rafts and swarms followed the movement of scouts. Interestingly, scouts that detached from swarms/rafts typically traveled away from the predation wave and in the direction of the prey (Fig. 3A). Strikingly, the trail left by the movement of scouts/loners was followed by other cells, and increased in width as more groups of cells used it (Fig. 3A). These observations suggest that A-motile cells are not only required to direct the movement of scouts (Figs. 1KL) but also of larger groups of cells (i.e. rafts and swarms).

We tested this hypothesis by segmenting the trails left by scouts (Fig. 1B, left) and those followed by loners/rafts/swarms (Fig. 1B, middle), and calculating the similarity index (SI) map between them. The SI map would be close to zero if scouts and loners/rafts/swarms followed different paths, and close to unity if their paths overlapped spatially. In fact, we observed that loners/rafts/swarms tended to follow the trails left by scouts over the whole predation front (Fig. 3B).

Then, we explored whether the ability of loners/rafts/swarms to follow scouts was impacted in a community unable to glide by A-motility (A-S+). Notably, the number and length of overlapping trails was dramatically affected in A-S+ communities (Fig. 3C). Interestingly, A+S- cells displayed similar trails than wild-type (Fig. 3D). These results can be quantified by calculating the histogram of similarity track lengths for these three communities (Fig. 3E), which clearly showed a large decrease in the number of common trails for all trail lengths for the A-S+ community. All in all, these results demonstrate that A-motility in rafts and swarms is required for their ability to follow the trails of scouts.

Finally, we investigated if large multicellular groups (rafts/swarms) also used trails within the active predation region. For this, we built a trail map by overlapping the single-cell trajectories of all cell groups color-coded by time (Fig. 3F). We clearly observe the existence of trails within the predation front, but also well behind the predation front occupied primarily by rafts and swarms. Thus, trails are widely used not only by scouts (Fig. 3B) but also by large multicellular groups.

To determine whether formation of these trails required A- or S-motilities, we constructed time-colored trail maps for A-S+ and A+S- communities (Fig. 3G-H). Notably, formation and use of trails within the predation zone requires A-motility. Interestingly, in A+S- communities, trails tend to display smaller widths likely due to the absence of swarms. To further characterize this behavior, we calculated the distribution of directionalities of all cell classes for wild-type, A-S+ and A+S- communities (Fig. 3I), and observed that loss of A-motility led to less directed and more confined/brownian motions. Overall, these results show that A-motility is key for the dynamic movements and strategies of all multicellular groups in the community ahead and behind the predation front.

Efficient killing requires the synergistic action of A- and S-motile cells

Finally, we set out to investigate why wild-type communities would require both motility mechanisms during predation, given that assembling and maintaining both gliding engines probably engenders a considerable cost, and that the role of S-motility during predation was unclear. To address these issues, we explored the consumption of prey during the process of predation by resorting to the ability of our method to perform semantic segmentation over large areas and over extended periods of time (Fig. 4A). From semantic segmentations we defined areas where active predation took place during our acquisition time, and regions that were not predated (Fig. 4A, right panel). To obtain an accurate estimation of prey consumption, we quantified the total fluorescence signal of the prey outside the predation zone (zone 2) and in a region within the predation area (zone 1, Fig. 4B). The total normalized prey fluorescence decreased monotonically over time in zone 1 due to photobleaching. Notably, the reduction in total normalized fluorescence was dramatically faster in zone 2 where prey was killed and consumed.

Next, we tested the roles of A- and S-motilities in this process by performing a similar quantification of predation assays from either A-S+ or A+S- communities. The absence of A-motile cells led to a noted reduction in the ability of myxococcus to kill prey, possibly linked to the reduced ability of this community to move directionally, efficiently explore ahead of the predation zone, and to form and follow trails. Interestingly, lack of S-motile cells led to a marked reduction in killing efficiency. Remarkably, these results show that efficient prey killing requires the synergistic action of both gliding machineries.

Discussion

The ability of *M. Xanthus* to glide on solid surfaces relies on two distinct and independent molecular machines that could be alternatively used to adapt to the mechanical properties of the substrate (Shi and Zusman 1993). Critically, since its discovery, A-motility was thought to be responsible for the movement of single cells, while S-motility was recognized as the hallmark for collective cell movement (Muñoz-Dorado et al. 2016; Zhang et al. 2012; Jonathan Hodgkin and Kaiser 1979). In this study, we developed an innovative multiscale single-cell tracking approach that allows us to revise these long standing views and shed light onto the manner in which these distinct molecular machines are deployed on the field.

Classically, A- and S-motile cells were thought to segregate spatially and to behave in two distinct manners: A-motile cells moving in isolation ahead of the invasion front acting as foragers searching for nutrients, and S-motile cells assembling large collective cell groups or “herds” (i.e. rafts, swarms) at the rear by promoting social interactions (Muñoz-Dorado et al. 2016). In contrast, our data shows that S-motile cells intermingled with A-motile cells in all cell groups, including herds. Thus, A- and S-motile cells are not spatially segregated during predation. Importantly, the speed and directionality of herds was impacted by the lack of A-motile cells. Therefore, the multiscale spatial intermingling of A-motile cells within herds drives their dynamic behaviour during predation (herding).

As expected, A-motility was not required for the formation of herds, consistent with previous studies (Jonathan Hodgkin and Kaiser 1979). This suggests that herding may instead play a role in guiding herds through existing trails layed by scouts, which in turn leads to the observed consolidation of the trail network behind the invasion front. The consolidation and use of existing trails likely increases foraging efficiency and prey consumption (Theraulaz and Bonabeau 1999). The presence of multiple A-motile cells within herds provides the ability of decentralized navigation (Manrique et al. 2019) which is known to increase the robustness and efficiency of reaching a target

in biological (Berni et al. 2012) and autonomous driving systems (Manrique et al. 2019). Future research, however, will be required to elucidate the mechanism by which A-motile cells may herd collective groups (Shamay-Tsoory et al. 2019).

Interestingly, in analogous animal ecosystems, herding dogs not only drive collective movement but also protect the herd by attacking predators. The coupling of A-motility and contact-dependent killing was recently shown to be the main mechanism driving the first steps of prey colony invasion (Seef et al. 2021). However, this mechanism may also be important for the penetration of prey micro-colonies within the prey-community. In this scenario, the presence of A-motile cells within herds would enhance the killing ability of herds after colony invasion.

Scouts and loners were observed with the same frequency in A+S- and A-S+ communities, challenging the finding that only A-motile cells are frequently found as isolated single cells (Muñoz-Dorado et al. 2016; Zhang et al. 2012; Jonathan Hodgkin and Kaiser 1979). However, S-motile scouts were mostly immobile, exhibited a reduced directionality, and displayed a limited ability to explore areas far from the predation front. Thus, while isolated and small groups of S-motile cells can be found ahead of the predation front, A-motility is required for their mobility and foraging ability.

Strikingly, collective cell groups frequently merged together or split apart, highlighting the plasticity and highly dynamic behavior of cells during predation. In addition, this finding suggests that collective cell groups are not pre-assembled and that there is likely a low energetic barrier for group fusion or splitting. Thus, groups can be made or unmade depending on the local environmental conditions to provide flexibility and adaptation. Interestingly, the transition frequencies between collective cell groups were in all cases symmetric, ensuring the long-term equilibrium of the system. This equilibrium may be perturbed to respond to local changes in prey distribution, providing another avenue for adaptation. Importantly, removal of either motility apparatus did not change the ability of collective groups to mix or split, but rather the transition frequencies and their final proportions at equilibrium. Fine tuning of transition frequencies would thus provide a mechanism to rapidly change the relative proportions of collective cell groups to adapt to the local ecosystem.

Early studies showed that A- and S-motilities enable *M. xanthus* to move on a wider range of substrates, from soft to hard, suggesting that both machines may be needed to provide flexibility and adaptation to the physical properties of the local environment (Shi and Zusman 1993). This arguably minor fitness gain was often deemed insufficient to outweigh the evolutionary burden of simultaneously maintaining both motility machines. Our results, however, show that A- and S- motile cells work in unison to synergistically drive predation. Critically, this combined action improves the efficiency of prey exploration and invasion, and leads to more efficient killing.

We are aware that the spatial organization of the prey community is likely to modulate the relative roles of A- and S-motilities during predation. For instance, A-motility may be more determinant than S-motility in close-knit prey communities, as the ability to penetrate the outer wall of these communities may depend acutely on A-motility and contact-dependent killing (Seef et al. 2021). Thus, the presence of cells with both motility systems in all collective cell groups enhances the ability of *M. xanthus* to adapt to the varying spatial organization and diversity of prey encountered in natural ecosystems. Finally, we envision that collective movement of A- and S-motile cells may enable *M. xanthus* communities to adapt their strategy to the defense and attack mechanisms of competing communities. All in all, these fitness advantages may largely outweigh the evolutionary costs associated with maintaining both motility systems.

Acknowledgements

This project was funded by the European Union's Horizon 2020 Research and Innovation Program (Grant ID 724429) (M.N.). We acknowledge the Bettencourt-Schueller Foundation for their prize 'Coup d'élan pour la recherche Française', the France-BioImaging infrastructure supported by the French National Research Agency (grant ID ANR-10-INBS-04, "Investments for the Future"). Additional funding was provided by the European Union's Horizon 2020 Research and Innovation Program (Grant ID 885145) (T.M.).

Methods

Bacterial strains

The bacterial strains used in this work can be found in the table below.

Strain	Genotype	Strain origin
<i>E. coli</i>	MG1655 wildtype	
<i>E. coli</i> HU-mCherry	MG1655 HU-mCherry	Espeli laboratory collection
<i>M. xanthus</i>	DZ2 wildtype	Mignot laboratory collection
<i>M. xanthus</i> cytosolic-sfGFP	DZ2 pSWU19-pm3068-sfGFP	Mignot laboratory collection
<i>M. xanthus</i> A+S-OMss-sfGFP	DZ2 Ω pilA pSWU19-PpilA-OMss-sfGFP	Mignot laboratory collection
<i>M. xanthus</i> A+S-OMss-sfGFP	DZ2 GltJ DNterm222 pSWU19-PpilA-OMss-sfGFP	Mignot laboratory collection
<i>M. xanthus</i> A+S-OMss-mCherry	DZ2 DpilA pSWU19-PpilA-OMss-mCherry	Mignot laboratory collection
<i>M. xanthus</i> AglZ-NeonGreen	Allelic replacement of <i>aglZ</i> by <i>aglZ-NeonGreen</i>	Mignot laboratory collection

Bacterial cultures

E. coli cells used in predation assays were grown overnight in 10 ml Luria-Bertani (LB) medium at 32°C under agitation (200 rpm). To ensure that *E. coli* cells were in exponential phase after overnight growth, a 1:10 dilution of the starter culture was made in fresh LB medium and incubated for approximately four hours.

M. xanthus cells were grown overnight in 10 ml Casitone Yeast Extract (CYE) rich medium as was described before (Bustamante et al. 2004) at 32°C under agitation (200 rpm), supplemented with antibiotics (Ampicillin 1 μ g/ml) when necessary. Cells were harvested when the OD₆₀₀ reached 0.1-0.5.

Predation assays

Bacterial predation was established in laboratory conditions by setting up a predation assay. In short, *E. coli* and *M. xanthus* cells were harvested from the LB and CYE media, respectively. Cells were concentrated by centrifugation on a tabletop centrifuge at 2100 g for 5 min at room temperature and resuspended in CF medium (10 mM MOPS (pH 7.6), 1 mM KH₂PO₄, 8 mM MgSO₄, 0.02% (NH₄)₂SO₄, 0.2% sodium citrate, 0.015% bacto casitone peptone). *M. xanthus* cells were concentrated to an OD₆₀₀ of 5, *E. coli* cells were concentrated to an OD₆₀₀ of 0.005. Cell suspensions of 1 μ l were spotted at close distance of approximately 1 mm on CF 1.5% agar pads supported on a coverslip.

The agar pads used for time lapse imaging were made with ultrapure agar (UltraPure Agarose 1000, Invitrogen) to limit autofluorescence by impurities in the agar solutions. Pads were made by pipetting 550 μ l of melted agar onto a 25mm coverslip and by placing a second coverslip on the drop of agar, allowing the latter to solidify between two flat surfaces. Once the agar pad was made, the top coverslip was removed and the agar was cut to a diameter of 20 mm.

The prepared predation assays were then placed onto a layer of CF 1.5% agar in a petri dish and the petri dish was closed with parafilm to avoid agar pad evaporation and drying. Samples were incubated 24h to 48h on 32°C to allow *M. xanthus* cells to invade the *E. coli* colony.

Microscopy

Fast time lapse and hubble imaging were done on a homemade fully-automated hardware-accelerated wide-field epifluorescence microscope built on a RAMM modular microscope system (Applied Scientific Instrumentation). Samples were imaged using a 60x Plan-Achromat water-immersion objective (NA = 1.2, Nikon, Japan). The objective lens was mounted on a closed-loop piezoelectric stage (Nano-F100, Mad City Labs Inc. - USA). Illumination was provided by a brightfield illumination source and 2 lasers (OBIS-488 nm and Sapphire-LP-561 nm, Coherent – USA). Images were acquired using a sCMOS camera (ORCA Flash 4.0V3, Hamamatsu – Japan), with a final pixel size calibrated to 106 nm. A custom-built autofocus system was used to correct for axial drift in real-time and maintain the sample in focus. Software-controlled microscope components, including camera, stages, brightfield illumination and lasers were run using a custom-made software package developed in LabView 2015 (National Instrument).

Hubble imaging

Hubble images, in which the predation assay is fully captured, was carried out by constructing a mosaic patchwork of MxN size. Each FOV of the mosaic overlaps with the neighbouring FOVs by 200 pixels. Acquisition of such a large mosaic was achieved by following a snake-like pattern. For each FOV a 3D stack of brightfield and fluorescence images was acquired of 12 planes interspaced with 250 nm. Laser powers were adjusted to have optimal signal for the target fluorescent proteins. Exposure times were set to 50 ms and brightfield illumination was decreased with a neutral density filter (OD 2).

Fast time lapse imaging

For imaging of the predation assay, the sample was covered with an imaging coverslip. The imaging coverslip was washed consecutively with acetone, Milli-Q water, 70% ethanol (v/v) and Milli-Q water, and flamed to remove any fluorescence impurities and residues. The coverslip was cooled down to room temperature and placed hermetically on the sample while avoiding bubbles between the sample and the coverslip. The sample was mounted in an attofluor and onto the microscope for imaging. A region of interest spanning an area of approximately 0.36 mm² was selected. This large area was imaged by constructing a mosaic patchwork of 3 by 3 fields of view (FOVs) or mosaic tiles of 2048x2048 pixels, each theoretically overlapping with 200 pixels. An imaging cycle, in which the 3-by-3 mosaic was imaged by sample displacement following a snake-like pattern, was thus made up of 9 consecutive acquisitions. For each FOV, a 3D-stack was acquired to account for sample tilt in brightfield and in the fluorescence channel of 561 nm for *E. coli* carrying a HU-mCherry fusion. An additional fluorescent channel was added for *M. xanthus* when the used strain was carrying a fluorescent protein as well. A 3D-stack was generally made up of 7-12 planes interspaced with 250-500 nm. Exposure times were set at 50 ms. The laser powers used were kept at low intensity to limit phototoxic effects on the live cells during time lapse acquisition. Brightfield illumination was attenuated with a neutral density filter with optical density two. Imaging cycles were generally completed in 30-40 seconds and were repeated 700 times to construct an hours-long time lapse series of the mosaic area.

Treatment of fast time lapse data

To increase imaging speed, all images from one imaging cycle were pooled into one DCIMG file. First, the DCIMG files were converted to tiff files with software from Hamamatsu and sorted for each FOV, channel and time point. Tiff images of the fluorescent channel of *E. coli* were deconvolved with Huygens Professional version 20.04 (Scientific Volume Imaging, the Netherlands, <https://svi.nl/>). Deconvolved *E. coli* stacks were z-projected by calculating the standard deviation. 3D brightfield stacks were converted to 2D images by dividing each stack in 16 ROIs of 512x512 pixels, selecting automatically or manually the in-focus plane for each ROI and restitching the 16 ROIs. The code for calculating the in-focus brightfield image (`im_straighter_FTL.m` or `im_straighter_FTL_manual.m`) can be found in https://github.com/jbfiche/DCIMG_to_TIFF_conversion/tree/master/Fast_TL_windows. 2D brightfield and *E. coli* fluorescence images were used as input for an in-house developed MATLAB code using a convolutional neural network with U-Net architecture for semantic segmentation (Ronneberger, Fischer, and Brox 2015; Van Valen et al. 2016). Semantic segmentation was performed with five independently trained networks to converge towards a high confidence result, outputting an image with pixel values representing the pixel assignment confidence to a given class. The code for semantic segmentation (`Reconstruct_image_FCN_FTL.m`) can be found in https://github.com/jbfiche/Deep_Learning_segmentation/tree/Myxo_segmentation_predation_fluo_Unet/For_image_reconstruction.

Segmented images were then used to reconstruct the mosaic image by tiling the 9 images. Exact image overlap for tiling was calculated by image-based pixel-resolution cross correlation. Drift in time was corrected by aligning the mosaic images based on cross correlation calculated from segmented images of stationary *E. coli* microcolonies. *M. xanthus* segments from mosaic images were post-processed to reduce segmentation artefacts. In short, binary masks were generated from the masks by exploiting the assignment of confidence values, masks were filtered for size and finally, tortuous masks and fused masks were rejected. *E. coli* masks were post-processed to avoid overlap between *E. coli* and *M. xanthus* masks and filtered for size to reject isolated pixels. The code for cross-correlation calculation (`MosaicImages_CC_BFNormalized_MyxoSegmented.py` and `Mosaic_DriftCorrection_GlidingRef_MiddelROI5.py`), and tiling, drift correction and mask post-processing (`function_DriftCorr_MosaicTiling_Ecoli.m`) can be found in https://github.com/SaraRombouts/ProjectFTL_Predation.

Single cell tracking

Single cell trajectories were reconstructed with an in-house developed MATLAB pipeline. For each timepoint in the time lapse image series, pairwise tracks were constructed between cells in frame k and cells in frame $k+1$. Briefly, the enlarged bounding box of the cell mask in frame k was utilized to select a number of possible candidates in frame $k+1$. Ultimately, the optimal candidate was found by ranking the candidates with Analytical Hierarchy Processing (AHP) (Saaty 1986) based on several parameters of the masks including cell area, cell length and mask overlap area between the cell and its candidates. To correct for multiple assignments of a candidate, an inverse AHP approach was used in which the optimal cell from frame k was selected for the candidate of frame $k+1$. Finally, pairwise tracks over all timepoints were combined to form complete single cell trajectories. The code for single-cell trajectory reconstruction (`function_Tracking_TiledMosaic.m`) can be found in https://github.com/SaraRombouts/ProjectFTL_Predation.

MSD

To characterize directionality of bacterial movement, individual bacterial trajectories were analysed with the Python trackpy package. For each track, the Mean Squared Displacement (MSD)

was computed and the five first time points were fitted with a power law. The resulting scaling exponent, α , was used to characterize the directionality of bacterial movement (from confined with $\alpha < 1$, brownian with $\alpha = 1$, to directed with $\alpha > 1$). The code used to calculate the MSD (Myxo_trackpy.py) can be found in https://github.com/SaraRombouts/ProjectFTL_Predation.

Speed

Instantaneous cell speed was calculated using the straight distance traveled in the five frames before and five frames after a given time point, normalized by the time between 10 frames. The code used to calculate speed (matfiles_to_umap_format.py) can be found in https://github.com/SaraRombouts/ProjectFTL_Predation.

Voronoi tessellation

To measure the local density of *M. xanthus* cells, a Voronoi tessellation was performed with the Voronoi function of MATLAB. The voronoi tessellation was calculated on the centers of the backbones of all masks that were included for tracking. Centers of gravity of the masks that were filtered for tortuosity and mask fusion based on branchpoints were included as well. For masks which contained a branchpoint in their backbone, the branchpoint was deleted, essentially breaking up the backbone. The centers of the newly generated backbones were calculated and included for the tessellation. For masks filtered out for tortuosity, the centers of the backbones were calculated as well and included for the tessellation. The area of the polygon to which the mask belongs was used as a measure for local density, with large polygon areas for low cell density and small polygon areas for high cell density. The code used to calculate the local density of *M. xanthus* cells (function_Voronoi_backbone_OverlapFlag.m) can be found in https://github.com/SaraRombouts/ProjectFTL_Predation.

Long range clustering

Long range clustering of cells was performed by dilating the binary cell masks of *Myxococcus xanthus* cells using a 10x10 pixels kernel ($\sim 1 \times 1 \mu\text{m}$). Then, merged cell masks were identified as clusters using the regionprops module of the skimage package in Python. For each identified cluster, the number of cells per cluster was determined and its size was measured as the area covered by the non dilated cell masks comprising each cluster. The code used to perform long-range clustering (scratch_multiscale_segmentation.py) can be found in https://github.com/SaraRombouts/ProjectFTL_Predation.

Classes

Bacterial populations were categorized into four groups: loners, scouts, rafts and swarms. Two criteria were used to determine the group to which a cell belongs to at each time point in the time lapse: the Voronoi cell density, V , and the number of cells per cluster, N . For loners: $\log_{10}(V) \leq 4.5$ and $N \leq 2$; for scouts: $\log_{10}(V) \leq 4.5$ and $N \leq 20$; for rafts: $2 < N \leq 600$; and for swarms: $600 < N$. When scouts functionality was used as an additional criterion, only cells with a speed higher than 3 pixels/frame were selected. The code used to cluster cells into classes (Figure2_myxo_classes.py) can be found in https://github.com/SaraRombouts/ProjectFTL_Predation.

2D Histograms

Two dimensional data points and trajectories histograms were both computed using the Python Datashader package, with canvas mapping data to pixels as points or lines, respectively. For histogram differences, the histograms were first normalized by the sum of their bin values. For histograms of trajectory fluxes, the spatial coordinates of each bacterial trajectory were replaced with new coordinates corresponding to the classification of the bacteria, being either loner, scout, raft or swarm, at each time point along the track with Gaussian noise added to reduce the overlap of the tracks. The code used to reproduce the histograms in Figures 1 and 2

(Figure1_2D_Histograms_ratio_2.py, Figure1_2D_Histograms.py, Figure1_Histo1D_speed_scouts.py, Figure2_2D_Histograms_ratio_0.py, scratch_compute_tracks_datashader_maps.py) can be found in https://github.com/SaraRombouts/ProjectFTL_Predation.

Similarity index map

To quantify the similarity between the trajectories of the scouts and the rest of the population, the trajectories of the two populations were split apart to map them on separated 2D arrays. Each array map was then binarized and used to compute a structural similarity index map with the Python Scikit-image package (sliding window of three pixels). Finally, the resulting similarity index map was binarized to extract the area of each portion of trajectory shared by the two populations. These areas of shared trajectories were used to quantify the amount of scout trajectories shared with the rest of the bacterial population. The code used to calculate similarity index maps (Figure3_load_and_analyse_tracks_datashader_maps.py) can be found in https://github.com/SaraRombouts/ProjectFTL_Predation.

Prey consumption

To quantify the consumption of prey cells by *M. xanthus* during invasion, the fluorescence of *E. coli* HU-mCherry was used. For each time point in the movies, the fluorescence intensity of the central plane of each z-stack was first normalized by the Gaussian profile of the excitation laser and then projected along the perpendicular direction of invasion. The mean intensity was then truncated into three equal parts to quantify *E. coli* HU-mCherry intensity changes in the portion of the field of view (FOV) that gets invaded by *M. xanthus* cells during the acquisitions (bottom part of the stitched FOV) and in a portion that does not get invaded during the acquisition (Top part of the stitched FOV), the central portion not being used. For the bottom and top parts of the FOV, the mean fluorescence intensity of *E. coli* HU-mCherry was quantified for each frame of the movies to characterize the disappearance of *E. coli* cells over time. The code used to calculate prey consumption (Figure4_EC_killing_load.py) can be found in https://github.com/SaraRombouts/ProjectFTL_Predation.

AgIZ foci detection

AgIZ foci were automatically detected to highlight the position of AgIZ complexes in single cells. For this, the raw fluorescent z-stacks were first band pass filtered to remove noise and low spatial frequencies in single planes and then a local normalization was applied to equalize signal strength heterogeneities due to the Gaussian excitation profile. Finally, the four central images of the z-stack were summed and used to localize AgIZ complexes as diffraction-limited spots using the DAOSTarFinder utility from the Astropy package (<https://www.astropy.org/>).

Figure Legends

Figure 1: Multiscale dynamic imaging reveals four distinct cell classes.

A) Schematic of large-scale imaging and semantic segmentation of the predation zone. Scalebars = 10 μm .

B) Example of a single-cell trajectory (yellow line) reconstructed by connecting segmented cell masks of the same cell (green mask) over time. Scalebar = 5 μm .

C) Example of a semantically segmented large ROI at the predation front containing the masks for *M. xanthus* (white) and *E. coli* (red) (left) Scalebar = 100 μm . The zoom of the boxed area shows single segmented cells in high and low cell density areas (right) Scalebar = 20 μm .

D) Voronoi tessellation of a large ROI at the predation forefront calculated from the middle points of the *M. xanthus* mask backbones (left) Scalebar = 100 μm . The zoom of the boxed area shows small polygon areas for *M. xanthus* cells in high *M. xanthus* cell density regions and large polygon areas for cells in low *M. xanthus* cell density regions (right) Scalebar = 20 μm .

E) Long-range clustering of *M. xanthus* cells in close spatial proximity in a large ROI at the predation forefront (left) Scalebar = 100 μm . The zoom of the boxed area shows several cell clusters with varying cluster sizes (right) Scalebar = 20 μm .

F) 2D Voronoi area-cluster size histogram for wildtype. Red, yellow, green and blue boxed areas correspond to scout, loner, raft and swarm cell classes, respectively.

G) Spatial occupation of scout, loner, raft and swarm trajectories for wildtype at the predation forefront. Yellow line delimitates the predation front, the green arrow indicates the direction in which *M. xanthus* predator cells move through the prey colony (predation direction). Scalebars = 100 μm .

H) 2D Voronoi area-cluster size histogram for A-motile cells (A+S-). Blue arrow points to non-existent swarm cell class.

I) 2D Voronoi area-cluster size histogram for S-motile cells (A-S+). Red arrow points to scout cell class.

J) Spatial occupation of scouts trajectories in S-motile communities (A-S+). Scalebar = 100 μm .

K) Histogram of instantaneous speed of scouts cells in wildtype, A-motile (A+S-) and S-motile (A-S+) communities.

L) Histogram of movement directionality of scouts cells in wildtype, A-motile (A+S-) and S-motile (A-S+) communities with directionality < 1 being confined motion, = 1 being Brownian motion and > 1 being directed motion.

Figure 2: A-motile cells mix with S-motile cells in all population classes.

A-B) Fluorescence image of A-motility complexes (AglZ-NeonGreen) in isolated cells (A) or in groups of cells (B) at the predation front. Green circles highlight automatically detected AglZ-clusters in single cells. Scalebar = 10 μm .

C) Migration of a 50/50 mixed community of A-motile (A+S-) (outer-membrane-ssGFP, green) and S-motile (A-S+) (outer-membrane-mCherry, red) cells at the predation front towards *E. coli* micro-colonies (top left, bright field).

D) Difference 2D Voronoi area-cluster size histogram of A+S- and wildtype. Cyan box highlights the increased population with reduced Voronoi areas for A-motile (A+S-) cells.

- E) 2D instantaneous speed-cluster size histogram of wildtype. Red, yellow, green and blue boxed areas correspond to scout, loner, raft and swarm cell classes, respectively.
- F) Difference 2D instantaneous speed-cluster size histogram of A+S- and wildtype.
- G) Difference 2D instantaneous speed-cluster size histogram of A-S+ and wildtype.
- H) Schematic line plot of cell class transitions observed in a single-cell trajectory.
- I) Examples of state transitions occurring in single-cell trajectories of wildtype cells. Track IDs are indicated in each example.
- J) Histogram of number of transitions per trajectory.
- K) Overlay of state transitions from all wildtype trajectories.
- L) State transition probabilities for wildtype.
- M-N) Same representations as in panels I,K and L but for A-motile (A+S-) cells (M) and S-motile (A-S+) cells (N).

Figure 3: A-motile cells drive collective cell movement along trails.

- A) Example of scout cells (red line) traveling away from an *E. coli* island (bright field) followed by rafts (purple lines).
- B-D) Trail maps of scout and loner/raft/swarm cells and similarity index map for wildtype (B), A-S+ (C) and A+S- cells (D). Yellow lines delimitate the predation front. Scalebars = 100 μm . Scalebars zooms of boxed areas = 20 μm .
- E) Histogram of length of overlapping tracks (Similarity track length) for wildtype, A-S+ and A+S-.
- F-H) Overlays of all trajectories for wildtype (F), S-motile (A-S+) cells (G) and A-motile (A+S-) cells (H). Green arrows indicate the predation direction, yellow lines delimitate the predation front. White arrows in the zoom of the boxed areas point to examples of trails.
- I) Histogram of movement directionality of all cell classes for wildtype, A-motile (A+S-) and S-motile (A-S+) communities with directionality < 1 being confined motion, = 1 being Brownian motion and > 1 being directed motion.

Figure 4: A- or S-motility mutations affect predation efficiency.

- A) Evolution of predation over time at the predation forefront visualised with semantically segmented large ROI containing the masks for *M. xanthus* (white) and *E. coli* (green). Two zones were defined: i) where no predation occurred (orange boxed area) and ii) predation zone (blue boxed area). Scalebars = 100 μm .
- B) Evolution of the total fluorescence signal from *E. coli* cells over time in zone: i) no predation and ii) predation. Scalebars = 100 μm .
- C-E) Quantification of the total fluorescence signal from *E. coli* cells over time in zone 1 and 2 for wildtype (C), S-motile (A-S+) (D) and A-motile (A+S-) (E) predators.

Supplementary figure 1

- A) 2D Voronoi area-cluster size histograms for wildtype, S-motile cells (A-S+) and A-motile (A+S-) cells thresholded for normalized distance higher than 2 pixels/track length.

B) Spatial occupation of scout, loner, raft and swarm trajectories for S-motile (A-S+) cells at the predation forefront. Yellow line delimitates the predation front, the green arrow indicates the direction in which *M. xanthus* predator cells move through the prey colony (predation direction).

C) Spatial occupation of scout, loner, raft and swarm trajectories for A-motile (A-S-) cells at the predation forefront.

D) Cluster size-number of cells per cluster scatter plot.

References

- Berni, Jimena, Stefan R. Pulver, Leslie C. Griffith, and Michael Bate. 2012. "Autonomous Circuitry for Substrate Exploration in Freely Moving *Drosophila* Larvae." *Current Biology: CB* 22 (20): 1861–70.
- Bustamante, Víctor H., Irma Martínez-Flores, Hera C. Vlamakis, and David R. Zusman. 2004. "Analysis of the Frz Signal Transduction System of *Myxococcus Xanthus* Shows the Importance of the Conserved C-Terminal Region of the Cytoplasmic Chemoreceptor FrzCD in Sensing Signals." *Molecular Microbiology*. <https://doi.org/10.1111/j.1365-2958.2004.04221.x>.
- Chtanova, Tatyana, Marie Schaeffer, Seong-Ji Han, Giel G. van Dooren, Marcelo Nollmann, Paul Herzmark, Shiao Wei Chan, et al. 2008. "Dynamics of Neutrophil Migration in Lymph Nodes during Infection." *Immunity* 29 (3): 487–96.
- "Collective Motion." 2012. *Physics Reports* 517 (3-4): 71–140.
- Faure, Laura M., Jean-Bernard Fiche, Leon Espinosa, Adrien Ducret, Vivek Anantharaman, Jennifer Luciano, Sébastien Lhospice, et al. 2016. "The Mechanism of Force Transmission at Bacterial Focal Adhesion Complexes." *Nature*, October. <https://doi.org/10.1038/nature20121>.
- Hodgkin, J., and D. Kaiser. 1977. "Cell-to-Cell Stimulation of Movement in Nonmotile Mutants of *Myxococcus*." *Proceedings of the National Academy of Sciences of the United States of America* 74 (7): 2938–42.
- Hodgkin, Jonathan, and Dale Kaiser. 1979. "Genetics of Gliding Motility in *Myxococcus Xanthus* (Myxobacterales): Two Gene Systems Control Movement." *Molecular and General Genetics MGG*. <https://doi.org/10.1007/bf00270004>.
- Kaiser, D. 1979. "Social Gliding Is Correlated with the Presence of Pili in *Myxococcus Xanthus*." *Proceedings of the National Academy of Sciences of the United States of America* 76 (11): 5952–56.
- Kaiser, Dale. 2003. "Coupling Cell Movement to Multicellular Development in Myxobacteria." *Nature Reviews. Microbiology* 1 (1): 45–54.
- Kern, Lara, Suhaib K. Abdeen, Aleksandra A. Kolodziejczyk, and Eran Elinav. 2021. "Commensal Inter-Bacterial Interactions Shaping the Microbiota." *Current Opinion in Microbiology* 63 (August): 158–71.
- Kienle, Korbinian, and Tim Lämmermann. 2016. "Neutrophil Swarming: An Essential Process of the Neutrophil Tissue Response." *Immunological Reviews* 273 (1): 76–93.
- Manrique, Pedro D., Mason Klein, Yao Sheng Li, Chen Xu, Pak Ming Hui, and Neil F. Johnson. 2019. "Getting Closer to the Goal by Being Less Capable." *Science Advances* 5 (2): eaau5902.
- Mercier, Romain, and Tâm Mignot. 2016. "Regulations Governing the Multicellular Lifestyle of *Myxococcus Xanthus*." *Current Opinion in Microbiology* 34 (December): 104–10.
- Merz, A. J., M. So, and M. P. Sheetz. 2000. "Pilus Retraction Powers Bacterial Twitching Motility." *Nature* 407 (6800): 98–102.
- Mignot, Tâm, Joshua W. Shaevitz, Patricia L. Hartzell, and David R. Zusman. 2007. "Evidence That Focal Adhesion Complexes Power Bacterial Gliding Motility." *Science* 315 (5813): 853–56.
- Muñoz-Dorado, José, Francisco J. Marcos-Torres, Elena García-Bravo, Aurelio Moraleda-Muñoz, and Juana Pérez. 2016. "Myxobacteria: Moving, Killing, Feeding, and Surviving Together." *Frontiers in Microbiology* 7 (May): 781.

- Nan, Beiyan, and David R. Zusman. 2011. "Uncovering the Mystery of Gliding Motility in the Myxobacteria." *Annual Review of Genetics* 45 (September): 21–39.
- Panigrahi, Swapnesh, Dorothée Murat, Antoine Le Gall, Eugénie Martineau, Kelly Goldlust, Jean-Bernard Fiche, Sara Rombouts, Marcelo Nöllmann, Leon Espinosa, and Tâm Mignot. 2021. "MiSiC, a General Deep Learning-Based Method for the High-Throughput Cell Segmentation of Complex Bacterial Communities." *eLife* 10 (September). <https://doi.org/10.7554/eLife.65151>.
- Ronneberger, Olaf, Philipp Fischer, and Thomas Brox. 2015. "U-Net: Convolutional Networks for Biomedical Image Segmentation." In *Medical Image Computing and Computer-Assisted Intervention – MICCAI 2015*, 234–41. Springer International Publishing.
- Saaty, Thomas L. 1986. "Absolute and Relative Measurement with the AHP. The Most Livable Cities in the United States." *Socio-Economic Planning Sciences* 20 (6): 327–31.
- Seef, Sofiene, Julien Herrou, Paul de Boissier, Laetitia My, Gael Brasseur, Donovan Robert, Rikesh Jain, et al. 2021. "A Tad-like Apparatus Is Required for Contact-Dependent Prey Killing in Predatory Social Bacteria." *eLife* 10 (September). <https://doi.org/10.7554/eLife.72409>.
- Shamay-Tsoory, Simone G., Nira Saporta, Inbar Z. Marton-Alper, and Hila Z. Gvirts. 2019. "Herding Brains: A Core Neural Mechanism for Social Alignment." *Trends in Cognitive Sciences* 23 (3): 174–86.
- Shi, W., and D. R. Zusman. 1993. "The Two Motility Systems of Myxococcus Xanthus Show Different Selective Advantages on Various Surfaces." *Proceedings of the National Academy of Sciences*. <https://doi.org/10.1073/pnas.90.8.3378>.
- Skerker, J. M., and H. C. Berg. 2001. "Direct Observation of Extension and Retraction of Type IV Pili." *Proceedings of the National Academy of Sciences of the United States of America* 98 (12): 6901–4.
- Theraulaz, G., and E. Bonabeau. 1999. "A Brief History of Stigmergy." *Artificial Life* 5 (2): 97–116.
- Thiery, Susanne, and Christine Kaimer. 2020. "The Predation Strategy of." *Frontiers in Microbiology* 11 (January): 2.
- Urban, Constantin F., and Emelie Backman. 2020. "Eradicating, Retaining, Balancing, Swarming, Shuttling and Dumping: A Myriad of Tasks for Neutrophils during Fungal Infection." *Current Opinion in Microbiology* 58 (December): 106–15.
- Van Valen, David A., Takamasa Kudo, Keara M. Lane, Derek N. Macklin, Nicolas T. Quach, Mialy M. DeFelice, Inbal Maayan, Yu Tanouchi, Euan A. Ashley, and Markus W. Covert. 2016. "Deep Learning Automates the Quantitative Analysis of Individual Cells in Live-Cell Imaging Experiments." *PLoS Computational Biology* 12 (11): e1005177.
- Zhang, Yong, Adrien Ducret, Joshua Shaevitz, and Tâm Mignot. 2012. "From Individual Cell Motility to Collective Behaviors: Insights from a prokaryote, Myxococcus Xanthus." *FEMS Microbiology Reviews*. <https://doi.org/10.1111/j.1574-6976.2011.00307.x>.

Figure 1

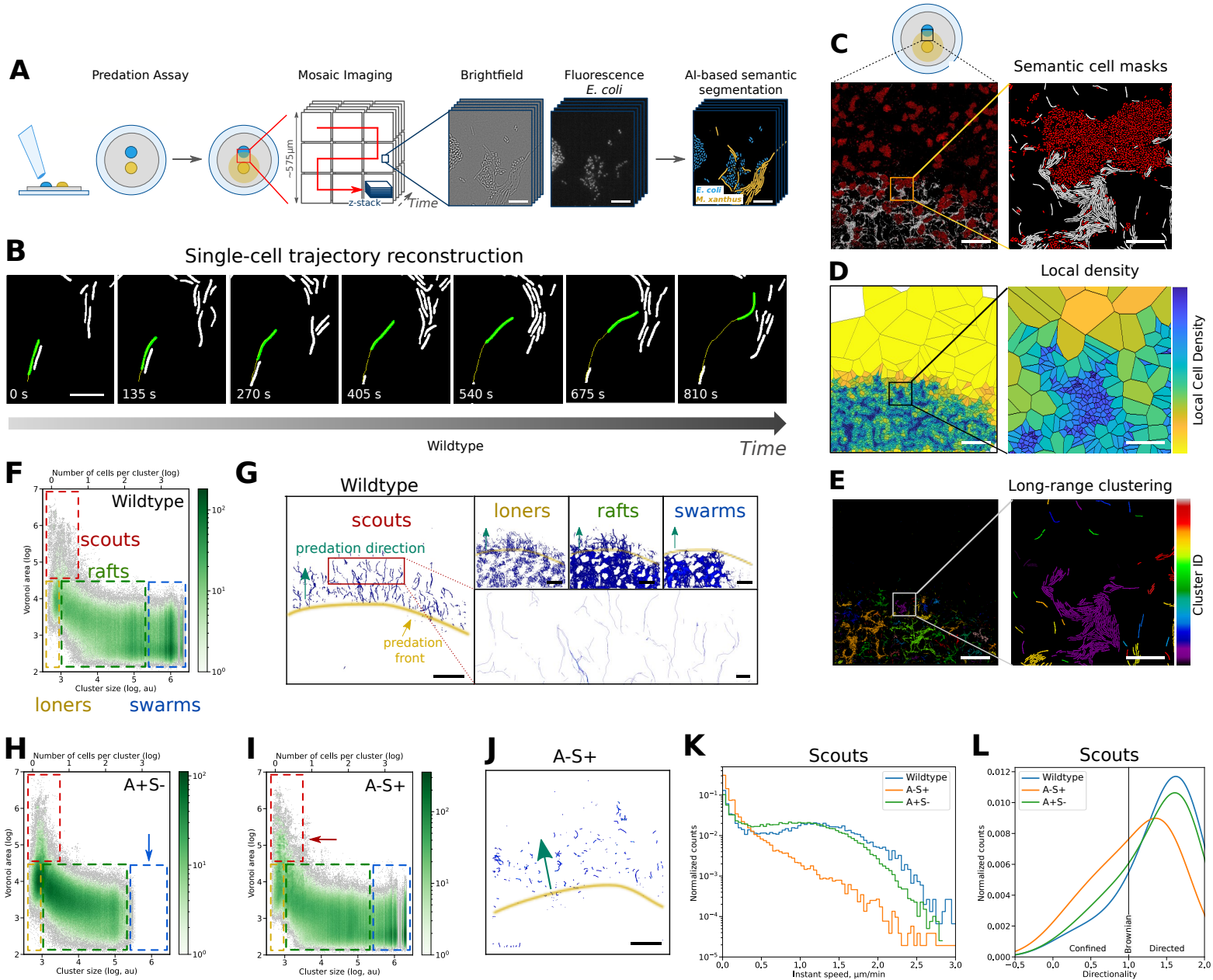


Figure 2

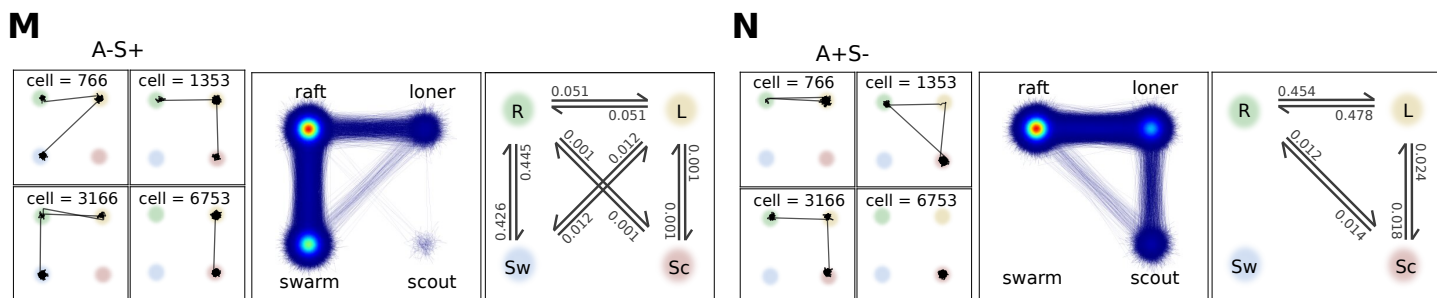
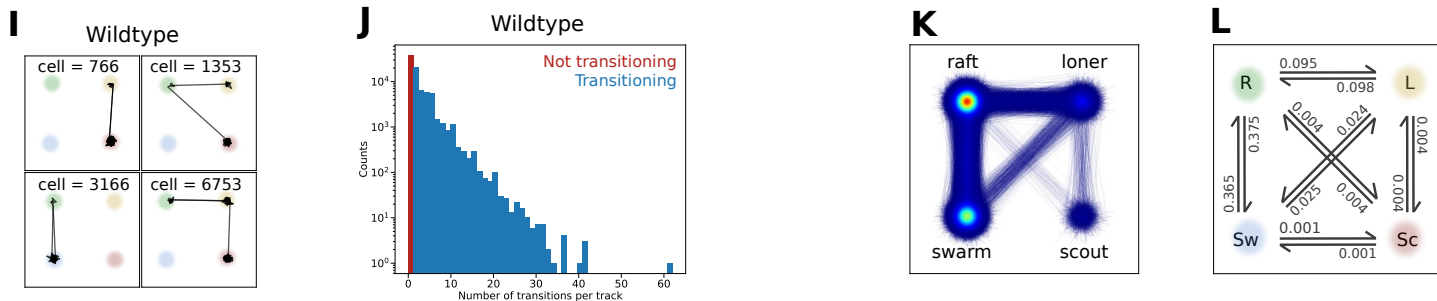
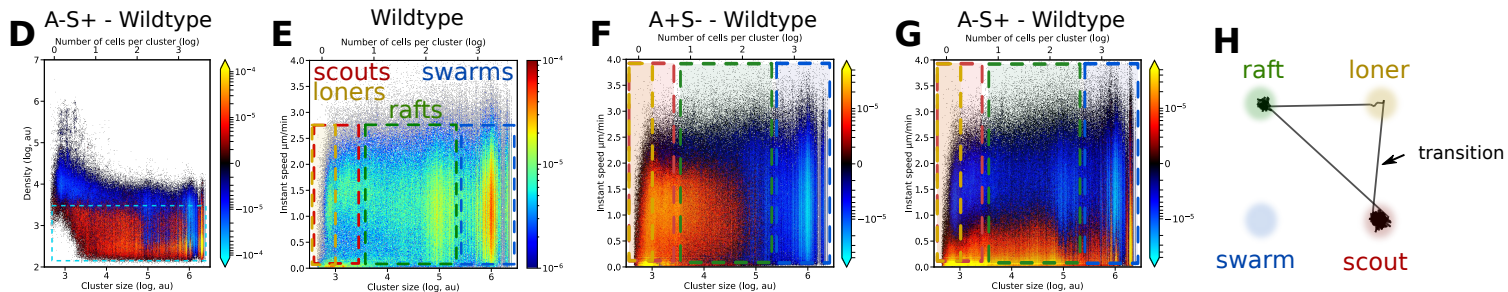
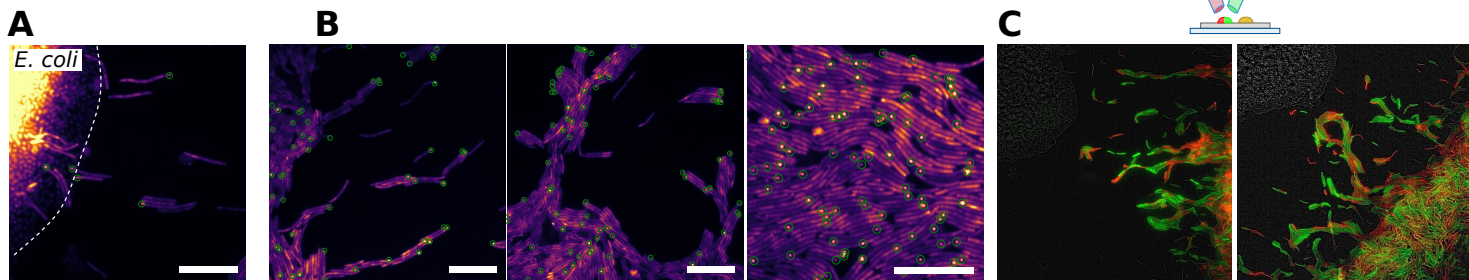
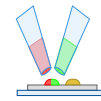


Figure 3

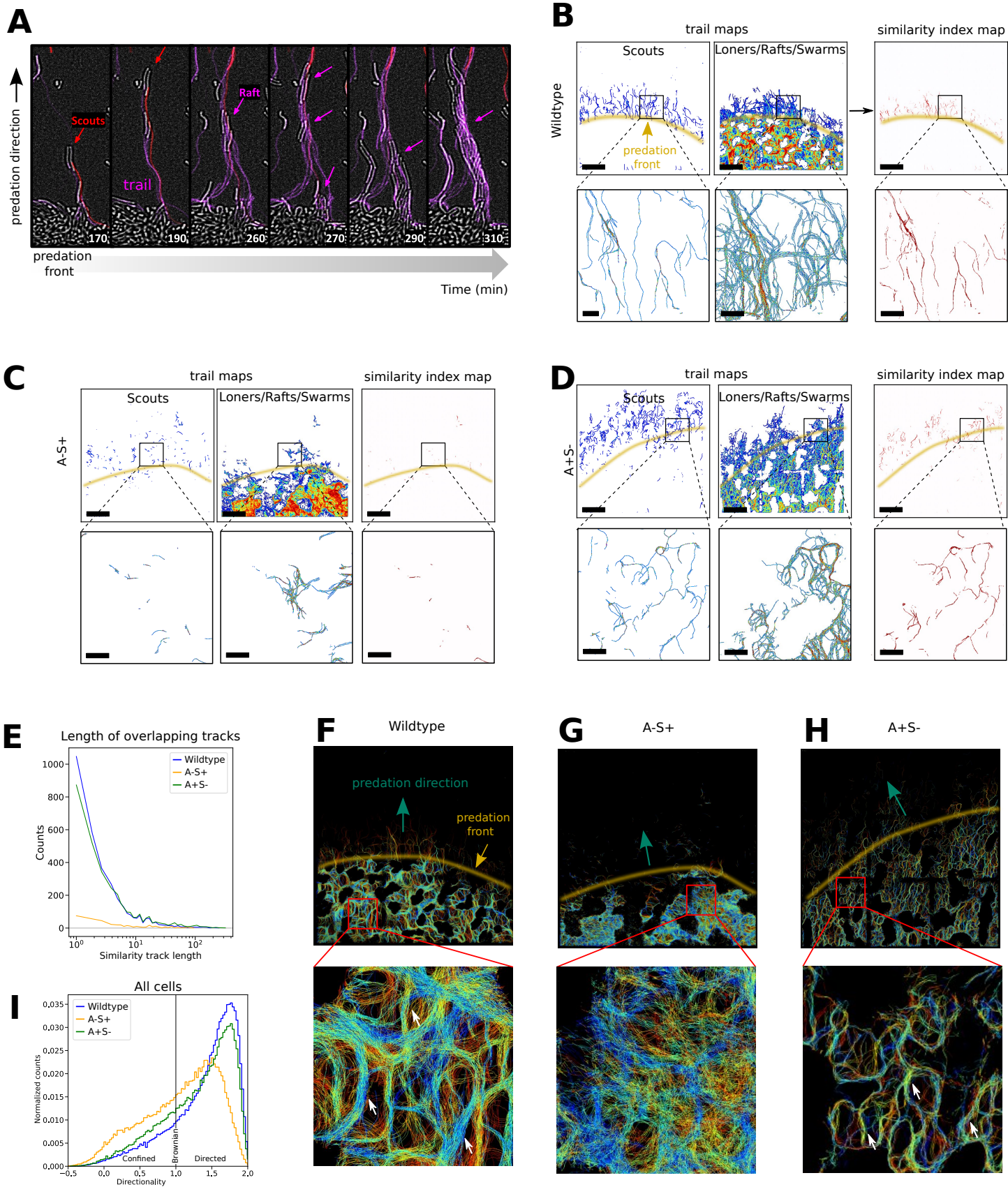
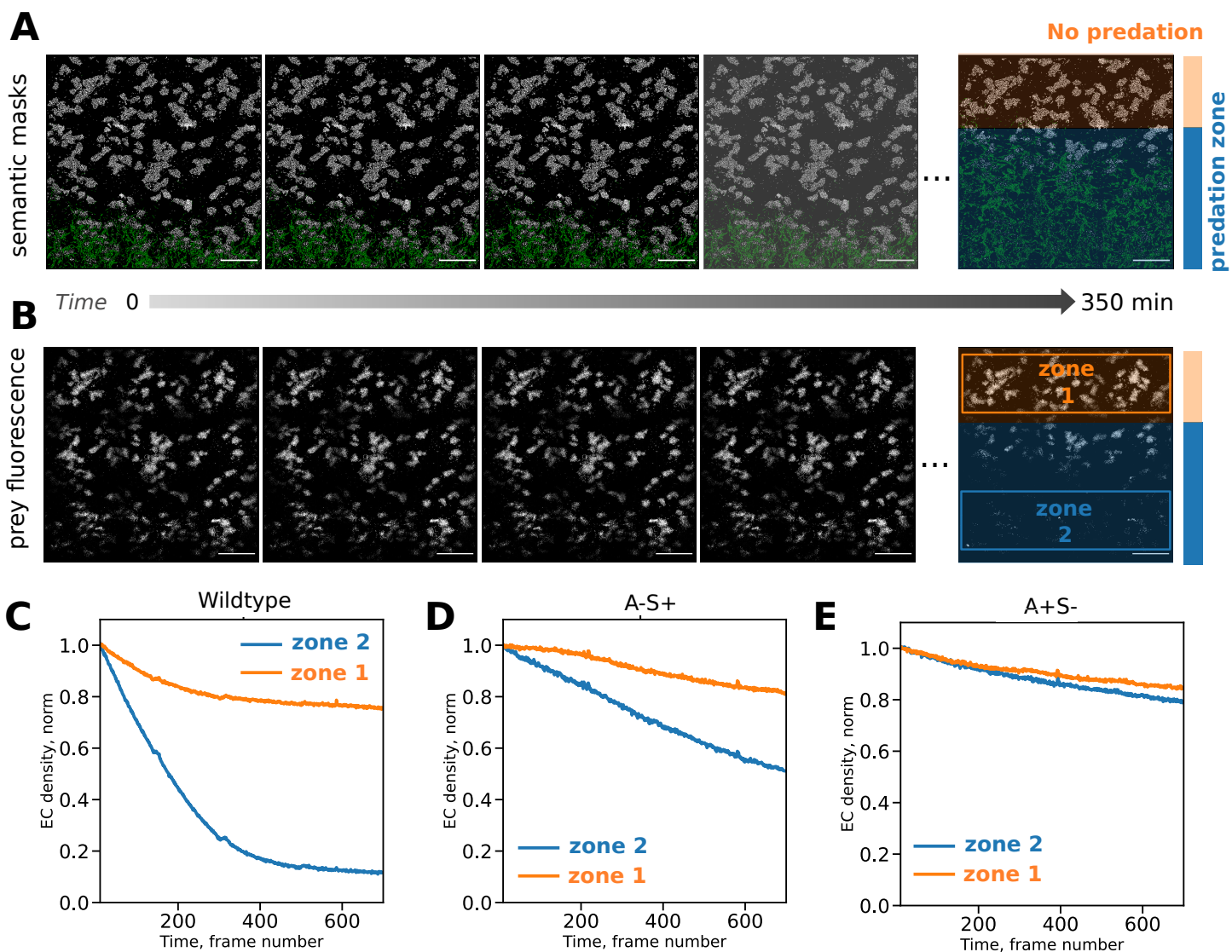
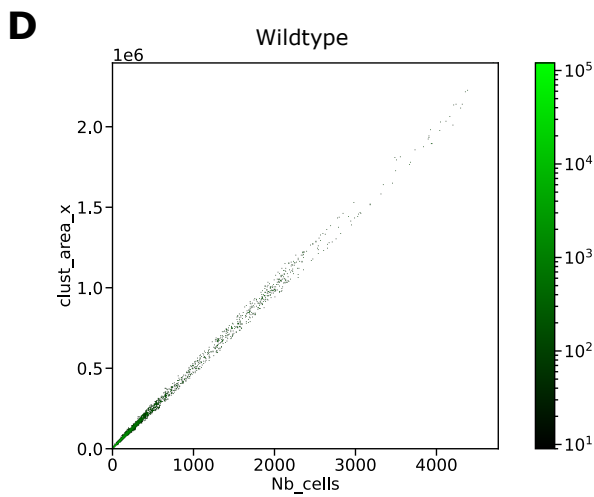
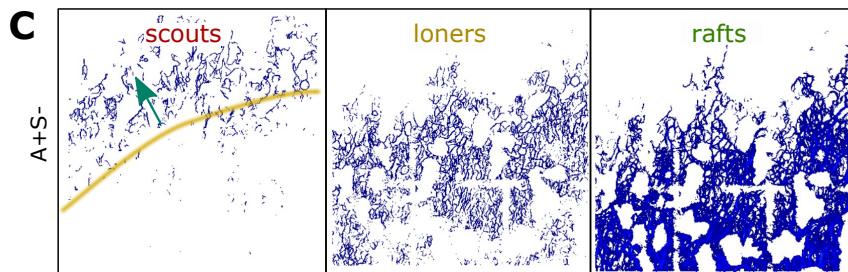
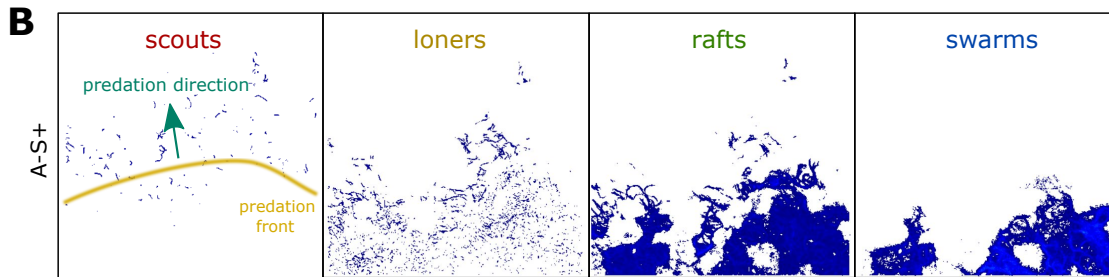
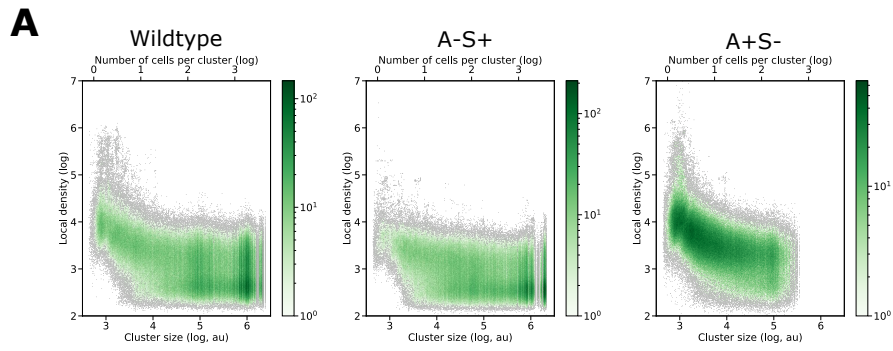


Figure 4



Supplementary Figure 1



3 Transcriptome heterogeneity in *M. xanthus* colonies

3.1 Introduction

Biofilms are an example of complex microbiological communities in which a great level of phenotypic heterogeneity exists (Stewart and Franklin 2008; An and Parsek 2007). Cells from an isogenic population are able to respond to changes in their microenvironments, for example by changing the biofilm architecture, resulting in division of labor and thus, cell specialization (Bridier et al. 2017). This specialization arises from differential gene expression programmes in the cells of the community and has been shown for several species including *B. subtilis*, Staphylococcus species *S. aureus* and *S. epidermidis* and *Pseudomonas aeruginosa* (Rani et al. 2007; Lenz et al. 2008; López and Kolter 2010).

A predating *M. xanthus* colony, like a biofilm, shows great intercellular diversity. From the microscopic timelapse experiments presented in chapter 1 of the results section, a great variation of functionality and motion behavior could be observed. Additionally, a wide range of behaviors have been described as well based on macroscopic-scale qualitative studies of the predation assay (Thiery and Kaimer 2020). These observations gave rise to the hypothesis that behavioral heterogeneity observed in the predating *M. xanthus* colony is a result of differential transcriptomic programs.

Transcriptomic variation in *M. xanthus* cells has been studied before for developmental cells (Muñoz-Dorado et al. 2019). Using a bulk RNA-seq method on cells sampled at different timepoints after the induction of the developmental cycle, this study showed that differential gene expression patterns can be observed between sampled timepoints. This suggests that developmental cells go through several transcriptional programs and that the evolution of the transcriptome might coincide with different cell behavior observed over time from the onset of development and cell aggregation to sporulation and fruiting body formation.

A myriad of imaging-based methods for the study of RNA in bacteria have been reported, which we summarized in a comprehensive review (Rombouts and Nollmann 2021) (Annex 0). To investigate transcriptomic heterogeneity in cells of a predating *M. xanthus* colony, we used one of these pioneering techniques, Fluorescence In Situ Hybridization (FISH). Here, I developed a workflow which allows me to label RNA species of interest in fixed cells while conserving the spatial context of the cell in the colony. This required the optimization of a protocol for RNA labeling and the development of a method to achieve labeling in a fragile biofilm while maintaining the spatial organization of cells in the colony. To simplify this endeavor, I first optimized the RNA labeling in cells from liquid culture. This included an extensive search of experimental conditions to ensure target-specific labeling and sufficient clearing of off-target probes. Subsequently, I focused on the development of a non-disruptive method which allows fixation and permeabilization of cells in a *M. xanthus* colony. I validated the workflow by studying the transcriptomic levels of one target RNA species, expressed under the promoter of the EF-TU gene. Ultimately, I show that differential gene expression can be detected in cells from the same predating colony and that their expression level is correlated with their spatial positioning within the colony.

3.2 RNA FISH labeling optimization in cells harvested from liquid cultures

To optimize the protocol for labeling and imaging of RNAs in *M. xanthus* cells from rich liquid culture, we used a wildtype strain carrying a fluorescent reporter, the superfolder Green Fluorescent Protein (sfGFP), under control of the promoter of EF-TU (elongation factor thermo unstable). Concentrations of this protein construct were monitored by directly visualizing the fluorescence signal of sfGFP or by using immunofluorescence (IF) with a commercially available antibody labeled with Atto-647 targeting sfGFP. To monitor the RNA levels of this fluorescent reporter, I adopted an indirect labeling approach based on RNA-FISH (**Figure 10a**).

First, the target transcript was labeled with primary probes, which contain a homologous region complementary to the transcript, and a tail region containing two unique read-out sequences from (Beliveau et al. 2015) and (Boettiger et al. 2016) (**Figure 10b**). Second, two fluorescently labeled secondary oligos were hybridized to the read-out sequences in the tail region of the primary probe (**Figure 10a**). For the sfGFP transcript, a set of 28 primary probes with a length of 20 nucleotides was designed with the Stellaris Probe Designer webtool spanning the total length of the transcript (**Figure 10b**).

To achieve labeling of the sfGFP transcript, the protocol published by Skinner et al. was adapted as described in (Material and Methods) (Skinner et al. 2013a). In short, cells in the exponential phase were harvested from liquid culture and directly fixed and permeabilized. Successful fixation and permeabilization is essential for preservation of transcripts present in the cell and to allow penetration of the cell envelope by primary and secondary probes. First, I verified the proper permeabilization of cells by labeling and imaging the sfGFP construct using IF microscopy. I reasoned that if the antibody was able to penetrate inside the cell and label its epitope within the soluble sfGFP construct, then a short oligonucleotide should also be able to diffuse into the cell given its considerably smaller size. For the strain carrying a cytosolic sfGFP label, I observed a cytosolic signal in the 641 nm channel (Atto-647) (**Figure 10c**). To confirm the specificity of this labeling, I used a strain where RomR was fused to GFP. RomR is a response regulator that induces polarity switching of the A-motility machinery and localizes at the cell poles with a predominant cluster at the lagging pole where RomR-GFP forms a fluorescent focus (Leonardy et al. 2007; Zhang, Guzzo, et al. 2012). As expected, the fluorescent signal from the IF labeling of RomR-GFP was located at the cell poles in the 647 nm channel (**Figure 10c (right)**). As a negative control, a WT strain without GFP labeling was used and showed no immunolabeling (**Figure 10c (middle)**). Altogether, these results show that the cell envelope of *M. xanthus* cells is well permeabilized after the fixation and permeabilization. Additionally, the immunolabeling of localized GFP at the cell pole suggests that the intracellular organization of cell components remains conserved during the fixation and permeabilization protocol.

Next, I optimized the protocol in search for conditions displaying specific labeling of the sfGFP transcript. For this, I varied the concentration of formamide in the hybridization and washing buffers (from 10% to 40%), as well as the primary probe incubation temperatures (from 30°C to 47°C). For each condition, I labeled WT and sfGFP strains with primary probes (PPs) in presence and absence of secondary probes (SPs). I expected to observe fluorescence from labeled RNA only in sfGFP cells in the presence of PPs and SPs. Successful labeling was only achieved at a probe incubation temperature of 30°C and a formamide concentration of 10% to 40% in the hybridization buffer (**Figure 10d**). The three negative controls (sfGFP-PPs+SPs, WT+PPs+SPs and WT-PPs+SPs) did not show significant

fluorescence, indicating that the labeling in the sample is specific to the target transcript, and that the washing conditions are sufficient to minimize off-target binding.

To quantify the degree of labeling, I integrated the total fluorescence signal normalized by the cell size for all the samples (**Figure 10e**). Such a quantification does not take the labeling pattern into account, and thus might result in large variations between single cells, however it does provide a good quantification of the degree of specific labeling as the non-specific fluorescence intensity in control samples is well below the fluorescence intensity in sfGFP cells labeled with PPs and SPs (**Figure 10e**). For all samples incubated at 30°C, I observed that the integrated fluorescence signal was significantly higher for sfGFP cells labeled with PPs and SPs than the signal in negative controls (**Figure 10e – bars 1-4**). To further optimize the RNA labeling protocol, I varied the formamide concentration in the hybridization and washing buffers. Formamide is known to destabilize RNA-DNA and DNA-DNA hybrids formed between the transcript and the PPs and between the tail of the PP and the fluorescently labeled secondary probes. Thus, higher formamide concentrations decrease off-target binding but can also destabilize on-target binding. I observed a considerable decrease in the integrated fluorescence signal of the sfGFP sample labeled with PPs and SPs when the formamide concentration in the hybridization buffer was increased from 10 to 40% (**Figure 10e**). It is worth noting that the integrated signal remained similar for the negative controls, suggesting that an increase in formamide concentration from 10% to 40% for PP incubation did not reduce off-target and non-specific probe binding.

Finally, I tested the effects of the hybridization temperature. For this, I incubated the sample at 37°C instead of 30°C for a formamide concentration of 10% in both the hybridization and washing buffers. The fluorescence signal in sfGFP cells labeled by PPs and SPs dropped to similar levels as the negative controls. Thus, under these hybridization conditions the probe did not bind stably to the target transcript. Our results confirm the important interplay between formamide concentrations in the hybridization and washing buffers and the incubation temperature to drive the stable RNA-DNA and DNA-DNA hybrid formation to achieve specific RNA labeling conditions.

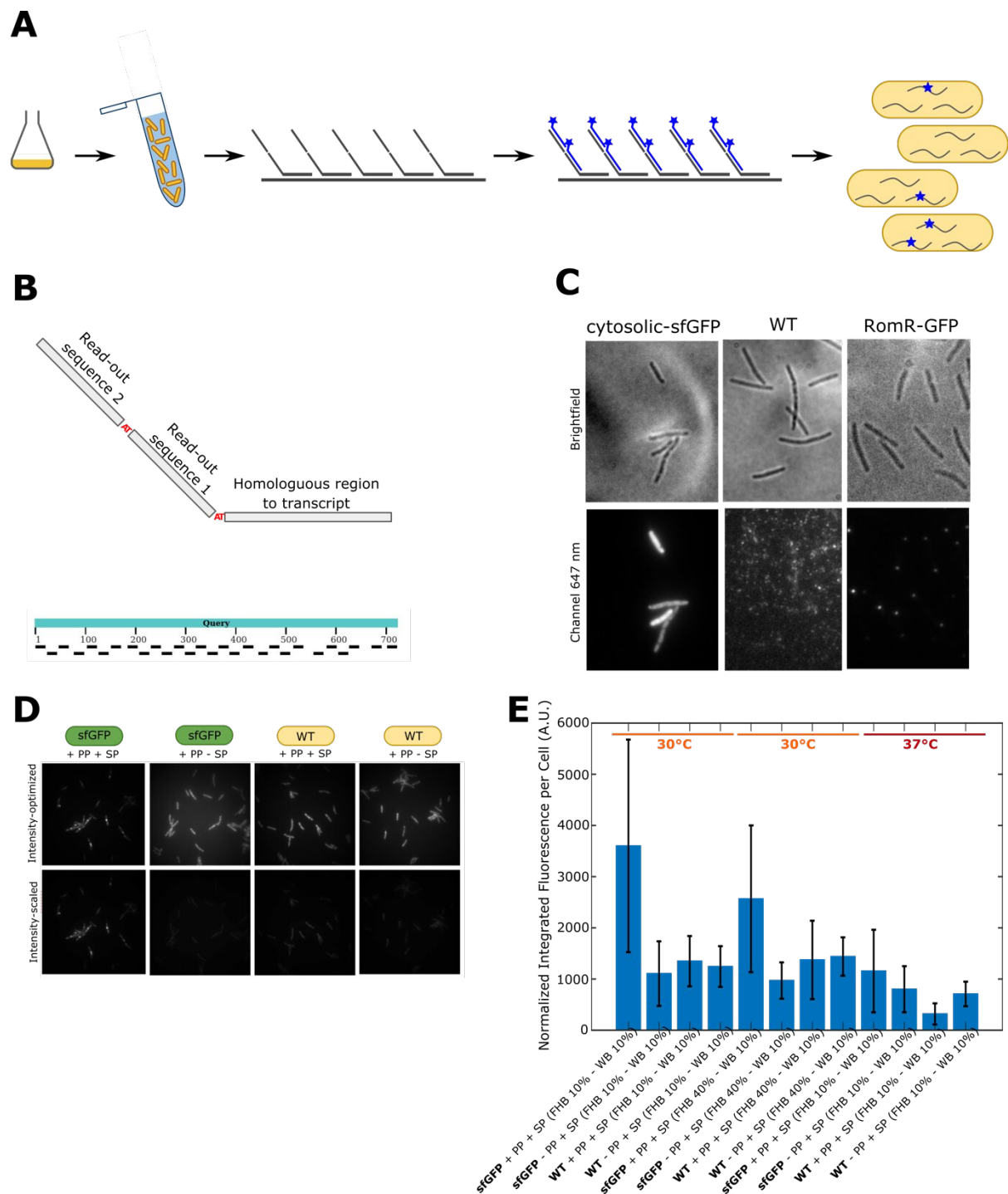


Figure 10. Probe design and labeling of sfGFP transcript in *Myxococcus xanthus* from liquid culture. A) Workflow of *M. xanthus* cells harvested from liquid culture. B) Design of a set of 28 primary probes spanning the total length of the target sfGFP transcript, consisting of a homologous region to sfGFP and 2 unique read-out sequences which can bind a fluorescently labeled read-out oligo. C) Immunofluorescence microscopy of anti-GFP Atto-647N to verify permeabilization of *M. xanthus* cells. D) RNA labeling of *M. xanthus* cells. E) Integrated fluorescence signal normalized for cell size for sample and the corresponding controls for different labeling protocols

To explore whether other temperature and formamide concentration conditions could improve the labeling results even further, I calculated the theoretical melting temperature of the homologous regions of the primary probe and the effect of the volume/volume percentage of formamide in the buffer based on the linear relationship between formamide concentration and melting temperature (McConaughy, Laird, and McCarthy 1969). For an increasing concentration of formamide in the buffer, the melting temperature of the hybrid decreased linearly (**Figure 11a**). This effect was confirmed by experiments where I gradually increased the formamide concentration in the washing buffer (**Figure 11**). The overall integrated fluorescence in sfGFP cells labeled with PPs and SPs decreased with increasing formamide concentration in both the PP and SP incubation buffers (**Figure 11b – right panel**). The integrated fluorescence in control samples followed a similar trend indicating that nonspecific or off-target binding of SPs decreases when the formamide concentration increases. The intensity of single fluorescence foci, representing the diffraction limited fluorescence signal originating from SPs, decreased with increasing formamide concentration as well (**Figure 11b – left panel**).

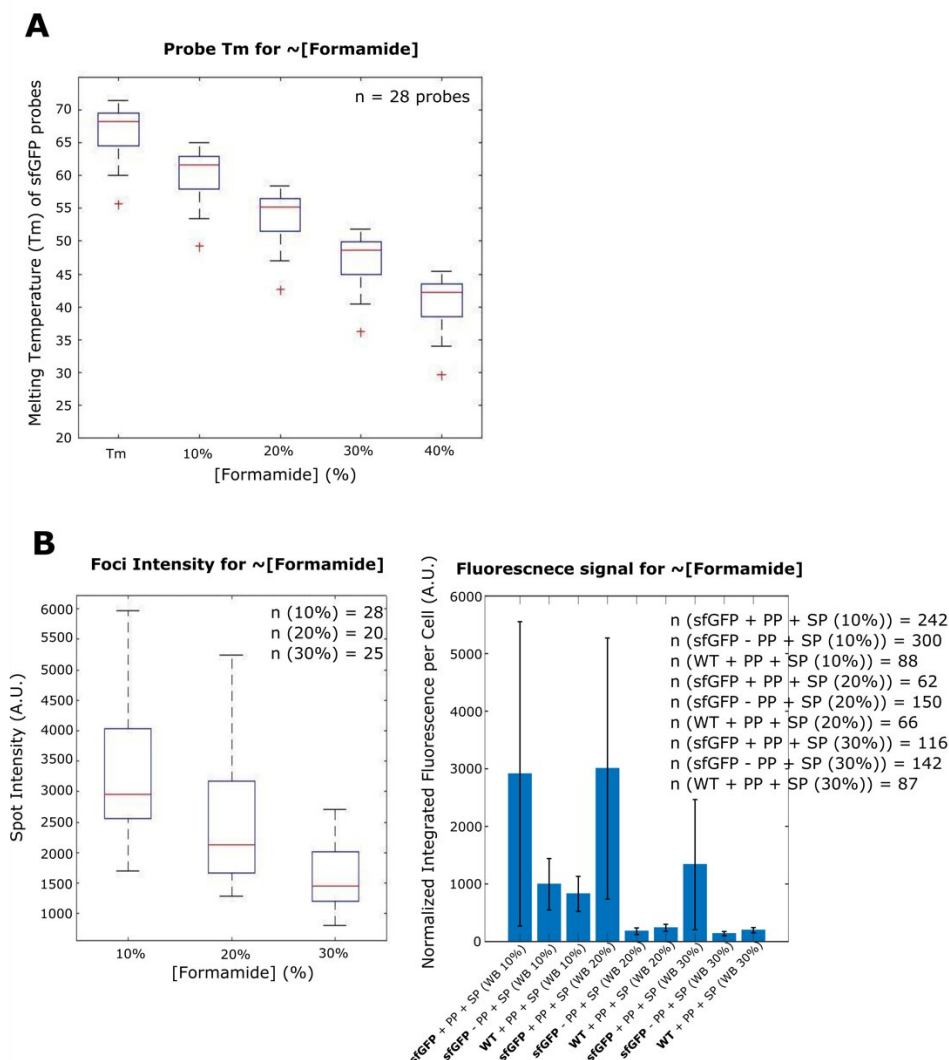


Figure 11. Influence of formamide concentration on melting temperatures and RNA labeling. A) Effect of formamide concentration on theoretically defined melting temperatures of homologous regions in primary probes. B) Foci Intensity and integrated fluorescence signal normalized for cell size for gradually.

3.3 RNA FISH labeling optimization in biofilms

In the second stage, I applied this protocol to detect mRNAs by RNA-FISH within predation assays where spatial organization of the predating *M. xanthus* colony and the *E. coli* microcolonies are preserved. In my original protocol, cells were harvested from liquid culture and treated in cell suspension. Therefore, a method to ensure colony preservation needed to be engineered.

A colony of *M. xanthus* deviates from the classical biofilm where cells are embedded in a matrix of extracellular material which can be carefully submerged in solution without disruption (Dar et al. 2021a). In fact, *M. xanthus* cells only loosely associate to form a colony. Additionally, *M. xanthus* cells can move over the solid surface on which they find themselves but do not tightly adhere to this surface. Because of these reasons, the predation assay cannot be submerged in liquid for fixation, permeabilization and probe hybridization without disrupting its architecture.

One possibility to circumvent this issue would be to rely on diffusion of liquids through the agarpad. To do so, cells need to be compressed between the agarpad and the coverslip to ensure stabilization of the biofilm. Then, chemicals can diffuse laterally through the agarpad from the outside. This approach would work for solutions that are not too viscous. However, the hybridization buffer is a very viscous solution due to the presence of dextran. We tested this approach nonetheless, but found that the diffusion of probes through the agar pad is too slow to make it experimentally possible, either due to the size of the probes which do not diffuse through the agarpad meshwork or due to the length scale over which the probes need to diffuse in order to reach the cells resulting in an unreasonably slow process.

Alternatively, I devised a method to make a print of a *M. xanthus* colony to a coverslip in which the spatial organization of cells is conserved (**Figure 12a**). The method consisted in the inoculation of a *M. xanthus* colony on a hard agar surface, either as a radially expanding colony or as a predation assay. Then, a second coverslip, the imaging coverslip, was hermetically placed on the agar pad avoiding air bubbles between the agar pad and the coverslip. Cells were compressed between the agar pad and the imaging coverslip by placing an in-house fabricated weight of around 50 gr on the support coverslip. This allowed the use of a liquid handling system that did not change the architecture of the colony. This sample was, weight included, placed in a petri dish, which was subsequently flushed with fixative. During incubation, these solutions diffused through the agar pad and fixed cells to the glass.

First, we used 3.7% Formaldehyde-PBS to fix the cells by allowing it to diffuse through the agarpad and reach the cells. We determined an incubation time of 90 min based on empirical observations made from real-time live imaging. Because *M. xanthus* cells are motile, we can essentially define the moment cells are effectively fixed when they arrest motion. Diffusion through the agar pad happens gradually, therefore cells located at the edge of the biofilm are stalling motion first, and thus are being fixed first. The critical time for the 3.7% Formaldehyde-PBS fixative to reach the middle of the agarpad was around 60 min for the agar pad dimensions we used. To achieve efficient fixation of cells located in the middle of the pad, another 30 min of incubation was added to the incubation time, resulting in a total incubation time of 90 min. Then the sample was then incubated with ethanol overnight, after which the agar pad was carefully removed, leaving cells adhered (or printed) to the glass.

From that point on, the sample was treated as a tissue slice adhered to the glass for further permeabilization and probe hybridization steps. Despite the successful colony preservation on the coverslip, the fixation of the full colony with 3.7% formaldehyde-PBS was slow and cells were only gradually exposed to fixative due to slow diffusion. This could lead to the induction of stress and thus, transcriptomic changes. To limit these effects, an alternative fixative containing formaldehyde, alcohol (ethanol) and acetic acid (FAA) was used. With this fixative, the incubation time could be reduced drastically because motion arrest in *M. xanthus* cells in the middle of the agar pad was observed almost instantaneously. We hypothesize that the fast diffusion of FAA through the agar pad is related to the ethanol in the solution. As agar is essentially a polymer meshwork containing water molecules, exposure to ethanol will rapidly expel the water content from the agar mesh and replace it with ethanol. After FAA incubation, the agar pad could be removed and cells remained printed onto the coverslip surface. Robustness of adhesion of cells to the coverslip, and thus preservation of the spatial colony organization, was enhanced with increased FAA incubation times, with ideal incubation times being between 10 to 30 min. After FAA incubation, the *M. xanthus* colony was post-fixed with 3,7% formaldehyde-PBS and permeabilized with 0.4% Triton-X PBS before probe hybridization.

As for cells in liquid culture, the efficiency of the fixation and permeabilization was verified by immunofluorescence labeling and imaging of a sfGFP fusion strain. Anti-GFP antibodies were used in a colony of *M. xanthus* cells carrying the cytosolic-sfGFP protein and a WT strain without GFP target as negative control (**Figure 12b**). IF assays showed successful labeling in the strain carrying cytosolic sfGFP, indicating that the protocol for fixation and permeabilization of cells in biofilms was efficient.

Next, the protocol for probe hybridization optimized on cells from liquid cultures was applied to printed colonies. In the first stage, RNA labeling was tested on cells from a pure *M. xanthus* colony in nutrient-rich conditions. As the cytosolic sfGFP was expressed under the promoter of EF-TU, a protein which is highly conserved and abundantly expressed in exponential phase prokaryotes (Harvey et al. 2019), such as *E. coli* and *M. xanthus*, we expected similar RNA labeling patterns as for cells harvested from exponential nutrient-rich liquid cultures.

Indeed, I observed that *M. xanthus* cells displayed a fluorescence signal in the 647 nm channel, originating from fluorescently labeled RNA (**Figure 12c**). To test the influence of prolonged FAA exposure, leading to more robust cell adhesion to the substrate, on RNA labeling, total integrated fluorescence of cells was calculated for increasing FAA incubation times. Interestingly, no significant difference could be observed between the experiments (**Figure 12d**), indicating that RNA remains intact under prolonged FAA exposure. Therefore, longer FAA incubation times can be used to ensure robust cell printing onto the coverslip without compromising RNA labeling.

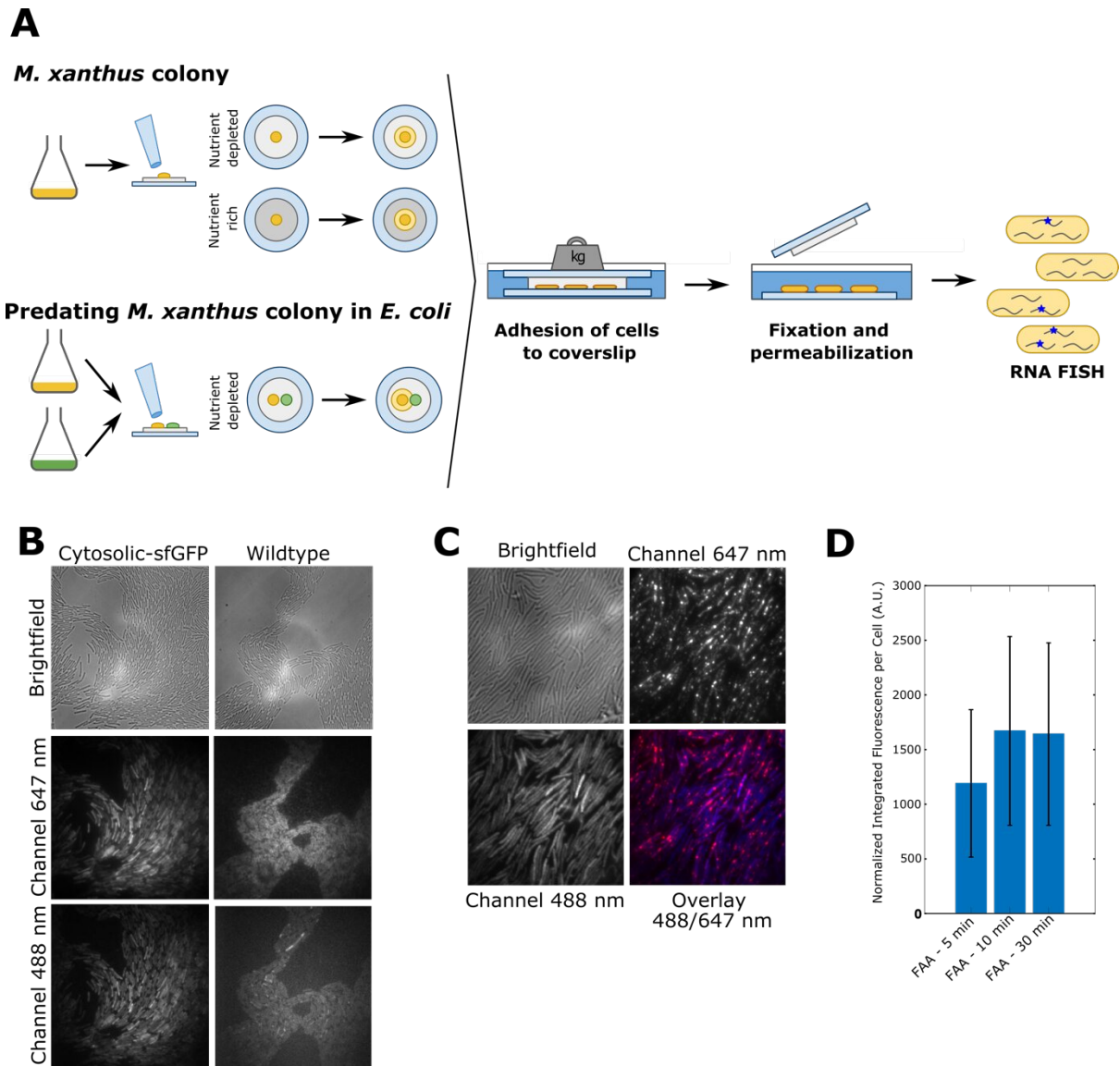


Figure 12. IF and RNA FISH labeling in printed *M. xanthus* cells. A) Workflow of RNA labeling of printed *M. xanthus* biofilm and predation assay. B) Immunofluorescence microscopy of anti-GFP Atto-647N in strain carrying cytosolic sfGFP (left) and wildtype (right). C) RNA labeling of printed *M. xanthus* biofilm on rich culture. D) Integrated fluorescence signal normalized for cell size for increasing FAA incubation times.

3.4 Nutrient-dependent differential gene expression in *M. xanthus*

Because *M. xanthus* in a predation assay is grown on a nutrient-depleted pad and thus, under starvation, the transcriptomic state of cells is different from *M. xanthus* cells from a biofilm in nutrient-rich conditions. Therefore, I quantified the fluorescence signal from sfGFP RNA in cells from a biofilm in nutrient-depleted conditions and compared it to the signal from cells from a *M. xanthus* biofilm formed in nutrient-rich conditions. I observed that the fluorescence signal originating from RNA labeling in cells in nutrient-depleted conditions disappeared, suggesting that the transcript sfGFP was produced to undetectable levels in these cells (**Figure 13a**). This indicates that differential expression of certain target genes arises from nutrient availability. Additionally, this result supports the validity of the RNA labeling and colony immobilization protocol presented above.

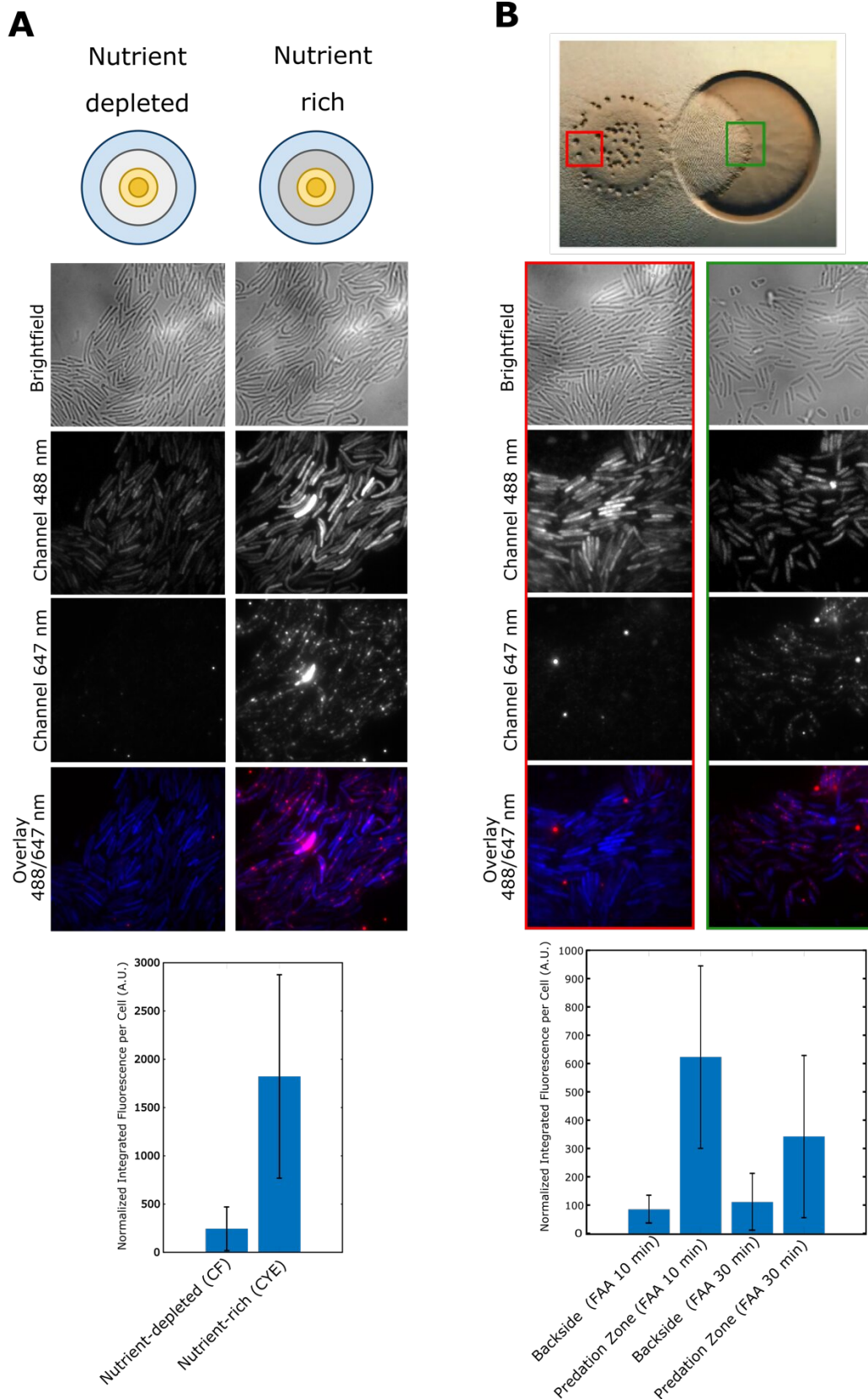


Figure 13. Differential expression of sfGFP under EF-TU promoter in *M. xanthus*. A) RNA labeling of *M. xanthus* biofilm formed in nutrient-depleted and nutrient-rich conditions. B) RNA labeling of *M. xanthus* predating biofilm in predation assay zoomed in on *M. xanthus* cells in predation zone and at colony backside, quantification for two samples with various FAA incubation times.

3.5 Differential gene expression in predating biofilms

Finally, the printing and RNA labeling protocol were applied to the predation assay. *M. xanthus* cells in nutrient-depleted conditions were allowed to predate on *E. coli*, creating a predation zone. Predation is thought to include both killing and consumption of prey cells, suggesting that *M. xanthus* cells actively feed on prey cells. However, not all cells in the *M. xanthus* predating colony are in contact with *E. coli*. In fact, a multitude of cells remain distant in space from prey microcolonies (e.g. in the backside of the predating colony).

To study whether gene expression variation could be observed in a predating *M. xanthus* colony, I imaged the fluorescence signal originating from labeled RNA throughout the predating colony. I observed a fluorescence signal in cells in the predation zone (**Figure 13b**). Surprisingly, no fluorescence signal could be observed for cells at the backside of the colony (**Figure 13b**). Comparing these results to the observations made previously for cells in nutrient-rich and nutrient-depleted conditions, the cells in the backside of the colony show, just like cells in nutrient-depleted conditions, no RNA labeling. In both conditions, the expression of the transcript of interest under the control of the EF-TU promoter dropped below detectable limits. For cells in the predation zone, which are in contact with *E. coli* and are thought to participate in prey killing and feeding, showed similar labeling patterns, albeit lower integrated fluorescence signals, as cells in nutrient-rich conditions.

Together, these results confirm that transcriptomic variation, here represented by the labeling and detection of one transcript of interest, can be observed in predating biofilms. Furthermore, these results suggest that *M. xanthus* cells making up a predating colony can be in different cell states, depending on their spatial positioning in the colony.

3.6 Discussion

Here, I propose a method for transcriptome profiling in spatially conserved *M. xanthus* colonies by RNA FISH. To do so, I designed a workflow to tightly adhere, or print, the cells in a colony to an imaging coverslip. The protocol for RNA FISH labeling was optimized in cells from exponential liquid cultures using the sfGFP transcript under the control of the EF-TU promoter, and was then applied to printed cells. From pure printed *M. xanthus* colonies, a differential expression of the transcript of interest could be observed between cells from colonies inoculated on a nutrient-rich and nutrient-depleted surface. Furthermore, RNA labeling in a predating colony showed variations in sfGFP expression between cells at the predation forefront and the colony backside within that same colony. This suggests that transcriptome heterogeneity exists between cells from *M. xanthus* colonies formed under different environmental conditions, and among cells in the same *M. xanthus* predating biofilm.

The transcript of interest used in this work was transcribed from the gene encoding a cytosolic sfGFP under control of the promoter for EF-TU expression. EF-TU is a highly conserved protein and among the most abundant in bacteria (Harvey et al. 2019). Two-dimensional immobilized pH/SDS-PAGE studies carried out on bulk protein extraction of vegetative and developmental *M. xanthus* cells showed that EF-TU is differentially expressed in both conditions, with high expression levels detected in vegetative cells and a decrease to very low levels in developmental cells (Horiuchi et al. 2002). This corresponds with the observations made here from RNA labeling of cells in nutrient-rich, or exponential, conditions and cells in nutrient-depleted, or starvation, conditions. The gene expression variation that could be observed within a predating colony indicates that cells located at the forefront

are in an exponential cell state and thus, actively feed on the *E. coli* prey. In contrast, cells at the colony backside seem to have entered the developmental cycle, suggesting that nutrients released from prey lysis are not redistributed over the length scales of this predating colony.

The implementation of high-throughput labeling strategies, such as sequential or multiplexed FISH, can help generate nearly-whole transcriptome profiles at the single cell level (Lubeck et al. 2014a; K. H. Chen et al. 2015a). Recently, high-throughput spatial transcriptomics was used to uncover different cell states in sessile *P. aeruginosa* communities (Dar et al. 2021a). Likewise, I expect that transcriptomic profiling in predating colonies might uncover a myriad of co-occurring cell states that might otherwise remain uncharacterized based on behavioral or phenotypic approaches.

4 Obstacle sensing by *M. xanthus*

4.1 Abstract

Correlative approaches combining AFM and optical microscopy are powerful methods to study a myriad of biological phenomena, including mechanobiology. The way living cells sense, transduce and respond to external stimuli of biological or mechanical nature can greatly influence several cellular processes, including motility behavior. Certain prokaryotes, such as the Gram-negative bacterium *Myxococcus xanthus*, achieve locomotion through Focal Adhesions (FAs). Similar to eukaryotic cells where G-proteins of the Ras superfamily link signal transduction and FA assembly to promote response to environmental stimuli, the assembly of FAs in *M. xanthus* is regulated by the Ras-like G-protein MglA. MglA in turn is regulated by the Frz-signaling pathway, which transduces environmental cues and enables cell reversal. Until now, it remains unclear what environmental cues trigger the Frz signaling pathway and thus, cell reversals. To explore whether cell reversals in *M. xanthus* cells employing FA-powered motility can be induced by mechanical stimuli, we set-up a single-cell assay using correlative Atomic Force Microscopy-Optical Microscopy in which the AFM tip is used to mechanically probe the cell. Here, I implemented this assay and tested the importance of sample preparation, and choice of AFM tip in terms of shape and size. I show that cell motility behavior can be affected by tip-cell collisions and discuss several challenges and caveats of such an experiment.

4.2 Introduction

The development of AFM revolutionized the fields of nanoscience and nanotechnology (Gerber and Lang 2006; Binnig, Quate, and Gerber 1986). The ability to image topological features in samples with extraordinary resolution resulted in incremental advances in numerous fields ranging from material science to life sciences and medicine, and triggered the development of a myriad of AFM-derived techniques. The design of the experiment needs to be such as to maintain the native state of the sample and approach physiological conditions by tightly controlling the direct environment of the sample. This is achieved by working in physiological buffers and controlling parameters such as temperature, pH, salt concentrations etc. Therefore, the development of the optical detection of cantilever deflection which allows the measurement of an immersed sample in aqueous solution was indispensable for bio-AFM (Drake et al. 1989; Radmacher et al. 1992; Meyer and Amer 1988). The development and fabrication of soft cantilevers pushed the field of bio-AFM even further. By decreasing the cantilever spring constant or stiffness, delicate soft matter, such as biological specimens, can be imaged or mechanically probed with high sensitivity.

Not only can biological specimen be imaged at high resolution in physiologically relevant conditions, a chemically modified AFM probe can be used to study specific interactions between the biological sample and the functional groups attached to the AFM probe or the AFM probe can be used to mechanically manipulate the sample or to evaluate its mechanical properties (Dufrêne et al. 2017; Krieg et al. 2019).

The ability to mechanically stimulate a biological specimen allows the study of mechanosensitivity and mechanotransduction. By combining AFM-based mechanical probing with other techniques in a correlative approach, the response of cells to the mechanical cues can be detected (Krieg et al. 2019). Conventional light microscopy allows the morphological characterization of the cell or the tracking of cell displacement over time. Additionally, fluorescence microscopy techniques allow the visualization of intracellular components of interest, such as target proteins. In short, cellular components can be labeled with fluorescent proteins in a translational fusion or with organic dyes. Thus, when the cell is mechanically stimulated, the labeled component can be followed in space and time. Combining AFM with optical microscopy approaches is a powerful tool in unravelling the relationship between the mechanobiological context and cell behavior, function or morphology.

4.2.1 Mechanosensitivity in the bacterial membrane

Cell motility is a crucial process in the lifecycle and development of many uni- and multicellular organisms and is thus an evolutionary conserved trait. In eukaryotic organisms, the precise regulation of cell motility in space and time drives several processes, such as embryonic development (Kurosaka and Kashina 2008). However, in pathophysiological conditions, the improper regulation of cell motility can lead to diseases, such as cancer metastasis (Stuelten, Parent, and Montell 2018). Eukaryotic cells generally regulate motility by dynamically reorganizing their actin cytoskeleton and assembling Focal Adhesions (FAs) at the leading cell edge (Heasman and Ridley 2008). Such FAs power locomotion by establishing an adhesive complex through which traction forces are transduced to the underlying substratum. Despite the heterogeneous molecular composition of FAs between different cell-types, their assembly/disassembly is largely regulated by small G-proteins of the Ras-superfamily. These GTPases act as nucleotide-binding molecular switches and are known to link signal transduction and

FA assembly to promote response to external stimuli (Charest and Firtel 2007). Indeed, GTPase-mediated cytoskeleton reorganizations in response to chemotactic signals are well understood. However, the sensing and transduction mechanisms of mechanical stimuli remain poorly understood.

Certain prokaryotes employ similar mechanisms to power locomotion and can be used as a model system to study FA-powered cell locomotion. Especially bacteria, which are not only fast and easy to culture but also genetically tractable, can be used as a proxy to unravel complex mechanisms in higher-order organisms. One example is *Myxococcus xanthus*, a rod-shaped gram-negative bacterium used for decades as a model system for its particular self-organization and motility properties. During vegetative growth, *M. xanthus* cells move over solid surfaces as multicellular swarms, enabling them to cooperatively prey on other microorganisms. When nutrients are depleted, cells enter the developmental cycle by coordinating their movement towards macroscopic multicellular fruiting bodies, containing spores (Muñoz-Dorado et al. 2016).

M. xanthus cell motility is powered by two motility engines (**Figure 14a**): i) Social (S-)motility based on a type IV pilus (Wu and Kaiser 1995; Sun, Zusman, and Shi 2000) and ii) Adventurous (A-)motility based on the assembly of the Agl-Glt molecular motor in Fas (**Figure 14b**) (Mignot et al. 2007; Faure et al. 2016a). Similar to eukaryotic cells where Ras G-proteins link signal transduction and FA assembly to promote response to environmental cues (Charest and Firtel 2007), the spatiotemporal FA assembly in *M. xanthus* is regulated by MglA, a Ras-like G-protein that directs motility by localizing at the leading cell pole (Zhang, Ducret, et al. 2012). MglA is in turn regulated by MglB, a GTPase activating protein that localizes at the lagging pole, and RomR, a multidomain response regulator recruiting MglA-GTP to the leading cell pole, which together make up the polarity control module of the cell. This module is regulated by the Frz signaling pathway, a bacterial chemotaxis-like system that transduces environmental cues and induces pole-to-pole switching of MglA/B leading to cell reversals (**Figure 14c**) (Mercier and Mignot 2016). Such environmental cues could include soluble and contact-dependent signals. Even though several studies have shown that certain solubles can artificially trigger the Frz system *in vitro* (Taylor and Welch 2008; Berleman et al. 2008a; McBride, Köhler, and Zusman 1992), no solubles have been identified to activate the Frz system *in vivo*. Contact-dependent signals, such as cell-cell collisions, have also been hypothesized to trigger Frz signaling (Mercier and Mignot 2016). However, it remains unclear whether those signals are of mechanical or (bio)-chemical nature.

To explore whether cell reversals in cells employing FA-powered motility (A-motility) can be induced by mechanical stimulation, we set-up a single-cell assay using correlative Atomic Force Microscopy-Optical Microscopy.

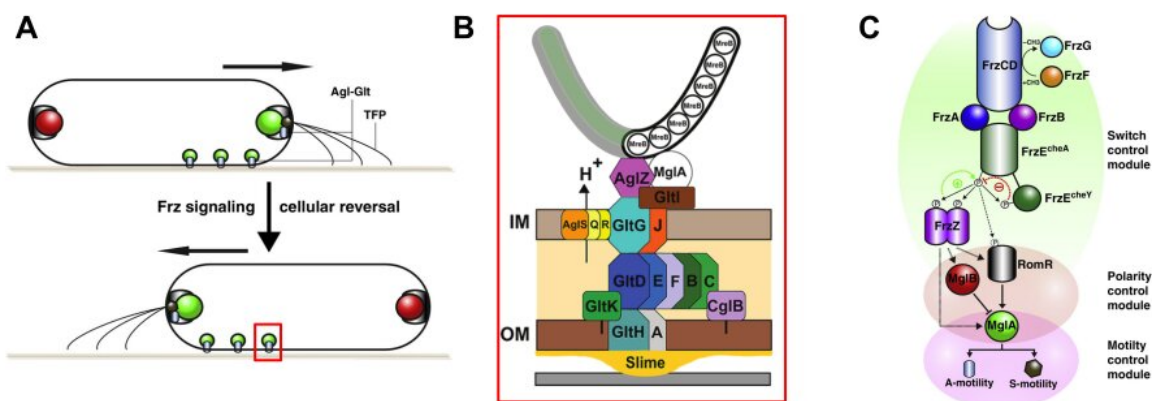


Figure 14. Motility systems of *M. xanthus*. A) Motility machinery and polarity control protein dynamics during cell reversals. RomR (black) recruits MglA (green) to the leading cell pole where it activates the Agl-Glt or A-motility machinery (blue) and the Type-IV pilus or S-motility machinery. MglB (red) co-localizes with RomR at the lagging cell pole where it activates GTP hydrolysis by MglA and ultimately prevents MglA accumulation. Frz signaling induces the polarity switching of MglA and MglB which allows the assembly of the A- and S-motility at the new leading pole and ultimately, cell movement in the opposite direction. Adapted from (Mercier and Mignot 2016). B) Schematic representation of all proteins of the Agl-Glt molecular motor. This motor is assembled and forms a FA traversing the bacterial cell membrane. IM = inner-membrane and OM = outer-membrane. Adapted from (Yang and Higgs 2014). C) Schematic representation of the Frz signaling pathway (Switch control module) and its downstream effects on the Polarity control module and the Motility Control Module. Dashed red line = suggested by recent evidence, dashed green arrow = unknown mechanisms, dashed black arrow = possible connections between Switch and Polarity control modules and plain arrow = established interactions. Adapted from (Mercier and Mignot 2016).

4.3 Correlative AFM and Fluorescence Microscopy

Our correlative AFM-SMLM (Single Molecule Localization Microscopy) set-up, which was previously described by Dahmane et al, combines a Nanowizard 4 microscope (JPK, Berlin) with an in-house built objective-type TIRF inverted optical microscope (Zeiss, Le Pecq, France) (**Figure 15**) (Dahmane et al. 2019). In short, four lasers are used for excitation or photoactivation, including a 405 nm (OBIS, LX 405-50, Coherent Inc.), 488 nm (OBIS, LX 488-50, Coherent Inc.), 561 nm (Sapphire, LX 561-50, Coherent Inc.) and 640 nm (OBIS, LX 640-100, Coherent Inc.). These laser lines are expanded and coupled into a single beam with dichroic mirrors (427, 552 and 613 nm laser MUXTM, Semrock). Laser intensities are modulated with an acousto-optic tunable filter (AOTFnc-400.650-TN, AA optoelectronics). Two achromatic lenses are used to expand the excitation laser and an additional dichroic mirror (zt405/488/561/638rpc, Chroma) is implemented to direct the laser lines to the back focal plane of an oil-immersion objective (Plan-Apochromat 100x, 1.4 DIC, Zeiss). A 1.5x telescope is used to achieve a final image magnification of 150-fold, resulting in a pixel size of 107 nm. Emission filters (ET525/50m, ET605/50m and ET700/75m, Chroma Technology) mounted onto a filter wheel are used to spectrally filter the emitted fluorescence light, which is then imaged using an EMCCD camera (iXon Ultra897, Andor Technologies). A piezo Tip Assisted Optics (TAO) module (JPK, Berlin) allows sample displacement in the x-, y- and z-directions (100x100x10 μm). Finally, an in-house built autofocus system corrects z-drift during acquisition: four percent of the 640 nm laser is deviated from the optical path; this beam is directed to the sample/glass coverslip interface, reflected towards the objective lens and redirected to a homemade QPD following the same path as the incident beam; the QPD

detects all transverse displacements, which are then corrected by the TAO piezo stage. LABVIEW (National Instruments) software controls the camera, laser intensities and filter wheel.

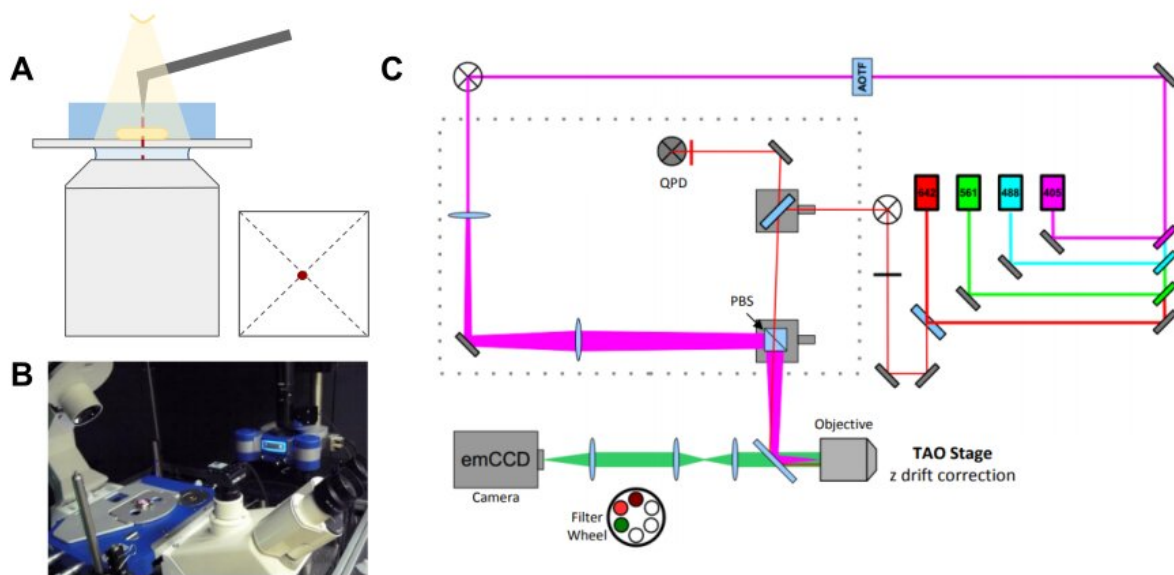


Figure 15. The AFM-SMLM set-up. A) Schematic representation of SMLM-AFM set-up. B) Nanowizard 4 microscope (JPK, Berlin) mounted on top of the objective type TIRF inverted optical microscope. C) Schematic lay-out of SMLM.

4.4 The experimental system: *Myxococcus xanthus*

To explore the ability of a *M. xanthus* cell to sense and transduce mechanical cues and induce an Frz-signalling pathway triggered cell reversal, we set-up a single-cell approach in which the cell is mechanically stimulated by the AFM tip and the response of the cell is followed in real-time by conventional light or fluorescence microscopy. When designing such an experiment, care needs to be taken regarding the sample preparation, the choice of AFM tip shape and size and the experimental set-up, including illumination geometry in the case where fluorescence is used.

4.4.1 The sample preparation

As mentioned before, *M. xanthus* cells move over solid surfaces relying on two distinct motility systems based on a Type IV pilus (S-motility) and the assembly of the Agl-Glt molecular motor in a Focal Adhesion (A-motility). Thus, a single cell on the surface could actually move by either motility mechanism. In this study, we aim to unravel whether cell reversals can be mechanically induced in cells using only the A-motility system. Thus, to completely suppress the possibility that cell motility originates completely or partially from the S-motility system, a mutant was used in which the gene *pilA* is deleted ($\Delta pilA$). This mutant lacks the fimbrial protein that makes up the pilus, and that is required for S-motility. Within this mutant strain, a protein of the Agl-Glt molecular motor is fluorescently tagged through a translational fusion between AglZ and the yellow fluorescent protein (YFP), AglZ-YFP. The AglZ protein in complex with other Agl-Glt proteins travels in a helical pattern from the cell pole to the basal membrane and forms a stationary fluorescent focus, corresponding to the assembly of a FA, when cells are moving (Faure et al. 2016a). The physiological buffer in which these cells are immersed in the following experiments is TPM (10 mM Tris-HCl, pH 7.6, 8 mM MgSO₄, and 1 mM KH₂PO₄) or TPM supplemented with 1 mM CaCl₂.

When combining AFM with optical microscopy, two experimental requirements need to be met to achieve a correlative approach. First, the sample is mounted on a high NA, oil-immersion objective to achieve high resolution optical imaging. Therefore, the sample needs to be prepared on a thin glass coverslip. Usually, living bacterial cells are flattened on the coverslip by placing them between the coverslip and a millimeter-thick agar pad. This, however, makes it impossible to access the cells from above, which is necessary when using AFM. To solve this problem, the glass coverslip can be functionalized with polymers such as chitosan or poly-L-lysine to create an adhesive layer and allow bacterial cell adsorption (Cattoni et al. 2013). However, care must be taken to select polymers that do not affect cell physiology or the ability of cells to move. In the case of the cationic polymer, poly-L-lysine, cell envelope stress as well as membrane potential decreases have been reported in both Gram-negative and Gram-positive bacteria (Strahl and Hamoen 2010; Katsu, Tsuchiya, and Fujita 1984; Colville et al. 2010). The properties and biological applicability of chitosan, on the other hand, is highly dependent on the molecular composition of the polymer mix, ranging from biocompatibility in terms of cell growth, adhesion and motility to antimicrobial activity (Raafat and Sahl 2009; Tréguier et al. 2019). Accordingly, commercial chitosan often leads to low reproducibility in experimental results due to batch-to-batch composition variations.

As an alternative to these coating molecules, we experimented with agar-coated coverslips as agar surfaces are highly biocompatible and an ideal substrate for *M. xanthus* cell motility. The agar needs to be spread on the coverslip as a very thin layer, in the order of a few micrometers, to be able to image the sample as the working distance of the objective is only 170 μm . On top of the layer the bacterial cells are deposited by spotting 3 μl of TPM-containing cells so that AFM can still be used to probe the sample from the top. One caveat of this approach is that bacterial cells usually do not strongly adhere to agar surfaces and thus, the cells tend to detach when immersing the sample in a buffer. We attempted to circumvent this problem by: i) working in air, and ii) supplying the thin agar layer with a physiologically relevant buffer at well-defined time intervals so that it is absorbed by the agar. Unfortunately, both approaches were unsuccessful because the agar coating is quickly susceptible to water evaporation, thinning the agar layer as it dries. This then results in large (tens of micrometers) axial drift of the sample. Even when the agar coating is supplied with a physiological buffer to counteract the evaporation, the salt concentration rapidly increases which ultimately compromises the physiological state of living cells. Counterbalancing the evaporation with Milli-Q water was another solution, however, the axial drift was still significant. The most important tested conditions for surface coating and their respective results are listed in Table 1.

Table 1. Tested surface coating and respective results.

Coating	Effect on living <i>M. xanthus</i> cells
1,5% CyE-agar	Coating too thick to image cells
0,75% CyE-agar	The TPM buffer containing cells evaporates over time, resulting in sedimentation of cells TPM buffer evaporation leads to salt sedimentation and formation of ion crystals Agar coating dehydrates over time resulting in a thinner layer, creating significant z-drift Cells are in air which leads to cell death
0,75% CyE agar + immersion in buffer	Cells are not well adhered to the agar coating even though FAs are established, resulting in the detachment of cells when adding TPM buffer
0,75% CyE agar + adding droplets of buffer at defined time intervals to hydrate the agar pad through absorption	Adding droplets of buffer creates fluctuations of the agar coating thickness over time After sedimentation of cells on the surface, cells remain in the thin liquid layer of the hydrated agar coating but motility is stalled after a while followed by cell death due to increased salt concentrations in the coating
0,75% CyE agar + adding droplets of Milli-Q at defined time intervals to hydrate the agar pad through absorption	Adding droplets of buffer creates fluctuations of the agar layer thickness over time Salt concentration decreases in the coating over time, deviating as well from physiological conditions
Poly-L-lysine 1/10	Reproducible adherence of cells Reduced motility speed
Poly-L-lysine 1/100	Reproducible adherence of cells Reduced motility speed
Chitosan	Irreproducible adherence and motility

Because of the unsuccessful attempts to construct a sample in which bacterial cells are deposited on an agar coating, we continued to explore polymer coatings. We tested the adherence and motility behavior of *M. xanthus* cells on poly-L-lysine (Sigma-Aldrich) in different concentrations and commercial chitosan (Sigma-Aldrich) while immersed in TPM buffer. As expected, commercial chitosan did not yield reproducible results. Poly-L-lysine on the other hand did result in reproducible adherence, and therefore we performed a control to test whether FA-powered motility behavior was

as expected. First, we tested motility speed by tracking cells over time on different surfaces. Lower speeds are detected when *M. xanthus* cells move over a poly-L-lysine coated surface as compared to an agar surface, and motility speed is dependent on the concentration of poly-L-lysine that was used to coat the surface (Figure 16a). Then, we tested the formation of FAs and the occurrence of cell reversals by following the fluorescently tagged AglZ protein (Figure 16b-c). Both on poly-L-lysine 1/10 and 1/100 concentrations cells are able to move by A-motility.

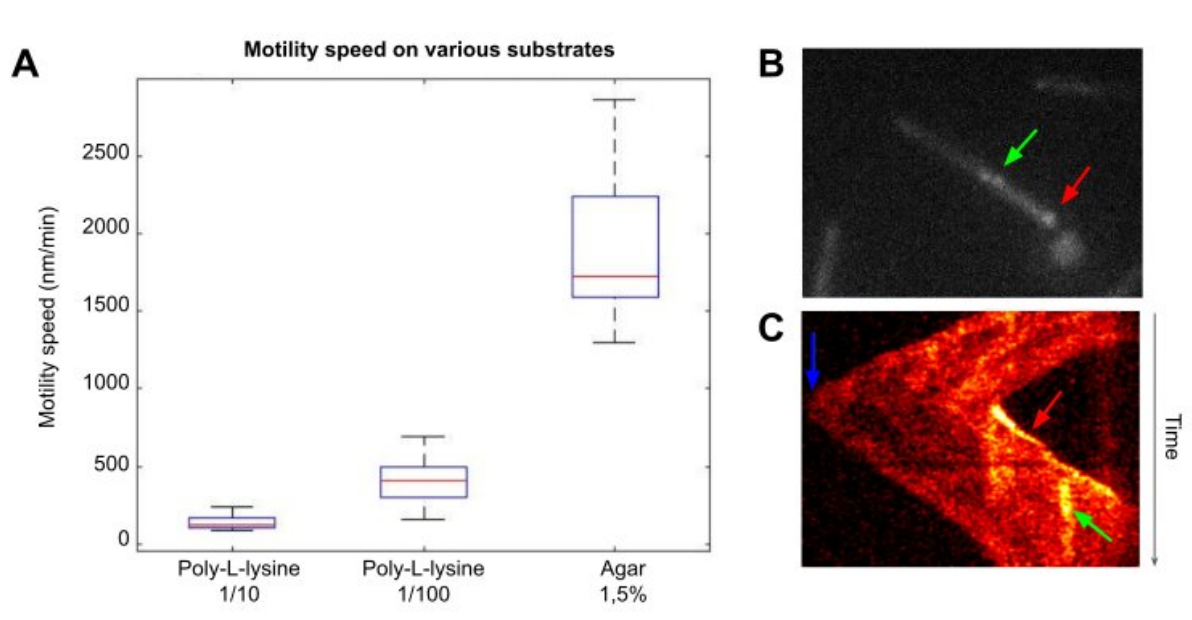


Figure 16. A-motility of *M. xanthus* on poly-L-lysine coated surfaces. A) Motility speed of *M. xanthus* (Δ pilA) on poly-L-lysine coated glass coverslips in 1/10 and 1/100 dilutions, and an agar substrate. B) Fluorescently labeled cells (Δ pilA AglZ-YFP) moving on a poly-L-lysine 1/100 coated glass coverslip forming fluorescent foci where Agl-Glt molecular motor assembles. C) Kymograph showing motility behavior of cell over time, including cell reversal (blue arrow), leading cells pole where Agl-Glt motor is assembled (red arrow), stationary FAs (green arrow).

4.4.2 AFM tip size and shape

Several different cantilevers and tips can be used to mechanically stimulate cells. The first set of cantilevers that we used, the MLCT-BIO-DC (Bruker AFM probes) with a nominal tip radius of 20 nm, proved to be ideal for imaging the sample but we deemed this probe not compatible with the experiment in terms of size (see below).

One working hypothesis that we wanted to test was that cell-cell collisions can induce cell reversals. Therefore, we aimed for a tip radius with a size similar to or larger than the diameter of a single cell. *M. xanthus* is a rod-shaped bacterium with a length of few μ m and a diameter of 1 μ m. To this end, we tested the Nanosensors ATEC-CONT (Nanosensors) where the tip is protruding from the cantilever which has a reported tip radius of 10 nm (Figure 17b-c) and the Nanotools Biosphere B1000-CONT (Nanotools) which has a spherical shaped tip with a radius of 1000 nm (Figure 18a). A polystyrene bead (Spherotech Inc.) with an approximate diameter of 2.7 μ m was attached to the ATEC-CONT tip to artificially enhance the tip radius. The protocol is described in Figure 17a. First, a glass coverslip is prepared containing a drop of glue and some beads. Prior to the deposition of the beads on the glass coverslip, the beads are dissolved and diluted in Milli-Q water, vortexed for several minutes and sonicated for 30 min. Then, 5 μ l of this solution is spotted on the glass coverslip and

allowed to dry for 45 min. This coverslip is mounted on the sample stage, while the cantilever with protruding tip is mounted onto the AFM cantilever holder. The tip of the AFM cantilever is then automatically approached to the glue (setpoint 5.0 V) and retracted when touching the glue. Finally, the AFM tip is automatically approached to an isolated bead on the glass coverslip (setpoint 0.2 V) and retracted. The tip containing the newly attached bead is then dried for 15 min (**Figure 17d-e**).

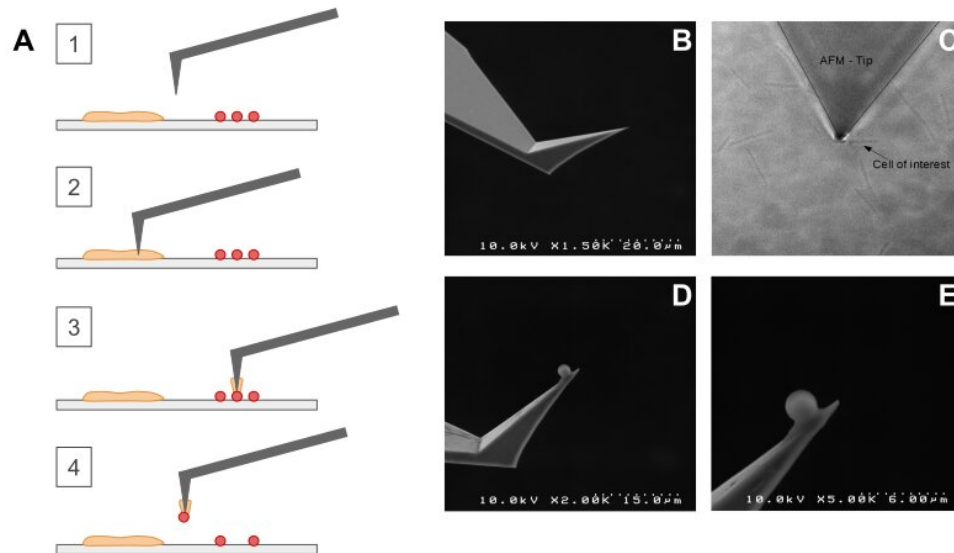


Figure 17. Bead attachment to the Nanosensors ATEC-CONT. A) Schematic protocol for attachment of microsized polystyrene bead on the Nanosensors ATEC-CONT protruding tip. B) Scanning Electron Microscopy (SEM) image of the Nanosensors ATEC-CONT tip. C) Field of view containing the protruding tip and cells. D) SEM image of Nanosensors ATEC-CONT tip with microsized polystyrene bead attached to it. E) Zoom of D.

4.4.3 The experimental set-up

When imaging live cells, care needs to be taken regarding phototoxicity and photobleaching. Light-induced damage can impair cell physiology, alter cell behavior and lead to cell death. Aside from the damage inflicted on the biological sample itself, the loss of fluorescent signal from labeled cellular components over time can impair the detection of target molecules. These effects are usually managed by decreasing the excitation illumination laser light as much as possible, while maintaining acceptable signal-to-noise ratios. In our experiment, the sample is illuminated by pulsing the excitation laser (with a T_{on} of 50 ms and a T_{off} ranging from 50 to 450 ms) which reduces the illumination time of the sample significantly. Nonetheless, the AgIZ-YFP fluorescent signal does decrease over time (**Figure 18d**). Despite the advantages of utilizing a pulsed excitation illumination in terms of phototoxicity and photobleaching (Boudreau et al. 2016), care needs to be taken when employing this manner of sample irradiation in correlative AFM-fluorescence microscopy. Pulsing the excitation laser can induce optomechanical forces resulting in cantilever oscillation and in non-constant and periodic tip-cell interaction force (Fernandes et al. 2020).

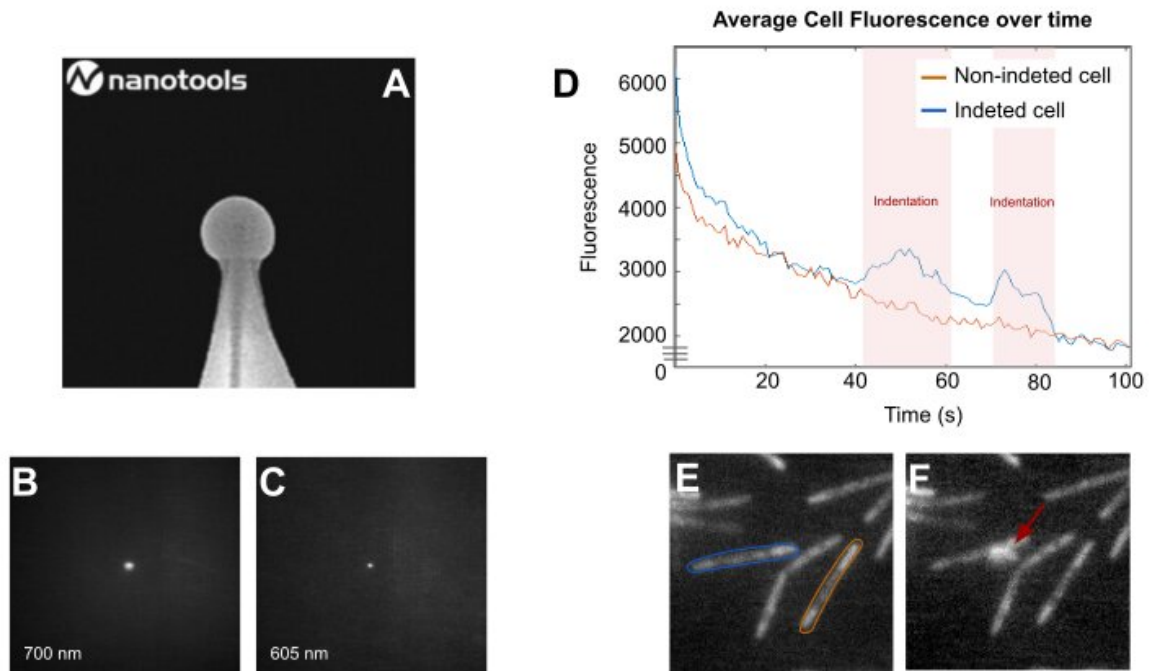


Figure 18. Fluorescence of Nanotools Biosphere B1000-CONT. A) Tip geometry of Nanotools Biosphere B1000-CONT. Derived from www.nanomore.com. B) Nanotools Biosphere B1000-CONT tip fluorescence emission at 700 nm. C) Nanotools Biosphere B1000-CONT tip fluorescence emission at 605 nm. D) Pixel average cell fluorescence over time for target cell for indentation (blue curve) and non-target cell. E) Fluorescently labeled cells (Δ pilA AglZ-YFP) on gliding on a poly-L-lysine coated glass coverslip before indentation. Blue (target cell for indentation) and orange encircled cells correspond to curve colors (D). F) Fluorescently labeled cells (Δ pilA AglZ-YFP) on gliding on a poly-L-lysine coated glass coverslip during indentation of the target cell.

A final parameter that needs to be evaluated is how, where and for how long the cell needs to be probed by the AFM tip to produce a mechanical stimulus detected by the cell (Gavara 2017). These three parameters might induce various cellular responses. In our experiment, we have explored three different ways of probing the cells, depending on the cantilevers and tips used (Figure 19). The Nanotools Biosphere B1000-CONT was used to stimulate cells normally and laterally targeting the cell body and not the cell poles. The internal cellular response of the AglZ-YFP protein was detected with fluorescence microscopy. While stimulating the cells, we observed that this tip is fluorescent in most fluorescence channels and at laser powers used to image the fluorescently labeled bacteria (AglZ-YFP) (Figure 18b-e). As such, the emitted fluorescence from the tip interferes with the observation of emitted fluorescence from AglZ-YFP.

An alternative approach is to use conventional light microscopy to observe the movement of cells over time. This does not allow us to follow the formation of FA complex through observation of fluorescence, but would permit measurement of cell displacements upon introduction of mechanical stimuli. In this case, the sample is imaged by the objective using brightfield illumination (Figure 15a), and thus the cantilever is visible in the image. For the Nanotools Biosphere B1000-CONT probes which have the tip attached perpendicular to and underneath the cantilever, this means that the tip is not visible and thus, the exact location of the tip is unknown or can only be estimated. To circumvent this

problem, as previously mentioned, we used the Nanosensors ATEC-CONT (Nanosensors) with a micrometric bead attached to the tip. This tip was mostly used as a physical obstacle placed close to the leading cell pole of a cell (**Figure 17c**).

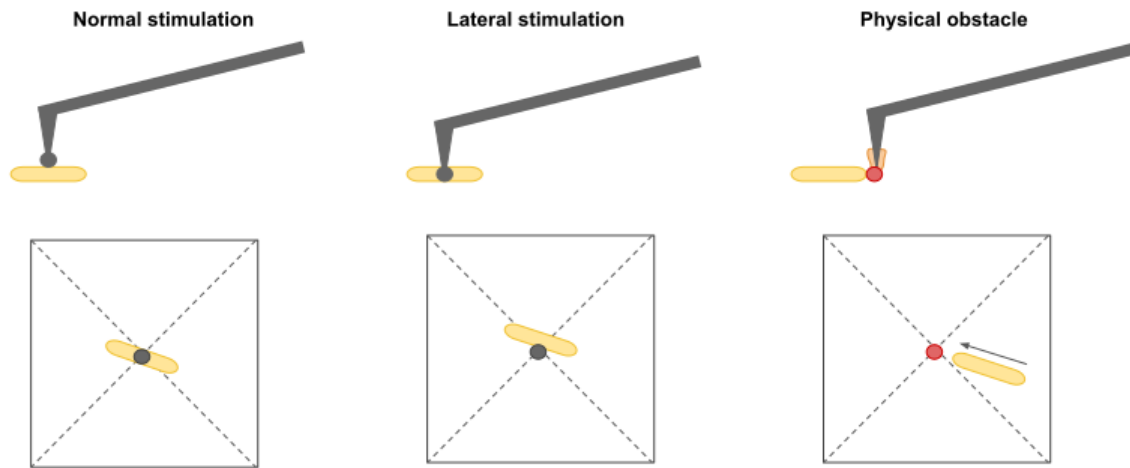


Figure 19. Different configurations for probing *M. xanthus* cells. Schematic representation of three different tip-cell interactions. Cells were probed normally or laterally when using a Nanotools Biosphere B1000-CONT. The Nanotools ATEC-CONT tip-size enhanced tips were used as a physical obstacle.

4.5 Results

We probed several tens of cells in numerous experimental replicates using the tip as a physical obstacle for moving cells (Δ pilA AglZ-YFP) on a glass coverslip coated with 1/100 poly-L-lysine and immersed in TPM buffer. In isolated moving cells - where no biological stimulus through contact with another cell is influencing cell behavior - we were able to observe cell reversal upon collision with the tip (**Figure 20a-b**). Other responses included: i) a short interaction between the tip and cell after which the cell stalled movement, and ii) the cell evading the tip after sensing and continuing the movement in the same direction.

Despite the observed cell reversals and interactions between cells and tips upon cell-tip collision, the slow motility rate of *M. xanthus* cells on poly-L-lysine made these experiments time-consuming and labor-intensive, which ultimately resulted in low statistics. Additionally, cells reacted in different manners to cell-tip collisions, deeming our results inconclusive at this moment. And finally, using only conventional light microscopy we could not probe the intracellular response to mechanical stimuli.

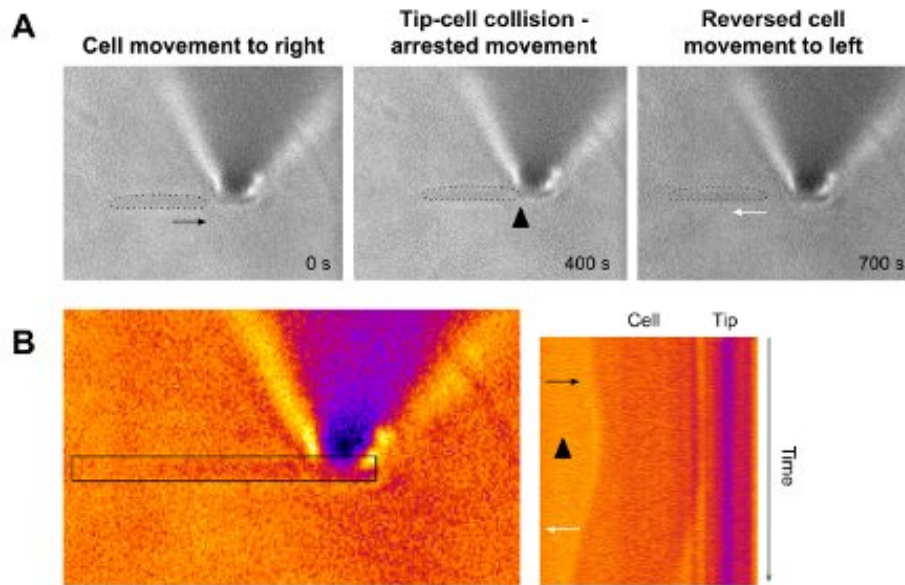


Figure 20. Tip-cell collision induced cell reversal. A) Snapshots taken at $t = 0\text{s}$, 400s and 700s of cell moving and colliding with the tip, after which it arrests movement and reverses. B) Kymograph (right) constructed from the boxed area, with the tip colored purple, the cell orange and the background yellow.

In this study, we did not utilize non-fluorescent large colloidal tips. However, the use of these probes would allow the detection and characterization of fluorescently-labeled target proteins of the Frz-signaling pathway or the Agl-Glt molecular motor. When using the AFM-SMLM set-up to its full potential, super-resolution imaging of those proteins would allow the determination of their precise localization and dynamics before, during and after mechanical stimulation of the cell. Ultimately, mutant deletion strains can be used to discover which proteins are essential to establish mechanically-induced cell reversals.

4.6 Conclusion

Despite the observed cell reversals and interactions between cells and tips upon cell-tip collision, the slow motility rate of *M. xanthus* cells on poly-L-lysine made these experiments time-consuming and labor-intensive, which ultimately resulted in low statistics. Additionally, cells reacted in different manners to cell-tip collisions, deeming our results inconclusive at this moment. And finally, using only conventional light microscopy we could not probe the intracellular response to mechanical stimuli.

In this study, we did not utilize non-fluorescent large colloidal tips. However, the use of these probes would allow the detection and characterization of fluorescently-labeled target proteins of the Frz-signaling pathway or the Agl-Glt molecular motor. When using the AFM-SMLM set-up to its full potential, super-resolution imaging of those proteins would allow the determination of their precise localization and dynamics before, during and after mechanical stimulation of the cell. Ultimately, mutant deletion strains can be used to discover which proteins are essential to establish mechanically-induced cell reversals.

III Conclusion and perspectives

In this thesis, I developed and applied several imaging technologies to investigate the mechanisms by which *M. xanthus* communities predate and kill *E. coli* colonies. First, I implemented a predation assay in which a colony of *M. xanthus* is spotted at a millimeter distance from a high density colony of *E. coli* on a hard agar surface. Over time, collective groups of *M. xanthus* cells move away from their community towards the *E. coli* colony and invade it, creating a predation zone. Second, to dissect the dynamics of collective cell movements during predation with single-cell resolution, I introduced a multiscale cell tracking approach that enabled semantic tracking of single predator and prey cells during relevant acquisition times. Importantly, this new imaging method enabled the quantitative analysis of single-cell and collective cell motion in a dense sample composed of multiple bacterial species partially overlapping in space and displaying complex dynamic behaviors. We used this method to investigate bacterial predation and more specifically, the respective roles of the motility systems during predation. We believe that this method is easily adaptable for different quantitative studies of *M. xanthus* communities as well, for example to study the motion dynamics during developmental aggregation occurring before fruiting body formation. Additionally, we envision that a similar approach can be useful to many other applications, such as study of bacterial dynamics within biofilms, or of other complex ecosystems (e.g. neutrophil migration and killing during parasitic infection).

Notably, this method enabled the tracking of most *M. xanthus* cells over extended time periods, even of cells within dense swarms. The approach, however, displays a number of limitations. For instance, cell tracking often stopped when cells entered *E. coli* microcolonies because *M. xanthus* cells frequently penetrate the prey microcolony by gliding over or under prey cells, creating a multilayer of cells that could not be segmented with our current method. The main reason for this limitation was that we segmented cells in 2D, thus cells outside of the main focal plane were often not detected. Use of 3D segmentation approaches could help solve this issue and permit tracking of *M. xanthus* motility in 3D within *E. coli* microcolonies and increase the tracking ability of cells within dense swarms. Previous efforts to follow the dynamics of *M. xanthus* cells within dense *E. coli* colonies resorted to the fluorescent labeling of only a small fraction of *M. xanthus* cells ([Berleman et al. 2008b](#)) representing a small subset of the predator population. Thus, this improvement in 3D tracking might provide insights into prey-predator interactions and the dynamics of collective prey killing at the single-cell level.

An alternative method to solve this issue would be to consistently use a fluorescently-labeled predator strain and allow the AI-network to assign more than one class per pixel during the semantic segmentation. This would allow the detection of 3D overlapping masks. This would require, however, a rethinking of the training data, as we currently assume only one cell be present at a given location, and thus only one class can be assigned per pixel. A new training database containing an additional layer of *M. xanthus* fluorescence information would be a prerequisite. The outputs of such a network would be a 2D labeled image containing *M. xanthus* cell masks and a second 2D labeled image containing *E. coli* masks. Such an adaptation of the semantic segmentation would allow us to reuse our tracking methodology for motile *M. xanthus* cells. Alternatively, voxel, instead of pixel, classification methods can be used for 3D cell segmentation. This, however, would require a redesign

of the tracking approach. Mask parameters, such as cell area and mask overlap become either challenging to compute based on voxel information or are no longer relevant in a 3D context. Therefore, these parameters need to evolve into concepts such as cell volume and volume overlap. To overcome these challenges, inspiration can be drawn from the recent advances made to adapt 2D U-net based approaches to 3D methods. These advances apply to high-resolution microscopy data ([Weigert et al. 2018](#); [Çiçek et al. 2016](#)), but are also extensively exploited for biomedical image analysis ([Islam et al. 2020](#); [W. Chen et al. 2019](#); [Kaur, Kaur, and Singh 2021](#)).

Finally, imaging an even larger area by increasing the mosaic size would allow us to visualize larger-scale collective phenomena, such as rippling. As we discussed in chapter II.1, robust tracking of cells requires that the time between images be smaller than half the distance travelled by a cell. Thus, increasing imaging areas would require a faster microscope. Potentially, use of light-sheet microscopy methods could accelerate 3D acquisitions over large areas, while also diminishing photo-toxicity and improving optical sectioning of multi-layered samples.

From microscopy timelapsing assays, a wide range of motion behaviors among *M. xanthus* cells could be observed. We found that, in contrast with the canonical view that the A-motility system powers motion of solitary cells and the S-motility system powers motion of swarms, that groups of cells (e.g. rafts and swarms) consist of both A- and S-motile cells. This raises the question whether this motility system diversity is reflected in the transcriptome and, moreover, whether a transcriptional control exists to modulate the use of these motility engines.

To study differential gene expression, I developed a spatial transcriptomics workflow in which an RNA species of interest could be labeled using In Situ Fluorescence Hybridization in fixed *M. xanthus* cells while conserving the spatial organization of the cell in the colony. This workflow was validated by studying the transcriptomic levels of one target RNA species, expressed under the promoter of the EF-TU gene, involved in translation and associated with cell growth, metabolic activity and proliferation. To provide such an experimental framework to understand transcriptome variation in complex microbial communities is of large interest for the community. Not so long ago, spatial transcriptomics were applied to sessile communities of *Pseudomonas aeruginosa* to study metabolic heterogeneity ([Dar et al. 2021b](#)). This study was carried out in collaboration with the Cai group and utilized its high-throughput sequential FISH method ([Eng et al. 2019](#); [Lubeck et al. 2014b](#)). The novelty of the work presented in this thesis and in the recent study of Dar and colleagues is that transcriptome profiling of cells in organized microbial communities is now possible without disrupting the spatial context. This allows to detect transcriptome heterogeneity and to link this information to the community context. More specifically, the spatial localization, cluster patterns or scattering of cells with similar transcriptome profiles can be studied. Another high-throughput multiplexed FISH technique, called merFISH ([K. H. Chen et al. 2015b](#)), was previously used to show the spatial patterning of distinct neural populations in the mouse hypothalamic preoptic region ([Moffitt et al. 2018](#)). It is only a matter of time before these spatial omics methods are consistently applied to microbial communities.

For the *M. xanthus* predating colony specifically, spatial transcriptomics might provide insight into the mechanisms of, for example, prey killing and feeding. Prey killing by *M. xanthus* has been proposed to happen by OMVs containing lethal cargo or by a tad-like apparatus in a contact-dependent manner ([Seef et al. 2021a](#); [Evans et al. 2012](#)). To date, however, it remains unclear how and which cells feed on these nutrients and what nutrients are metabolized. Transcriptomic profiling

of cells at the predation forefront might detect the expression of gene products for metabolic activity which might lead to a better understanding of which macromolecules derived from prey-lysis are metabolized during the feeding process and in which cells metabolic activity occurs. It has been hypothesized that the multicellular phenomenon of rippling contributes to efficient nutrient scavenging ([Berleman et al. 2006](#)). A high-throughput spatial transcriptomics profiling of *M. xanthus* cells might be able to consolidate this hypothesis. Finally, motion behavior can be studied with transcriptome profiling. To date, it is unclear whether *M. xanthus* is attracted to prey or whether it encounters it by chance through efficient surface colonization. The expression of genes playing a role in chemotaxis pathways might shed light on predator attraction by prey cells and on how *M. xanthus* cells coordinate their motion through a prey colony.

Aside from transcriptome profiling, the workflow that I presented can be extended to other spatial omics methods. We showed that immunolabeling could be achieved on the printed *M. xanthus* assays. This means that imaging-based proteomics studies through antibody labeling can be carried out for protein expression and localization studies. Additionally, spatial genomics methods relying on DNA FISH labelling can be applied to the printed predation assay and be exploited for chromosome architecture experiments.

Overall, the technological and experimental frameworks presented in this thesis contribute to the field of *M. xanthus* and open the door for a myriad of experiments. With the arrival of more accessible, open-source deep learning tools and their applications to the field of biology, studies which were up thus far qualitative, can now be studied with data-driven approaches. Additionally, the recent work done on complex microbial communities using spatial transcriptomics showcases the interest of in-depth profiling of single-cells in their native microenvironments. It is exciting to anticipate the new waves of biological discoveries that these techniques will bring.

IV Annex

1 Material and Methods

Bacterial strains

A list of all bacterial strains used in the thesis can be found **Table 2**. This table contains the strain name, genotype and strain origin.

Table 2. List of bacterial strains.

Strain	Genotype	Strain origin
<i>E. coli</i>	MG1655 wildtype	
<i>E. coli</i> HU-mCherry	MG1655 HU-mCherry	Espeli laboratory collection
<i>M. xanthus</i>	DZ2 wildtype	Mignot laboratory collection
<i>M. xanthus</i> cytosolic-sfGFP	DZ2 pSWU19-pm3068-sfGFP	Mignot laboratory collection
<i>M. xanthus</i> A+S- OMss-sfGFP	DZ2 Ω pilA pSWU19-PpilA-OMss-sfGFP	Mignot laboratory collection
<i>M. xanthus</i> A-S+ OMss-sfGFP	DZ2 GltJ DNterm222 pSWU19-PpilA-OMss-sfGFP	Mignot laboratory collection
<i>M. xanthus</i> A+S- OMss-mCherry	DZ2 DpilA pSWU19-PpilA-OMss-mCherry	Mignot laboratory collection
<i>M. xanthus</i> AglZ-NeonGreen	Allelic replacement of <i>aglZ</i> by <i>aglZ-NeonGreen</i>	Mignot laboratory collection
<i>M. xanthus</i> RomR-GFP	DZ2 pSWU30-pilA-RomR-GFP, Tcr	Mignot laboratory collection
<i>M. xanthus</i> Δ KillDEF	DZ2 Δ 3105-3107	Mignot laboratory collection (Seef et al. 2021b)
<i>M. xanthus</i> (A+S-) AglZ-YFP	DZ2 pilA::tet aglZ-YFP, Tcr Kmr	Mignot laboratory collection (Faure et al. 2016b)

Bacterial cultures

E. coli cells used in predation assay were grown overnight in 10 ml Luria-Bertani (LB) medium at 32°C under agitation (200 rpm). To ensure that *E. coli* cells were in exponential phase after overnight growth, a 1:10 dilution of the starter culture was made in fresh LB medium and incubated for approximately four hours.

M. xanthus cells were grown overnight in 10 ml Casitone Yeast Extract (CYE) rich medium as was described before (Bustamante et al. 2004) at 32°C under agitation (200 rpm), supplemented with antibiotics (Ampicillin 1 μ g/ml) when necessary. Cells were harvested when the OD₆₀₀ reached 0.1-0.5.

***M. xanthus* biofilms and predation assays**

Bacterial predation was established in laboratory conditions by setting up a predation assay. In short, *E. coli* and *M. xanthus* cells were harvested from the LB and CYE media, respectively. Cells were concentrated by centrifugation on a tabletop centrifuge at 2100 g for 5 min at room temperature and resuspended in CF medium (10 mM MOPS (pH 7.6), 1 mM KH₂PO₄, 8 mM MgSO₄, 0.02% (NH₄)₂SO₄, 0.2% sodium citrate, 0.015% bacto casitone peptone). *M. xanthus* cells were concentrated to an OD₆₀₀ of 5, *E. coli* cells were concentrated to an OD₆₀₀ of 0.005 or 5 for the time lapse imaging experiments and the RNA FISH experiments, respectively. Cell suspensions of 1 µl were spotted at close distance of approximately 1 mm on CF 1.5% agar pads supported on a coverslip.

The agar pads used for time lapse imaging were made with ultrapure agar (UltraPure Agarose 1000, Invitrogen) to limit autofluorescence by impurities in the agar solutions. Pads were made by pipetting 550 µl of melted agar onto a 25mm coverslip and by placing a second coverslip on the drop of agar, allowing the latter to solidify between two flat surfaces. Once the agar pad was made, the top coverslip was removed and the agar was cut to a diameter of 20 mm.

The prepared predation assays were then placed onto a layer of CF 1.5% agar in a petri dish and the petri dish was closed with parafilm to avoid agar pad evaporation and drying. Samples were incubated 24h to 48h on 32°C to allow *M. xanthus* cells to invade the *E. coli* colony.

M. xanthus biofilms, in the absence of prey, were created by spotting the concentrated *M. xanthus* suspension on either a thin CF 1.5% agar pad or on a thin CYE 1.5% agar pad, created as described above.

Microscopy

Fast time lapse and hubble imaging were done on a homemade fully-automated hardware-accelerated wide-field epifluorescence microscope built on a RAMM modular microscope system (Applied Scientific Instrumentation). Samples were imaged using a 60x Plan-Achromat water-immersion objective (NA = 1.2, Nikon, Japan). The objective lens was mounted on a closed-loop piezoelectric stage (Nano-F100, Mad City Labs Inc. - USA). Illumination was provided by a brightfield illumination source and 2 lasers (OBIS-488 nm and Sapphire-LP-561 nm, Coherent – USA). Images were acquired using a sCMOS camera (ORCA Flash 4.0V3, Hamamatsu – Japan), with a final pixel size calibrated to 106 nm. A custom-built autofocus system was used to correct for axial drift in real-time and maintain the sample in focus. Software-controlled microscope components, including camera, stages, brightfield illumination and lasers were run using a custom-made software package developed in LabView 2015 (National Instrument).

Hubble imaging

Hubble images, in which the predation assay is fully captured, was carried out by constructing a mosaic patchwork of MxN size. Each FOV of the mosaic overlaps with the neighbouring FOVs by 200 pixels. Acquisition of such a large mosaic was achieved by following a snake-like pattern. For each FOV a 3D stack of brightfield and fluorescence images was acquired of 12 planes interspaced with 250 nm. Laser powers were adjusted to have optimal signal for the target fluorescent proteins. Exposure times were set to 50 ms and brightfield illumination was decreased with a neutral density filter (OD 2).

Fast time lapse imaging

For imaging of the predation assay, the sample was covered with an imaging coverslip. The imaging coverslip was washed consecutively with acetone, Milli-Q water, 70% ethanol (v/v) and Milli-Q water, and flamed to remove any fluorescence impurities and residues. The coverslip was cooled down to room temperature and placed hermetically on the sample while avoiding bubbles between the sample and the coverslip. The sample was mounted in an attofluor and onto the microscope for imaging. A region of interest spanning an area of approximately 0.36 mm² was selected. This large area was imaged by constructing a mosaic patchwork of 3 by 3 fields of view (FOVs) or mosaic tiles of 2048x2048 pixels, each theoretically overlapping with 200 pixels. An imaging cycle, in which the 3-by-3 mosaic was imaged by sample displacement following a snake-like pattern, was thus made up of 9 consecutive acquisitions. For each FOV, a 3D-stack was acquired to account for sample tilt in brightfield and in the fluorescence channel of 561 nm for *E. coli* carrying a HU-mCherry fusion. An additional fluorescent channel was added for *M. xanthus* when the used strain was carrying a fluorescent protein as well. A 3D-stack was generally made up of 7-12 planes interspaced with 250-500 nm. Exposure times were set at 50 ms. The laser powers used were kept at low intensity to limit phototoxic effects on the live cells during time lapse acquisition. Brightfield illumination was attenuated with a neutral density filter with optical density two. Imaging cycles were generally completed in 30-40 seconds and were repeated 700 times to construct an hours-long time lapse series of the mosaic area.

Treatment of fast time lapse data

To increase imaging speed, all images from one imaging cycle were pooled into one DCIMG file. First, the DCIMG files were converted to tiff files with software from Hamamatsu and sorted for each FOV, channel and time point. Tiff images of the fluorescent channel of *E.coli* were deconvolved with Huygens Professional version 20.04 (Scientific Volume Imaging, the Netherlands, <https://svi.nl/>). Deconvolved *E. coli* stacks were z-projected by calculating the standard deviation. 3D brightfield stacks were converted to 2D images by dividing each stack in 16 ROIs of 512x512 pixels, selecting automatically or manually the in-focus plane for each ROI and restitching the 16 ROIs. The code for calculating the in-focus brightfield image (`im_straighter_FTL.m` or `im_straighter_FTL_manual.m`) can be found in https://github.com/jbfiche/DCIMG_to_TIFF_conversion/tree/master/Fast_TL_windows.

2D brightfield and *E. coli* fluorescence images were used as input for an in-house developed MATLAB code using a convolutional neural network with U-Net architecture for semantic segmentation (Ronneberger, Fischer, and Brox 2015; Van Valen et al. 2016). Semantic segmentation was performed with five independently trained networks to converge towards a high confidence result, outputting an image with pixel values representing the pixel assignment confidence to a given class. The code for semantic segmentation (`Reconstruct_image_FCN_FTL.m`) can be found in https://github.com/jbfiche/Deep_Learning_segmentation/tree/Myxo_segmentation_predation_fluo_Unet/For_image_reconstruction.

Segmented images were then used to reconstruct the mosaic image by tiling the 9 images. Exact image overlap for tiling was calculated by image-based pixel-resolution cross correlation. Drift in time was corrected by aligning the mosaic images based on cross correlation calculated from

segmented images of stationary *E. coli* microcolonies. *M. xanthus* segments from mosaic images were post-processed to reduce segmentation artefacts. In short, binary masks were generated from the masks by exploiting the assignment of confidence values, masks were filtered for size and finally, tortuous masks and fused masks were rejected. *E. coli* masks were post-processed to avoid overlap between *E. coli* and *M. xanthus* masks and filtered for size to reject isolated pixels. The code for cross-correlation calculation (`MosaicImages_CC_BFNormalized_MyxoSegmented.py` and `Mosaic_DriftCorrection_GlidingRef_MiddelROI5.py`), and tiling, drift correction and mask post-processing (`function_DriftCorr_MosaicTiling_Ecoli.m`) can be found in https://github.com/SaraRombouts/ProjectFTL_Predation.

Single cell tracking

Single cell trajectories were reconstructed with an in-house developed MATLAB pipeline. For each timepoint in the time lapse image series, pairwise tracks were constructed between cells in frame k and cells in frame $k+1$. Briefly, the enlarged bounding box of the cell mask in frame k was utilized to select a number of possible candidates in frame $k+1$. Ultimately, the optimal candidate was found by ranking the candidates with Analytical Hierarchy Processing (AHP) (Saaty 1986) based on several parameters of the masks including cell area, cell length and mask overlap area between the cell and its candidates. To correct for multiple assignments of a candidate, an inverse AHP approach was used in which the optimal cell from frame k was selected for the candidate of frame $k+1$. Finally, pairwise tracks over all timepoints were combined to form complete single cell trajectories. The code for single-cell trajectory reconstruction (`function_Tracking_TiledMosaic.m`) can be found in https://github.com/SaraRombouts/ProjectFTL_Predation.

MSD

To characterize bacterial movement, individual bacterial trajectories were analysed with the Python trackpy package. For each track, the Mean Squared Displacement (MSD) was computed and the five first time points were fitted with a power law. The resulting scaling exponent, α , was used to characterize the directionality of bacterial movement (from confined with $\alpha < 1$, brownian with $\alpha = 1$, to directed with $\alpha > 1$). The code used to calculate the MSD (`Myxo_trackpy.py`) can be found in https://github.com/SaraRombouts/ProjectFTL_Predation.

Speed

Instantaneous cell speed was calculated using the **straight** distance traveled in the five frames before and five frames after a given time point, normalized by the time between 10 frames. The code used to calculate speed (`matfiles_to_umap_format.py`) can be found in https://github.com/SaraRombouts/ProjectFTL_Predation.

Voronoi tessellation

To measure the local density of *M. xanthus* cells, a Voronoi tessellation was performed with the Voronoi function of MATLAB. The voronoi tessellation was calculated on the centers of the backbones of all masks that were included for tracking. Centers of gravity of the masks that were filtered for tortuosity and mask fusion based on branchpoints were included as well. For masks which

contained a branchpoint in their backbone, the branchpoint was deleted, essentially breaking up the backbone. The centers of the newly generated backbones were calculated and included for the tessellation. For masks filtered out for tortuosity, the centers of the backbones were calculated as well and included for the tessellation. The area of the polygon to which the mask belongs was used as a measure for local density, with large polygon areas for low cell density and small polygon areas for high cell density. The code used to calculate the local density of *M. xanthus* cells (function_Voronoi_backbone_OverlapFlag.m) can be found in https://github.com/SaraRombouts/ProjectFTL_Predation.

Long range clustering

Long range clustering of cells was performed by dilating the binary cell masks of *Myxococcus xanthus* cells using a 10x10 pixels kernel ($\sim 1 \times 1 \mu\text{m}$). Then, merged cell masks were identified as clusters using the regionprops module of the skimage package in Python. For each identified cluster, the number of cells per cluster was determined and its size was measured as the area covered by the non dilated cell masks comprising each cluster. The code used to perform long-range clustering (scratch_multiscale_segmentation.py) can be found in https://github.com/SaraRombouts/ProjectFTL_Predation.

Classes

Bacterial populations were categorized into four groups: loners, scouts, rafts and swarms. Two criteria were used to determine the group to which a cell belongs to at each time point in the time lapse: the Voronoi cell density, V , and the number of cells per cluster, N . For loners: $\log_{10}(V) \leq 4.5$ and $N \leq 2$; for scouts: $\log_{10}(V) \leq 4.5$ and $N \leq 20$; for rafts: $2 < N \leq 600$; and for swarms: $600 < N$. When scouts functionality was used as an additional criterion, only cells with a speed higher than 3 pixels/frame were selected. The code used to cluster cells into classes (Figure2_myxo_classes.py) can be found in https://github.com/SaraRombouts/ProjectFTL_Predation.

2D Histograms

Two dimensional data points and trajectories histograms were both computed using the Python Datashader package, with canvas mapping data to pixels as points or lines, respectively. For histogram differences, the histograms were first normalized by the sum of their bin values. For histograms of trajectory fluxes, the spatial coordinates of each bacterial trajectory were replaced with new coordinates corresponding to the classification of the bacteria, being either loner, scout, raft or swarm, at each time point along the track with Gaussian noise added to reduce the overlap of the tracks. The code used to reproduce the histograms in Figures 1 and 2 (Figure1_2D_Histograms_ratio_2.py, Figure1_2D_Histograms.py, Figure1_Histo1D_speed_scouts.py, Figure2_2D_Histograms_ratio_0.py, scratch_compute_tracks_datashader_maps.py) can be found in https://github.com/SaraRombouts/ProjectFTL_Predation.

Similarity index map

To quantify the similarity between the trajectories of the scouts and the rest of the population, the trajectories of the two populations were split apart to map them on separated 2D arrays. Each array map was then binarized and used to compute a structural similarity index map with the Python Scikit-image package (sliding window of three pixels). Finally, the resulting similarity index map was binarized to extract the area of each portion of trajectory shared by the two populations. These areas

of shared trajectories were used to quantify the amount of scout trajectories shared with the rest of the bacterial population. The code used to calculate similarity index maps (Figure3_load_and_analyse_tracks_datashader_maps.py) can be found in https://github.com/SaraRombouts/ProjectFTL_Predation.

Prey consumption

To quantify the consumption of prey cells by *M. xanthus* during invasion, the fluorescence of *E. coli* HU-mCherry was used. For each time point in the movies, the fluorescence intensity of the central plane of each z-stack was first normalized by the Gaussian profile of the excitation laser and then projected along the perpendicular direction of invasion. The mean intensity was then truncated into three equal parts to quantify *E. coli* HU-mCherry intensity changes in the portion of the field of view (FOV) that gets invaded by *M. xanthus* cells during the acquisitions (bottom part of the stitched FOV) and in a portion that does not get invaded during the acquisition (Top part of the stitched FOV), the central portion not being used. For the bottom and top parts of the FOV, the mean fluorescence intensity of *E. coli* HU-mCherry was quantified for each frame of the movies to characterize the disappearance of *E. coli* cells over time. The code used to calculate prey consumption (Figure4_EC_killing_load.py) can be found in https://github.com/SaraRombouts/ProjectFTL_Predation.

AgIZ foci detection

AgIZ foci were automatically detected to highlight the position of AgIZ complexes in single cells. For this, the raw fluorescent z-stacks were first band pass filtered to remove noise and low spatial frequencies in single planes and then a local normalization was applied to equalize signal strength heterogeneities due to the Gaussian excitation profile. Finally, the four central images of the z-stack were summed and used to localize AgIZ complexes as diffraction-limited spots using the DAOSTarFinder utility from the Astropy package (<https://www.astropy.org/>).

RNA FISH in liquid cultures and in predation prints

Probe design

Probes were designed against the transcript of superfolder GFP (sfGFP), a 718 nucleotide long transcript. A set of oligonucleotides was designed with the Stellaris Probe Designer version 4.2 (available at <https://www.biosearchtech.com/stellaris-designer>). The Stellaris Designer was set to generate homologous sequences of 20 nt long interspaced by at least 2 nt. The masking level, which masks simple repeats, species specific repeats and repetitive sequences with more or less stringency, was set to two. Under these conditions, 28 unique probes spanning the complete sfGFP transcript with GC contents ranging between 40% and 60% were generated. Each homologous sequence was further complemented at the 5'-end with two 32-mer sequences complementary to two unique and fluorescently-labeled oligonucleotide secondary probes. The final primary oligonucleotide probes (ordered from integrated DNA technologies, or IDT) thus contained a region homologous to the transcript appended by two read-out sequences on the 5'-end using an AT spacer. Secondary probes were labeled with Alexa-647N, their sequences can be found in **Table 3**.

Table 3. Sequences of probe set for sfGFP target transcript and read-out oligos.

Probe set sfGFP (28 homologous regions)	CAGTTCTTCACCTTTAGACA CAGGATCGGAACAACACCGG TTAACATCACCATCCAGTTC CCTTCACCACGAACAGAGAA TTTACCGTTGGTTGCATCAC GTGCAGATGAATTCAGGGT CATGGAACCGGCAGTTTACC AACACCATAGGTCAGGGTAG TCCGGGTAACGAGAAAAACA GAAATCATGCTGCTTCATGT CTTCCGGCATTGCAGATTTG AAATGGTGCCTCCTGTACA TAGGTGCCATCGTCTTTGAA TTAACCTCTGCACGGGTTT CAGTTCTTCACCTTTAGACA ATGCCTTTCAGTTCAATACG GTTGCCGCCTCTTTGAAAT GTTATATTCCAGTTTGTGGC GCGGTGATGTAAACGTTATG GATACCGTTCTTCTGTTTGT GGCGAATTTGAAGTTAGCT TGTACGCTACCGTCTTCAAC CATCACCGATCGGAGTGTTT TGGTTATCCGGCAGCAGAAC GAACAGACTGGGTGGACAGG TTTTCGTTCGGGTCTTTGGA ATACCTGCTGCAGTAACGAA ATTTGTAGAGCTCATCCATG
Read-out probe 1	CACACGCTCTCCGTTCTATGCGACGTCGGTG/iThioMC6-D//3AlexF647N/
Read-out probe 2	GACCAAGAGCGGACGTTGTGCCAATGATCGC/iThioMC6-D//3AlexF647N/

RNA FISH

RNA FISH labeling of *M. xanthus* cells was achieved by working in an RNase-free environment. All solutions were prepared in an RNase-free manner and sterilized by filtration through a 0.22 µm filter.

RNA labeling in *M. xanthus* cells from liquid culture was optimized by adapting the protocol of Skinner et al (Skinner et al. 2013b). In short, cells were grown overnight in 20 mL CYE. After overnight growth, a cell culture volume equal to $V=6/OD_{600}$ was harvested by transferring the culture to falcon tubes on ice. Cells were pelleted by centrifugation at 4500g for 5 min at 4°C. After centrifugation, cells were resuspended and fixed in 1 ml ice-cold 3.7% formaldehyde PBS solution for 30min. Cells were then washed by centrifugation at 600g for 3.5 min at room temperature and resuspended in 1 ml 0.1% Tween-20 PBS. Finally, cells were pelleted by centrifugation at 600g for 3.5 min at room temperature and permeabilized in 1 ml 0.4% Triton X-100 PBS for 15 min. Labeling of target RNAs was initiated by a prehybridization step. After pelleting the cells by centrifugation at 1000g for 7 min at room temperature, cells were resuspended in 1 ml washing buffer containing either

10% or 40% formamide (v/v) and 2X SSC for 5 min at room temperature. Cells were pelleted again by centrifugation at 1000g for 7 min at room temperature. Hybridization of the primary probes was achieved by resuspending the cell pellet in 50 µl hybridization buffer (10% dextran sulfate, 0.02% BSA (w/v), 10% *E. coli* tRNA (w/v), 2 mM ribonucleoside vanadyl complex, 10-40% formamide (v/v), 2X SSC) containing a total of 550 pmol, or 10 µM, primary probes and incubation overnight at 30°C. The next day, 200 µl washing buffer (10% formamide, 2x SSC) was added to and mixed with the cells in the hybridization buffer. Cells were then washed twice by centrifugation at 1000g for 5 min at room temperature, pellets were resuspended in 200 µl washing buffer (10% formamide, 2X SSC) and further incubated at 30°C for 30 min. Then, cells were centrifuged again at 1000g for 5 min at room temperature. Finally, the hybridization of the secondary fluorescent probes (RTs) to the read-out sequences in the tails of the primary probes was carried out by resuspending the pelleted cells in 500 µl RT solution (25 nM per secondary probe in washing buffer (10% formamide, 2X SSC)) and by incubating for 30 min at room temperature. Finally, cells were pelleted by centrifugation at 1000g for 5 min at room temperature and resuspended in 50 µl imaging buffer (1X PBS, 5% w/v glucose, 0.5 mg/mL glucose oxidase and 0.05 mg/mL catalase).

RNA labeling in a *M. xanthus* colony or *M. xanthus* predating colony was achieved by tightly adhering, or printing, cells to the imaging coverslip. This was done by compressing the intact colony between the supported agar pad and the imaging coverslip. First, the imaging coverslip was cleaned sequentially with acetone, Milli-Q water, 70% ethanol (v/v) and Milli-Q water, and flamed to remove any fluorescence impurities and residues. The coverslip was cooled down to room temperature, and placed hermetically on the agar pad, ensuring that no bubbles were formed between the agar pad and the imaging coverslip. An in-house fabricated weight of around 50 gr was placed on the support coverslip to compress cells against the imaging coverslip. This allowed the use of a liquid handling system that does not alter the spatial structure of the colony. To tightly adhere cells to the imaging coverslip, the sample was placed in a petri dish. The petri dish was either sequentially flushed with 5 ml ice-cold 3.7% formaldehyde PBS for 90 min on ice, 70% ethanol for 15 min at room temperature and 100% ethanol overnight at room temperature, or with 5 ml ice-cold FAA (50%-70% ethanol (v/v), 3.7% formaldehyde (v/v), 5% glacial acetic acid (v/v)) for 10-30 min on ice. During incubation, these solutions diffused through the agar pad and fixed cells to the glass.

After incubation with fixatives, the weight was removed and the agar pad was disassembled from the imaging coverslip leaving the intact colony attached to the imaging coverslip. FAA-treated colonies were additionally immersed in 5 ml ice-cold 3.7% formaldehyde PBS for 30 min on ice. After fixation, the sample was washed twice with 5 ml 0.1% Tween-20 PBS for 15 min at room temperature and permeabilized with 5 ml 0.4% Triton-X PBS for 15 min at room temperature. Samples were then immersed in prehybridization buffer (10% formamide (v/v), 2X SSC) for 15 min at room temperature. Hybridization of primary probes was done by overnight incubation on 30°C of the sample in 200 µl hybridization buffer (10% dextran sulfate, 0.02% BSA (w/v), 10% *E. coli* tRNA (w/v), 2 mM ribonucleoside vanadyl complex, 10% formamide (v/v), 2X SSC) containing 550 pmol primary probes, or 2.75 µM. To avoid evaporation of the hybridization buffer overnight, the coverslip was placed sample down onto a piece of parafilm spreaded on the bottom of a petri dish on which the hybridization buffer was pipetted. Afterwards, the coverslip was washed twice in 5 ml washing buffer (10% formamide (v/v), 2X SSC) for 30 min on 30°C. Secondary probes were hybridized in 100 µl RT solution (100 nM per secondary probe in washing buffer (10% formamide, 2X SSC)) for 30 min at room temperature. Samples were washed once more in 5ml washing buffer and subsequently imaged

in 200 μ l imaging buffer (1X PBS, 5% w/v glucose, 0.5 mg/mL glucose oxidase and 0.05 mg/mL catalase).

Immunofluorescence

Commercial antibodies against GFP (GFP-booster-ATTO647N, Chromotec) were used for immunofluorescence labeling of the sfGFP target protein. *M. xanthus* cells were fixed, washed and permeabilized in 3.7% formaldehyde PBS for 30 min, 0.1% Tween-20 PBS and 0.4% Triton-X PBS for 15 min, respectively. After permeabilization, cells were washed twice with 0.1% Tween-20 PBS and treated with blocking buffer (4% BSA (w/v), 0.1% Tween-20 (v/v), PBS) for 10 min at room temperature. Antibody incubation was done in 1 ml blocking buffer containing 1:200 GFP-booster for 1h at room temperature. Samples were washed three times with 1 ml 0.1% Tween-20 PBS for 5 min at room temperature. Samples were immersed in imaging buffer for microscopy.

RNA FISH Microscopy

Imaging of RNA labeled samples and immunofluorescence stained samples was performed on a home-built set-up based on a Zeiss Axiovert 200 equipped with a EM-CCD (iXon-897, Andor) and an oil-immersion objective (Zeiss, 1.45 NA, 100X).

Both the acquisition of the anti-GFP antibody labeled with ATTO-647N and the RNA read-out probes labeled with Alexa-647 were imaged by acquiring a time series of several tens of images at the focal plane with a 640 nm readout laser (OBIS-640, Coherent - USA) and an exposure time of 50 ms. The fluorescent protein (sfGFP or GFP) was imaged with a 488 nm readout laser (OBIS-488, Coherent - USA) with an exposure time of 50 ms. A bright field image was taken of each field of view for cell segmentation.

RNA FISH Image treatment

Image treatment was done with a home-made MATLAB code. For each acquired time series an average image was calculated based on the first 10 consecutive images of the time series. To correct for the inhomogeneous illumination pattern, images were flattened with an estimated image of the excitation profile. This estimated image was constructed by applying a butterworth filter to the average images. Cell segmentation was done with an in-house developed MATLAB-based AI approach. In short, bright field images were segmented with a Convolutional Neural Network (CNN) using five independently trained networks for *M. xanthus*. Images outputted by each of the five networks were averaged to construct the converged resulting segmented image. Single cell masks were obtained by binarizing the converged segmented image. The code for segmentation (Reconstruct_image_segmentation_bacteria_emCCD.m) can be found in https://github.com/jbfiche/Deep_Learning_segmentation/tree/emCCD_generalization.

Cell masks were used to retrieve the total integrated fluorescence for single cells by summing all pixel values per mask. This value was divided by the area under the mask to normalize for cell size.

Foci intensity determination

The intensity values of foci in cells were determined by selecting a line ROI on the average images and plotting the intensity profile along this line. From the intensity line profiles the peak intensity was determined.

Melting temperatures

The theoretical melting temperatures of DNA/RNA hybrids of the primary probes and their corresponding homologous region of the transcript were calculated with the online version of MELTING (<https://www.ebi.ac.uk/biomodels-static/tools/melting/>) (Le Novère 2001). Input parameters for this calculation included: i) nearest-neighbor parameters set as in (Sugimoto et al. 1995), ii) salt concentration equal to 0.303 M reflecting the salt concentration in the hybridization buffer, iii) excess nucleic acid concentration equal to 2.75 μ M in the hybridization buffer, and iv) the salt correction as in (SantaLucia 1998). The effect of formamide concentration (in volume/volume percentage) in the buffer is described in MELTING with the following equation:

$$T_m = T_m (\text{Formamide}=0) - 0.65 \times \text{Formamide concentration (\%)}$$

as described in the user guide (<https://www.ebi.ac.uk/biomodels-static/tools/melting/melting5-UserGuide.pdf>). This equation was applied on the theoretical melting temperatures calculated for the DNA/RNA hybrids for each primary probe for formamide concentrations ranging from 0-40% (v/v).

2 Review: RNA Imaging in Bacteria

REVIEW ARTICLE

RNA imaging in bacteria

Sara Rombouts and Marcelo Nollmann^{*,†}

Centre de Biochimie Structurale, CNRS UMR 5048, INSERM U1054, Université de Montpellier, 60 Rue de Navacelles, 34090, Montpellier, France

^{*}Corresponding author: 29 rue de Navacelles, Montpellier, France. Tel: +33 6 77 50 80 83; E-mail: marcelo.nollmann@cbs.cnrs.fr**One sentence summary:** Recent advances in RNA labeling make it possible to study transcript abundance, localization and dynamics in bacteria.

Editor: Tam Mignot

[†]Marcelo Nollmann, <http://orcid.org/0000-0003-3339-2349>

ABSTRACT

The spatiotemporal regulation of gene expression plays an essential role in many biological processes. Recently, several imaging-based RNA labeling and detection methods, both in fixed and live cells, were developed and now enable the study of transcript abundance, localization and dynamics. Here, we review the main single-cell techniques for RNA visualization with fluorescence microscopy and describe their applications in bacteria.

Keywords: RNA imaging; microscopy in bacteria; transcription

INTRODUCTION

RNA is one of the main actors in the cell, allowing the flow of information between DNA, the carrier of genetic material and proteins (Crick 1970). RNA transcripts are produced from double-stranded DNA by RNA polymerases in the process of transcription (Fig. 1). However, not all transcripts are messenger RNA (mRNA) and translated into proteins (Wagner, Gerhart and Romby 2015). In fact, most of the transcribed RNAs in bacteria are ribosomal RNAs (rRNA), transfer RNAs (tRNA) and other non-coding or regulatory small RNAs (srRNA) (Fig. 1) (Argaman et al. 2001; Rivas et al. 2001; Wassarman et al. 2001). These RNAs do not directly result in proteins; however, they influence the composition of the transcriptome and proteome of a cell by fine-tuning the expression of specific genes in response to environmental cues (Gottesman 2004; Papenfort and Vogel 2009; Waters and Storz 2009; Gottesman and Storz 2011; Storz, Vogel and Wassarman 2011; Wagner, Gerhart and Romby 2015). Regulation of transcription plays a crucial role in many biological processes such as development, cell differentiation and cell homeostasis (Browning and Busby 2016; Pope and Medzhitov 2018). Consequently, the detection and precise quantification of RNA levels in cells are important to understand how transcription is regulated, as well as to decipher the specific transcriptional patterns of different cell types.

Early pioneering techniques, such as northern blotting, qPCR and microarrays, enabled the detection and quantification of specific transcripts from a pool of RNA, and proved powerful in species identification and in differential gene expression studies (Jauregui et al. 2001; Sachse et al. 2005; Streit et al. 2009). Subsequently, high-density DNA microarrays and high-throughput RNA sequencing (RNAseq) were developed to detect whole transcriptomes (Lashkari et al. 1997; Bainbridge et al. 2006; Weber et al. 2007). These methods rely on the extraction of total RNA from a pool of cultured cells or a homogenized cell solution, and thus result in an ensemble average for the population of cells under study. Recent advances in fractionation techniques and RNAseq now enable transcriptome profiling of single cells, allowing further exploration of cell-to-cell variability and subpopulation identification (Shalek et al. 2014; Chen, Teichmann and Meyer 2018; Montoro et al. 2018). A major drawback of sequencing-based technologies is their inability to monitor single-cell dynamics and subcellular localization. These measurements prove to be critical in understanding the mechanism of transcriptional regulation and the functions of RNA in the cell.

A major advantage of imaging-based methods is that cellular processes and their associated actors can be visualized in time and space within their native context. This ability, when combined with the development of a myriad of strategies to

Received: 15 January 2020; Accepted: 1 October 2020

© The Author(s) 2020. Published by Oxford University Press on behalf of FEMS. All rights reserved. For permissions, please e-mail: journals.permissions@oup.com

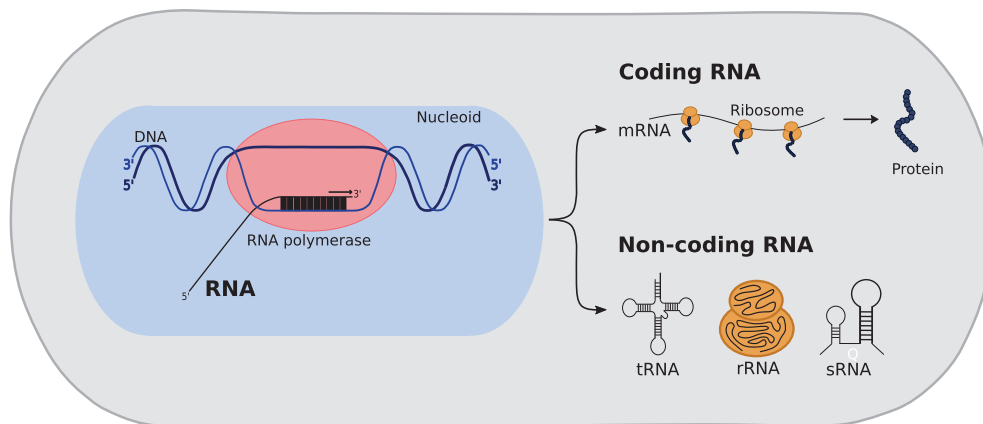


Figure 1. Synthesis of coding and non-coding RNA species in bacteria during transcription. In bacteria, both coding and non-coding RNA is synthesized from double-stranded DNA by RNA polymerase, presumably in the nucleoid periphery, in the process of transcription. Coding RNA or messenger RNA (mRNA) is translated to proteins by ribozymes, presumably in the nucleoid periphery as well. Non-coding RNA, such as transfer RNA (tRNA), ribosomal RNA (rRNA) and other small regulatory RNA (sRNA), will fold into distinct nanostructures and will play a role in downstream processes such as translation and gene expression regulation.

tag most macromolecules within a cell, has made fluorescence microscopy a popular tool for the study of many biological problems. Particularly, imaging-based methods have provided considerably new insight into the process of transcriptional regulation and more generally into the cellular roles of different RNA species.

In eukaryotic cells, transcription occurs in the nucleus and translation in the cytoplasm. As a result, these processes are decoupled in space and time. The translocation and final positioning of RNA molecules within the cytoplasm plays a regulatory role in asymmetric cell division, cell migration and development (Buxbaum, Haimovich and Singer 2015; Chin and Lécuyer 2017). In bacteria, on the other hand, the nucleoid and cytoplasm coexist within the same compartment. In addition, transcription and translation are often coupled and occur in the same nucleo-plasmic space (Bakshi et al. 2012; Bakshi, Choi and Weishaar 2015; Fan et al. 2017). This led to the early assumption that, in bacteria, RNA species lacked spatial compartmentalization or preferential subcellular localization. However, with the emergence of novel imaging-based techniques, several studies have recently evidenced that RNA molecules as well as proteins involved in their processing can indeed exhibit specific spatial patterns of subcellular localization (Montero Llopis et al. 2010; Nevo-Dinur et al. 2011; Moffitt et al. 2016; Weng et al. 2019). In addition, the ability of imaging-based methods to monitor changes in protein and transcript abundance and localization was fundamental to characterize the dynamics of transcription. This ability was key to characterize the different sources of noise in gene expression (Elowitz 2002; Ozbudak et al. 2002; Rosenfeld et al. 2005) or to understand the mechanism of promoter specificity (Ferguson et al. 2012).

In this review, we provide an overview of the most important and most recently developed single-cell approaches for the visualization of RNA with fluorescence microscopy, with a particular focus on those methods that were used in bacteria or that promise to be relevant to the study of transcriptional regulation in bacteria. We describe techniques for the read-out of RNA molecules in fixed cells, which have mostly helped to understand the abundance and subcellular spatial organization of RNA. In addition, we highlight the most established techniques for the imaging of RNA molecules in live cells, which enabled the description of gene expression and transcript dynamics in space and time. Finally, we illustrate recent advances made

towards the simultaneous visualization of multiple RNA species, approaching whole-transcriptome imaging.

Fixed-cell imaging

Fluorescence *in situ* hybridization (FISH) is one of the most powerful techniques for the visualization of nucleic acid molecules in fixed cells. This technique relies on the hybridization of single-stranded, fluorescently labeled oligonucleotide probes to a complementary DNA or RNA sequence (Femino 1998; Raj and van Oudenaarden 2009). Although the technique was initially developed for DNA labeling (Langer-Safer, Levine and Ward 1982), it is now the golden standard for the imaging of native transcripts, especially for mRNA quantification and localization studies.

Initially, the detection of single mRNA molecules by single-molecule FISH (smFISH) was challenging due to the low signal-to-noise ratio of the labeled mRNA with respect to the background signal arising from freely diffusing unbound probes and from non-specific binding or sticking of the probe to other cellular components (Femino 1998). To overcome this problem, the fluorescent signal emanating from a single RNA molecule needs to largely exceed the background signal. This problem was solved by increasing the number of fluorophores used to label a single mRNA molecule. Signal amplification can be achieved by the use of multiple, short, non-overlapping, fluorescently labeled oligonucleotide probes (Raj et al. 2008) (Fig. 2A). The image of this single transcript then appears as a diffraction-limited spot, because the multiple oligonucleotide probes remain closer than the diffraction limit of light (~250 nm). Thus, by counting the number of diffraction-limited spots per cell one can measure the number of single mRNA molecules in a given cell for a specific mRNA species. This approach has proven very powerful for the labeling of mRNA in eukaryotes and for the detection of different kinds of RNA in *Escherichia coli* and *Bacillus subtilis* (Maamar, Raj and Dubnau 2007; So et al. 2011; Skinner et al. 2013; Fei et al. 2015; Arbel-Goren et al. 2016; Sepúlveda et al. 2016) (Table 1) (Fig. 2B). However, bacterial genes are often short (~1 kb or less), thus limiting the number of distinct fluorescent oligonucleotide probes that can encode a single RNA species. This results in decreased detection efficiencies and calls for other experimental strategies.

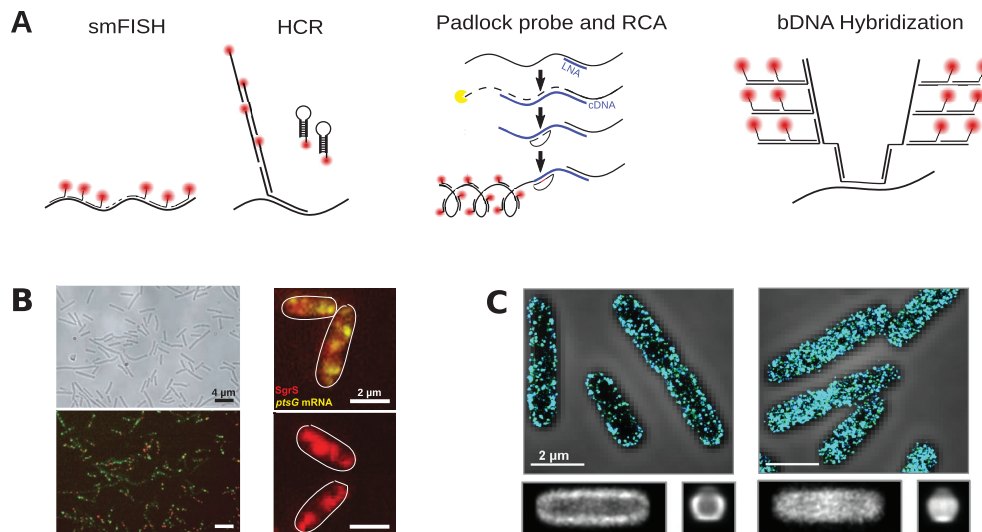


Figure 2. Methods for fixed cell imaging of RNA species at single-molecule resolution. (A) Signal amplification methods. Single molecule FISH (smFISH) (Raj et al. 2008), in which several fluorescently labeled oligonucleotides bind to the transcript. Hybridization chain reaction (HCR) (Dirks and Pierce 2004; Choi et al. 2010; Choi, Beck and Pierce 2014; Shah et al. 2016), in which a primary probe containing a homology region to the transcript of interest and a HCR initiator sequence binds to the transcript. Subsequently, the HCR initiator sequence triggers the self-assembly of the two fluorescently labeled hairpins into a long polymer chain. Padlock probes and rolling circle amplification (RCA) (Larsson et al. 2010), in which an LNA primer sequence hybridizes to the transcript of interest and initiates a reverse transcriptase reaction. The RNA-cDNA hybrid is then partially digested by RNase H, which in turn allows the hybridization of a padlock probe. Finally, this padlock probe is used as a template for the RCA. The amplified product contains binding sites for fluorescently labeled oligonucleotides. Branched DNA (bdNA) hybridization (Player et al. 2001; Kishi et al. 2019; Xia et al. 2019), in which an amplifier sequence is bound to the primary probe and provides a multitude of additional hybridizing sites for fluorescently labeled oligonucleotides. (B) Examples of smFISH in *B. subtilis* (left) and *E. coli* (right). Adapted from Maamar, Raj and Dubnau (2007) and Fei et al. (2015), respectively. (C) Example of fluorescent labeling and simultaneous imaging of well-defined populations of RNA in *E. coli*. Phase contrast and STORM cross-section images of cells stained with FISH probes against inner-membrane-protein mRNA (left) and cytosolic-protein mRNA (right). Adapted from Moffitt et al. (2016).

Indirect labeling strategies allow for more complex read-out schemes to increase the number of fluorophores per oligonucleotide probe. Generally, a primary probe is designed to contain two essential regions: (i) a complementary region to the RNA of interest and (ii) a tail sequence. For example, hybridization chain reaction (HCR) relies on the binding of the primary probe, containing an HCR initiator sequence in the tail, to the mRNA of interest (Dirks and Pierce 2004; Choi et al. 2010; Choi, Beck and Pierce 2014; Shah et al. 2016). This initiator sequence triggers the self-assembly of two fluorescently labeled metastable hairpins to a long polymer chain in which many fluorophores can be incorporated (Fig. 2A). When using the HCR method, care needs to be taken with non-specific probe hybridization to limit artefacts (Shah et al. 2016; Choi et al. 2018). In fact, off-target binding of probes to sequences containing the initiator sequence will also trigger the HCR, thus amplifying the background. Another strategy, based on the concept of rolling circle amplification (RCA), uses a padlock probe to initiate the amplification reaction (Larsson et al. 2004, 2010). In short, an LNA primary probe is used to target an mRNA and initiate a reverse transcriptase reaction resulting in an RNA-cDNA hybrid. This hybrid will be partially digested by Rnase H, allowing the binding of a padlock probe to the single-stranded cDNA. The padlock probe is ligated after hybridization and serves as a primer for the RCA reaction. Then, multiple fluorescently labeled oligonucleotide probes can hybridize to sequence repeats within the RCA product (Fig. 2A). A major advantage of both HCR and RCA is that the signal can be tuned and amplified as much as desired (Larsson et al. 2004, 2010; Shah et al. 2016). This, however, requires the precise modulation of self-assembly or polymerization times.

A more straightforward approach is branched DNA amplification (Player et al. 2001; Xia et al. 2019). Here, the primary probe has a tail on both sides of the complementary sequence, each

of which binds a primary amplifier. Such an amplifier sequence is made out of a sequence hybridizing to the tail of the primary probe and to several repeats, each of which can bind a secondary amplifier (Fig. 2A). The secondary amplifier also contains several repeats that can bind a tertiary amplifier and so on, or a fluorescently labeled oligonucleotide probe. Thus, in this method the degree of signal amplification is defined by the bdNA design.

Signal amplification methods, such as bdNA, HCR and RCA, are powerful strategies to upscale the fluorescent signal emitted from the labeled target transcript and thus to increase signal-to-noise ratios. However, care needs to be taken when using amplified signals for the localization and quantification of transcripts (Shah et al. 2016). As signal amplification generates foci of increased size, caution is required to avoid compromising the localization accuracy. Additionally, non-linear signal amplification can complicate the quantification of RNA copy numbers as the brightness of a fluorescent spot no longer correlates with the number of RNA molecules localized in that spot.

Although the above mentioned amplification approaches enable the detection of short RNA species, applications in prokaryotes so far remain limited. Only HCR has been successfully implemented in bacteria for species detection in complex samples and for the study of gene expression (Table 1) (Nikolakakis et al. 2015; Yamaguchi et al. 2015).

An additional complication to the accurate counting of single RNA molecules appears for highly expressed transcripts. In conventional fluorescence microscopy, the signal of one transcript labeled with multiple oligonucleotide probes results in a diffraction-limited spot. When transcripts are spatially well separated, they can be imaged, localized and quantified as distinct single molecules. However, when the RNA density increases, the fluorescence signal from several RNA molecules can overlap in space, making it impossible to resolve them as

Table 1. A summary of RNA imaging technologies reported in bacteria.

Method	Selected applications to bacteria	References
smFISH	Localization of mRNA and sRNA in <i>E. coli</i> and <i>B. subtilis</i> Examples: spatial localization of sRNA SgrS depends on its expression level, and transcriptome localization in <i>E. coli</i> , gene expression regulation in <i>E. coli</i> , noise in gene expression in <i>B. subtilis</i>	(Maamar, Raj and Dubnau 2007; So et al. 2011; Fei et al. 2015; Arbel-Goren et al. 2016; Moffitt et al. 2016; Sepúlveda et al. 2016)
MS2 system	Dynamics of transcription Examples: measurement of stochastic gene expression in <i>E. coli</i> , or transcript localization in several species, including <i>E. coli</i> , <i>Lactococcus lactis</i> and <i>B. subtilis</i>	(Golding et al. 2005; Nevo-Dinur et al. 2011; Santos et al. 2012; van Gijtenbeek et al. 2016)
HCR	Detection of bacterial species. The study of gene expression	(Nikolakakis et al. 2015; Yamaguchi et al. 2015)
3D-STORM-FISH RNA aptamers	Transcriptome localization in <i>E. coli</i> Study of conformational changes in RNA molecules Apta-FRET in <i>E. coli</i> where spinach and mango are expressed in close proximity on a tRNA scaffold to study the conformational changes in RNA nanostructures Spinach, broccoli, mango, corn, DNB and SRB-2 RNA aptamers were used in bacteria	(Moffitt et al. 2016) (Jepsen et al. 2018) (Sunbul and Jäschke 2013, 2018; Dolgosheina et al. 2014; Arora, Sunbul and Jäschke 2015; Zhang et al. 2015; Filonov and Jaffrey 2016; Song et al. 2017)
Fluorogenic dyes	Fluorogenic near-red and infra-red dyes used in <i>E. coli</i> for confocal imaging of tRNA/mRNA and STED imaging of mRNA	(Wirth et al. 2019)
Pumilio-based system	The tetramolecular fluorescence complementation (TetFC) system was used to label specific RNA targets in <i>E. coli</i>	(Kellermann and Rentmeister 2017)
FIT/QUAL probes Super-resolved SPT	Discrimination of bacterial species Dynamic localization of RNA polymerase and ribosomes in <i>E. coli</i> . Investigation of translation dynamics in <i>E. coli</i>	(Silverman and Kool 2005) (Sanamrad et al. 2014; Stracy et al. 2015; Volkov et al. 2018)

single transcripts. This often represents a major problem in bacteria, as their reduced cellular volume leads to considerably high global RNA densities. For this reason, signal overlapping occurs for many abundant RNA species, limiting detection with diffraction-limited microscopies to low abundance RNA species (Wang, Moffitt and Zhuang 2018). Several groups have circumvented this issue by estimating mRNA copy numbers from the total fluorescence signal for highly expressed target mRNA molecules in *E. coli* (Taniguchi et al. 2010; Skinner et al. 2013). Here, the fluorescence brightness of a single molecule is used to estimate the number of mRNA molecules from the total fluorescence signal in a given cell. Alternatively, this issue can be circumvented by using super-resolution techniques able to resolve smaller detection volumes and thus enable detection of single mRNA molecules in crowded environments (Lubeck and Cai 2012; Wang, Moffitt and Zhuang 2018). Both structured illumination microscopy (Gustafsson 2000) and stimulated-emission depletion microscopy (STED) (Hell and Wichmann 1994) have been employed to resolve RNA species labeled by smFISH in eukaryotic cells (Zhang et al. 2014; Mito et al. 2016). In bacteria, however, localization methods such as stochastic optical resolution microscopy (STORM) were more often used (Rust, Bates and Zhuang 2006). By combining three-dimensional (3D) STORM and whole-transcriptome FISH labeling, Moffitt and coworkers were able to demonstrate that the bacterial transcriptome in *E. coli* is spatially organized (Table 1) (Fig. 2C) (Moffitt

et al. 2016). Similarly, Fei and colleagues combined 3D-STORM with smFISH to label the bacterial sRNA SgrS and showed that the localization of SgrS depends on its expression level (Table 1) (Fei et al. 2015). More recently, a novel technique called expansion microscopy (ExM) was developed (Chen, Tillberg and Boyden 2015). The ExM approach relies on the embedding of the biological sample in a polymer hydrogel and the subsequent swelling of the hydrogel by immersion in a liquid. This results in a physical magnification of the embedded sample, making it possible to image cellular components at high resolution. ExM has proven successful for imaging FISH-labeled RNA species in eukaryotes (Chen et al. 2016; Tsanov et al. 2016; Asano et al. 2018; Wang, Moffitt and Zhuang 2018). In bacteria, the technique has been validated, but to date no study has reported the imaging of RNA content with ExM (Lim et al. 2019).

Even though techniques for fixed cell imaging enable the quantification and study of gene expression in space, the dynamics of gene expression remain unresolved with these approaches. Excitingly, a number of alternative technologies have been developed to enable transcript imaging in live cells.

Live cell imaging

Live cell imaging of RNA requires the labeling of transcripts *in vivo*. Many different strategies have been developed over the years to target specific mRNA molecules, involving the binding

of either a protein or a fluorogenic dye to an RNA-aptamer. The first of such strategies was developed in 1998 and makes use of the MS2 phage system to target a selected transcript (Bertrand et al. 1998). In short, a dimer of the MS2 phage coat protein (MCP) binds to one hairpin loop on the phage RNA (Lowary and Uhlenbeck 1987; Peabody 1993; Bertrand et al. 1998; Beach, Salmon and Bloom 1999). The high specificity of MCP binding to these hairpins was exploited to label other RNA species. Bertrand and coworkers fused multiple repeats of the MS2 RNA hairpin to the 3' UTR of a plasmid-encoded ASH1 gene from *Saccharomyces cerevisiae* (Bertrand et al. 1998). A Green Fluorescent Protein (GFP) fusion of the MS2 protein was then used to detect the ASH1 transcript (Bertrand et al. 1998) (Fig. 3A) and in later studies to follow it in space and time (Golding et al. 2005) (Fig. 3B). Genomic MS2-tagging of transcripts is now more regularly used (Tutucci et al. 2018). Aside from its application to yeast, the MS2 system was further developed for other systems, including bacteria (Rook, Lu and Kosik 2000; Forrest and Gavis 2003; Fusco et al. 2003; Zhang and Simon 2003; Golding and Cox 2004; Golding et al. 2005; So et al. 2011; Campbell et al. 2015). The first study in bacteria used 96 MS2 binding sites fused to the target RNA to investigate transcript kinetics in *E. coli* (Table 1) (Golding and Cox 2004). The results of this study uncovered cellular fluctuations in gene expression in single cells, supporting the hypothesis of stochastic transcription (Golding et al. 2005). The MS2 system has also proven to be a valuable tool for transcript localization in *E. coli* and other bacteria such as *B. subtilis* and *Lactococcus lactis* (Table 1) (Nevo-Dinur et al. 2011; Santos et al. 2012; Gijtenbeek et al. 2016). A major drawback of this approach to study transcript diffusion and localization is, however, that transcript lengthening can decrease the diffusion rate of the targeted RNA species and ultimately limit the applicability of this approach to highly dynamic transcripts (Golding and Cox 2004; Golding et al. 2005; Montero Llopis et al. 2010; Garcia and Parker 2015). Additionally, the high levels of expression of the MS2-GFP fusion lead to high levels of background signal (from freely diffusing MS2-GFP), making it difficult to distinguish RNA-specific signals from background fluorescence. In eukaryotes, this problem can be mitigated by targeting the unbound protein to other cellular compartments (Bertrand et al. 1998). Unfortunately, this approach is not feasible in bacteria, because bacteria lack canonical membrane-bound organelles. Another way of circumventing this issue, which was successfully used in both prokaryotic and eukaryotic systems, is to tweak the expression ratio of the reporter protein to its binding sites on the RNA (Fusco et al. 2003; Nevo-Dinur et al. 2011; Santos et al. 2012; Wu, Chao and Singer 2012; Gijtenbeek et al. 2016).

An orthogonal approach, involving the use of fluorogenic dyes for the labeling of specific RNA-aptamers was developed to circumvent the problem of background fluorescence. Fluorogenic dyes are molecules that display low levels of fluorescence when unbound and undergo a shift in fluorescence intensity upon binding to the RNA-aptamer (Wirth et al. 2019; Bouhedda et al. 2020). This aptamer sequence is then tethered to the RNA of interest as a genetically encoded tag. With this method, several RNA aptamers were developed, such as Spinach, Spinach2 and Broccoli, all binding 3,5-difluoro-4-hydroxybenzylidene (DFHBI), a non-toxic, cell-permeable dye (Table 1) (Paige, Wu and Jaffrey 2011; Strack, Disney and Jaffrey 2013; Filonov et al. 2014; Strack and Jaffrey 2015) (Fig. 3A). Both aptamer-dye systems were validated in *E. coli* (Zhang et al. 2015; Filonov and Jaffrey 2016) (Fig. 3C). In addition, Mango and Corn are aptamers that bind either thiazole orange or DFHO, respectively (Table 1) (Dolgosheina et al. 2014; Song et al. 2017; Autour et al. 2018). The

Mango and Corn RNA aptamers were also validated in *E. coli* (Dolgosheina et al. 2014; Song et al. 2017). In addition, the Mango RNA aptamer was used in combination with the Spinach RNA aptamer in an interesting method called apta-FRET (Table 1) (Jeppen et al. 2018). Here, the Mango and Spinach RNA aptamers were placed in close proximity on a tRNA scaffold and the FRET-signal generated when these aptamers are in close proximity were used to report on tRNA conformational changes. The concept of apta-FRET is an interesting development for the field of nanotechnology, as it allows one to study the specific folding and dynamics of RNA nanostructures in living cells.

To find the appropriate sequences that will bind the dye molecule of interest, a technique called systematic evolution of ligands by exponential enrichment (SELEX) was developed (Ellington and Szostak 1990; Holeman et al. 1998; Stoltenburg, Reinemann and Strehlitz 2007). This method allows for the selection, identification and amplification of the most optimal binding RNA aptamer from a random library. A drawback of SELEX is the suboptimal binding of target RNA sequences. This was partially solved by microfluidics-assisted *in vitro* compartmentalization, a technique relying on the use of selection pressure to find high-affinity aptamer sequences (Ryckelynck et al. 2015; Autour, Westhof and Ryckelynck 2016; Autour et al. 2018). Aside from the use of fluorogenic dyes, photostable organic dyes that are conditionally quenched were also used. Examples are the DNB and SRB-2 aptamers that bind a myriad of fluorophores quenched by dinitroaniline and aptamers binding black hole quenchers attached to fluorophores (Murata et al. 2011; Sunbul and Jäschke 2013, 2018; Arora, Sunbul and Jäschke 2015; Sato et al. 2015) (Fig. 3A). In *E. coli*, both the DNB and SRB-2 aptamers were validated (Table 1) (Sunbul and Jäschke 2013, 2018; Arora, Sunbul and Jäschke 2015) by simultaneous labeling and detection of two different RNA species (Arora, Sunbul and Jäschke 2015).

Recent advances in the RNA aptamer field have enabled the development of aptamer-binding silicon rhodamine-derived fluorophores in the far-red and near-infrared (Autour et al. 2018; Braselmann et al. 2018; Yerramilli and Kim 2018). These new dyes promise a significant reduction in phototoxicity and autofluorescence for live-cell imaging (Umezawa, Citterio and Suzuki 2014; Li et al. 2019) and allow super-resolution imaging of RNA in *E. coli* by STED microscopy (Table 1) (Wirth et al. 2019). Furthermore, spontaneously blinking rhodamine-derived fluorophores were used in other super-resolution microscopy techniques such as dSTORM (Lukinavičius et al. 2013; Uno et al. 2014). Unfortunately, such fluorophores are not yet reported in bacterial systems. A disadvantage of organic dyes is that, unlike fluorescent proteins, they are exogenous to cells, and rely mainly on diffusion through the cell membrane to enter the cell. This diffusion can be slow and challenging for certain bacterial species. Additionally, many dye molecules are toxic to cells and exhibit strong phototoxic effects (Hilderbrand and Weissleder 2010; Martynov et al. 2016; Bouhedda, Autour and Ryckelynck 2017).

Avoiding the modification of the RNA template enables the study of native transcripts and thus the endogenous behavior of transcription. This was achieved by resorting to the use of the Pumilio homology domain (PumHD), a protein that binds mRNA in a sequence-specific manner (Wang et al. 2002; Ozawa et al. 2007; Filipovska et al. 2011; Chen et al. 2017). Recently, PumHD was engineered to generate four protein modules, each recognizing a different RNA base. These building blocks can then be concatenated to form a chain of desired composition and length, which is expressed from a plasmid. Eventually, the PumHD protein chain binds a specific sequence on the target

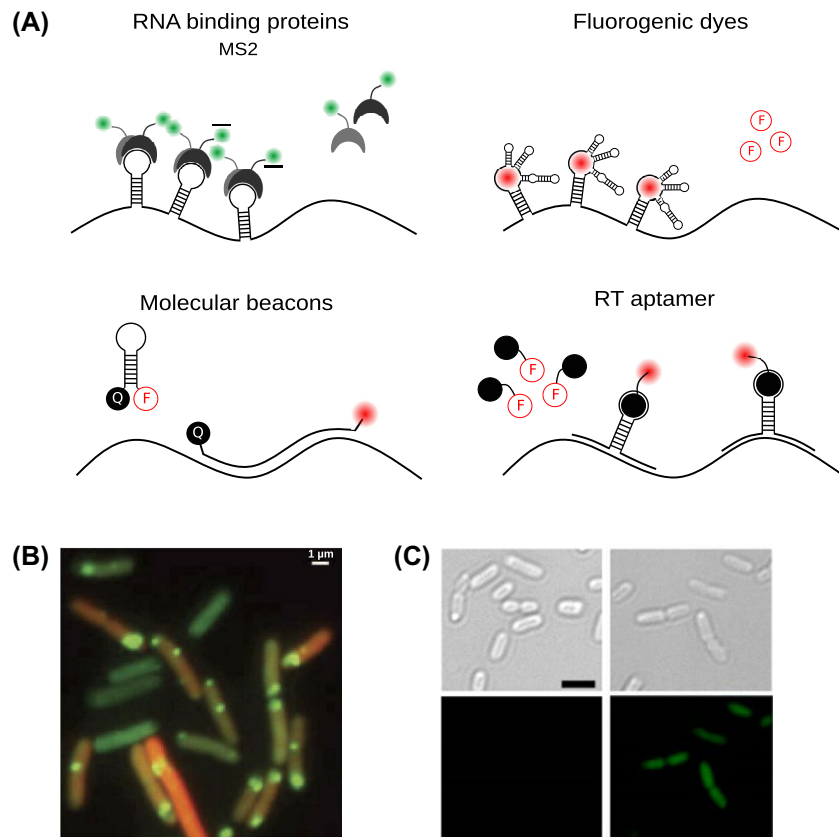


Figure 3. Methods for live cell imaging of RNA species at single-molecule resolution. (A) Genetically encoded RNA aptamers (top) tethered to the transcript of interest bind either an RNA binding protein fused to a reporter protein (MS2 system) (Bertrand et al. 1998) or fluorogenic dyes (Paige, Wu and Jaffrey 2011). Strategies for the study of native transcripts (bottom), based on conditionally quenched fluorophores. Opening of the hairpin structure upon binding of the molecular beacon (Tyagi and Kramer 1996) or by stable binding of the quencher to the RT aptamer (Sunbul and Jäschke 2013; Arora, Sunbul and Jäschke 2015) disables the quenching activity of the beacon and the dye molecule fluoresces. (B) Example of the MS2 system in *E. coli* with the protein mRFP1 (red) and its corresponding transcripts (green). MS2 aptamers are added to the mRFP1 transcript enabling binding of MS2 fused to GFP. Adapted from Golding et al. (2005). (C) Example of the Broccoli aptamer binding the fluorogenic dye DFHBI in *E. coli*. An empty plasmid and a plasmid carrying the Broccoli aptamer were transformed into *E. coli* cells. The empty plasmid does not give a fluorescence signal and functions as the control, while the Broccoli aptamer binds the dye molecules and fluoresces. Adapted from Filonov et al. (2014).

mRNA. When fusing a fluorescent protein to the PumHD chain, the native target mRNA can be visualized. An additional advantage of this method is that PumHD modules can be displaced by ribosomes, thus they can be exploited to study translation (Adamala, Martin-Alarcon and Boyden 2016).

In *E. coli*, an elegant tetramolecular fluorescence complementation (TetFC) system was used to label a specific mRNA target (Table 1) (Kellermann and Rentmeister 2017). The TetFC system contains two variants of the Pumilio protein and a three partite split GFP. Each Pumilio variant contains one β -strand of the GFP fluorescent protein and thus a fluorescence signal is generated only when the target mRNA is bound by both Pumilio variants and the detector GFP. This strategy was combined with Fluorescence-activated cell sorting (FACS) to sort *E. coli* cells in which the target mRNA was expressed from cells lacking the target mRNA.

Alternatively, endogenous RNA, such as mRNA and microRNA, can be labeled *in vivo* with molecular beacons (Sokol et al. 1998; Bratu et al. 2003; Tyagi and Alsmadi 2004; Matsuo 1998; Guk et al. 2019). Molecular beacons are probe-like structures made up of a binding domain that is complementary to the RNA of interest and of two flanking regions that form a hairpin structure when unbound to RNA (Tyagi and Kramer 1996; Zheng et al. 2015; Chen et al. 2017). At the 3' and 5' regions of the molecular beacon probe, a quencher and fluorophore

are attached, respectively. When the probe forms the hairpin through intermolecular base-pairing, the fluorophore and quencher are in close proximity, rendering the probe non-fluorescent. Upon binding to the target sequence, the hairpin opens and the quencher-fluorophore conjugate is broken, resulting in the emission of a fluorescence signal (Fig. 3A). In addition to molecular beacons, several other constructs, such as forced intercalation (FIT) or quenched autoligation (QUAL) probes, exist (Sando, Abe and Kool 2004; Köhler, Jarikote and Seitz 2005; Hövelmann et al. 2013; Hövelmann et al. 2016). For example, QUAL probes were used to discriminate between morphologically similar bacterial species (Table 1) (Silverman and Kool 2005) that hybridized *in vivo* to species-specific 16S rRNA sequences of either *E. coli*, *Salmonella enterica* or *Pseudomonas putida* and the detection using conventional fluorescence microscopy for identification.

Probe systems, such as the aforementioned molecular beacons, FIT probes and QUAL probes, share the same advantage. They are in the dark state when unbound and only generate a fluorescent signal upon binding to the RNA target, solving the problem of background fluorescence. However, these probes can be degraded by endogenous nucleases. Backbone modifications, such as 2'-O-methylation or with synthetic probes, such as PNA or LNA probes, can be used to stabilize probes in the native

environment of a cell (Dirks, Molenaar and Tanke 2003; Wiegant et al. 2010; Fontenete et al. 2013). These synthetic probes are exogenous and therefore have to be introduced into cells. Generally this is achieved by microinjection or by the formation of transient pores in the cell membrane with pore-forming agents (Tyagi and Kramer 1996; Matsuo 1998; Sokol et al. 1998; Bratu et al. 2003; Mhlanga 2005). These applications have been validated in eukaryotic cultures; however, applications in bacteria for *in vivo* RNA imaging have not been reported.

Live cell RNA imaging approaches have proven powerful for the study of transcription dynamics and transcript localization. When combined with the detection of translating transcripts, the intertwining between transcription and translation can be studied. Recently, the MS2 system was combined with SunTag labeling to follow both the formation of the transcript and its translation (Tanenbaum et al. 2014; Wang et al. 2016; Wu et al. 2016; Yan et al. 2016). The gene encoding the transcript is modified to include a tandem array of the sequence coding for GCN4 peptide epitopes in the open reading frame. Upon translation of the transcript, short peptides are produced that act as epitopes for a single-chain variable fragment antibody fused to a fluorescent protein coexpressed in the cell. Additionally, the transcript of interest is labeled by the MS2 system with a different fluorescent protein. In this way, translating transcripts will display a fluorescence signal for both fluorescent proteins, while transcribed but untranslated transcripts will only exhibit a fluorescence signal originating from the MS2 system. Thus, the combination of these two systems in single eukaryotic cells allowed the simultaneous study of both transcription and translation dynamics.

Alternative approaches focused on the labeling and imaging of other actors involved in gene expression, such as RNA polymerase (RNAP), ribosomes and tRNA, and enabled the detection of the dynamics and localization of the transcription and translation machineries, as well as their interaction with RNA or DNA, respectively (Sanamrad et al. 2014; Stracy et al. 2015; Volkov et al. 2018). In bacteria, super-resolved single-particle tracking (SPT) is a particularly suitable tool for distinguishing the diffusive states of a molecule within a 3D space of a cell, thereby enabling the distinction between freely diffusing and bound/static molecules (Table 1) (Stracy et al. 2015). More specifically, SPT-PALM has been used to track both RNAP and ribosomal subunits, through fusion of PAmCherry to the beta' subunit of RNAP and the fusion of mEos to the 50S ribosomal protein L1 and 30S ribosomal protein S2, respectively (Sanamrad et al. 2014; Stracy et al. 2015). In these studies, it was shown that both bound RNAP and bound ribosomes are mostly excluded from the nucleoid, while unbound RNAP and ribosomal subunits can diffuse through the nucleoid space. A similar technology was more recently introduced to study translation kinetics. Codon-specific, *in vitro* dye-labeled tRNA molecules were introduced into *E. coli* cells through electroporation and tracked with super-resolved SPT to measure the dwell times of tRNA on ribosomes as a proxy for translation rates (Volkov et al. 2018).

Multiplexed imaging

RNA aptamer-based approaches and smFISH have proven to be very powerful tools for the study of transcript localization and abundance. However, the detection of multiple RNA species at the same time in the same single cell would additionally enable the characterization of transcriptional patterns with spatial resolution.

For live cell imaging of eukaryotic systems, the multicolor read-out of several different mRNA was reported using RNA-binding protein systems. For instance, the MS2 system was combined with either the PP7 system, derived from the coat protein of bacteriophage PP7, or with the LambdaN system, derived from the lambda bacteriophage antiterminator protein N (Lange et al. 2008; Hocine et al. 2013). The main disadvantages of this approach are the extensive genetic/transcriptomic modifications required and the limited number of colors that can be detected at once. Both disadvantages limit the number of mRNA species that can be visualized simultaneously to only a few (2–3).

Recently, advances in labeling strategies, imaging and automated analysis led to the development of several *in situ* sequencing (ISS) and *in situ* hybridization (ISH) techniques for the read-out of tens to thousands of RNAs in fixed cells.

The first multiplexing ISH strategies that enabled the simultaneous measurement of tens of mRNA species relied on direct transcript labeling schemes where target mRNA were encoded with spectral barcodes and read-out by sequential hybridization and imaging rounds (Levsky 2002; Lubeck and Cai 2012; Levesque and Raj 2013; Lubeck et al. 2014). SeqFISH, the first protocol to realize sequential FISH (Lubeck et al. 2014), can suffer from high background autofluorescence when imaging thick and opaque tissue samples, thus limiting the accurate detection of mRNA molecules (Shah et al. 2016). This problem was circumvented by combining sequential imaging with single molecule HCR (smHCR) for signal amplification (Shah et al. 2016, 2017). Here, the complementary region of the primary probe hybridizes to the mRNA molecule of interest in each hybridization round and the HCR initiator sequence in the probe tail triggers the HCR reaction. After imaging, the probes are stripped off the transcripts by DNase treatment before a new round of hybridization is started. Both seqFISH and smHCR seqFISH enable the detection of tens to hundreds of mRNA species. Alongside seqFISH, another approach, called ouroboros single molecule FISH (osmFISH), was developed to address the issue of spatial overlapping of different RNA species in a diffraction-limited volume (Codeluppi et al. 2018). osmFISH employs a direct labeling scheme, similar to that of seqFISH, in which the number of target molecules is defined by the number of hybridization rounds and channels that are imaged. Even though the multiplexing capabilities of these approaches are limited, the advantage of seqFISH and osmFISH is that only one target RNA species is detected in each image, thus considerably reducing the signal overlapping of closely positioned mRNA molecules and therefore greatly facilitating the precise detection and localization of these mRNA molecules and limiting undercounting.

Alternatively, approaches using combinatorial encoding schemes allow the increase of the number of detected RNA species in a manner that is not proportional to the number of hybridization cycles. The specific combinatorial scheme implemented in multiplexed error-robust FISH (MERFISH) is able to detect and correct registration errors (Chen et al. 2015). The original publication reported the detection of 140 RNA species with error correction. The same study also reported the detection of 1001 RNA species but with no error correction (Chen et al. 2015). RNA species were encoded with a 16-bit binary word where each bit represents the on (1) or off (0) signal of the RNA molecule in each hybridization round. Each RNA species is designed to be labeled with a read-out probe and detected in only 4 out of 16 hybridization rounds. The use of 16-bit binary words that are separated from each other by a Hamming distance of four enabled robust error correction, as mutations of a single digit could be corrected without ambiguity. Transcript identities were

then decoded by reconstruction of the 16-bit words through the sequential imaging and localization of the 16 read-out probes. After decoding the transcripts, the abundance and localization of each RNA species in the sample was obtained. MERFISH has single-molecule detection capabilities, however, care must be taken when imaging highly abundant species, as transcripts located closer to each other than the diffraction limit and sharing one read-out probe cannot be decoded. The spatial overlap of RNA molecules in MERFISH was recently addressed by combining MERFISH with ExM to increase the RNA density limit (Wang, Moffitt and Zhuang 2018). In a complementary approach, abundant species were decoded using a sequential instead of a combinatorial encoding scheme (Moffitt et al. 2018). More recently, the multiplexing capabilities of MERFISH were increased by one order of magnitude to detect ~10 000 RNA species (Xia et al. 2019).

Alternatively, a second combinatorial approach was developed (seqFISH+) that makes it possible to image and detect up to ~10 000 mRNA molecules (Eng et al. 2019). SeqFISH+ employs an indirect labeling scheme in which barcodes are sequentially read-out using combinatorial encoding combined with multi-color imaging. Each target RNA species was encoded with a unique sequence of four pseudocolors. In SeqFISH+, the 60 pseudocolors were generated by including in each barcoding round 20 hybridization cycles in which probes are imaged in three color channels. This means that the labeling and detection of a specific RNA species in a given hybridization round and in a given color channel represents the pseudocolor of that barcoding round. Transcript identities were decoded by reconstructing the pseudocolor barcode through the labeling and detection of RNA molecules for each of the four barcoding rounds. This labeling and imaging strategy results in 60 unique images for each barcoding round, each representing a specific pseudocolor. Single molecule detection efficiency in seqFISH+ is thus achieved by detecting only a subset of the total ensemble of targeted mRNA molecules in each image, which avoids the spatial overlapping of different RNA species and ultimately allows for the precise localization of single target mRNA by Gaussian fitting without the use of super-resolution methods. Despite the successful application of these FISH-based methods to a wide variety of eukaryotic systems, their use in bacterial systems has still to be reported.

A second family of technologies perform the optical read-out of different RNA species by ISS. ISS methods allow the direct linking of the sequencing output information to the spatial localization of target RNAs. Generally, the ensemble of target transcripts are amplified *in situ* by using RCA-based methods to create DNA amplicons containing a detection target (i.e. the mRNA transcript of interest) and a sequencing target consisting of either the detection target itself or a barcode incorporated during RCA. The sequencing target is sequenced by 'sequencing by ligation' (SBL) or by 'sequencing by synthesis' (SBS) using fluorescently labeled probes or nucleotides, respectively. The first ISS development reported used reverse transcription of mRNA to cDNA, and hybridization of padlock probes to cDNA followed by RCA for amplification, ultimately creating a DNA amplicon called a 'rolling circle product' (RCP) (Ke et al. 2013). An RCP contains multiple repeats of the sequencing target and is thus essential for signal amplification. Depending on the design of the padlock probe, the detection target is directly sequenced or a sequencing target is incorporated in the RCA, which functions as an indirect barcode. In the original method, SBL is used to reconstruct a four base-long sequence and to identify the target transcript. Recently, the throughput of this approach reached a multiplexing capability of ~100 target RNAs (Qian et al. 2020). A

variation on this original work, called 'barcode *in situ* targeted sequencing' (BaristaSeq), employs the same strategy to generate RCPs of target transcripts and 15 nucleotide-long sequences by SBS (Chen et al. 2018). The increase in read length in BaristaSeq requires an increase in the number of imaging cycles to 15. To ensure the spatial stability of the RCP during imaging, the RCP is anchored to the cellular matrix. Concomitantly, spatially resolved transcript amplicon read-out mapping (Wang et al. 2018) avoids cDNA synthesis by using a 'specific amplification of nucleic acids via intramolecular ligation' (SNAIL) probe system, containing a padlock carrying a unique five nucleotide-long barcode and a primer that hybridizes partially to the target transcript and partially to the padlock probe. The primer of the SNAIL probe can then be used to initiate RCA. The RCPs are embedded into a hydrogel, which has the advantage that unbound protein and lipids can be washed out of this gel, resolving any background fluorescence (Wang et al. 2018). Finally, the barcode or sequencing target is reconstructed by SBL. A disadvantage of both *in situ* hybridization and *in situ* sequencing methods is that they require *a priori* knowledge of the RNA target sequences to be detected. Generally, this implies that only well-annotated transcripts can be targeted. An interesting development, relying on the use of fluorescence *in situ* sequencing for DNA amplicon sequencing (Mitra et al. 2003; Shendure et al. 2005; Kim et al. 2007), circumvents this issue by allowing the targeting and sequencing of transcripts for which no *a priori* sequence knowledge is available as well as of non-coding RNA species (Lee et al. 2014, 2015). Unbiased labeling of RNA species is achieved by using random hexamer primer sequences, which initiate reverse transcription of the primer tagged RNA species (Lee et al. 2014). Each of these primer sequences carries a tag, which later functions as the sequencing primer. After cDNA synthesis, the cDNA molecules are anchored to the cellular matrix, circularized by ligation and amplified by RCA. Then SBL results in a read length of 30 bases. By employing a partition sequencing strategy where the RCPs are randomly sampled and only a subset is sequenced, up to ~8000 different target RNA species can be discriminated. Despite the powerful multiplexing capabilities of ISS methods and their application to cultured eukaryotic cells and complex tissue samples, ISS methods have yet to be reported in bacteria.

CONCLUSION

The large palette of imaging-based methods described in this review have allowed researchers to gain incremental insights into the mechanisms involved in the regulation of RNA biosynthesis as well as in cellular RNA functions. The ability to either follow RNA molecules in space and time with single molecule sensitivity in live cells or the read-out of many RNA species simultaneously in fixed cells enabled the investigation of RNA dynamics, abundance and localization at the single cell level in their native context. These methods led to several pioneering discoveries. For example, both the MS2 system and smFISH were used to examine the stochastic nature of bacterial gene activity in *E. coli*, which underlies transcriptional bursting (Golding and Cox 2004; Golding et al. 2005; Zong et al. 2010; So et al. 2011; Skinner et al. 2013). Furthermore, smFISH has been used in *B. subtilis* to show that stochastic gene expression can drive cell states transitions resulting in cell competence (Maamar, Raj and Dubnau 2007).

Additionally, imaging-based methods have expanded our understanding of the subcellular spatial organization of RNA within bacterial cells that lack membrane-bound organelles. For instance, smFISH enabled the discovery of the subcellular

localization of small bacterial RNAs depending on their expression level (Fei et al. 2015). The use of whole-transcriptome FISH labeling contributed to the recent understanding that mRNA in bacteria can display specific patterns of subcellular localizations (Montero Llopis et al. 2010; Nevo-Dinur et al. 2011; Moffitt et al. 2016; Weng et al. 2019). Finally, labeling of pre-rRNA using smFISH and RNA polymerases using fluorescent protein tagging was used to show that the genomic organization within the bacterial nucleoid greatly influences the spatial organization of RNA polymerase clusters and of rRNA transcription sites (Weng et al. 2019).

Conversely, these important findings have also triggered novel biological questions regarding the mechanisms underlying RNA localization and its possible regulatory roles. One major question is whether the classical hypothesis of co-transcription and co-translation in bacteria holds true. On the one hand, localization studies of transcribed gene loci, RNAP and ribosomal subunits support a model in which active transcription seems to drive transcription and translation machineries towards the periphery of the nucleoid and the cytoplasmic space (Sanamrad et al. 2014; Stracy et al. 2015; Yang et al. 2019). On the contrary, imaging-based localization studies, cell fractionation and RNAseq-based studies are rather consistent with translation-independent patterning of a subset of mRNA species in several bacteria (Nevo-Dinur et al. 2011; Benhalevy et al. 2017; Kannaiah, Livny and Amster-Choder 2019). Aside from its implications for translation, the function of subcellular RNA enrichment remains largely unexplained. Deeper insights into the relationship between gene expression, transcriptome localization and the phenotype of the cell might uncover co-regulated and co-localized transcripts, ultimately leading to a better understanding of the molecular pathways involved and their implications to cell physiology.

Despite these many important applications of imaging-based RNA detection methods, many challenges remain to be addressed. For instance, in the development of new methods for tagging RNA without altering their regulatory function, diffusion behavior or localization (Golding et al. 2005; Garcia and Parker 2015, 2016; Haimovich et al. 2016; Heinrich et al. 2017; Tutucci et al. 2018). Diffraction of light within a microscope, and the intrinsically high densities of RNA in bacteria, can both degrade our ability to discriminate and accurately quantify the abundance and localization of large numbers of RNA species in bacteria. Approaches combining novel RNA labeling and sample preparation strategies with super-resolution fluorescence microscopies will likely help solve this issue in future.

Finally, while a large number of technologies to detect and quantify RNA in single cells have been developed in the past 2 decades, to date only a subset of them have been reported in bacteria. Established bacterial model systems can be genetically manipulated rather easily, and have proven to play a key role in the molecular dissection of important cellular processes, such as transcription, translation or DNA replication and repair. Thus, we envision that application of novel RNA imaging technologies to bacterial model systems will likely lead to new important discoveries, relevant to the study of RNA biology in general.

ACKNOWLEDGMENTS

We acknowledge funding from the European Research Council (ERC) under the European Union's Horizon 2020 research and innovation programme (Grant Agreement No 724429) to M.N.

and from the European Union's Horizon 2020 research and innovation programme under the Marie Skłodowska-Curie Grant Agreement No 721874 (SPM2.0) to S.R.

Conflict of interest. None declared.

REFERENCES

- Adamala KP, Martin-Alarcon DA, Boyden ES. Programmable RNA-binding protein composed of repeats of a single modular unit. *Proceedings of the National Academy of Sciences*, 2016 <https://doi.org/10.1073/pnas.1519368113>.
- Arbel-Goren R, Tal A, Parasar B et al. Transcript degradation and noise of small RNA-controlled genes in a switch activated network in *Escherichia coli*. *Nucleic Acids Res* 2016;**44**:6707–20.
- Argaman L, Hershberg R, Vogel J et al. Novel small RNA-encoding genes in the intergenic regions of *Escherichia coli*. *Curr Biol* 2001;**11**:941–50.
- Arora A, Sunbul M, Jäschke A. Dual-colour imaging of RNAs using quencher- and fluorophore-binding aptamers. *Nucleic Acids Res* 2015;**43**:e144.
- Asano SM, Gao R, Wassie AT et al. Expansion microscopy: protocols for imaging proteins and RNA in cells and tissues. *Curr Protocol Cell Biol* 2018;**80**:e56.
- Autour A, Jeng SCY, Cawte AD et al. Fluorogenic RNA mango aptamers for imaging small non-coding RNAs in mammalian cells. *Nat Commun* 2018;**9**:656.
- Autour A, Westhof E, Ryckelynck M. iSpinach: a fluorogenic RNA aptamer optimized for in vitro applications. *Nucleic Acids Res* 2016; <https://doi.org/10.1093/nar/gkw083>.
- Bainbridge MN, Warren RL, Hirst M et al. Analysis of the prostate cancer cell line LNCaP transcriptome using a sequencing-by-synthesis approach. *BMC Genomics* 2006;**7**:246.
- Bakshi S, Choi H, Weisshaar JC. The Spatial biology of transcription and translation in rapidly growing *Escherichia coli*. *Front Microbiol* 2015;**6**:636.
- Bakshi S, Siryaporn A, Goulian M et al. Superresolution imaging of ribosomes and RNA polymerase in live *Escherichia coli* cells. *Mol Microbiol* 2012;**85**:21–38.
- Beach DL, Salmon ED, Bloom K. Localization and anchoring of mRNA in budding yeast. *Curr Biol* 1999;**9**:569–78.
- Benhalevy D, Biran I, Bochkareva ES et al. Evidence for a cytoplasmic pool of ribosome-free mRNAs encoding inner membrane proteins in *Escherichia coli*. *PLoS One* 2017;**12**:e0183862.
- Bertrand E, Chartrand P, Schaefer M et al. Localization of ASH1 mRNA particles in living yeast. *Mol Cell* 1998;**2**:437–45.
- Bouhedda F, Autour A, Ryckelynck M. Light-up RNA aptamers and their cognate fluorogens: from their development to their applications. *Int J Mol Sci* 2017; <https://doi.org/10.3390/ijms19010044>.
- Bouhedda F, Fam KT, Collot M et al. A dimerization-based fluorogenic dye-aptamer module for RNA imaging in live cells. *Nat Chem Biol* 2020; <https://doi.org/10.1038/s41589-019-0381-8>.
- Brasemann E, Wierzbka AJ, Polaski JT et al. A multicolor riboswitch-based platform for imaging of RNA in live mammalian cells. *Nat Chem Biol* 2018; <https://doi.org/10.1038/s41589-018-0103-7>.
- Bratu DP, Cha B-J, Mhlanga MM et al. Visualizing the distribution and transport of mRNAs in living cells. *Proc Natl Acad Sci* 2003; <https://doi.org/10.1073/pnas.2233244100>.
- Browning DF, Busby SJW. Local and global regulation of transcription initiation in bacteria. *Nature Rev Microbiol* 2016;**14**:638–50.

- Buxbaum AR, Haimovich G, Singer RH. In the right place at the right time: visualizing and understanding mRNA localization. *Nature Rev Mol Cell Biol* 2015;16:95–109.
- Campbell PD, Chao JA, Singer RH et al. Dynamic Visualization of transcription and RNA subcellular localization in zebrafish. *Development* 2015; <https://doi.org/10.1242/dev.118968>.
- Chen F, Tillberg PW, Boyden ES. Optical imaging. expansion microscopy. *Science* 2015;347:543–8.
- Chen F, Wassie AT, Cote AJ et al. Nanoscale imaging of RNA with expansion microscopy. *Nat Methods* 2016; <https://doi.org/10.1038/nmeth.3899>.
- Chen KH, Boettiger AN, Moffitt JR et al. RNA Imaging. spatially resolved, highly multiplexed RNA profiling in single cells. *Science* 2015;348: aaa6090.
- Chen M, Ma Z, Wu X et al. A molecular beacon-based approach for live-cell imaging of RNA transcripts with minimal target engineering at the single-molecule level. *Sci Rep* 2017; <https://doi.org/10.1038/s41598-017-01740-1>.
- Chen X, Sun Y-C, Church GM et al. Efficient in situ barcode sequencing using padlock probe-based baristaseq. *Nucleic Acids Res* 2018;46:e22.a
- Chen X, Teichmann SA, Meyer KB. From tissues to cell types and back: single-cell gene expression analysis of tissue architecture. *Ann Rev Biomed Data Sci* 2018;1:29–51.
- Chin A, Lécuyer E. RNA localization: making its way to the center stage. *Biochim Biophys Acta Gen Subj* 2017;1861:2956–70.
- Choi HMT, Beck VA, Pierce NA. Next-generation in situ hybridization chain reaction: higher gain, lower cost, greater durability. *ACS Nano* 2014;8:4284–94.
- Choi HMT, Chang JY, Trinh LA et al. Programmable in situ amplification for multiplexed imaging of mRNA expression. *Nat Biotechnol* 2010;28:1208–12.
- Choi HMT, Schwarzkopf M, Fornace ME et al. Third-generation in situ hybridization chain reaction: multiplexed, quantitative, sensitive, versatile, robust. *Development* 2018;145. <https://doi.org/10.1242/dev.165753>.
- Codeluppi S, Borm LE, Zeisel A et al. Spatial organization of the somatosensory cortex revealed by osmFISH. *Nat Methods* 2018. <https://doi.org/10.1038/s41592-018-0175-z>.
- Crick F. Central dogma of molecular biology. *Nature* 1970;227:561–63.
- Dirks RM, Pierce NA. Triggered amplification by hybridization chain reaction. *PNAS* 2004;101:15275–78.
- Dirks RW, Molenaar C, Tanke HJ. Visualizing RNA molecules inside the nucleus of living cells. *Methods* 2003. [https://doi.org/10.1016/s1046-2023\(02\)00290-6](https://doi.org/10.1016/s1046-2023(02)00290-6).
- Dolgosheina EV, Jeng SCY, Panchapakesan SSS et al. RNA mango aptamer-fluorophore: a bright, high-affinity complex for RNA labeling and tracking. *ACS Chem Biol* 2014;9:2412–20.
- Ellington AD, Szostak JW. In vitro selection of RNA molecules that bind specific ligands. *Nature* 1990. <https://doi.org/10.1038/346818a0>.
- Elowitz MB. Stochastic gene expression in a single cell. *Science* 2002. <https://doi.org/10.1126/science.1070919>.
- Eng C-HL, Lawson M, Zhu Q et al. Transcriptome-scale super-resolved imaging in tissues by RNA seqFISH+. *Nature* 2019;568:235–9.
- Fan H, Conn AB, Williams PB et al. Transcription–translation coupling: direct interactions of RNA polymerase with ribosomes and ribosomal subunits. *Nucleic Acids Res* 2017. <https://doi.org/10.1093/nar/gkx719>.
- Fei J, Singh D, Zhang Q et al. RNA biochemistry. determination of in vivo target search kinetics of regulatory noncoding RNA. *Science* 2015;347:1371–4.
- Femino AM. Visualization of single RNA transcripts in situ. *Science* 1998. <https://doi.org/10.1126/science.280.5363.585>.
- Ferguson ML, Le Coq D, Jules M et al. Reconciling molecular regulatory mechanisms with noise patterns of bacterial metabolic promoters in induced and repressed states. *PNAS* 2012;109:155–60.
- Filipovska A, Razif MFM, Nygård KKA et al. A universal code for RNA recognition by PUF proteins. *Nat Chem Biol* 2011. <https://doi.org/10.1038/nchembio.577>.
- Filonov GS, Jaffrey SR. RNA imaging with dimeric broccoli in live bacterial and mammalian cells. *Curr Protocol Chem Biol* 2016. <https://doi.org/10.1002/9780470559277.ch150174>.
- Filonov GS, Moon JD, Svensen N et al. Broccoli: rapid selection of an RNA mimic of green fluorescent protein by fluorescence-based selection and directed evolution. *J Am Chem Soc* 2014;136:16299–308.
- Fontenete S, Guimarães N, Leite M et al. Hybridization-based detection of *Helicobacter pylori* at human body temperature using advanced locked nucleic acid (LNA) probes. *PLoS One* 2013. <https://doi.org/10.1371/journal.pone.0081230>.
- Forrest KM, Gavis ER. Live imaging of endogenous RNA reveals a diffusion and entrapment mechanism for nanos mRNA localization in *Drosophila*. *Curr Biol* 2003. [https://doi.org/10.1016/s0960-9822\(03\)00451-2](https://doi.org/10.1016/s0960-9822(03)00451-2).
- Fusco D, Accornero N, Lavoie B et al. Single mRNA molecules demonstrate probabilistic movement in living mammalian cells. *Curr Biol* 2003;13:161–67.
- Garcia JF, Parker R. MS2 coat proteins bound to yeast mRNAs block 5' to 3' degradation and trap mRNA decay products: implications for the localization of mRNAs by MS2-MCP system. *RNA* 2015;21:1393–95.
- Garcia JF, Parker R. Ubiquitous accumulation of 3' mRNA decay fragments in *Saccharomyces cerevisiae* RNAs with chromosomally integrated MS2 arrays. *RNA* 2016. <https://doi.org/10.1261/ma.056325.116>.
- Gijtenbeek LA, Robinson A, Oijen AM et al. On the spatial organization of mRNA, plasmids, and ribosomes in a bacterial host overexpressing membrane proteins. *PLoS Genet* 2016. <https://doi.org/10.1371/journal.pgen.1006523>.
- Golding I, Cox EC. RNA dynamics in live *Escherichia coli* cells. *Proc Natl Acad Sci* 2004. <https://doi.org/10.1073/pnas.0404443101>.
- Golding I, Paulsson J, Zawilski SM et al. Real-time kinetics of gene activity in individual bacteria. *Cell* 2005;123:1025–36.
- Gottesman S, Storz G. Bacterial small RNA regulators: versatile roles and rapidly evolving variations. *Cold Spring Harb Perspect Biol* 2011;3. <https://doi.org/10.1101/cshperspect.a003798>.
- Gottesman S. The small RNA regulators of *Escherichia coli*: roles and mechanisms. *Annu Rev Microbiol* 2004;58:303–28.
- Guk K, Hwang SG, Lim J et al. Fluorescence amplified sensing platforms enabling miRNA detection by self-circulation of a molecular beacon circuit. *Chem Commun* 2019;55:3457–60.
- Gustafsson MG. Surpassing the lateral resolution limit by a factor of two using structured illumination microscopy. *J Microsc* 2000;198:82–7.
- Haimovich G, Zabezhinsky D, Haas B et al. Use of the MS2 aptamer and coat protein for RNA localization in yeast: a response to 'MS2 coat proteins bound to yeast mRNAs block 5' to 3' degradation and trap mRNA decay products: implications for the localization of mRNAs by MS2-MCP system.' *RNA* 2016. <https://doi.org/10.1261/rna.055095.115>.
- Heinrich S, Sidler CL, Azzalin CM et al. Stem-loop RNA labeling can affect nuclear and cytoplasmic mRNA processing. *RNA* 2017. <https://doi.org/10.1261/rna.057786.116>.

- Hell SW, Wichmann J. Breaking the diffraction resolution limit by stimulated emission: stimulated-emission-depletion fluorescence microscopy. *Opt Lett* 1994;19:780–2.
- Hilderbrand SA, Weissleder R. Near-infrared fluorescence: application to in vivo molecular imaging. *Curr Opin Chem Biol* 2010. <https://doi.org/10.1016/j.cbpa.2009.09.029>.
- Hocine S, Raymond P, Zenklusen D et al. Single-molecule analysis of gene expression using two-color RNA labeling in live yeast. *Nat Methods* 2013. <https://doi.org/10.1038/nmeth.2305>.
- Holeman LA, Robinson SL, Szostak JW et al. Isolation and characterization of fluorophore-binding RNA aptamers. *Fold Des* 1998. [https://doi.org/10.1016/s1359-0278\(98\)00059-5](https://doi.org/10.1016/s1359-0278(98)00059-5).
- Hövelmann F, Gaspar I, Chamiolo J et al. LNA-enhanced DNA FIT-probes for multicolour RNA imaging. *Chem Sci* 2016. <https://doi.org/10.1039/c5sc03053f>.
- Hövelmann F, Gaspar I, Ephrussi A et al. Brightness enhanced DNA FIT-probes for wash-free RNA imaging in tissue. *J Am Chem Soc* 2013. <https://doi.org/10.1021/ja410674h>.
- Jauregui LH, Higgins J, Zarlenga D et al. Development of a real-time PCR assay for detection of toxoplasma gondii in pig and mouse tissues. *J Clin Microbiol* 2001;39:2065–71.
- Jepsen MDE, Sparvath SM, Nielsen TB et al. Development of a genetically encodable FRET system using fluorescent RNA aptamers. *Nat Commun* 2018;9:18.
- Kannaiah S, Livny J, Amster-Choder O. Spatiotemporal organization of the E. coli transcriptome: translation independence and engagement in regulation. *Mol Cell* 2019. <https://doi.org/10.1016/j.molcel.2019.08.013>.
- Kellermann SJ, Rentmeister A. A FACS-based screening strategy to assess sequence-specific RNA-binding of pumilio protein variants in E. coli. *Biol Chem* 2017;398:69–75.
- Ke R, Mignardi M, Pacureanu A et al. In situ sequencing for RNA analysis in preserved tissue and cells. *Nat Methods* 2013;10:857–60.
- Kim JB, Porreca GJ, Song L et al. Polony multiplex analysis of gene expression (PMAGE) in mouse hypertrophic cardiomyopathy. *Science* 2007;316:1481–4.
- Kishi JY, Lapan SW, Believeau BJ et al. SABER amplifies FISH: enhanced multiplexed imaging of RNA and DNA in cells and tissues. *Nat Methods* 2019;16:533–44.
- Köhler O, Jarikote DV, Seitz O. Forced intercalation probes (FIT probes): thiazole orange as a fluorescent base in peptide nucleic acids for homogeneous single-nucleotide-polymorphism detection. *ChemBioChem* 2005. <https://doi.org/10.1002/cbic.200400260>.
- Langer-Safer PR, Levine M, Ward DC. Immunological method for mapping genes on drosophila polytene chromosomes. *PNAS* 1982;79:4381–5.
- Lange S, Katayama Y, Schmid M et al. Simultaneous transport of different localized mRNA species revealed by live-cell imaging. *Traffic* 2008. <https://doi.org/10.1111/j.1600-0854.2008.00763.x>.
- Larsson C, Grundberg I, Söderberg O et al. In situ detection and genotyping of individual mRNA molecules. *Nat Methods* 2010;7:395–7.
- Larsson C, Koch J, Nygren A et al. In situ genotyping individual DNA molecules by target-primed rolling-circle amplification of padlock probes. *Nat Methods* 2004;1:227–32.
- Lashkari DA, DeRisi JL, McCusker JH et al. Yeast microarrays for genome wide parallel genetic and gene expression analysis. *PNAS* 1997;94:13057–62.
- Lee JH, Daugharthy ER, Scheiman J et al. Fluorescent in situ sequencing (FISSEQ) of RNA for gene expression profiling in intact cells and tissues. *Nat Protoc* 2015;10:442–58.
- Lee JH, Daugharthy ER, Scheiman J et al. Highly multiplexed sub-cellular RNA sequencing in situ. *Science* 2014. <https://doi.org/10.1126/science.1250212>.
- Levesque MJ, Raj A. Single-chromosome transcriptional profiling reveals chromosomal gene expression regulation. *Nat Methods* 2013. <https://doi.org/10.1038/nmeth.2372>.
- Levsky JM. Single-cell gene expression profiling. *Science* 2002. <https://doi.org/10.1126/science.1072241>.
- Li J-B, Liu H-W, Fu T et al. “Recent progress in small-molecule near-ir probes for bioimaging.” *Trends in Chemistry* 2019. <https://doi.org/10.1016/j.trechm.2019.03.002>.
- Lim Y, Shiver AL, Khariton M et al. Mechanically resolved imaging of bacteria using expansion microscopy. *PLoS Biol* 2019;17:e3000268.
- Lowary PT, Uhlenbeck OC. An RNA mutation that increases the affinity of an RNA–protein interaction. *Nucleic Acids Res* 1987. <https://doi.org/10.1093/nar/15.24.10483>.
- Lubeck E, Cai L. Single-cell systems biology by super-resolution imaging and combinatorial labeling. *Nat Methods* 2012. <https://doi.org/10.1038/nmeth.2069>.
- Lubeck E, Coskun AF, Zhiyentayev T et al. Single-cell in situ RNA profiling by sequential hybridization. *Nat Methods* 2014. <https://doi.org/10.1038/nmeth.2892>.
- Lukinavičius G, Umezawa K, Olivier N et al. A near-infrared fluorophore for live-cell super-resolution microscopy of cellular proteins. *Nat Chem* 2013. <https://doi.org/10.1038/nchem.1546>.
- Maamar H, Raj A, Dubnau D. Noise in gene expression determines cell fate in bacillus subtilis. *Science* 2007;317:526–9.
- Martynov VIPakhomov AA, Popova NV, et al., Pakhomov AA, Popova NV Synthetic fluorophores for visualizing biomolecules in living systems. *Acta Naturae* 2016. <https://doi.org/10.32607/20758251-2016-8-4-33-46>.
- Matsuo T. In situ visualization of messenger RNA for basic fibroblast growth factor in living cells. *Biochimica et Biophysica Acta* 1998. [https://doi.org/10.1016/s0304-4165\(97\)00090-1](https://doi.org/10.1016/s0304-4165(97)00090-1).
- Mhlanga MM. tRNA-linked molecular beacons for imaging mRNAs in the cytoplasm of living cells. *Nucleic Acids Res* 2005. <https://doi.org/10.1093/nar/gki302>.
- Mito M, Kawaguchi T, Hirose T et al. Simultaneous multi-color detection of RNA and proteins using super-resolution microscopy. *Methods* 2016;98:158–65.
- Mitra RD, Butty VL, Shendure J et al. Digital genotyping and haplotyping with polymerase colonies. *PNAS* 2003;100:5926–31.
- Moffitt J, Bambah-Mukku D, Eichhorn SW et al. Molecular, spatial, and functional single-cell profiling of the hypothalamic preoptic region. *Science* 2018;362:eaau5324.
- Moffitt JR, Pandey S, Boettiger AN et al. Spatial organization shapes the turnover of a bacterial transcriptome. *eLife* 2016;5:e13065.
- Montero Llopis P, Jackson AF, Sliusarenko O et al. Spatial organization of the flow of genetic information in bacteria. *Nature* 2010;466:77–81.
- Montoro DT, Haber AL, Biton M et al. A revised airway epithelial hierarchy includes CFTR-expressing ionocytes. *Nature* 2018;560:319–24.
- Murata A, Sato S-I, Kawazoe Y et al. Small-molecule fluorescent probes for specific RNA targets. *Chem Commun* 2011;47:4712–4.
- Nevo-Dinur K, Nussbaum-Shochat A, Ben-Yehuda S et al. Translation-independent localization of mRNA in E. coli. *Science* 2011. <https://doi.org/10.1126/science.1195691>.

- Nikolakakis K, Lehnert E, McFall-Ngai MJ *et al.* Use of hybridization chain reaction-fluorescent in situ hybridization to track gene expression by both partners during initiation of symbiosis. *Appl Environ Microbiol* 2015;**81**:4728–35.
- Ozawa T, Natori Y, Sato M *et al.* Imaging dynamics of endogenous mitochondrial RNA in single living cells. *Nat Methods* 2007. <https://doi.org/10.1038/nmeth1030>.
- Ozbudak EM, Thattai M, Kurtser I *et al.* Regulation of noise in the expression of a single gene. *Nat Genet* 2002;**31**:69–73.
- Paige JS, Wu KY, Jaffrey SR. RNA mimics of green fluorescent protein. *Science* 2011. <https://doi.org/10.1126/science.1207339>.
- Papenfert K, Vogel J. Multiple target regulation by small noncoding RNAs rewires gene expression at the post-transcriptional level. *Res Microbiol* 2009;**160**:278–87.
- Peabody DS. The RNA Binding site of bacteriophage MS2 coat protein. *EMBO J* 1993;**12**:595–600.
- Player AN, Shen LP, Kenny D *et al.* Single-copy gene detection using branched DNA (bDNA) in Situ hybridization. *J Histochem Cytochem* 2001;**49**:603–12.
- Pope SD, Medzhitov R. Emerging principles of gene expression programs and their regulation. *Mol Cell* 2018;**71**:389–97.
- Qian X, Harris KD, Hauling T *et al.* Probabilistic cell typing enables fine mapping of closely related cell types in situ. *Nat Methods* 2020;**17**:101–6.
- Raj A, van den Bogaard P, Rifkin SA *et al.* Imaging individual mRNA molecules using multiple singly labeled probes. *Nat Methods* 2008;**5**:877–9.
- Raj A, van Oudenaarden A. Single-molecule approaches to stochastic gene expression. *Annu Rev Biophys* 2009;**38**:255–70.
- Rivas E, Klein RJ, Jones TA *et al.* Computational identification of noncoding RNAs in *E. coli* by comparative genomics. *Curr Biol* 2001;**11**:1369–73.
- Rook MS, Lu M, Kosik KS. CaMKII α 3' untranslated region-directed mRNA translocation in living neurons: visualization by GFP linkage. *J Neurosci* 2000. <https://doi.org/10.1523/jneurosci.20-17-06385.2000>.
- Rosenfeld N, Young JW, Alon U *et al.* Gene regulation at the single-cell level. *Science* 2005;**307**:1962–5.
- Rust MJ, Bates M, Zhuang X. Sub-diffraction-limit imaging by stochastic optical reconstruction microscopy (STORM). *Nat Methods* 2006;**3**:793–5.
- Ryckelynck M, Baudrey S, Rick C *et al.* Using droplet-based microfluidics to improve the catalytic properties of RNA under multiple-turnover conditions. *RNA* 2015. <https://doi.org/10.1261/rna.048033.114>.
- Sachse K, Hotzel H, Slickers P *et al.* DNA Microarray-based detection and identification of chlamydia and chlamydothila spp. *Mol Cell Probes* 2005;**19**:41–50.
- Sanamrad A, Persson F, Lundius EG *et al.* Single-particle tracking reveals that free ribosomal subunits are not excluded from the *Escherichia coli* nucleoid. *Proc Natl Acad Sci* 2014. <https://doi.org/10.1073/pnas.1411558111>.
- Sando S, Abe H, Kool ET. Quenched auto-ligating DNAs: multi-color identification of nucleic acids at single nucleotide resolution. *J Am Chem Soc* 2004. <https://doi.org/10.1021/ja038665z>.
- Santos VT, Santos VT, Bisson-Filho AW *et al.* DivIVA-mediated polar localization of ComN, a posttranscriptional regulator of *Bacillus subtilis*. *J Bacteriol* 2012. <https://doi.org/10.1128/jb.05879-11>.
- Sato S-I, Watanabe M, Katsuda Y *et al.* Live-cell imaging of endogenous mRNAs with a small molecule. *Angew Chem* 2015. <https://doi.org/10.1002/ange.201410339>.
- Sepúlveda LA, Xu H, Zhang J *et al.* Measurement of gene regulation in individual cells reveals rapid switching between promoter states. *Science* 2016;**351**:1218–22.
- Shah S, Lubeck E, Schwarzkopf M *et al.* Single-molecule RNA detection at depth by hybridization chain reaction and tissue hydrogel embedding and clearing. *Development* 2016. <https://doi.org/10.1242/dev.138560>.
- Shah S, Lubeck E, Zhou W *et al.* Editorial note to: In situ transcription profiling of single cells reveals spatial organization of cells in the mouse hippocampus. *Neuron* 2017.
- Shalek AK, Satija R, Shuga J *et al.* Single-cell RNA-seq reveals dynamic paracrine control of cellular variation. *Nature* 2014;**510**:363–9.
- Shendure J, Porreca GJ, Reppas NB *et al.* Accurate multiplex polony sequencing of an evolved bacterial genome. *Science* 2005;**309**:1728–32.
- Silverman AP, Kool ET. Quenched autoligation probes allow discrimination of live bacterial species by single nucleotide differences in rRNA. *Nucleic Acids Res* 2005;**33**:4978–86.
- Skinner SO, Sepúlveda LA, Xu H *et al.* Measuring mRNA copy number in individual *Escherichia coli* cells using single-molecule fluorescent in situ hybridization. *Nat Protoc* 2013. <https://doi.org/10.1038/nprot.2013.066>.
- Sokol DL, Zhang X, Lu P *et al.* Real time detection of DNA RNA hybridization in living cells. *Proc Natl Acad Sci* 1998;**95**:11538–43.
- So L-H, Ghosh A, Zong C *et al.* General properties of transcriptional time series in *Escherichia coli*. *Nat Genet* 2011;**43**:554–60.
- Song W, Filonov GS, Kim H *et al.* Imaging RNA polymerase iii transcription using a photostable RNA-fluorophore complex. *Nat Chem Biol* 2017;**13**:1187–94.
- Stoltenburg R, Reinemann C, Strehlitz B. SELEX—a (r)evolutionary method to generate high-affinity nucleic acid ligands. *Biomol Eng* 2007. <https://doi.org/10.1016/j.bioeng.2007.06.001>.
- Storz G, Vogel J, Wassarman KM. Regulation by small RNAs in bacteria: expanding frontiers. *Mol Cell* 2011;**43**:880–91.
- Strack RL, Disney MD, Jaffrey SR. A superfolder Spinach2 reveals the dynamic nature of trinucleotide repeat-containing RNA. *Nat Methods* 2013;**10**:1219–24.
- Strack RL, Jaffrey SR. Live-cell imaging of mammalian RNAs with Spinach2. *Methods Enzymol* 2015;**550**:129–46.
- Stracy M, Lesterlin C, de Leon FG *et al.* Live-cell superresolution microscopy reveals the organization of RNA polymerase in the bacterial nucleoid. *Proc Natl Acad Sci* 2015. <https://doi.org/10.1073/pnas.1507592112>.
- Streit S, Michalski CW, Erkan M *et al.* Northern blot analysis for detection and quantification of RNA in pancreatic cancer cells and tissues. *Nat Protoc* 2009;**4**:37–43.
- Sunbul M, Jäschke A. Contact-mediated quenching for RNA imaging in bacteria with a fluorophore-binding aptamer. *Angew Chem* 2013;**52**:13401–4.
- Sunbul M, Jäschke A. SRB-2: a promiscuous rainbow aptamer for live-cell RNA imaging. *Nucleic Acids Res* 2018. <https://doi.org/10.1093/nar/gky543>.
- Tanenbaum ME, Gilbert LA, Qi LS *et al.* A protein-tagging system for signal amplification in gene expression and fluorescence imaging. *Cell* 2014; <https://doi.org/10.1016/j.cell.2014.09.039>.
- Taniguchi Y, Choi PJ, Li G-W *et al.* Quantifying *E. coli* proteome and transcriptome with single-molecule sensitivity in single cells. *Science* 2010;**329**:533–38.

- Tsanov N, Samacoits A, Chouaib R et al. smiFISH and FISH-Quant - a flexible single RNA detection approach with super-resolution capability. *Nucleic Acids Res* 2016;**44**:e165.
- Tutucci E, Vera M, Biswas J et al. An improved MS2 System for accurate reporting of the mRNA life cycle. *Nat Methods* 2018;**15**:81–89.
- Tyagi S, Alsmadi O. Imaging native beta-actin mRNA in motile fibroblasts. *Biophys J* 2004;**87**:4153–62.
- Tyagi S, Kramer FR. Molecular beacons: probes that fluoresce upon hybridization. *Nat Biotechnol* 1996;**14**:303–8.
- Umezawa K, Citterio D, Suzuki K. New trends in near-infrared fluorophores for bioimaging. *Anal Sci* 2014. <https://doi.org/10.2116/analsci.30.327>.
- Uno S-N, Kamiya M, Yoshihara T et al. A spontaneously blinking fluorophore based on intramolecular spirocyclization for live-cell super-resolution imaging. *Nature Chem* 2014. <https://doi.org/10.1038/nchem.2002>.
- Volkov IL, Lindén M, Rivera JA et al. tRNA tracking for direct measurements of protein synthesis kinetics in live cells. *Nat Chem Biol* 2018. <https://doi.org/10.1038/s41589-018-0063-y>.
- Wagner E, Gerhart H, Romby P. Small RNAs in bacteria and archaea: who they are, what they do, and how they do it. *Adv Genet* 2015;**90**:133–208.
- Wang C, Han B, Zhou R et al. Real-time imaging of translation on single mRNA transcripts in live cells. *Cell* 2016;**165**:990–1001.
- Wang G, Moffitt JR, Zhuang X. Multiplexed imaging of high-density libraries of RNAs with MERFISH and expansion microscopy. *Sci Rep* 2018;**8**:4847.
- Wang X, Allen WE, Wright MA et al. Three-dimensional intact-tissue sequencing of single-cell transcriptional states. *Science* 2018;**361**. <https://doi.org/10.1126/science.aat5691>.
- Wang X, McLachlan J, Zamore PD et al. Modular recognition of RNA by a human pumilio-homology domain. *Cell* 2002. [https://doi.org/10.1016/s0092-8674\(02\)00873-5](https://doi.org/10.1016/s0092-8674(02)00873-5).
- Wassarman KM, Repoila F, Rosenow C et al. Identification of novel small RNAs using comparative genomics and microarrays. *Genes & Development* 2001;**15**:1637–51.
- Waters LS, Storz G. Regulatory RNAs in bacteria. *Cell* 2009;**136**:615–28.
- Weber APM, Weber KL, Carr K et al. Sampling the arabidopsis transcriptome with massively parallel pyrosequencing. *Plant Physiol* 2007. <https://doi.org/10.1104/pp.107.096677>.
- Weng X, Bohrer CH, Bettridge K et al. Spatial organization of RNA polymerase and its relationship with transcription in *Escherichia coli*. *PNAS* 2019;**116**:20115–23.
- Wiegant J, Brouwer AK, Tanke HJ et al. Visualizing nucleic acids in living cells by fluorescence in vivo hybridization. *Methods Mol Biol* 2010. <https://doi.org/10.1007/978-1-60761-789-1.17>.
- Wirth R, Gao P, Nienhaus GU et al. SiRA: a silicon rhodamine-binding aptamer for live-cell super-resolution RNA imaging. *J Am Chem Soc* 2019. <https://doi.org/10.1021/jacs.9b02697>.
- Wu B, Chao JA, Singer RH. Fluorescence fluctuation spectroscopy enables quantitative imaging of single mRNAs in living cells. *Biophys J* 2012. <https://doi.org/10.1016/j.bpj.2012.05.017>.
- Wu B, Elisavich C, Yoon YJ et al. Translation dynamics of single mRNAs in live cells and neurons. *Science* 2016;**352**:1430–35.
- Xia C, Babcock HP, Moffitt JR et al. Multiplexed detection of RNA using MERFISH and branched DNA amplification. *Sci Rep* 2019;**9**:7721.
- Yamaguchi T, Fuchs BM, Amann R et al. Rapid and sensitive identification of marine bacteria by an improved in situ DNA hybridization chain reaction (quickHCR-FISH). *Syst Appl Microbiol* 2015;**38**:400–5.
- Yang S, Kim S, Kim D-K et al. Transcription and translation contribute to gene locus relocation to the nucleoid periphery in *E. coli*. *Nat Commun* 2019. <https://doi.org/10.1038/s41467-019-13152-y>.
- Yan X, Hoek TA, Vale RD et al. Dynamics of translation of single mRNA molecules in vivo. *Cell* 2016. <https://doi.org/10.1016/j.cell.2016.04.034>.
- Yerramilli VS, Kim KH. Labeling RNAs in live cells using malachite green aptamer scaffolds as fluorescent probes. *ACS Synthetic Biology* 2018;**7**:758–66.
- Zhang F, Simon AE. A novel procedure for the localization of viral RNAs in protoplasts and whole plants. *Plant J* 2003. <https://doi.org/10.1046/j.1365-313x.2003.01837.x>.
- Zhang J, Fei J, Leslie BJ et al. Tandem spinach array for mRNA imaging in living bacterial cells. *Sci Rep* 2015. <https://doi.org/10.1038/srep17295>.
- Zhang WI, Röhse H, Rizzoli SO et al. Fluorescent in situ hybridization of synaptic proteins imaged with super-resolution STED microscopy. *Microsc Res Tech* 2014. <https://doi.org/10.1002/jemt.22367>.
- Zheng J, Yang R, Shi M et al. Rationally designed molecular beacons for bioanalytical and biomedical applications. *Chem Soc Rev* 2015. <https://doi.org/10.1039/c5cs00020c>.
- Zong C, So L-H, Sepúlveda LA et al. Lysogen stability is determined by the frequency of activity bursts from the fate-determining gene. *Mol Syst Biol* 2010;**6**:440.

V References

- Abebe, Gedif Meseret. 2020. "The Role of Bacterial Biofilm in Antibiotic Resistance and Food Contamination." *International Journal of Microbiology* 2020 (August): 1705814.
- Aguilar, Claudio, Aurelien Carlier, Kathrin Riedel, and Leo Eberl. 2009. "Cell–Cell Communication in Biofilms of Gram-negative Bacteria." *Bacterial Signaling*. Wiley. <https://doi.org/10.1002/9783527629237.ch2>.
- Aguilar, Claudio, Catherine Eichwald, and Leo Eberl. 2015. "Multicellularity in Bacteria: From Division of Labor to Biofilm Formation." In *Evolutionary Transitions to Multicellular Life: Principles and Mechanisms*, edited by Iñaki Ruiz-Trillo and Aurora M. Nedelcu, 79–95. Dordrecht: Springer Netherlands.
- Aguilar, Claudio, Hera Vlamakis, Alejandra Guzman, Richard Losick, and Roberto Kolter. 2010. "KinD Is a Checkpoint Protein Linking Spore Formation to Extracellular-Matrix Production in *Bacillus Subtilis* Biofilms." *MBio* 1 (1). <https://doi.org/10.1128/mBio.00035-10>.
- An, Dingding, and Matthew R. Parsek. 2007. "The Promise and Peril of Transcriptional Profiling in Biofilm Communities." *Current Opinion in Microbiology* 10 (3): 292–96.
- Armbruster, Catherine R., and Matthew R. Parsek. 2018. "New Insight into the Early Stages of Biofilm Formation." *Proceedings of the National Academy of Sciences of the United States of America*.
- Arnold, J. W., and L. J. Shimkets. 1988. "Cell Surface Properties Correlated with Cohesion in *Myxococcus Xanthus*." *Journal of Bacteriology* 170 (12): 5771–77.
- Avery, Simon V. 2006. "Microbial Cell Individuality and the Underlying Sources of Heterogeneity." *Nature Reviews. Microbiology* 4 (8): 577–87.
- Bak-Coleman, Joseph B., Mark Alfano, Wolfram Barfuss, Carl T. Bergstrom, Miguel A. Centeno, Iain D. Couzin, Jonathan F. Donges, et al. 2021. "Stewardship of Global Collective Behavior." *Proceedings of the National Academy of Sciences of the United States of America* 118 (27). <https://doi.org/10.1073/pnas.2025764118>.
- Balagam, Rajesh, Douglas B. Litwin, Fabian Czerwinski, Mingzhai Sun, Heidi B. Kaplan, Joshua W. Shaevitz, and Oleg A. Igoshin. 2014. "Myxococcus Xanthus Gliding Motors Are Elastically Coupled to the Substrate as Predicted by the Focal Adhesion Model of Gliding Motility." *PLoS Computational Biology* 10 (5): e1003619.
- Barken, Kim B., Sünje J. Pamp, Liang Yang, Morten Gjermansen, Jacob J. Bertrand, Mikkel Klausen, Michael Givskov, Cynthia B. Whitchurch, Joanne N. Engel, and Tim Tolker-Nielsen. 2008. "Roles of Type IV Pili, Flagellum-Mediated Motility and Extracellular DNA in the Formation of Mature Multicellular Structures in *Pseudomonas Aeruginosa* Biofilms." *Environmental Microbiology*. <https://doi.org/10.1111/j.1462-2920.2008.01658.x>.
- Beliveau, Brian J., Alistair N. Boettiger, Maier S. Avendaño, Ralf Jungmann, Ruth B. McCole, Eric F. Joyce, Caroline Kim-Kiselak, et al. 2015. "Single-Molecule Super-Resolution Imaging of Chromosomes and in Situ Haplotype Visualization Using Oligopaint FISH Probes." *Nature Communications* 6 (May): 7147.
- Bergman, B. 1997. "N₂ Fixation by Non-Heterocystous Cyanobacteria." *FEMS Microbiology Reviews*. [https://doi.org/10.1016/s0168-6445\(96\)00028-9](https://doi.org/10.1016/s0168-6445(96)00028-9).
- Berleman, James E., Simon Allen, Megan A. Danielewicz, Jonathan P. Remis, Amita Gorur, Jack Cunha, Masood Z. Hadi, et al. 2014. "The Lethal Cargo of *Myxococcus Xanthus* Outer Membrane Vesicles." *Frontiers in Microbiology*. <https://doi.org/10.3389/fmicb.2014.00474>.
- Berleman, James E., Tatiana Chumley, Patricia Cheung, and John R. Kirby. 2006a. "Rippling Is a Predatory Behavior in *Myxococcus Xanthus*." *Journal of Bacteriology*. <https://doi.org/10.1128/jb.00559-06>.
- . 2006b. "Rippling Is a Predatory Behavior in *Myxococcus Xanthus*." *Journal of Bacteriology*. <https://doi.org/10.1128/jb.00559-06>.

- . 2006c. “Rippling Is a Predatory Behavior in *Myxococcus Xanthus*.” *Journal of Bacteriology* 188 (16): 5888–95.
- Berleman, James E., and John R. Kirby. 2009a. “Deciphering the Hunting Strategy of a Bacterial Wolfpack.” *FEMS Microbiology Reviews* 33 (5): 942–57.
- . 2009b. “Deciphering the Hunting Strategy of a Bacterial Wolfpack.” *FEMS Microbiology Reviews* 33 (5): 942–57.
- Berleman, James E., Jodie Scott, Tatiana Chumley, and John R. Kirby. 2008a. “Predataxis Behavior in *Myxococcus Xanthus*.” *Proceedings of the National Academy of Sciences of the United States of America* 105 (44): 17127–32.
- . 2008b. “Predataxis Behavior in *Myxococcus Xanthus*.” *Proceedings of the National Academy of Sciences of the United States of America* 105 (44): 17127–32.
- . 2008c. “Predataxis Behavior in *Myxococcus Xanthus*.” *Proceedings of the National Academy of Sciences of the United States of America* 105 (44): 17127–32.
- Berleman, James E., Marcin Zemla, Jonathan P. Remis, Hong Liu, Annie E. Davis, Alexandra N. Worth, Zachary West, et al. 2016. “Exopolysaccharide Microchannels Direct Bacterial Motility and Organize Multicellular Behavior.” *The ISME Journal* 10 (11): 2620–32.
- Bertolaso, Marta, and Anna Maria Dieli. 2017. “Cancer and Intercellular Cooperation.” *Royal Society Open Science*. <https://doi.org/10.1098/rsos.170470>.
- Binnig, G., C. F. Quate, and C. Gerber. 1986. “Atomic Force Microscope.” *Physical Review Letters* 56 (9): 930–33.
- Biro, Dora, Takao Sasaki, and Steven J. Portugal. 2016. “Bringing a Time–Depth Perspective to Collective Animal Behaviour.” *Trends in Ecology & Evolution*. <https://doi.org/10.1016/j.tree.2016.03.018>.
- Bjarnsholt, Thomas. 2013. “The Role of Bacterial Biofilms in Chronic Infections.” *APMIS Supplementum*, no. 136 (May): 1–51.
- Blackhart, B. D., and D. R. Zusman. 1985. “‘Frizzy’ Genes of *Myxococcus Xanthus* Are Involved in Control of Frequency of Reversal of Gliding Motility.” *Proceedings of the National Academy of Sciences of the United States of America* 82 (24): 8767–70.
- Bodman, S. B. von, D. R. Majerczak, and D. L. Coplin. 1998. “A Negative Regulator Mediates Quorum-Sensing Control of Exopolysaccharide Production in *Pantoea Stewartii* Subsp. *Stewartii*.” *Proceedings of the National Academy of Sciences of the United States of America* 95 (13): 7687–92.
- Boettiger, Alistair N., Bogdan Bintu, Jeffrey R. Moffitt, Siyuan Wang, Brian J. Beliveau, Geoffrey Fudenberg, Maxim Imakaev, Leonid A. Mirny, Chao-Ting Wu, and Xiaowei Zhuang. 2016. “Super-Resolution Imaging Reveals Distinct Chromatin Folding for Different Epigenetic States.” *Nature* 529 (7586): 418–22.
- Bonner, John Tyler. 1998. “The Origins of Multicellularity.” *Integrative Biology* 1 (1): 27–36.
- Boudreau, Colton, Tse-Luen Erika Wee, Yan-Rung Silvia Duh, Melissa P. Couto, Kimya H. Ardakani, and Claire M. Brown. 2016. “Excitation Light Dose Engineering to Reduce Photo-Bleaching and Photo-Toxicity.” *Scientific Reports* 6 (August): 30892.
- Branda, S. S., J. E. González-Pastor, S. Ben-Yehuda, R. Losick, and R. Kolter. 2001. “Fruiting Body Formation by *Bacillus Subtilis*.” *Proceedings of the National Academy of Sciences of the United States of America* 98 (20): 11621–26.
- Branda, Steven S., Shild Vik, Lisa Friedman, and Roberto Kolter. 2005. “Biofilms: The Matrix Revisited.” *Trends in Microbiology* 13 (1): 20–26.
- Bridier, Arnaud, Jean-Christophe Piard, Caroline Pandin, Simon Labarthe, Florence Dubois-Brissonnet, and Romain Briandet. 2017. “Spatial Organization Plasticity as an Adaptive Driver of Surface Microbial Communities.” *Frontiers in Microbiology* 8 (July): 1364.
- Brinkhoff, Thorsten, Doreen Fischer, John Vollmers, Sonja Voget, Christine Beardsley, Sebastian Thole, Marc Mussmann, et al. 2012. “Biogeography and Phylogenetic Diversity of a Cluster of Exclusively Marine Myxobacteria.” *The ISME Journal* 6 (6): 1260–72.

- Brown, Sam P., and Angus Buckling. 2008. "A Social Life for Discerning Microbes." *Cell* 135 (4): 600–603.
- Brunet, Thibaut, and Nicole King. 2017. "The Origin of Animal Multicellularity and Cell Differentiation." *Developmental Cell* 43 (2): 124–40.
- Bull, C. T., K. G. Shetty, and K. V. Subbarao. 2002. "Interactions Between Myxobacteria, Plant Pathogenic Fungi, and Biocontrol Agents." *Plant Disease* 86 (8): 889–96.
- Bulyha, Iryna, Carmen Schmidt, Peter Lenz, Vladimir Jakovljevic, Andrea Höne, Berenike Maier, Michael Hoppert, and Lotte Sjøgaard-Andersen. 2009. "Regulation of the Type IV Pili Molecular Machine by Dynamic Localization of Two Motor Proteins." *Molecular Microbiology* 74 (3): 691–706.
- Burchard, R. P. 1981. "Gliding Motility of Prokaryotes: Ultrastructure, Physiology, and Genetics." *Annual Review of Microbiology* 35: 497–529.
- . 1982. "Trail Following by Gliding Bacteria." *Journal of Bacteriology* 152 (1): 495–501.
- Bustamante, Víctor H., Irma Martínez-Flores, Hera C. Vlamakis, and David R. Zusman. 2004a. "Analysis of the Frz Signal Transduction System of Myxococcus Xanthus Shows the Importance of the Conserved C-Terminal Region of the Cytoplasmic Chemoreceptor FrzCD in Sensing Signals." *Molecular Microbiology*. <https://doi.org/10.1111/j.1365-2958.2004.04221.x>.
- . 2004b. "Analysis of the Frz Signal Transduction System of Myxococcus Xanthus Shows the Importance of the Conserved C-Terminal Region of the Cytoplasmic Chemoreceptor FrzCD in Sensing Signals." *Molecular Microbiology* 53 (5): 1501–13.
- . 2004c. "Analysis of the Frz Signal Transduction System of Myxococcus Xanthus Shows the Importance of the Conserved C-Terminal Region of the Cytoplasmic Chemoreceptor FrzCD in Sensing Signals." *Molecular Microbiology* 53 (5): 1501–13.
- Caberoy, Nora B., Roy D. Welch, Jimmy S. Jakobsen, Steven C. Slater, and Anthony G. Garza. 2003. "Global Mutational Analysis of NtrC-Like Activators in Myxococcus Xanthus : Identifying Activator Mutants Defective for Motility and Fruiting Body Development." *Journal of Bacteriology*. <https://doi.org/10.1128/jb.185.20.6083-6094.2003>.
- Cao, Pengbo, Arup Dey, Christopher N. Vassallo, and Daniel Wall. 2015a. "How Myxobacteria Cooperate." *Journal of Molecular Biology* 427 (23): 3709–21.
- . 2015b. "How Myxobacteria Cooperate." *Journal of Molecular Biology* 427 (23): 3709–21.
- Cascales, E., M. Gavioli, J. N. Sturgis, and R. Lloubès. 2000. "Proton Motive Force Drives the Interaction of the Inner Membrane TolA and Outer Membrane Pal Proteins in Escherichia Coli." *Molecular Microbiology* 38 (4): 904–15.
- Cattoni, Diego I., Jean-Bernard Fiche, Alessandro Valeri, Tâm Mignot, and Marcelo Nöllmann. 2013. "Super-Resolution Imaging of Bacteria in a Microfluidics Device." *PloS One* 8 (10): e76268.
- Chang, Yi-Wei, Lee A. Rettberg, Anke Treuner-Lange, Janet Iwasa, Lotte Sjøgaard-Andersen, and Grant J. Jensen. 2016a. "Architecture of the Type IVa Pilus Machine." *Science* 351 (6278): aad2001.
- . 2016b. "Architecture of the Type IVa Pilus Machine." *Science* 351 (6278): aad2001.
- Chao, L., and B. R. Levin. 1981. "Structured Habitats and the Evolution of Anticompetitor Toxins in Bacteria." *Proceedings of the National Academy of Sciences of the United States of America* 78 (10): 6324–28.
- Chao, Yashuan, Laura R. Marks, Melinda M. Pettigrew, and Anders P. Hakansson. 2015. "Streptococcus Pneumoniae Biofilm Formation and Dispersion during Colonization and Disease." *Frontiers in Cellular and Infection Microbiology*. <https://doi.org/10.3389/fcimb.2014.00194>.
- Charest, Pascale G., and Richard A. Firtel. 2007. "Big Roles for Small GTPases in the Control of Directed Cell Movement." *Biochemical Journal* 401 (2): 377–90.
- Chater, Keith F., Sandor Biró, Kye Joon Lee, Tracy Palmer, and Hildgund Schrempf. 2010. "The Complex Extracellular Biology of Streptomyces." *FEMS Microbiology Reviews* 34 (2): 171–98.
- Chauhan, Ashwini, Murty V. V. S. Madiraju, Marek Fol, Hava Lofton, Erin Maloney, Robert Reynolds, and Malini Rajagopalan. 2006. "Mycobacterium Tuberculosis Cells Growing in Macrophages Are Filamentous and Deficient in FtsZ Rings." *Journal of Bacteriology* 188 (5): 1856–65.

- Chen, Kok Hao, Alistair N. Boettiger, Jeffrey R. Moffitt, Siyuan Wang, and Xiaowei Zhuang. 2015a. "RNA Imaging. Spatially Resolved, Highly Multiplexed RNA Profiling in Single Cells." *Science* 348 (6233): aaa6090.
- . 2015b. "RNA Imaging. Spatially Resolved, Highly Multiplexed RNA Profiling in Single Cells." *Science* 348 (6233): aaa6090.
- Chen, Wei, Boqiang Liu, Suting Peng, Jiawei Sun, and Xu Qiao. 2019. "S3D-UNet: Separable 3D U-Net for Brain Tumor Segmentation." In *Brainlesion: Glioma, Multiple Sclerosis, Stroke and Traumatic Brain Injuries*, 358–68. Springer International Publishing.
- Çiçek, Özgün, Ahmed Abdulkadir, Soeren S. Lienkamp, Thomas Brox, and Olaf Ronneberger. 2016. "3D U-Net: Learning Dense Volumetric Segmentation from Sparse Annotation." In *Medical Image Computing and Computer-Assisted Intervention – MICCAI 2016*, 424–32. Springer International Publishing.
- Claessen, Dennis, Wouter de Jong, Lubbert Dijkhuizen, and Han A. B. Wösten. 2006. "Regulation of Streptomyces Development: Reach for the Sky!" *Trends in Microbiology* 14 (7): 313–19.
- Claessen, Dennis, Daniel E. Rozen, Oscar P. Kuipers, Lotte Søgaard-Andersen, and Gilles P. van Wezel. 2014a. "Bacterial Solutions to Multicellularity: A Tale of Biofilms, Filaments and Fruiting Bodies." *Nature Reviews. Microbiology* 12 (2): 115–24.
- . 2014b. "Bacterial Solutions to Multicellularity: A Tale of Biofilms, Filaments and Fruiting Bodies." *Nature Reviews. Microbiology* 12 (2): 115–24.
- Cohen, Susan E., and Susan S. Golden. 2015. "Circadian Rhythms in Cyanobacteria." *Microbiology and Molecular Biology Reviews: MMBR* 79 (4): 373–85.
- Colville, Keegan, Nicolas Tompkins, Andrew D. Rutenberg, and Manfred H. Jericho. 2010. "Effects of Poly(L-Lysine) Substrates on Attached Escherichia Coli Bacteria." *Langmuir: The ACS Journal of Surfaces and Colloids* 26 (4): 2639–44.
- Corno, Gianluca. 2006. "Effects of Nutrient Availability and Ochromonas Sp. Predation on Size and Composition of a Simplified Aquatic Bacterial Community." *FEMS Microbiology Ecology*. <https://doi.org/10.1111/j.1574-6941.2006.00185.x>.
- Corno Gianluca, and Jürgens Klaus. 2006. "Direct and Indirect Effects of Protist Predation on Population Size Structure of a Bacterial Strain with High Phenotypic Plasticity." *Applied and Environmental Microbiology* 72 (1): 78–86.
- Crawford, E. W., Jr, and L. J. Shimkets. 2000. "The Myxococcus Xanthus SocE and CsgA Genes Are Regulated by the Stringent Response." *Molecular Microbiology* 37 (4): 788–99.
- Crespi, B. J. 2001. "The Evolution of Social Behavior in Microorganisms." *Trends in Ecology & Evolution* 16 (4): 178–83.
- Curtis, Patrick D., James Atwood 3rd, Ron Orlando, and Lawrence J. Shimkets. 2007. "Proteins Associated with the Myxococcus Xanthus Extracellular Matrix." *Journal of Bacteriology* 189 (21): 7634–42.
- Curtis, Patrick D., Rion G. Taylor, Roy D. Welch, and Lawrence J. Shimkets. 2007. "Spatial Organization of Myxococcus Xanthus during Fruiting Body Formation." *Journal of Bacteriology* 189 (24): 9126–30.
- Dahmane, Selma, Christine Doucet, Antoine Le Gall, Célia Chamontin, Patrice Dosset, Florent Murcy, Laurent Fernandez, et al. 2019. "Nanoscale Organization of Tetraspanins during HIV-1 Budding by Correlative DSTORM/AFM." *Nanoscale* 11 (13): 6036–44.
- Dana, J. R., and L. J. Shimkets. 1993. "Regulation of Cohesion-Dependent Cell Interactions in Myxococcus Xanthus." *Journal of Bacteriology* 175 (11): 3636–47.
- Danhorn, Thomas, and Clay Fuqua. 2007. "Biofilm Formation by Plant-Associated Bacteria." *Annual Review of Microbiology*. <https://doi.org/10.1146/annurev.micro.61.080706.093316>.
- Dar, Daniel, Nina Dar, Long Cai, and Dianne K. Newman. 2021a. "Spatial Transcriptomics of Planktonic and Sessile Bacterial Populations at Single-Cell Resolution." *Science* 373 (6556). <https://doi.org/10.1126/science.abi4882>.

- . 2021b. “Spatial Transcriptomics of Planktonic and Sessile Bacterial Populations at Single-Cell Resolution.” *Science* 373 (6556). <https://doi.org/10.1126/science.abi4882>.
- Darouiche, Rabih O. 2004. “Treatment of Infections Associated with Surgical Implants.” *New England Journal of Medicine*. <https://doi.org/10.1056/nejmra035415>.
- Dawid, W. 2000. “Biology and Global Distribution of Myxobacteria in Soils.” *FEMS Microbiology Reviews* 24 (4): 403–27.
- Dey, Arup, and Daniel Wall. 2014. “A Genetic Screen in *Myxococcus Xanthus* Identifies Mutants That Uncouple Outer Membrane Exchange from a Downstream Cellular Response.” *Journal of Bacteriology* 196 (24): 4324–32.
- Dhar, Neeraj, and John D. McKinney. 2007. “Microbial Phenotypic Heterogeneity and Antibiotic Tolerance.” *Current Opinion in Microbiology* 10 (1): 30–38.
- Diodati, Michelle E., Ronald E. Gill, Lynda Plamann, and Mitchell Singer. 2014. “Initiation and Early Developmental Events.” In *Myxobacteria*, 41–76. Washington, DC, USA: ASM Press.
- Doekes, Hilje M., Rob J. de Boer, and Rutger Hermsen. 2019. “Toxin Production Spontaneously Becomes Regulated by Local Cell Density in Evolving Bacterial Populations.” *PLoS Computational Biology* 15 (8): e1007333.
- Donlan Rodney M., and Costerton J. William. 2002. “Biofilms: Survival Mechanisms of Clinically Relevant Microorganisms.” *Clinical Microbiology Reviews* 15 (2): 167–93.
- Dow, J. M., L. Crossman, K. Findlay, Y-Q He, J-X Feng, and J-L Tang. 2003. “Biofilm Dispersal in *Xanthomonas Campestris* Is Controlled by Cell-Cell Signaling and Is Required for Full Virulence to Plants.” *Proceedings of the National Academy of Sciences*. <https://doi.org/10.1073/pnas.1833360100>.
- Dragoš, Anna, Heiko Kiesewalter, Marivic Martin, Chih-Yu Hsu, Raimo Hartmann, Tobias Wechsler, Carsten Eriksen, et al. 2018. “Division of Labor during Biofilm Matrix Production.” *Current Biology: CB* 28 (12): 1903-1913.e5.
- Drake, B., C. B. Prater, A. L. Weisenhorn, S. A. Gould, T. R. Albrecht, C. F. Quate, D. S. Cannell, H. G. Hansma, and P. K. Hansma. 1989. “Imaging Crystals, Polymers, and Processes in Water with the Atomic Force Microscope.” *Science* 243 (4898): 1586–89.
- Dufrène, Yves F., Toshio Ando, Ricardo Garcia, David Alsteens, David Martinez-Martin, Andreas Engel, Christoph Gerber, and Daniel J. Müller. 2017. “Imaging Modes of Atomic Force Microscopy for Application in Molecular and Cell Biology.” *Nature Nanotechnology* 12 (4): 295–307.
- Dugatkin, Lee Alan, Michael Perlin, J. Scott Lucas, and Ronald Atlas. 2005. “Group-Beneficial Traits, Frequency-Dependent Selection and Genotypic Diversity: An Antibiotic Resistance Paradigm.” *Proceedings. Biological Sciences / The Royal Society* 272 (1558): 79–83.
- Dworkin, Martin. 1963. “NUTRITIONAL REGULATION OF MORPHOGENESIS IN *MYXOCOCCUS XANTHUS*.” *Journal of Bacteriology* 86 (1): 67–72.
- Eiff, Christof von, Christof von Eiff, Bernd Jansen, Wolfgang Kohnen, and Karsten Becker. 2005. “Infections Associated with Medical Devices.” *Drugs*. <https://doi.org/10.2165/00003495-200565020-00003>.
- Eng, Chee-Huat Linus, Michael Lawson, Qian Zhu, Ruben Dries, Noushin Koulana, Yodai Takeji, Jina Yun, et al. 2019. “Transcriptome-Scale Super-Resolved Imaging in Tissues by RNA SeqFISH.” *Nature* 568 (7751): 235–39.
- Evans, Alun G. L., Hazel M. Davey, Alan Cookson, Heather Currinn, Gillian Cooke-Fox, Paulina J. Stanczyk, and David E. Whitworth. 2012a. “Predatory Activity of *Myxococcus Xanthus* Outer-Membrane Vesicles and Properties of Their Hydrolase Cargo.” *Microbiology* 158 (Pt 11): 2742–52.
- . 2012b. “Predatory Activity of *Myxococcus Xanthus* Outer-Membrane Vesicles and Properties of Their Hydrolase Cargo.” *Microbiology* 158 (Pt 11): 2742–52.
- Faure, Laura M., Jean-Bernard Fiche, Leon Espinosa, Adrien Ducret, Vivek Anantharaman, Jennifer Luciano, Sébastien Lhospice, et al. 2016a. “The Mechanism of Force Transmission at Bacterial Focal Adhesion Complexes.” *Nature* 539 (7630): 530–35.

- . 2016b. “The Mechanism of Force Transmission at Bacterial Focal Adhesion Complexes.” *Nature* 539 (7630): 530–35.
- . 2016c. “The Mechanism of Force Transmission at Bacterial Focal Adhesion Complexes.” *Nature* 539 (7630): 530–35.
- Fernandes, Thales F. D., Oscar Saavedra, Emmanuel Margeat, Pierre-Emmanuel Milhiet, and Luca Costa. 2020. “Synchronous, Crosstalk-Free Correlative AFM and Confocal Microscopies/Spectroscopies.” *Scientific Reports*. <https://doi.org/10.1038/s41598-020-62529-3>.
- Fiegna, Francesca, and Gregory J. Velicer. 2003. “Competitive Fates of Bacterial Social Parasites: Persistence and Self-Induced Extinction of *Myxococcus Xanthus* Cheaters.” *Proceedings. Biological Sciences / The Royal Society* 270 (1523): 1527–34.
- . 2005. “Exploitative and Hierarchical Antagonism in a Cooperative Bacterium.” *PLoS Biology* 3 (11): e370.
- Findlay, Brandon L. 2016. “The Chemical Ecology of Predatory Soil Bacteria.” *ACS Chemical Biology*. <https://doi.org/10.1021/acscchembio.6b00176>.
- Fisher, Robert A., Bridget Gollan, and Sophie Helaine. 2017. “Persistent Bacterial Infections and Persister Cells.” *Nature Reviews. Microbiology* 15 (8): 453–64.
- Flärdh, Klas. 2003. “Growth Polarity and Cell Division in *Streptomyces*.” *Current Opinion in Microbiology* 6 (6): 564–71.
- Flärdh, Klas, and Mark J. Buttner. 2009. “*Streptomyces* Morphogenetics: Dissecting Differentiation in a Filamentous Bacterium.” *Nature Reviews. Microbiology* 7 (1): 36–49.
- Flores, Enrique, and Antonia Herrero. 2010. “Compartmentalized Function through Cell Differentiation in Filamentous Cyanobacteria.” *Nature Reviews. Microbiology* 8 (1): 39–50.
- Floyd, K. A., A. R. Eberly, and M. Hadjifrangiskou. 2017. “3 - Adhesion of Bacteria to Surfaces and Biofilm Formation on Medical Devices.” In *Biofilms and Implantable Medical Devices*, edited by Ying Deng and Wei Lv, 47–95. Woodhead Publishing.
- Folse, Henry J., 3rd, and Steven D. Allison. 2012. “Cooperation, Competition, and Coalitions in Enzyme-Producing Microbes: Social Evolution and Nutrient Depolymerization Rates.” *Frontiers in Microbiology* 3 (September): 338.
- Friedrich, Carmen, Iryna Bulyha, and Lotte Sogaard-Andersen. 2014. “Outside-in Assembly Pathway of the Type IV Pilus System in *Myxococcus Xanthus*.” *Journal of Bacteriology* 196 (2): 378–90.
- Funken, Horst, Kai-Malte Bartels, Susanne Wilhelm, Melanie Brocker, Michael Bott, Manjeet Bains, Robert E. W. Hancock, Frank Rosenau, and Karl-Erich Jaeger. 2012. “Specific Association of Lectin LecB with the Surface of *Pseudomonas Aeruginosa*: Role of Outer Membrane Protein OprF.” *PloS One* 7 (10): e46857.
- Galicia, Christian, Sébastien Lhospice, Paloma Fernández Varela, Stefano Trapani, Wenhua Zhang, Jorge Navaza, Julien Herrou, Tãm Mignot, and Jacqueline Cherfils. 2019. “MglA Functions as a Three-State GTPase to Control Movement Reversals of *Myxococcus Xanthus*.” *Nature Communications* 10 (1): 5300.
- Garcia, Ronald, Klaus Gerth, Marc Stadler, Irineo J. Dogma, and Rolf Müller. 2010. “Expanded Phylogeny of Myxobacteria and Evidence for Cultivation of the ‘Unculturable.’” *Molecular Phylogenetics and Evolution*. <https://doi.org/10.1016/j.ympev.2010.08.028>.
- Gavara, Núria. 2017. “A Beginner’s Guide to Atomic Force Microscopy Probing for Cell Mechanics.” *Microscopy Research and Technique* 80 (1): 75–84.
- Gerber, Christoph, and Hans Peter Lang. 2006. “How the Doors to the Nanoworld Were Opened.” *Nature Nanotechnology* 1 (1): 3–5.
- Gibiansky, Maxim L., Wei Hu, Karin A. Dahmen, Wenyuan Shi, and Gerard C. L. Wong. 2013. “Earthquake-like Dynamics in *Myxococcus Xanthus* Social Motility.” *Proceedings of the National Academy of Sciences of the United States of America* 110 (6): 2330–35.
- Giglio, Krista M., Nora Caberoy, Garret Suen, Dale Kaiser, and Anthony G. Garza. 2011. “A Cascade of Coregulating Enhancer Binding Proteins Initiates and Propagates a Multicellular

- Developmental Program." *Proceedings of the National Academy of Sciences*. <https://doi.org/10.1073/pnas.1105876108>.
- Golden, James W., and Ho-Sung Yoon. 2003. "Heterocyst Development in *Anabaena*." *Current Opinion in Microbiology* 6 (6): 557–63.
- Grande, Rossella, Laura Nistico, Karthik Sambanthamoorthy, Mark Longwell, Antonio Iannitelli, Luigina Cellini, Antonio Di Stefano, Luanne Hall Stoodley, and Paul Stoodley. 2014. "Temporal Expression Of agrB, CidA, Andalsin the Early Development Of *Staphylococcus Aureus* UAMS-1 Biofilm Formation and the Structural Role of Extracellular DNA and Carbohydrates." *Pathogens and Disease*. <https://doi.org/10.1111/2049-632x.12158>.
- Gronewold, Thomas M. A., and Dale Kaiser. 2007. "Mutations of the Act Promoter in *Myxococcus Xanthus*." *Journal of Bacteriology* 189 (5): 1836–44.
- Grosberg, Richard K., and Richard R. Strathmann. 2007. "The Evolution of Multicellularity: A Minor Major Transition?," December. <https://doi.org/10.1146/annurev.ecolsys.36.102403.114735>.
- Gu, Huan, Shuyu Hou, Chanokpon Yongyat, Suzanne De Tore, and Dacheng Ren. 2013. "Patterned Biofilm Formation Reveals a Mechanism for Structural Heterogeneity in Bacterial Biofilms." *Langmuir*. <https://doi.org/10.1021/la402608z>.
- Guiseppi, Annick, Juan Jesus Vicente, Julien Herrou, Deborah Byrne, Aurelie Barneoud, Audrey Moine, Leon Espinosa, et al. 2019. "A Divergent CheW Confers Plasticity to Nucleoid-Associated Chemosensory Arrays." *PLoS Genetics* 15 (12): e1008533.
- Gupta, Priya, Subhasis Sarkar, Bannhi Das, Surajit Bhattacharjee, and Prosun Tribedi. 2016. "Biofilm, Pathogenesis and Prevention—a Journey to Break the Wall: A Review." *Archives of Microbiology*. <https://doi.org/10.1007/s00203-015-1148-6>.
- Guzzo, Mathilde, Seán M. Murray, Eugénie Martineau, Sébastien Lhospice, Grégory Baronian, Laetitia My, Yong Zhang, et al. 2018. "A Gated Relaxation Oscillator Mediated by FrzX Controls Morphogenetic Movements in *Myxococcus Xanthus*." *Nature Microbiology* 3 (8): 948–59.
- Hahn, M. W., E. R. Moore, and M. G. Höfle. 1999. "Bacterial Filament Formation, a Defense Mechanism against Flagellate Grazing, Is Growth Rate Controlled in Bacteria of Different Phyla." *Applied and Environmental Microbiology* 65 (1): 25–35.
- Hamilton, W. D. 1964. "The Genetical Evolution of Social Behaviour. I." *Journal of Theoretical Biology* 7 (1): 1–16.
- . 1970. "Selfish and Spiteful Behaviour in an Evolutionary Model." *Nature* 228 (5277): 1218–20.
- Hammer, Brian K., and Bonnie L. Bassler. 2004. "Quorum Sensing Controls Biofilm Formation in *Vibrio Cholerae*." *Molecular Microbiology*. <https://doi.org/10.1111/j.1365-2958.2004.03939.x>.
- Hammer, Neal D., and Eric P. Skaar. 2011. "Molecular Mechanisms Of *Staphylococcus Aureus* Iron Acquisition." *Annual Review of Microbiology*. <https://doi.org/10.1146/annurev-micro-090110-102851>.
- Harris, B. Z., D. Kaiser, and M. Singer. 1998. "The Guanosine Nucleotide (p)PpGpp Initiates Development and A-Factor Production in *Myxococcus Xanthus*." *Genes & Development*. <https://doi.org/10.1101/gad.12.7.1022>.
- Hartzell, P., and D. Kaiser. 1991. "Function of MglA, a 22-Kilodalton Protein Essential for Gliding in *Myxococcus Xanthus*." *Journal of Bacteriology* 173 (23): 7615–24.
- Harvey, Kate L., Veronica M. Jarocki, Ian G. Charles, and Steven P. Djordjevic. 2019. "The Diverse Functional Roles of Elongation Factor Tu (EF-Tu) in Microbial Pathogenesis." *Frontiers in Microbiology* 10 (October): 2351.
- Haselkorn, R. 1978. "Heterocysts." *Annual Review of Plant Physiology* 29 (1): 319–44.
- Heasman, Sarah J., and Anne J. Ridley. 2008. "Mammalian Rho GTPases: New Insights into Their Functions from in Vivo Studies." *Nature Reviews. Molecular Cell Biology* 9 (9): 690–701.
- Higgs, Penelope I., Patricia L. Hartzell, Carina Holkenbrink, and Egbert Hoiczyk. 2013. "Myxococcus Xanthus Vegetative and Developmental Cell Heterogeneity." In *Myxobacteria: Genomics, Cellular and Molecular Biology*, 51–77. Horizon Scientific press and Caister Academic Press.

- Hillesland, Kristina L., Richard E. Lenski, and Gregory J. Velicer. 2007. "Ecological Variables Affecting Predatory Success in *Myxococcus Xanthus*." *Microbial Ecology* 53 (4): 571–78.
- Hillesland, Kristina L., and Gregory J. Velicer. 2005. "Resource Level Affects Relative Performance of the Two Motility Systems of *Myxococcus Xanthus*." *Microbial Ecology* 49 (4): 558–66.
- Hillesland, Kristina L., Gregory J. Velicer, and Richard E. Lenski. 2009. "Experimental Evolution of a Microbial Predator's Ability to Find Prey." *Proceedings. Biological Sciences / The Royal Society* 276 (1656): 459–67.
- Hinohara, Kunihiko, and Kornelia Polyak. 2019. "Intratumoral Heterogeneity: More Than Just Mutations." *Trends in Cell Biology* 29 (7): 569–79.
- Hodgkin, J., and D. Kaiser. 1977. "Cell-to-Cell Stimulation of Movement in Nonmotile Mutants of *Myxococcus*." *Proceedings of the National Academy of Sciences of the United States of America* 74 (7): 2938–42.
- Hodgkin, Jonathan, and Dale Kaiser. 1979. "Genetics of Gliding Motility in *Myxococcus Xanthus* (Myxobacteriales): Two Gene Systems Control Movement." *Molecular and General Genetics MGG*. <https://doi.org/10.1007/bf00270004>.
- Horiuchi, Takayuki, Masato Taoka, Toshiaki Isobe, Teruya Komano, and Sumiko Inouye. 2002. "Role of FruA and CsgA Genes in Gene Expression during Development of *Myxococcus Xanthus*." *Journal of Biological Chemistry*. <https://doi.org/10.1074/jbc.m111214200>.
- Hu, Wei, Maksim L. Gibiansky, Jing Wang, Chuandong Wang, Renate Lux, Yuezhong Li, Gerard C. L. Wong, and Wenyan Shi. 2016. "Interplay between Type IV Pili Activity and Exopolysaccharides Secretion Controls Motility Patterns in Single Cells of *Myxococcus Xanthus*." *Scientific Reports* 6 (January): 17790.
- Iizuka, T., Y. Jojima, R. Fudou, and S. Yamanaka. 1998. "Isolation of Myxobacteria from the Marine Environment." *FEMS Microbiology Letters* 169 (2): 317–22.
- Iizuka, Takashi, Mitsunori Tokura, Yasuko Jojima, Akira Hiraishi, Shigeru Yamanaka, and Ryosuke Fudou. 2006. "Enrichment and Phylogenetic Analysis of Moderately Thermophilic Myxobacteria from Hot Springs in Japan." *Microbes and Environments / JSME* 21 (3): 189–99.
- Inhülsen, Silja, Claudio Aguilar, Nadine Schmid, Angela Suppiger, Kathrin Riedel, and Leo Eberl. 2012. "Identification of Functions Linking Quorum Sensing with Biofilm Formation in *Burkholderia Cenocepacia* H111." *MicrobiologyOpen*. <https://doi.org/10.1002/mbo3.24>.
- Islam, Mobarakol, V. S. Vibashan, V. Jeya Maria Jose, Navodini Wijethilake, Uppal Utkarsh, and Hongliang Ren. 2020. "Brain Tumor Segmentation and Survival Prediction Using 3D Attention UNet." *Brainlesion: Glioma, Multiple Sclerosis, Stroke and Traumatic Brain Injuries*. https://doi.org/10.1007/978-3-030-46640-4_25.
- Islam, Salim T., and Tâm Mignot. 2015. "The Mysterious Nature of Bacterial Surface (Gliding) Motility: A Focal Adhesion-Based Mechanism in *Myxococcus Xanthus*." *Seminars in Cell & Developmental Biology* 46 (October): 143–54.
- Izano, Era A., Matthew A. Amarante, William B. Kher, and Jeffrey B. Kaplan. 2008. "Differential Roles of Poly- N -Acetylglucosamine Surface Polysaccharide and Extracellular DNA in *Staphylococcus Aureus* and *Staphylococcus Epidermidis* Biofilms." *Applied and Environmental Microbiology*. <https://doi.org/10.1128/aem.02073-07>.
- Jakobczak, Beata, Daniela Keilberg, Kristin Wuichet, and Lotte Sjøgaard-Andersen. 2015. "Contact- and Protein Transfer-Dependent Stimulation of Assembly of the Gliding Motility Machinery in *Myxococcus Xanthus*." *PLoS Genetics* 11 (7): e1005341.
- Jelsbak, L., and L. Sjøgaard-Andersen. 2000. "Pattern Formation: Fruiting Body Morphogenesis in *Myxococcus Xanthus*." *Current Opinion in Microbiology* 3 (6): 637–42.
- Jelsbak, Lars, and Lotte Sjøgaard-Andersen. 2002. "Pattern Formation by a Cell Surface-Associated Morphogen in *Myxococcus Xanthus*." *Proceedings of the National Academy of Sciences of the United States of America* 99 (4): 2032–37.
- Jenal, Urs, Alberto Reinders, and Christian Lori. 2017. "Cyclic Di-GMP: Second Messenger Extraordinaire." *Nature Reviews. Microbiology* 15 (5): 271–84.

- Jiang, De-Ming, Chiaki Kato, Xiu-Wen Zhou, Zhi-Hong Wu, Takako Sato, and Yue-Zhong Li. 2010. "Phylogeographic Separation of Marine and Soil Myxobacteria at High Levels of Classification." *The ISME Journal* 4 (12): 1520–30.
- Jong, Imke G. de, Patsy Haccou, and Oscar P. Kuipers. 2011. "Bet Hedging or Not? A Guide to Proper Classification of Microbial Survival Strategies." *BioEssays: News and Reviews in Molecular, Cellular and Developmental Biology* 33 (3): 215–23.
- Joo, Hwang-Soo, and Michael Otto. 2012. "Molecular Basis of in Vivo Biofilm Formation by Bacterial Pathogens." *Chemistry & Biology* 19 (12): 1503–13.
- Jousset, Alexandre. 2012. "Ecological and Evolutive Implications of Bacterial Defences against Predators." *Environmental Microbiology* 14 (8): 1830–43.
- Jurcisek, Joseph A., and Lauren O. Bakaletz. 2007. "Biofilms Formed by Nontypeable Haemophilus Influenzae In Vivo Contain Both Double-Stranded DNA and Type IV Pilin Protein." *Journal of Bacteriology*. <https://doi.org/10.1128/jb.01935-06>.
- Kahnt, Jörg, Kryssia Aguiluz, Jürgen Koch, Anke Treuner-Lange, Anna Konovalova, Stuart Huntley, Michael Hoppert, Lotte Søggaard-Andersen, and Reiner Hedderich. 2010. "Profiling the Outer Membrane Proteome during Growth and Development of the Social Bacterium Myxococcus Xanthus by Selective Biotinylation and Analyses of Outer Membrane Vesicles." *Journal of Proteome Research*. <https://doi.org/10.1021/pr1004983>.
- Kaiser, D., M. Robinson, and L. Kroos. 2010. "Myxobacteria, Polarity, and Multicellular Morphogenesis." *Cold Spring Harbor Perspectives in Biology*. <https://doi.org/10.1101/cshperspect.a000380>.
- Kaiser, Dale. 2003. "Coupling Cell Movement to Multicellular Development in Myxobacteria." *Nature Reviews Microbiology*. <https://doi.org/10.1038/nrmicro733>.
- Kaiser, Dale, and Cathy Crosby. 1983. "Cell Movement and Its Coordination in Swarms of Myxococcus Xanthus." *Cell Motility* 3 (3): 227–45.
- Kang, Sung Gyun, and Kye Joon Lee. 1997. "Kinetic Analysis of Morphological Differentiation and Protease Production in Streptomyces Albidoflavus SMF301." *Microbiology* 143 (8): 2709–14.
- Kaplan, H. B., and L. Plamann. 1996. "A Myxococcus Xanthus Cell Density-Sensing System Required for Multicellular Development." *FEMS Microbiology Letters* 139 (2–3): 89–95.
- Kataoka, M., T. Seki, and T. Yoshida. 1991. "Regulation and Function of the Streptomyces Plasmid PSN22 Genes Involved in Pock Formation and Inviability." *Journal of Bacteriology* 173 (24): 7975–81.
- Katsu, T., T. Tsuchiya, and Y. Fujita. 1984. "Dissipation of Membrane Potential of Escherichia Coli Cells Induced by Macromolecular Polylysine." *Biochemical and Biophysical Research Communications* 122 (1): 401–6.
- Kaur, Amrita, Lakhwinder Kaur, and Ashima Singh. 2021. "GA-UNet: UNet-Based Framework for Segmentation of 2D and 3D Medical Images Applicable on Heterogeneous Datasets." *Neural Computing & Applications*, June. <https://doi.org/10.1007/s00521-021-06134-z>.
- Keane, Ryan, and James Berleman. 2016a. "The Predatory Life Cycle of Myxococcus Xanthus." *Microbiology* 162 (1): 1–11.
- . 2016b. "The Predatory Life Cycle of Myxococcus Xanthus." *Microbiology* 162 (1): 1–11.
- Keilberg, Daniela, Kristin Wuichet, Florian Drescher, and Lotte Søggaard-Andersen. 2012. "A Response Regulator Interfaces between the Frz Chemosensory System and the MglA/MglB GTPase/GAP Module to Regulate Polarity in Myxococcus Xanthus." *PLoS Genetics* 8 (9): e1002951.
- Keim, Carolina N., Juliana L. Martins, Fernanda Abreu, Alexandre Soares Rosado, Henrique Lins de Barros, Radovan Borojevic, Ulysses Lins, and Marcos Farina. 2004. "Multicellular Life Cycle of Magnetotactic Prokaryotes." *FEMS Microbiology Letters* 240 (2): 203–8.
- Keren, Iris, Niilo Kaldalu, Amy Spoering, Yipeng Wang, and Kim Lewis. 2004. "Persister Cells and Tolerance to Antimicrobials." *FEMS Microbiology Letters* 230 (1): 13–18.

- Kerr, Benjamin, Margaret A. Riley, Marcus W. Feldman, and Brendan J. M. Bohannan. 2002. "Local Dispersal Promotes Biodiversity in a Real-Life Game of Rock-Paper-Scissors." *Nature* 418 (6894): 171–74.
- Khatoon, Zohra, Christopher D. McTiernan, Erik J. Suuronen, Thien-Fah Mah, and Emilio I. Alarcon. 2018. "Bacterial Biofilm Formation on Implantable Devices and Approaches to Its Treatment and Prevention." *Heliyon* 4 (12): e01067.
- Kiedrowski, Megan R., and Alexander R. Horswill. 2011. "New Approaches for Treating Staphylococcal Biofilm Infections." *Annals of the New York Academy of Sciences* 1241 (December): 104–21.
- Kim, S. K., and D. Kaiser. 1990a. "C-Factor: A Cell-Cell Signaling Protein Required for Fruiting Body Morphogenesis of *M. Xanthus*." *Cell* 61 (1): 19–26.
- . 1990b. "Cell Alignment Required in Differentiation of *Myxococcus Xanthus*." *Science* 249 (4971): 926–28.
- Kim, Wook, Stuart B. Levy, and Kevin R. Foster. 2016. "Rapid Radiation in Bacteria Leads to a Division of Labour." *Nature Communications* 7 (February): 10508.
- Kobayashi Kazuo. 2007. "Bacillus Subtilis Pellicle Formation Proceeds through Genetically Defined Morphological Changes." *Journal of Bacteriology* 189 (13): 4920–31.
- Köhler, T., L. K. Curty, F. Barja, C. van Delden, and J. C. Pechère. 2000. "Swarming of *Pseudomonas Aeruginosa* Is Dependent on Cell-to-Cell Signaling and Requires Flagella and Pili." *Journal of Bacteriology* 182 (21): 5990–96.
- Konovalova, Anna, Stephanie Löbach, and Lotte Sjøgaard-Andersen. 2012. "A RelA-Dependent Two-Tiered Regulated Proteolysis Cascade Controls Synthesis of a Contact-Dependent Intercellular Signal in *Myxococcus Xanthus*." *Molecular Microbiology* 84 (2): 260–75.
- Konovalova, Anna, Tobias Petters, and Lotte Sjøgaard-Andersen. 2010. "Extracellular Biology Of *Myxococcus Xanthus*." *FEMS Microbiology Reviews*. <https://doi.org/10.1111/j.1574-6976.2009.00194.x>.
- Konovalova, Anna, Sigrun Wegener-Feldbrügge, and Lotte Sjøgaard-Andersen. 2012. "Two Intercellular Signals Required for Fruiting Body Formation in *Myxococcus Xanthus* Act Sequentially but Non-Hierarchically." *Molecular Microbiology* 86 (1): 65–81.
- Koutsoudis, Maria D., Dimitrios Tsaltas, Timothy D. Minogue, and Susanne B. von Bodman. 2006. "Quorum-Sensing Regulation Governs Bacterial Adhesion, Biofilm Development, and Host Colonization in *Pantoea Stewartii* Subspecies *Stewartii*." *Proceedings of the National Academy of Sciences of the United States of America* 103 (15): 5983–88.
- Kraemer, S. A., and G. J. Velicer. 2011. "Endemic Social Diversity within Natural Kin Groups of a Cooperative Bacterium." *Proceedings of the National Academy of Sciences of the United States of America* 108 Suppl 2 (Suppl 2). <https://doi.org/10.1073/pnas.1100307108>.
- Kramer, Jos, Özhan Özkaya, and Rolf Kümmerli. 2020. "Bacterial Siderophores in Community and Host Interactions." *Nature Reviews. Microbiology* 18 (3): 152–63.
- Krieg, Michael, Gotthold Fläschner, David Alsteens, Benjamin M. Gaub, Wouter H. Roos, Gijs J. L. Wuite, Hermann E. Gaub, Christoph Gerber, Yves F. Dufrêne, and Daniel J. Müller. 2019. "Atomic Force Microscopy-Based Mechanobiology." *Nature Reviews Physics* 1 (1): 41–57.
- Kroos, Lee. 2007. "The *Bacillus* and *Myxococcus* Developmental Networks and Their Transcriptional Regulators." *Annual Review of Genetics*. <https://doi.org/10.1146/annurev.genet.41.110306.130400>.
- Kroos, Lee, and Sumiko Inouye. 2014. "Transcriptional Regulatory Mechanisms during *Myxococcus Xanthus* Development." *Myxobacteria*. <https://doi.org/10.1128/9781555815677.ch9>.
- Kruse, T., S. Lobedanz, N. M. Berthelsen, and L. Sjøgaard-Andersen. 2001. "C-Signal: A Cell Surface-Associated Morphogen That Induces and Co-Ordinates Multicellular Fruiting Body Morphogenesis and Sporulation in *Myxococcus Xanthus*." *Molecular Microbiology* 40 (1): 156–68.
- Kumar, Krithika, Rodrigo A. Mella-Herrera, and James W. Golden. 2010. "Cyanobacterial Heterocysts." *Cold Spring Harbor Perspectives in Biology* 2 (4): a000315.

- Kurosaka, Satoshi, and Anna Kashina. 2008a. "Cell Biology of Embryonic Migration." *Birth Defects Research. Part C, Embryo Today: Reviews* 84 (2): 102–22.
- . 2008b. "Cell Biology of Embryonic Migration." *Birth Defects Research. Part C, Embryo Today: Reviews* 84 (2): 102–22.
- Kuspa, A., L. Kroos, and D. Kaiser. 1986. "Intercellular Signaling Is Required for Developmental Gene Expression in *Myxococcus Xanthus*." *Developmental Biology* 117 (1): 267–76.
- Kuspa, A., L. Plamann, and D. Kaiser. 1992a. "Identification of Heat-Stable A-Factor from *Myxococcus Xanthus*." *Journal of Bacteriology*. <https://doi.org/10.1128/jb.174.10.3319-3326.1992>.
- . 1992b. "A-Signalling and the Cell Density Requirement for *Myxococcus Xanthus* Development." *Journal of Bacteriology* 174 (22): 7360–69.
- Lasa, Iñigo, and José R. Penadés. 2006. "Bap: A Family of Surface Proteins Involved in Biofilm Formation." *Research in Microbiology*. <https://doi.org/10.1016/j.resmic.2005.11.003>.
- Le Novère, N. 2001. "MELTING, Computing the Melting Temperature of Nucleic Acid Duplex." *Bioinformatics* 17 (12): 1226–27.
- Lee, Bongsoo, Carina Holkenbrink, Anke Treuner-Lange, and Penelope I. Higgs. 2012. "Myxococcus Xanthus Developmental Cell Fate Production: Heterogeneous Accumulation of Developmental Regulatory Proteins and Reexamination of the Role of MazF in Developmental Lysis." *Journal of Bacteriology*. <https://doi.org/10.1128/jb.06756-11>.
- Lee, Jun-Seok, Bongjun Son, Poorna Viswanathan, Paul M. Luethy, and Lee Kroos. 2011. "Combinatorial Regulation of FmgD by MrpC2 and FruA during *Myxococcus Xanthus* Development." *Journal of Bacteriology* 193 (7): 1681–89.
- Lenz, Ailyn P., Kerry S. Williamson, Betsey Pitts, Philip S. Stewart, and Michael J. Franklin. 2008a. "Localized Gene Expression in *Pseudomonas Aeruginosa* Biofilms." *Applied and Environmental Microbiology* 74 (14): 4463–71.
- . 2008b. "Localized Gene Expression in *Pseudomonas Aeruginosa* Biofilms." *Applied and Environmental Microbiology* 74 (14): 4463–71.
- Leonardy, Simone, Gerald Freymark, Sabrina Hebener, Eva Ellehauge, and Lotte Sjøgaard-Andersen. 2007. "Coupling of Protein Localization and Cell Movements by a Dynamically Localized Response Regulator in *Myxococcus Xanthus*." *The EMBO Journal* 26 (21): 4433–44.
- Lewis, Kim. 2007. "Persister Cells, Dormancy and Infectious Disease." *Nature Reviews. Microbiology* 5 (1): 48–56.
- Li, Yinuo, Hong Sun, Xiaoyuan Ma, Ann Lu, Renate Lux, David Zusman, and Wenyuan Shi. 2003. "Extracellular Polysaccharides Mediate Pilus Retraction during Social Motility of *Myxococcus Xanthus*." *Proceedings of the National Academy of Sciences of the United States of America* 100 (9): 5443–48.
- Livingstone, Paul G., Andrew D. Millard, Martin T. Swain, and David E. Whitworth. 2018. "Transcriptional Changes When *Myxococcus Xanthus* Preys on *Escherichia Coli* Suggest Myxobacterial Predators Are Constitutively Toxic but Regulate Their Feeding." *Microbial Genomics* 4 (2). <https://doi.org/10.1099/mgen.0.000152>.
- Livingstone, Paul G., Russell M. Morphew, and David E. Whitworth. 2017. "Myxobacteria Are Able to Prey Broadly upon Clinically-Relevant Pathogens, Exhibiting a Prey Range Which Cannot Be Explained by Phylogeny." *Frontiers in Microbiology* 8 (August): 1593.
- López, Daniel, and Roberto Kolter. 2010a. "Extracellular Signals That Define Distinct and Coexisting Cell Fates In *Bacillus Subtilis*." *FEMS Microbiology Reviews*. <https://doi.org/10.1111/j.1574-6976.2009.00199.x>.
- . 2010b. "Extracellular Signals That Define Distinct and Coexisting Cell Fates In *Bacillus Subtilis*." *FEMS Microbiology Reviews*. <https://doi.org/10.1111/j.1574-6976.2009.00199.x>.
- López, Daniel, Hera Vlamakis, Richard Losick, and Roberto Kolter. 2009. "Cannibalism Enhances Biofilm Development in *Bacillus Subtilis*." *Molecular Microbiology* 74 (3): 609–18.

- Lu, Ann, Kyunyoung Cho, Wesley P. Black, Xue-Yan Duan, Renate Lux, Zhaomin Yang, Heidi B. Kaplan, David R. Zusman, and Wen Yuan Shi. 2005. "Exopolysaccharide Biosynthesis Genes Required for Social Motility in *Myxococcus Xanthus*." *Molecular Microbiology* 55 (1): 206–20.
- Lubeck, Eric, Ahmet F. Coskun, Timur Zhiyentayev, Mubhij Ahmad, and Long Cai. 2014a. "Single-Cell in Situ RNA Profiling by Sequential Hybridization." *Nature Methods*. <https://doi.org/10.1038/nmeth.2892>.
- . 2014b. "Single-Cell in Situ RNA Profiling by Sequential Hybridization." *Nature Methods*. <https://doi.org/10.1038/nmeth.2892>.
- Luciano, Jennifer, Rym Agrebi, Anne Valérie Le Gall, Morgane Wartel, Francesca Fiegna, Adrien Ducret, Céline Brochier-Armanet, and Tâm Mignot. 2011. "Emergence and Modular Evolution of a Novel Motility Machinery in Bacteria." *PLoS Genetics* 7 (9): e1002268.
- Lyons, Nicholas A., and Roberto Kolter. 2015a. "On the Evolution of Bacterial Multicellularity." *Current Opinion in Microbiology* 24 (April): 21–28.
- . 2015b. "On the Evolution of Bacterial Multicellularity." *Current Opinion in Microbiology* 24 (April): 21–28.
- Manhes, Pauline, and Gregory J. Velicer. 2011. "Experimental Evolution of Selfish Policing in Social Bacteria." *Proceedings of the National Academy of Sciences of the United States of America* 108 (20): 8357–62.
- Manoil, C., and D. Kaiser. 1980a. "Guanosine Pentaphosphate and Guanosine Tetraphosphate Accumulation and Induction of *Myxococcus Xanthus* Fruiting Body Development." *Journal of Bacteriology*. <https://doi.org/10.1128/jb.141.1.305-315.1980>.
- . 1980b. "Purine-Containing Compounds, Including Cyclic Adenosine 3',5'-Monophosphate, Induce Fruiting of *Myxococcus Xanthus* by Nutritional Imbalance." *Journal of Bacteriology*. <https://doi.org/10.1128/jb.141.1.374-377.1980>.
- Manteca, Angel, Dennis Claessen, Carmen Lopez-Iglesias, and Jesus Sanchez. 2007. "Aerial Hyphae in Surface Cultures of *Streptomyces Lividans* and *Streptomyces Coelicolor* Originate from Viable Segments Surviving an Early Programmed Cell Death Event." *FEMS Microbiology Letters* 274 (1): 118–25.
- Manteca, Ángel, Marisol Fernández, and Jesús Sánchez. 2005. "A Death Round Affecting a Young Compartmentalized Mycelium Precedes Aerial Mycelium Dismantling in Confluent Surface Cultures of *Streptomyces Antibioticus*." *Microbiology* 151 (Pt 11): 3689–97.
- Masters, Elysia A., Ryan P. Trombetta, Karen L. de Mesy Bentley, Brendan F. Boyce, Ann Lindley Gill, Steven R. Gill, Kohei Nishitani, et al. 2019. "Evolving Concepts in Bone Infection: Redefining 'Biofilm', 'Acute vs. Chronic Osteomyelitis', 'the Immune Proteome' and 'Local Antibiotic Therapy.'" *Bone Research*. <https://doi.org/10.1038/s41413-019-0061-z>.
- Mauriello, Emilia M. F., Tâm Mignot, Zhaomin Yang, and David R. Zusman. 2010. "Gliding Motility Revisited: How Do the Myxobacteria Move without Flagella?" *Microbiology and Molecular Biology Reviews*. <https://doi.org/10.1128/mubr.00043-09>.
- Mauriello, Emilia M. F., Fabrice Mouhamar, Beiyan Nan, Adrien Ducret, David Dai, David R. Zusman, and Tâm Mignot. 2010. "Bacterial Motility Complexes Require the Actin-like Protein, MreB and the Ras Homologue, MglA." *The EMBO Journal* 29 (2): 315–26.
- McBride, M. J., T. Köhler, and D. R. Zusman. 1992. "Methylation of FrzCD, a Methyl-Accepting Taxic Protein of *Myxococcus Xanthus*, Is Correlated with Factors Affecting Cell Behavior." *Journal of Bacteriology* 174 (13): 4246–57.
- McBride, M. J., R. A. Weinberg, and D. R. Zusman. 1989. "'Frizzly' Aggregation Genes of the Gliding Bacterium *Myxococcus Xanthus* Show Sequence Similarities to the Chemotaxis Genes of Enteric Bacteria." *Proceedings of the National Academy of Sciences of the United States of America* 86 (2): 424–28.
- McBride, M. J., and D. R. Zusman. 1996a. "Behavioral Analysis of Single Cells of *Myxococcus Xanthus* in Response to Prey Cells of *Escherichia Coli*." *FEMS Microbiology Letters* 137 (2–3): 227–31.

- . 1996b. “Behavioral Analysis of Single Cells of *Myxococcus Xanthus* in Response to Prey Cells of *Escherichia Coli*.” *FEMS Microbiology Letters* 137 (2–3): 227–31.
- McConaughy, B. L., C. D. Laird, and B. J. McCarthy. 1969. “Nucleic Acid Reassociation in Formamide.” *Biochemistry* 8 (8): 3289–95.
- McCormick, Joseph R., and Klas Flärdh. 2012. “Signals and Regulators That Govern *Streptomyces* Development.” *FEMS Microbiology Reviews* 36 (1): 206–31.
- Meeks, John C., and Jeff Elhai. 2002. “Regulation of Cellular Differentiation in Filamentous Cyanobacteria in Free-Living and Plant-Associated Symbiotic Growth States.” *Microbiology and Molecular Biology Reviews: MMBR* 66 (1): 94–121; table of contents.
- Mendes-Soares, Helena, and Gregory J. Velicer. 2013. “Decomposing Predation: Testing for Parameters That Correlate with Predatory Performance by a Social Bacterium.” *Microbial Ecology* 65 (2): 415–23.
- Mercier, Romain, Sarah Bautista, Maëlle Delannoy, Margaux Gibert, Annick Guiseppi, Julien Herrou, Emilia M. F. Mauriello, and Tâm Mignot. 2020. “The Polar Ras-like GTPase MglA Activates Type IV Pilus via SgmX to Enable Twitching Motility In *Myxococcus Xanthus*.” *Proceedings of the National Academy of Sciences*. <https://doi.org/10.1073/pnas.2002783117>.
- Mercier, Romain, and Tâm Mignot. 2016a. “Regulations Governing the Multicellular Lifestyle of *Myxococcus Xanthus*.” *Current Opinion in Microbiology* 34 (December): 104–10.
- . 2016b. “Regulations Governing the Multicellular Lifestyle of *Myxococcus Xanthus*.” *Current Opinion in Microbiology* 34 (December): 104–10.
- . 2016c. “Regulations Governing the Multicellular Lifestyle of *Myxococcus Xanthus*.” *Current Opinion in Microbiology* 34 (December): 104–10.
- Merino-Puerto, Victoria, Heinz Schwarz, Iris Maldener, Vicente Mariscal, Conrad W. Mullineaux, Antonia Herrero, and Enrique Flores. 2011. “FraC/FraD-Dependent Intercellular Molecular Exchange in the Filaments of a Heterocyst-Forming Cyanobacterium, *Anabaena* Sp.” *Molecular Microbiology*. <https://doi.org/10.1111/j.1365-2958.2011.07797.x>.
- Meyer, Gerhard, and Nabil M. Amer. 1988. “Novel Optical Approach to Atomic Force Microscopy.” *Applied Physics Letters* 53 (12): 1045–47.
- Mignot, Tâm, Joshua W. Shaevitz, Patricia L. Hartzell, and David R. Zusman. 2007a. “Evidence That Focal Adhesion Complexes Power Bacterial Gliding Motility.” *Science* 315 (5813): 853–56.
- . 2007b. “Evidence That Focal Adhesion Complexes Power Bacterial Gliding Motility.” *Science* 315 (5813): 853–56.
- Miguélez, Elisa M., Carlos Hardisson, and Manuel B. Manzanal. 1999. “Hyphal Death during Colony Development in *Streptomyces Antibioticus*: Morphological Evidence for the Existence of a Process of Cell Deletion in a Multicellular Prokaryote.” *Journal of Cell Biology*. <https://doi.org/10.1083/jcb.145.3.515>.
- Mittal, Sheenu, and Lee Kroos. 2009a. “A Combination of Unusual Transcription Factors Binds Cooperatively to Control *Myxococcus Xanthus* Developmental Gene Expression.” *Proceedings of the National Academy of Sciences of the United States of America* 106 (6): 1965–70.
- . 2009b. “Combinatorial Regulation by a Novel Arrangement of FruA and MrpC2 Transcription Factors during *Myxococcus Xanthus* Development.” *Journal of Bacteriology* 191 (8): 2753–63.
- Moffitt, Jeffrey R., Dhananjay Bambah-Mukku, Stephen W. Eichhorn, Eric Vaughn, Karthik Shekhar, Julio D. Perez, Nimrod D. Rubinstein, et al. 2018. “Molecular, Spatial, and Functional Single-Cell Profiling of the Hypothalamic Preoptic Region.” *Science* 362 (6416). <https://doi.org/10.1126/science.aau5324>.
- Mohr, Kathrin I. 2018. “Diversity of Myxobacteria—We Only See the Tip of the Iceberg.” *Microorganisms* 6 (3): 84.
- Mohr, Kathrin I., Marc Stechling, Joachim Wink, Elke Wilharm, and Marc Stadler. 2016. “Comparison of Myxobacterial Diversity and Evaluation of Isolation Success in Two Niches: Kiritimati Island and German Compost.” *MicrobiologyOpen* 5 (2): 268–78.

- Mohr, Kathrin I., Tanja Zindler, Joachim Wink, Elke Wilharm, and Marc Stadler. 2017. "Myxobacteria in High Moor and Fen: An Astonishing Diversity in a Neglected Extreme Habitat." *MicrobiologyOpen*. <https://doi.org/10.1002/mbo3.464>.
- Monds, Russell D., and George A. O'Toole. 2009. "The Developmental Model of Microbial Biofilms: Ten Years of a Paradigm up for Review." *Trends in Microbiology* 17 (2): 73–87.
- Morgan, Andrew D., R. Craig MacLean, Kristina L. Hillesland, and Gregory J. Velicer. 2010. "Comparative Analysis of Myxococcus Predation on Soil Bacteria." *Applied and Environmental Microbiology* 76 (20): 6920–27.
- Morikawa, Masaaki, Shinji Kagihiro, Mitsuru Haruki, Kazufumi Takano, Steve Branda, Roberto Kolter, and Shigenori Kanaya. 2006. "Biofilm Formation by a *Bacillus Subtilis* Strain That Produces γ -Polyglutamate." *Microbiology*. <https://doi.org/10.1099/mic.0.29060-0>.
- Mukherjee, Sampri, and Bonnie L. Bassler. 2019. "Bacterial Quorum Sensing in Complex and Dynamically Changing Environments." *Nature Reviews Microbiology*. <https://doi.org/10.1038/s41579-019-0186-5>.
- Muñoz-Dorado, José, Francisco J. Marcos-Torres, Elena García-Bravo, Aurelio Moraleda-Muñoz, and Juana Pérez. 2016a. "Myxobacteria: Moving, Killing, Feeding, and Surviving Together." *Frontiers in Microbiology* 7 (May): 781.
- . 2016b. "Myxobacteria: Moving, Killing, Feeding, and Surviving Together." *Frontiers in Microbiology* 7 (May): 781.
- . 2016c. "Myxobacteria: Moving, Killing, Feeding, and Surviving Together." *Frontiers in Microbiology* 7 (May): 781.
- Muñoz-Dorado, José, Aurelio Moraleda-Muñoz, Francisco Javier Marcos-Torres, Francisco Javier Contreras-Moreno, Ana Belen Martin-Cuadrado, Jared M. Schrader, Penelope I. Higgs, and Juana Pérez. 2019. "Transcriptome Dynamics of the *Myxococcus Xanthus* Multicellular Developmental Program." *ELife* 8 (October). <https://doi.org/10.7554/eLife.50374>.
- Nadell, Carey D., Joao B. Xavier, and Kevin R. Foster. 2009. "The Sociobiology of Biofilms." *FEMS Microbiology Reviews* 33 (1): 206–24.
- Nadell, Carey D., Joao B. Xavier, Simon A. Levin, and Kevin R. Foster. 2008. "The Evolution of Quorum Sensing in Bacterial Biofilms." *PLoS Biology* 6 (1): e14.
- Nan, Beiyan, Jing Chen, John C. Neu, Richard M. Berry, George Oster, and David R. Zusman. 2011. "Myxobacteria Gliding Motility Requires Cytoskeleton Rotation Powered by Proton Motive Force." *Proceedings of the National Academy of Sciences of the United States of America* 108 (6): 2498–2503.
- Nariya, Hirofumi, and Masayori Inouye. 2008. "MazF, an mRNA Interferase, Mediates Programmed Cell Death during Multicellular *Myxococcus* Development." *Cell*. <https://doi.org/10.1016/j.cell.2007.11.044>.
- Nariya, Hirofumi, and Sumiko Inouye. 2006. "A Protein Ser/Thr Kinase Cascade Negatively Regulates the DNA-Binding Activity of MrpC, a Smaller Form of Which May Be Necessary for the *Myxococcus Xanthus* Development." *Molecular Microbiology* 60 (5): 1205–17.
- Nelson, D. E., and K. D. Young. 2000. "Penicillin Binding Protein 5 Affects Cell Diameter, Contour, and Morphology of *Escherichia Coli*." *Journal of Bacteriology* 182 (6): 1714–21.
- Neu, Thomas R., and John R. Lawrence. 2010. "Extracellular Polymeric Substances in Microbial Biofilms." *Microbial Glycobiology*. <https://doi.org/10.1016/b978-0-12-374546-0.00037-7>.
- Ng, Wai-Leung, and Bonnie L. Bassler. 2009. "Bacterial Quorum-Sensing Network Architectures." *Annual Review of Genetics* 43: 197–222.
- Nguyen, Alexander, Mitsukuni Yoshida, Hani Goodarzi, and Sohail F. Tavazoie. 2016. "Highly Variable Cancer Subpopulations That Exhibit Enhanced Transcriptome Variability and Metastatic Fitness." *Nature Communications*. <https://doi.org/10.1038/ncomms11246>.
- Nudleman, Eric, Daniel Wall, and Dale Kaiser. 2005. "Cell-to-Cell Transfer of Bacterial Outer Membrane Lipoproteins." *Science* 309 (5731): 125–27.

- O'Connor, K. A., and D. R. Zusman. 1991. "Development in Myxococcus Xanthus Involves Differentiation into Two Cell Types, Peripheral Rods and Spores." *Journal of Bacteriology* 173 (11): 3318–33.
- Oppenheimer-Shaanan, Yaara, Nitai Steinberg, and Ilana Kolodkin-Gal. 2013. "Small Molecules Are Natural Triggers for the Disassembly of Biofilms." *Trends in Microbiology* 21 (11): 594–601.
- Ostrowski, Adam, Angela Mehert, Alan Prescott, Taryn B. Kiley, and Nicola R. Stanley-Wall. 2011. "YuaB Functions Synergistically with the Exopolysaccharide and TasA Amyloid Fibers To Allow Biofilm Formation by Bacillus Subtilis." *Journal of Bacteriology*. <https://doi.org/10.1128/jb.00223-11>.
- Paharik, Alexandra E., and Alexander R. Horswill. 2016. "The Staphylococcal Biofilm: Adhesins, Regulation, and Host Response." *Microbiology Spectrum*. <https://doi.org/10.1128/microbiolspec.vmbf-0022-2015>.
- Parsek, Matthew R., and E. P. Greenberg. 2005. "Sociomicrobiology: The Connections between Quorum Sensing and Biofilms." *Trends in Microbiology* 13 (1): 27–33.
- Pathak, Darshankumar T., Xueming Wei, Alex Bucuvalas, Daniel H. Haft, Dietlind L. Gerloff, and Daniel Wall. 2012a. "Cell Contact-Dependent Outer Membrane Exchange in Myxobacteria: Genetic Determinants and Mechanism." *PLoS Genetics* 8 (4): e1002626.
- . 2012b. "Cell Contact-Dependent Outer Membrane Exchange in Myxobacteria: Genetic Determinants and Mechanism." *PLoS Genetics* 8 (4): e1002626.
- Pathak, Darshankumar T., Xueming Wei, Arup Dey, and Daniel Wall. 2013. "Molecular Recognition by a Polymorphic Cell Surface Receptor Governs Cooperative Behaviors in Bacteria." *PLoS Genetics* 9 (11): e1003891.
- Pathak, Darshankumar T., Xueming Wei, and Daniel Wall. 2012. "Myxobacterial Tools for Social Interactions." *Research in Microbiology* 163 (9–10): 579–91.
- Patra, Pintu, Kimberley Kissoon, Isabel Cornejo, Heidi B. Kaplan, and Oleg A. Igoshin. 2016. "Colony Expansion of Socially Motile Myxococcus Xanthus Cells Is Driven by Growth, Motility, and Exopolysaccharide Production." *PLoS Computational Biology* 12 (6): e1005010.
- Pelling, A. E., Y. Li, W. Shi, and J. K. Gimzewski. 2005. "Nanoscale Visualization and Characterization of Myxococcus Xanthus Cells with Atomic Force Microscopy." *Proceedings of the National Academy of Sciences*. <https://doi.org/10.1073/pnas.0501207102>.
- Pérez, Juana, José I. Jiménez-Zurdo, Francisco Martínez-Abarca, Vicenta Millán, Lawrence J. Shimkets, and José Muñoz-Dorado. 2014. "Rhizobial Galactoglucan Determines the Predatory Pattern of Myxococcus Xanthus and Protects Sinorhizobium Meliloti from Predation." *Environmental Microbiology* 16 (7): 2341–50.
- Pérez, Juana, Aurelio Moraleda-Muñoz, Francisco Javier Marcos-Torres, and José Muñoz-Dorado. 2016. "Bacterial Predation: 75 Years and Counting!" *Environmental Microbiology*. <https://doi.org/10.1111/1462-2920.13171>.
- Pérez, Juana, José Muñoz-Dorado, Alfredo F. Braña, Lawrence J. Shimkets, Laura Sevillano, and Ramón I. Santamaría. 2011. "Myxococcus Xanthus Induces Actinorhodin Overproduction and Aerial Mycelium Formation by Streptomyces Coelicolor." *Microbial Biotechnology* 4 (2): 175–83.
- Pérez-Núñez, Daniel, Romain Briandet, Blandine David, Céline Gautier, Pierre Renault, Bernard Hallet, Pascal Hols, Rut Carballido-López, and Eric Guédon. 2011. "A New Morphogenesis Pathway in Bacteria: Unbalanced Activity of Cell Wall Synthesis Machineries Leads to Coccus-to-Rod Transition and Filamentation in Ovococci." *Molecular Microbiology*. <https://doi.org/10.1111/j.1365-2958.2010.07483.x>.
- Pham, Vinh D., Conrad W. Shebelut, Michelle E. Diodati, Carolee T. Bull, and Mitchell Singer. 2005. "Mutations Affecting Predation Ability of the Soil Bacterium Myxococcus Xanthus." *Microbiology* 151 (Pt 6): 1865–74.
- Plamann, L., A. Kuspa, and D. Kaiser. 1992. "Proteins That Rescue A-Signal-Defective Mutants of Myxococcus Xanthus." *Journal of Bacteriology*. <https://doi.org/10.1128/jb.174.10.3311-3318.1992>.

- Potluri, Lakshmi-Prasad, Miguel A. de Pedro, and Kevin D. Young. 2012. "Escherichia Coli Low-Molecular-Weight Penicillin-Binding Proteins Help Orient Septal FtsZ, and Their Absence Leads to Asymmetric Cell Division and Branching." *Molecular Microbiology* 84 (2): 203–24.
- Powell, James T., Aspasia D. Chatziefthimiou, Sandra Anne Banack, Paul Alan Cox, and James S. Metcalf. 2015. "Desert Crust Microorganisms, Their Environment, and Human Health." *Journal of Arid Environments* 112 (January): 127–33.
- Raafat, Dina, and Hans-Georg Sahl. 2009. "Chitosan and Its Antimicrobial Potential--a Critical Literature Survey." *Microbial Biotechnology* 2 (2): 186–201.
- Radmacher, M., R. W. Tillmann, M. Fritz, and H. E. Gaub. 1992. "From Molecules to Cells: Imaging Soft Samples with the Atomic Force Microscope." *Science* 257 (5078): 1900–1905.
- Rainey, P. B., and M. Travisano. 1998. "Adaptive Radiation in a Heterogeneous Environment." *Nature* 394 (6688): 69–72.
- Raj, Arjun, and Alexander van Oudenaarden. 2008. "Nature, Nurture, or Chance: Stochastic Gene Expression and Its Consequences." *Cell* 135 (2): 216–26.
- Rani, Suriani Abdul, Betsey Pitts, Haluk Beyenal, Raja Angathevar Veluchamy, Zbigniew Lewandowski, William M. Davison, Kelli Buckingham-Meyer, and Philip S. Stewart. 2007a. "Spatial Patterns of DNA Replication, Protein Synthesis, and Oxygen Concentration within Bacterial Biofilms Reveal Diverse Physiological States." *Journal of Bacteriology*. <https://doi.org/10.1128/jb.00107-07>.
- . 2007b. "Spatial Patterns of DNA Replication, Protein Synthesis, and Oxygen Concentration within Bacterial Biofilms Reveal Diverse Physiological States." *Journal of Bacteriology*. <https://doi.org/10.1128/jb.00107-07>.
- Rankin, Daniel J., Katja Bargum, and Hanna Kokko. 2007. "The Tragedy of the Commons in Evolutionary Biology." *Trends in Ecology & Evolution* 22 (12): 643–51.
- REICHENBACH, and H. 1993. "Biology of the Myxobacteria Ecology and Taxonomy." *Myxobacteria II*. <https://ci.nii.ac.jp/naid/10018533594/>.
- Reichenbach, H. 1999. "The Ecology of the Myxobacteria." *Environmental Microbiology* 1 (1): 15–21.
- Rippka, R., J. Deruelles, and J. B. Waterbury. 1979. "Generic Assignments, Strain Histories and Properties of Pure Cultures of Cyanobacteria." <https://www.microbiologyresearch.org/content/journal/micro/10.1099/00221287-111-1-1?TRACK=RSS>.
- Robinson, Mark, Bongjun Son, David Kroos, and Lee Kroos. 2014. "Transcription Factor MrpC Binds to Promoter Regions of Hundreds of Developmentally-Regulated Genes in Myxococcus Xanthus." *BMC Genomics* 15 (December): 1123.
- Rodrigues, Lígia R. 2011. "Inhibition of Bacterial Adhesion on Medical Devices." *Advances in Experimental Medicine and Biology* 715: 351–67.
- Rombouts, Sara, and Marcelo Nollmann. 2021. "RNA Imaging in Bacteria." *FEMS Microbiology Reviews* 45 (2). <https://doi.org/10.1093/femsre/fuaa051>.
- Romero, Diego, Claudio Aguilar, Richard Losick, and Roberto Kolter. 2010. "Amyloid Fibers Provide Structural Integrity to Bacillus Subtilis Biofilms." *Proceedings of the National Academy of Sciences*. <https://doi.org/10.1073/pnas.0910560107>.
- Romero, Diego, Hera Vlamakis, Richard Losick, and Roberto Kolter. 2011. "An Accessory Protein Required for Anchoring and Assembly of Amyloid Fibres in B. Subtilis Biofilms." *Molecular Microbiology*. <https://doi.org/10.1111/j.1365-2958.2011.07653.x>.
- Ronneberger, Olaf, Philipp Fischer, and Thomas Brox. 2015. "U-Net: Convolutional Networks for Biomedical Image Segmentation." In *Medical Image Computing and Computer-Assisted Intervention – MICCAI 2015*, 234–41. Springer International Publishing.
- Rosenberg, E., K. H. Keller, and M. Dworkin. 1977. "Cell Density-Dependent Growth of Myxococcus Xanthus on Casein." *Journal of Bacteriology* 129 (2): 770–77.

- Rosenberg, Eugene, and Mazal Varon. 1984. "Antibiotics and Lytic Enzymes." In *Myxobacteria: Development and Cell Interactions*, edited by Engene Rosenberg, 109–25. New York, NY: Springer New York.
- Rossetti, Valentina, Bettina E. Schirrmester, Marco V. Bernasconi, and Homayoun C. Bagheri. 2010. "The Evolutionary Path to Terminal Differentiation and Division of Labor in Cyanobacteria." *Journal of Theoretical Biology* 262 (1): 23–34.
- Rutherford, Steven T., and Bonnie L. Bassler. 2012. "Bacterial Quorum Sensing: Its Role in Virulence and Possibilities for Its Control." *Cold Spring Harbor Perspectives in Medicine* 2 (11). <https://doi.org/10.1101/cshperspect.a012427>.
- Saaty, Thomas L. 1986. "Absolute and Relative Measurement with the AHP. The Most Livable Cities in the United States." *Socio-Economic Planning Sciences* 20 (6): 327–31.
- Sachs, Joel L., Ulrich G. Mueller, Thomas P. Wilcox, and James J. Bull. 2004. "The Evolution of Cooperation." *The Quarterly Review of Biology* 79 (2): 135–60.
- Sah, Govind Prasad, and Daniel Wall. 2020. "Kin Recognition and Outer Membrane Exchange (OME) in Myxobacteria." *Current Opinion in Microbiology* 56 (August): 81–88.
- Sakuragi, Yumiko, and Roberto Kolter. 2007. "Quorum-Sensing Regulation of the Biofilm Matrix Genes (Pel) of *Pseudomonas Aeruginosa*." *Journal of Bacteriology* 189 (14): 5383–86.
- SantaLucia, J., Jr. 1998. "A Unified View of Polymer, Dumbbell, and Oligonucleotide DNA Nearest-Neighbor Thermodynamics." *Proceedings of the National Academy of Sciences of the United States of America* 95 (4): 1460–65.
- Schirrmester, Bettina E., Alexandre Antonelli, and Homayoun C. Bagheri. 2011. "The Origin of Multicellularity in Cyanobacteria." *BMC Evolutionary Biology* 11 (February): 45.
- Schluter, Jonas, Armin P. Schoech, Kevin R. Foster, and Sara Mitri. 2016. "The Evolution of Quorum Sensing as a Mechanism to Infer Kinship." *PLOS Computational Biology*. <https://doi.org/10.1371/journal.pcbi.1004848>.
- Seef, Sofiene, Julien Herrou, Paul de Boissier, Laetitia My, Gael Brasseur, Donovan Robert, Rikesh Jain, et al. 2021a. "A Tad-like Apparatus Is Required for Contact-Dependent Prey Killing in Predatory Social Bacteria." *BioRxiv*. <https://doi.org/10.1101/2021.02.25.432843>.
- . 2021b. "A Tad-like Apparatus Is Required for Contact-Dependent Prey Killing in Predatory Social Bacteria." *ELife* 10 (September). <https://doi.org/10.7554/eLife.72409>.
- . 2021c. "A Tad-like Apparatus Is Required for Contact-Dependent Prey Killing in Predatory Social Bacteria." *ELife* 10 (September). <https://doi.org/10.7554/eLife.72409>.
- Shah, Devang, Zhigang Zhang, Arkady Khodursky, Niilo Kaldalu, Kristi Kurg, and Kim Lewis. 2006. "Persisters: A Distinct Physiological State of *E. Coli*." *BMC Microbiology* 6 (June): 53.
- Shapiro, J. A. 1998. "Thinking about Bacterial Populations as Multicellular Organisms." *Annual Review of Microbiology* 52: 81–104.
- Shapiro, James A. 1988. "Bacteria as Multicellular Organisms." *Scientific American*. <https://doi.org/10.1038/scientificamerican0688-82>.
- Shi, W., and D. R. Zusman. 1993. "The Two Motility Systems of *Myxococcus Xanthus* Show Different Selective Advantages on Various Surfaces." *Proceedings of the National Academy of Sciences of the United States of America* 90 (8): 3378–82.
- Shilo, M. 1970a. "Lysis of Blue-Green Algae by *Myxobacter*." *Journal of Bacteriology* 104 (1): 453–61.
- . 1970b. "Lysis of Blue-Green Algae by *Myxobacter*." *Journal of Bacteriology* 104 (1): 453–61.
- Shimkets, L. J. 1999. "Intercellular Signaling during Fruiting-Body Development of *Myxococcus Xanthus*." *Annual Review of Microbiology* 53: 525–49.
- Shimkets, L. J., M. Dworkin, and H. Reichenbach. 2006. "The Myxobacteria, p 31--115." *The Prokaryotes*. Springer, New York, NY.
- Shimkets, L. J., and D. Kaiser. 1982. "Induction of Coordinated Movement of *Myxococcus Xanthus* Cells." *Journal of Bacteriology* 152 (1): 451–61.

- Shimkets, L., and C. R. Woese. 1992. "A Phylogenetic Analysis of the Myxobacteria: Basis for Their Classification." *Proceedings of the National Academy of Sciences of the United States of America* 89 (20): 9459–63.
- Skerker, J. M., and H. C. Berg. 2001. "Direct Observation of Extension and Retraction of Type IV Pili." *Proceedings of the National Academy of Sciences of the United States of America* 98 (12): 6901–4.
- Skinner, Samuel O., Leonardo A. Sepúlveda, Heng Xu, and Ido Golding. 2013a. "Measuring mRNA Copy Number in Individual Escherichia Coli Cells Using Single-Molecule Fluorescent in Situ Hybridization." *Nature Protocols*. <https://doi.org/10.1038/nprot.2013.066>.
- . 2013b. "Measuring mRNA Copy Number in Individual Escherichia Coli Cells Using Single-Molecule Fluorescent in Situ Hybridization." *Nature Protocols* 8 (6): 1100–1113.
- Smits, Wiep Klaas, Oscar P. Kuipers, and Jan-Willem Veening. 2006. "Phenotypic Variation in Bacteria: The Role of Feedback Regulation." *Nature Reviews. Microbiology* 4 (4): 259–71.
- Son, Bongjun, Yu Liu, and Lee Kroos. 2011. "Combinatorial Regulation by MrpC2 and FruA Involves Three Sites in the FmgE Promoter Region during Myxococcus Xanthus Development." *Journal of Bacteriology* 193 (11): 2756–66.
- Speziale, Pietro, Giampiero Pietrocola, Timothy J. Foster, and Joan A. Geoghegan. 2014. "Protein-Based Biofilm Matrices in Staphylococci." *Frontiers in Cellular and Infection Microbiology*. <https://doi.org/10.3389/fcimb.2014.00171>.
- Spröer, C., H. Reichenbach, and E. Stackebrandt. 1999. "The Correlation between Morphological and Phylogenetic Classification of Myxobacteria." *International Journal of Systematic Bacteriology* 49 Pt 3 (July): 1255–62.
- Stanley, Nicola R., and Beth A. Lazazzera. 2005. "Defining the Genetic Differences between Wild and Domestic Strains of Bacillus Subtilis That Affect Poly-Gamma-DL-Glutamic Acid Production and Biofilm Formation." *Molecular Microbiology* 57 (4): 1143–58.
- Steinberger, R. E., and P. A. Holden. 2005. "Extracellular DNA in Single- and Multiple-Species Unsaturated Biofilms." *Applied and Environmental Microbiology*. <https://doi.org/10.1128/aem.71.9.5404-5410.2005>.
- Stewart, Philip S., and Michael J. Franklin. 2008. "Physiological Heterogeneity in Biofilms." *Nature Reviews. Microbiology* 6 (3): 199–210.
- Stoica, P., M. C. Chifiriuc, M. Rapa, and V. Lazăr. 2017. "1 - Overview of Biofilm-Related Problems in Medical Devices." In *Biofilms and Implantable Medical Devices*, edited by Ying Deng and Wei Lv, 3–23. Woodhead Publishing.
- Strahl, Henrik, and Leendert W. Hamoen. 2010. "Membrane Potential Is Important for Bacterial Cell Division." *Proceedings of the National Academy of Sciences of the United States of America* 107 (27): 12281–86.
- Stuelten, Christina H., Carole A. Parent, and Denise J. Montell. 2018. "Cell Motility in Cancer Invasion and Metastasis: Insights from Simple Model Organisms." *Nature Reviews. Cancer* 18 (5): 296–312.
- Sugimoto, N., S. Nakano, M. Katoh, A. Matsumura, H. Nakamuta, T. Ohmichi, M. Yoneyama, and M. Sasaki. 1995. "Thermodynamic Parameters to Predict Stability of RNA/DNA Hybrid Duplexes." *Biochemistry* 34 (35): 11211–16.
- Sumpter, D. J. T. 2006. "The Principles of Collective Animal Behaviour." *Philosophical Transactions of the Royal Society B: Biological Sciences*. <https://doi.org/10.1098/rstb.2005.1733>.
- Sumpter, David J. T. 2010. "Collective Animal Behavior." <https://doi.org/10.1515/9781400837106>.
- Sun, H., and W. Shi. 2001a. "Genetic Studies of Mrp, a Locus Essential for Cellular Aggregation and Sporulation of Myxococcus Xanthus." *Journal of Bacteriology* 183 (16): 4786–95.
- . 2001b. "Analyses of Mrp Genes during Myxococcus Xanthus Development." *Journal of Bacteriology* 183 (23): 6733–39.
- Sun, H., D. R. Zusman, and W. Shi. 2000. "Type IV Pilus of Myxococcus Xanthus Is a Motility Apparatus Controlled by the Frz Chemosensory System." *Current Biology: CB* 10 (18): 1143–46.

- Sun, Mingzhai, Morgane Wartel, Eric Cascales, Joshua W. Shaevitz, and Tâm Mignot. 2011. "Motor-Driven Intracellular Transport Powers Bacterial Gliding Motility." *Proceedings of the National Academy of Sciences of the United States of America* 108 (18): 7559–64.
- Tamulonis, Carlos, Marten Postma, and Jaap Kaandorp. 2011. "Modeling Filamentous Cyanobacteria Reveals the Advantages of Long and Fast Trichomes for Optimizing Light Exposure." *PloS One* 6 (7): e22084.
- Taylor, Rion G., and Roy D. Welch. 2008. "Chemotaxis as an Emergent Property of a Swarm." *Journal of Bacteriology* 190 (20): 6811–16.
- Thiery, Susanne, and Christine Kaimer. 2020a. "The Predation Strategy of Myxococcus Xanthus." *Frontiers in Microbiology* 11 (January): 2.
- . 2020b. "The Predation Strategy of Myxococcus Xanthus." *Frontiers in Microbiology* 11 (January): 2.
- Thomasson, Bobbie, Jason Link, Angela G. Stassinopoulos, Neal Burke, Lynda Plamann, and Patricia L. Hartzell. 2002. "MglA, a Small GTPase, Interacts with a Tyrosine Kinase to Control Type IV Pili-Mediated Motility and Development of Myxococcus Xanthus." *Molecular Microbiology*. <https://doi.org/10.1046/j.1365-2958.2002.03258.x>.
- Torres, Pablo S., Florencia Malamud, Luciano A. Rigano, Daniela M. Russo, María Rosa Marano, Atilio P. Castagnaro, Angeles Zorreguieta, Kamal Bouarab, John Maxwell Dow, and Adrián A. Vojnov. 2007. "Controlled Synthesis of the DSF Cell-Cell Signal Is Required for Biofilm Formation and Virulence in Xanthomonas Campestris." *Environmental Microbiology*. <https://doi.org/10.1111/j.1462-2920.2007.01332.x>.
- Tréguier, Julie, Loïc Bugnicourt, Guillaume Gay, Mamoudou Diallo, Salim Timo Islam, Alexandre Toro, Laurent David, Olivier Théodoly, Guillaume Sudre, and Tâm Mignot. 2019. "Chitosan Films for Microfluidic Studies of Single Bacteria and Perspectives for Antibiotic Susceptibility Testing." *MBio* 10 (4). <https://doi.org/10.1128/mBio.01375-19>.
- Treuner-Lange, Anke, Eric Macia, Mathilde Guzzo, Edina Hot, Laura M. Faure, Beata Jakobczak, Leon Espinosa, et al. 2015. "The Small G-Protein MglA Connects to the MreB Actin Cytoskeleton at Bacterial Focal Adhesions." *The Journal of Cell Biology* 210 (2): 243–56.
- Ueki, Toshiyuki, and Sumiko Inouye. 2003. "Identification of an Activator Protein Required for the Induction of FruA, a Gene Essential for Fruiting Body Development in Myxococcus Xanthus." *Proceedings of the National Academy of Sciences of the United States of America* 100 (15): 8782–87.
- Van Gestel, Jordi, Hera Vlamakis, and Roberto Kolter. 2015. "Division of Labor in Biofilms: The Ecology of Cell Differentiation." *Microbial Biofilms*. <https://doi.org/10.1128/9781555817466.ch4>.
- Van Valen, David A., Takamasa Kudo, Keara M. Lane, Derek N. Macklin, Nicolas T. Quach, Mialy M. DeFelice, Inbal Maayan, Yu Tanouchi, Euan A. Ashley, and Markus W. Covert. 2016. "Deep Learning Automates the Quantitative Analysis of Individual Cells in Live-Cell Imaging Experiments." *PLoS Computational Biology* 12 (11): e1005177.
- Vassallo, Christopher, Darshankumar T. Pathak, Pengbo Cao, David M. Zuckerman, Egbert Hoiczyk, and Daniel Wall. 2015. "Cell Rejuvenation and Social Behaviors Promoted by LPS Exchange in Myxobacteria." *Proceedings of the National Academy of Sciences of the United States of America* 112 (22): E2939–46.
- Veening, Jan-Willem, Oleg A. Igoshin, Robyn T. Eijlander, Reindert Nijland, Leendert W. Hamoen, and Oscar P. Kuipers. 2008. "Transient Heterogeneity in Extracellular Protease Production by Bacillus Subtilis." *Molecular Systems Biology* 4 (April): 184.
- Veening, Jan-Willem, Wiep Klaas Smits, and Oscar P. Kuipers. 2008. "Bistability, Epigenetics, and Bet-Hedging in Bacteria." *Annual Review of Microbiology* 62: 193–210.
- Veening, Jan-Willem, Eric J. Stewart, Thomas W. Berngruber, François Taddei, Oscar P. Kuipers, and Leendert W. Hamoen. 2008. "Bet-Hedging and Epigenetic Inheritance in Bacterial Cell Development." *Proceedings of the National Academy of Sciences of the United States of America* 105 (11): 4393–98.

- Veerachamy, Suganthan, Tejasri Yarlagadda, Geetha Manivasagam, and Prasad Kdv Yarlagadda. 2014. "Bacterial Adherence and Biofilm Formation on Medical Implants: A Review." *Proceedings of the Institution of Mechanical Engineers. Part H, Journal of Engineering in Medicine* 228 (10): 1083–99.
- Velicer, G. J., L. Kroos, and R. E. Lenski. 2000. "Developmental Cheating in the Social Bacterium *Myxococcus Xanthus*." *Nature* 404 (6778): 598–601.
- Velicer, Gregory J. 2003. "Social Strife in the Microbial World." *Trends in Microbiology* 11 (7): 330–37.
- Velicer, Gregory J., and Michiel Vos. 2009. "Sociobiology of the Myxobacteria." *Annual Review of Microbiology* 63: 599–623.
- Velicer, Gregory J., and Yuen-Tsu N. Yu. 2003a. "Evolution of Novel Cooperative Swarming in the Bacterium *Myxococcus Xanthus*." *Nature* 425 (6953): 75–78.
- . 2003b. "Evolution of Novel Cooperative Swarming in the Bacterium *Myxococcus Xanthus*." *Nature* 425 (6953): 75–78.
- Vilain, Sébastien, Jakobus M. Pretorius, Jacques Theron, and Volker S. Brözel. 2009. "DNA as an Adhesin: *Bacillus Cereus* Requires Extracellular DNA To Form Biofilms." *Applied and Environmental Microbiology*. <https://doi.org/10.1128/aem.01317-08>.
- Vlamakis, Hera, Claudio Aguilar, Richard Losick, and Roberto Kolter. 2008. "Control of Cell Fate by the Formation of an Architecturally Complex Bacterial Community." *Genes & Development* 22 (7): 945–53.
- Vos, Michiel, and Gregory J. Velicer. 2009. "Social Conflict in Centimeter- and Global-Scale Populations of the Bacterium *Myxococcus Xanthus*." *Current Biology: CB* 19 (20): 1763–67.
- Wall, D., S. S. Wu, and D. Kaiser. 1998. "Contact Stimulation of Tgl and Type IV Pili in *Myxococcus Xanthus*." *Journal of Bacteriology* 180 (3): 759–61.
- Wang, Guangqiang, Yu Xia, Jing Cui, Zhennan Gu, Yuanda Song, Yong Q. Chen, Haiqin Chen, Hao Zhang, and Wei Chen. 2014. "The Roles of Moonlighting Proteins in Bacteria." *Current Issues in Molecular Biology* 16: 15–22.
- Ward, M. J., and D. R. Zusman. 1997. "Regulation of Directed Motility in *Myxococcus Xanthus*." *Molecular Microbiology* 24 (5): 885–93.
- Wei, Guopeng, Connor Walsh, Irina Cazan, and Radu Marculescu. 2015. "Molecular Tweeting." *Proceedings of the 6th ACM Conference on Bioinformatics, Computational Biology and Health Informatics*. <https://doi.org/10.1145/2808719.2808757>.
- Wei, Xueming, Darshankumar T. Pathak, and Daniel Wall. 2011. "Heterologous Protein Transfer within Structured Myxobacteria Biofilms." *Molecular Microbiology* 81 (2): 315–26.
- Weigert, Martin, Uwe Schmidt, Tobias Boothe, Andreas Müller, Alexandr Dibrov, Akanksha Jain, Benjamin Wilhelm, et al. 2018. "Content-Aware Image Restoration: Pushing the Limits of Fluorescence Microscopy." *Nature Methods* 15 (12): 1090–97.
- West, S. A., A. S. Griffin, and A. Gardner. 2007. "Social Semantics: Altruism, Cooperation, Mutualism, Strong Reciprocity and Group Selection." *Journal of Evolutionary Biology* 20 (2): 415–32.
- West, Stuart A., and Guy A. Cooper. 2016. "Division of Labour in Microorganisms: An Evolutionary Perspective." *Nature Reviews. Microbiology* 14 (11): 716–23.
- West, Stuart A., Stephen P. Diggle, Angus Buckling, Andy Gardner, and Ashleigh S. Griffin. 2007. "The Social Lives of Microbes." *Annual Review of Ecology, Evolution, and Systematics* 38 (1): 53–77.
- Whitchurch, C. B. 2002. "Extracellular DNA Required for Bacterial Biofilm Formation." *Science*. <https://doi.org/10.1126/science.295.5559.1487>.
- Whitfield, Damion L., Gaurav Sharma, Gregory T. Smaldone, and Mitchell Singer. 2020. "Peripheral Rods: A Specialized Developmental Cell Type in *Myxococcus Xanthus*." *Genomics* 112 (2): 1588–97.
- Whitworth, David E. 2015. "Genome-Wide Analysis of Myxobacterial Two-Component Systems: Genome Relatedness and Evolutionary Changes." *BMC Genomics* 16 (October): 780.

- Whitworth, David E., and Bethan H. Morgan. 2015. "Synergism Between Bacterial GAPDH and OMVs: Disparate Mechanisms but Co-Operative Action." *Frontiers in Microbiology* 6 (November): 1231.
- Whitworth, David E., Susan E. Slade, and Adrian Mironas. 2015. "Composition of Distinct Sub-Proteomes in *Myxococcus Xanthus*: Metabolic Cost and Amino Acid Availability." *Amino Acids* 47 (12): 2521–31.
- Wildermuth, H. 1970. "Development and Organization of the Aerial Mycelium in *Streptomyces Coelicolor*." *Journal of General Microbiology* 60 (1): 43–50.
- Wireman, J. W., and M. Dworkin. 1977. "Developmentally Induced Autolysis during Fruiting Body Formation by *Myxococcus Xanthus*." *Journal of Bacteriology*. <https://doi.org/10.1128/jb.129.2.798-802.1977>.
- Wolgemuth, Charles, Egbert Hoiczyk, Dale Kaiser, and George Oster. 2002. "How Myxobacteria Glide." *Current Biology: CB* 12 (5): 369–77.
- Wu, S. S., and D. Kaiser. 1995. "Genetic and Functional Evidence That Type IV Pili Are Required for Social Gliding Motility in *Myxococcus Xanthus*." *Molecular Microbiology* 18 (3): 547–58.
- Xavier, João B., Esteban Martinez-Garcia, and Kevin R. Foster. 2009. "Social Evolution of Spatial Patterns in Bacterial Biofilms: When Conflict Drives Disorder." *The American Naturalist* 174 (1): 1–12.
- Xiao Yao, Wei Xueming, Ebright Richard, and Wall Daniel. 2011. "Antibiotic Production by Myxobacteria Plays a Role in Predation." *Journal of Bacteriology* 193 (18): 4626–33.
- Yang, Zhaomin, and Penelope I. Higgs. 2014. *Myxobacteria: Genomics, Cellular and Molecular Biology*. Caister Academic Press.
- Zhang, Wenchao, Yan Wang, Huining Lu, Qin Liu, Chuandong Wang, Wei Hu, and Kun Zhao. 2020. "Dynamics of Solitary Predation by *Myxococcus Xanthus* on *Escherichia Coli* Observed at the Single-Cell Level." *Applied and Environmental Microbiology* 86 (3). <https://doi.org/10.1128/AEM.02286-19>.
- Zhang, Yong, Adrien Ducret, Joshua Shaevitz, and Tãm Mignot. 2012a. "From Individual Cell Motility to Collective Behaviors: Insights from a Prokaryote, *Myxococcus Xanthus*." *FEMS Microbiology Reviews* 36 (1): 149–64.
- . 2012b. "From Individual Cell Motility to Collective Behaviors: Insights from a Prokaryote, *Myxococcus Xanthus*." *FEMS Microbiology Reviews* 36 (1): 149–64.
- Zhang, Yong, Mathilde Guzzo, Adrien Ducret, Yue-Zhong Li, and Tãm Mignot. 2012a. "A Dynamic Response Regulator Protein Modulates G-Protein-Dependent Polarity in the Bacterium *Myxococcus Xanthus*." *PLoS Genetics* 8 (8): e1002872.
- . 2012b. "A Dynamic Response Regulator Protein Modulates G-Protein-Dependent Polarity in the Bacterium *Myxococcus Xanthus*." *PLoS Genetics* 8 (8): e1002872.
- Zhang, Yu-Qing, Yue-Zhong Li, Bing Wang, Zhi-Hong Wu, Cui-Ying Zhang, Xun Gong, Zhi-Jun Qiu, and Yong Zhang. 2005. "Characteristics and Living Patterns of Marine Myxobacterial Isolates." *Applied and Environmental Microbiology* 71 (6): 3331–36.
- Zhou, Xiu-Wen, Shu-Guang Li, Wei Li, De-Ming Jiang, Kui Han, Zhi-Hong Wu, and Yue-Zhong Li. 2014. "Myxobacterial Community Is a Predominant and Highly Diverse Bacterial Group in Soil Niches." *Environmental Microbiology Reports* 6 (1): 45–56.
- Zusman, D. R., and K. A. O'Connor. 1991. "Development in *Myxococcus Xanthus* Involves Aggregation and Sporulation as Well as Non-Aggregation and Nonsporulation." In *Seminars in Developmental Biology*, 2:37–45.
- Zusman, David R., Ansley E. Scott, Zhaomin Yang, and John R. Kirby. 2007a. "Chemosensory Pathways, Motility and Development in *Myxococcus Xanthus*." *Nature Reviews. Microbiology* 5 (11): 862–72.
- . 2007b. "Chemosensory Pathways, Motility and Development in *Myxococcus Xanthus*." *Nature Reviews. Microbiology* 5 (11): 862–72.

